Alma Mater Studiorum – Università di Bologna

DOTTORATO DI RICERCA IN

Chimica

Ciclo XXXIV

Settore Concorsuale: 03/C1

Settore Scientifico Disciplinare: CHIM/06

Novel Hydroxystearoyl-, Heterocyclic and Carbocyclic derivatives: Synthesis and Applications in Biological Field

Presentata da: Dario Telese

Coordinatore del Dottorato

Prof.ssa Domenica Tonelli

Supervisore

Prof.ssa Carla Boga

Co-relatore

Dott. Gabriele Micheletti

Esame finale anno 2022

-"Sapete la differenza tra i fisici e noi chimici?"

[silenzio]

-"I fisici cercano di INTERPRETARE i fenomeni che circondano il nostro universo, noi chimici invece,

beh noi LI CREIAMO"

G. Longoni

Table of contents

Chapter I: Synthesis, biological effects and drug delivery of hydroxystearic acids (HSAs) and their derivatives

1.1. Introduction

1.1.1. Epigenetics

The terms “epigenesis” and “epigenetics”, although both refer to processes related to development of complex organisms, suggest different phenomena.

The term “epigenesis” has been introduced in the second half of XVIII century by physiologist Caspar Friedrich Wolff to indicate a development mechanism, starting from something simple and no-form, leading to the progressive differentiation and development of tissues and organs up to the formation of a complex organism.[1] However the idea has very ancient origins, in according to the development of individual forms (phenotype) which occured from no-formed matter (genotype): already Aristotele postulated the existence of genetic phenomena in the IV century in his treatise "Physics".[2] This vision was in contrast with the preformism theory, that interpreted the development as the simple growth of a little organism but already completely preformed.

The term “epigenetics” means “over genetics” and it was introduced in 1942 by Conrad Waddington to describe the branch of biology that studies the phenomena leading from genotype to phenotype, but it assumed several meanings over time.[2] Initially this term was used to indicate the study of interactions between genes and environment for the formation of organism. Later it was used to indicate in direct manner the mechanisms of time and space control of activity of genes during the growth of complex organisms up to a unifying definition of epigenetic events by Adrian Bird in 2007: the structural adaptation of chromosomal regions so as to register, signal or perpetuate altered activity states.[3]

The study of phenomena and epigenetic regulations was strictly correlated to that of human disease. Just the study on hereditary diseases, which showed an anomalous inheritance compared to the classic laws of genetics, allowed to identify and analyse phenomena of epigenetic regulation. Although the mechanism of inheritance of epigenetic modifications is still unclear, epigenetic changes counteracted by chemical agents is where the most important difference between epigenetic and genetic mechanism lies.[4,5]

The main epigenetic mechanisms of regulation of the genetic activity are DNA methylation and the process of chromatin remodeling. These mechanisms play an important role into biologic research and affect several fields, *i.e.* cancer, viral latency, somatic gene therapies, parental genomic imprinting.[6] For example, a deregulation of genes subjected to cytosine methylation imprinting is the

basis of some diseases of the nervous system, including Rett syndrome, Prader-Willi syndrome and Angelman syndrome. One of the various examples of genetic diseases involving the alteration of chromatin remodelling is the CHARGE syndrome (Coloboma, Heart defect, Atresia choanae, Retarded growth and development, Genital hypoplasia, Ear anomalies/deafness). Indeed, it has been found that patients afflicted with CHARGE syndrome are characterized by haploinsufficiency of CHD7, an ATP-dependent chromatin remodeler.[1] A general change in epigenetic terms, among the features of tumor cells, suggested that alterations of epigenetic processes could be at the base of changes in gene activity that accompany the malignant transformation of cells. Infact, a remarkable reprogramming of the various epigenetic components was explained during the phases of initiation and progression of cancer cells, including DNA methylation, histone changes and repositioning of nucleosomes.[1]

1.1.2. DNA methylation

DNA methylation is a heritable epigenetic mark involving the methylation at the C-5 position of the cytosine belonging to DNA by action of DNA methyltransferases (DNMTs). In mammals, mainly cytosine rings are methylated and followed by guanine in 5'-CG-3' sequence, where the two bases are bound through a phosphate group. These stretches of DNA are called CpG islands where "p" indicates the presence of phosphate group. It was observed that CpG sequences (methylated or not) are not evenly distributed along the genomic sequence, but they appear clustered in regions about 1-2 Kpb long and composed of more than 500 couple of bases with a cytosine and guanine content above 55%.[1,7]

The action of DNMTs is able to modify DNA conformation to which proteins capable of interacting with the DNA itself are bound. In particular it involves some alterations into the structure of chromatin and also a decrease or increase of transcription rate, depending on regulatory elements (positive or negative) of the genes involved. Especially the methylation of a promoter of CpG island leds to bound different proteins, to shape highly condensed chromatin structures, forbidding access to transcription factors (TFs).[8] Methylated DNA participates in the formation of chromatin through interactions with various other epigenetic modifications such as the histone code, polycomb complexes, nucleosome positioning, noncoding RNA, and ATP-dependent chromatin remodeling proteins.[9]

Post-translational histone modifications (PTM), *i.e.* phosphorylation, methylation, proline isomerization and acetylation, are part of epigenetic modifications. Potentially these are good therapeutic targets, thanks to their reversibility and they are very useful as tumor biomarkers.

DNA methylation, with organization of chromatin and regulation of histone acetylation/deacetylation, can play an important role during the whole carcinogenic process.

During mammalian development and cancer, DNA methylation and specific histone modifications appear to reciprocally influence each other: histone methylation may direct DNA methylation patterns, and DNA methylation may serve as a template for the establishment of certain histone modifications after DNA replication.[10] This relationship between DNA methylation and histone modifications supported researchers to introduce combined therapies based on methylation and deacetylation inhibitors.

1.1.3. Acetylation, deacetylation and chromatin remodeling

Histones are basic proteins characterized by apolar central domain with globular structure, N-terminal regions, called histone tails, and C-terminal regions which contain mainly basic aminoacids, such as lysine and arginine.

Five major classes of histones exist: H1, H2A, H2B, H3 and H4. Histones H2A, H2B, H3 and H4 are known as the core histones, while histones H1 are known as the linker histones. These proteins compose the proteic octamer around which the DNA turns itself in a left-handed helix to form the nucleosome, essential unit of chromatin.[11]

Histones are subjected to many post-translational modifications (PTM) to the point of *N*-terminal tails, *i.e.* acetylations, methylations, phosphorylations, ADP-ribosylations and ubiquitinations.[12] These modifications lead to the formation of several recognition sites for enzimatic complexes involved in important processes, for example DNA repair and replication and chromatin assembly. In general once PTM occur, the chromatin is susceptible to structural variations, which in turn determine different transcriptional states: the condensed form of chromatin (heterochromatin) is less accessible to transcription factors (TF), involving a repression of transcription, while when chromatin is in a relaxed form (eucromatin), TFs are able to reach the promoter areas, activating the transcription (**Figure 1**).

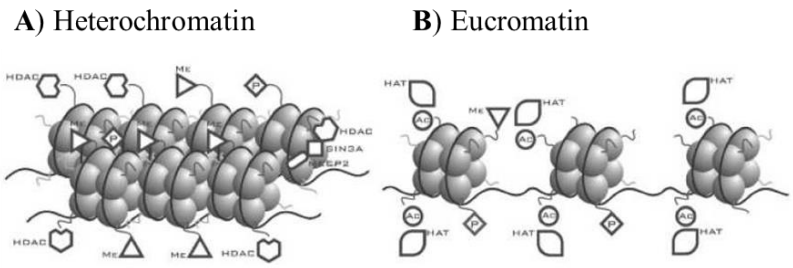

Figure 1. A) Condensed form and **B)** relaxed form of chromatin.

It is noteworthy that the structure of chromosomes is dynamic, thus there is an equilibrium between the condensed and relaxed form of chromatin.

Histone tails H3 and H4 are the principal targets of PTM catalyzed by several enzymes, *i.e.* histone acetyltransferases (HAT), histone deacetylases (HDAC) which I will focus on because it is one of the topics of this thesis, methyltransferases (HMT) and kinases (HK), whose reactions are able to regulate gene expression. The existence of a real "histone code" or "epigenetic code" has been proposed by the set of modifications that are able to regulate the transcriptional activity of specific genes.[13]

The state of histone acetylation is controlled by the activity of two families of enzymes: HAT and HDAC, which preferentially interact with the ε-amino groups of the lysine residues of the N-terminal tails. The positive charges of hypo-acetylated histones in the nucleosome, interact with the negatively charged phosphate groups of DNA, keeping the chromatin in a compact and therefore silent structure. Acetylation neutralizes that positive charge on histones, inducing the formation of eucromatin and making promoter regions more accessible to TFs, transcription regulation complexes and RNA polymerase (**Figure 2**).

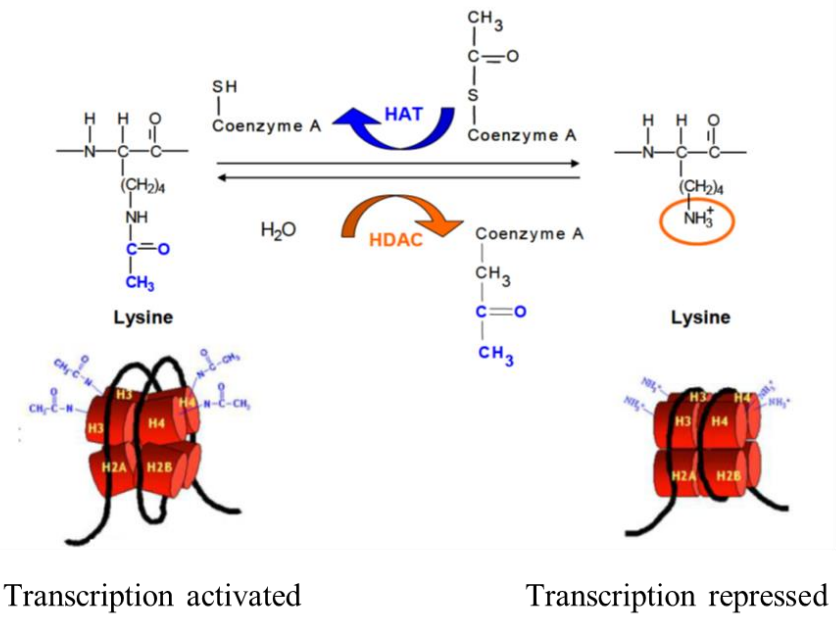

Figure 2. Role of HAT and HDAC during acetylation.

The enzymes belonging to these families can be divided into various classes according to their different characteristics, such as cell location, size, structural homology and mechanism of action.

Based on the homolgy with the yeast deacetylases, HDACs are composed by four classes: classes I, II and IV are similar in sequence and structure and they have a zinc-dependent catalytic activity. Instead the class III, called also sirtuins, needs the presence of nicotinamide adenine dinucleotide ($NAD^{+)}$, an oxidoreduction coenzyme whose role is the electron transfer.[14]

The class I is composed by HDAC 1, 2, 3 and 8, located into the nucleus, and it is belived to be particularly involved in histone acetylation, but not all HDACs of this class react in the same manner. The knock-down, that is the abolition of functions without physical elimination, of different HDACs of class I caused several cellular effects. For example, a study showed how the knock-down of HDAC 1 and 2 induces an antiproliferative activity against colon cancer cell lines *in vitro*[15], in contrast with HDAC 3 which showed a growth inhibition of a different colon cancer cell set[16]; moreover the knock-down of HDAC 2 and 3 induced a damage to DNA and apoptosis.[17]

Instead the class II is composed by HDAC 4, 5, 6, 7 and 9, located into cytoplasm, and the analysis of this class led the same conclusions of class I. The knock-down of HDAC 4 involved proliferation inhibition and apoptosis[18], while the knock-down of HDAC 7 in endothelial cells showed no effects on growth or survival but on the migratory capacity and formation of capillary structures.[19] The activity of these enzymes depends on cell type and context but it is possible to deduce that HDACs of class I are mainly engaged in the regulation of proliferative activity and apoptosis, while those of class II appear to be involved in migration and angiogenesis.

1.1.4. HDACs: carcinogenesis and its inhibitors

Recently it has been observed that aberrant HDAC and HAT levels are involved in carcinogenesis: HDAC and HAT are able to deacetylate/acetylate not only histone proteins, but also proteins able to control cell cycle progression and/or apoptosis.[20]

The arrest of the cell cycle and apoptosis are important events in the differentiation process; for this reason the chromatin remodeling, regulated by the action of HAT and HDAC, which can involve the aberrant expression of some genes, could interfere with these processes finely controlled and induce the proliferation of undifferentiated cells and therefore the onset of the tumor.[21]

Several research groups are interested in the design and synthesis of compounds with low toxicity able to inhibit the activity of these enzymatic classes. Moreover, these compounds must be able to block the cell proliferation stopping the cell cycle in phases G0/G1 and/or G2 and/or inducing apoptosis of cells; they must show to be active against a wide range of cell lines of both, solid and blood cancers; in this context some of compounds exhibiting these properties have been clinically tested.[22,23]

The research group in which I carried out my PhD showed that an endogenous lipoperoxidation product, 9-hydroxystearic acid (9-HSA), when administered to HT29 colon carcinoma cells induced an antiproliferative effect at least partially associated with a molecular mechanism involving HDAC 1 inhibition. The enzymatic activity assay showed that 9-HSA inhibited 66.4% of the HDAC 1 activity *in vitro*. The molecular interaction of 9-HSA with HDAC 1 was investigated through a computational approach, demonstrating that the binding of 9-HSA to the active site of HDAC 1 was rather similar to that of trichostatin A (TSA), a well-known HDAC inhibitor.[24]

Treatments with HDAC inhibitors (HDACi) cause an increase in histone acetylation levels both in normal cells and in cancer cells; nevertheless cancer cells are more sensitive to growth inhibiting effects and apoptotic effects compared to normal cells. A peculiar ability of HDACi is to selectively manipulate gene expression of transformed cells. These compounds induce an accumulation of hyperacetylated histones into chromatin, but only a little part of expressed genes show a change in the transcription pattern.

After treatment with HDACi, among several genes in many transformed cells, it is present a gene, called CDKN1A, which codes for the cyclin-dependent kinase (CDK) inhibitor p^{21WAF1}.[25]

Kinases are enzymes involved in many biological pathways, including cell cycle control in which they perform their functions at the level of the two checkpoints located at transitions G1/S and G2/M (**Figure 3**).

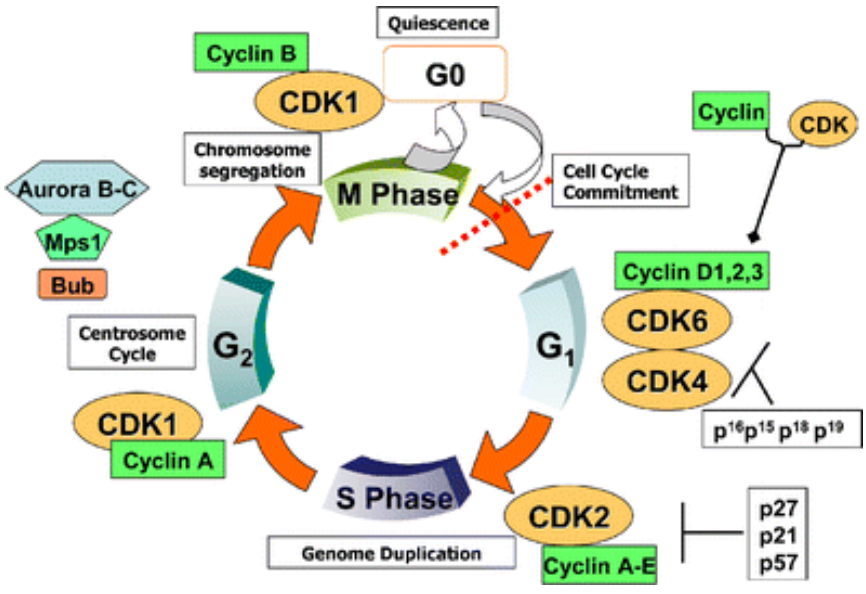

Figure 3. Cell cycle and action of cyclins.

Thanks to a particular class of proteins, the cyclins, they allow the regular progress of cell cycle. Being a tumor suppressor, cyclin inhibits the activity of CDK when it is bounded to it, inducing a

hypophosphorylation of the proteins pRb, p107 and p130, the suppression of cell proliferation and the arrest of the cell cycle in phase G1.[25]

Another gene, whose altered expression is generally low in cancer cells, is that codifying for thioredoxin-binding protein 2 (TBP2).[26] The suberoylanilide hydroxamic acid (SAHA), a well-known HDAC inhibitor, increases selectively the TBP2 expression, which bounds and inactivates the thioredoxin reducted.[27] This protein is very important for redox reactions of cell: SAHA increases the sensibility of cells towards oxidative stress and it could induce apoptosis. Following the treatment of this agent, the activation of TBP2, generally repressed in cancer cells, can contribute in the arrest of cell growth and /or apoptosis.

Although molecules with inhibitory activity towards HDACs are classified according to chemical structures, most of them could be related through a common pharmacophore: the basic structure, similar to the structure of Trichostatin A (TSA), is characterized by a functional group chelating the zinc atom in the active site, a linker that accommodates the tubular access to the active site, and a recognition group for interactions with the external surface, connected by a small unit to the linker (**Figure 4**).[28]

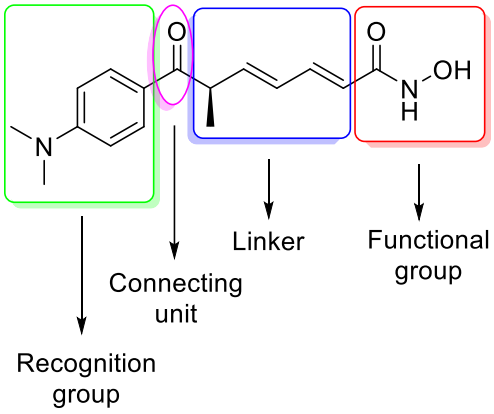

Figure 4. Structure of TSA as HDACi.

Four classes of HDACi are known and object of clinical trials: short chain carboxylic acids, hydroxamic acids, benzamides and cyclic tetrapeptides.

- Short chain carboxylic acids: this class of compounds (shown in **Figure 5**) is characterized by a short plasma half-life, non-specificity and low inhibitory power due to weak contact of the short aliphatic chain with the catalytic pocket of the HDAC.[29] Valproic acid was the first one to be subjected to analysis: it has long been used as an antiepileptic and also tested against leukemia considering its mild side effects, but showed small effect as HDAC.[30] Later, butyric acid and phenylbutyrate were also studied, but with poor results.

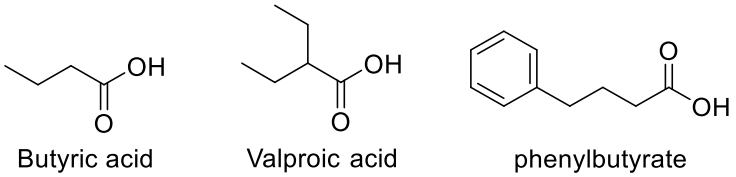

Figure 5. Examples of short chain carboxyl acids as HDACi.

- Hydroxamic acids: the general structure is made of a hydrophobic linker that allows the hydroxamic group to chelate the cation on the bottom of the enzymatic pocket, thus preventing access of the substrate to the zinc ion.[31] TSA was one of the first HDAC inhibitors identified and it is often used as a reference in biological studies (**Figure 6**). It causes apoptosis in hepatocellular carcinoma cells, blocks the cell cycle in Hela cells and the differentiation of ovarian cancer cells.[32] However, its toxicity and poor specificity led to the search for other molecules: suberanilohydroxamic acid (SAHA), also known as Vorinostat (shown in **Figure 6**), is sold under the name Zolinza by Merck for the treatment of cutaneous T cell lymphoma (CTCL).[33] It was the first histone deacetylase inhibitor approved by FDA (Food and Drug Administration) for clinical use, able to inhibit any zinc-dependent HDAC, except for enzymes belonging to class IIa, on which it has weak effects.[34]

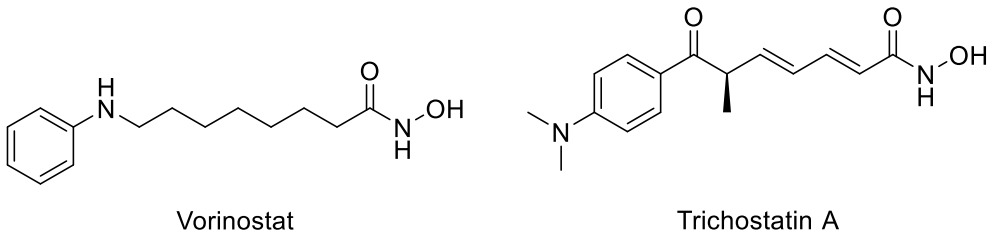

Figure 6. Examples of hydroxamic acids as HDACi.

- Benzamides: the mechanism of action of this class is not yet entirely clear; however they showed to inhibit the cell proliferation acting between G1 and S phase of the cell cycle[35] and the presence of amino-amide group is very important to chelate the zinc ion in the catalytic site.[36] Entinostat (shown in **Figure 7**), also called MS275, is the most powerful of its derivatives: it inhibits selectively HDAC1 and HDAC3 with IC_{50} of 0.18 μM and 0.74 μM, respectively.[35] The activity of MS275 involves an increase in the transcription of the $p^{21WAF/Cip1}$ inhibitor of cyclin dependent kinases and therefore an arrest of the cell cycle in G1.[37] Moreover it showed anticancer activity against several human cancer cell lines.[38]

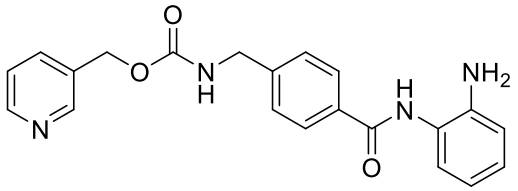

Entinostat

Figure 7. Example of benzamide as HDACi.

- Cyclic tetrapeptides: cyclic peptides (shown in **Figure 8**), such as Apicidin, interact with the active site and exhibit the antiproliferative effects through selective induction of $p^{21WAF1/Cip1}$ already in nanomolar doses.[39] Moreover, Apicidin showed apoptosis against endometrial, ovarian and human acute promyelocytic leukemia cell lines.[39,40] Instead Trapoxin is a fungal product that causes accumulation of highly acetylated core histones in a variety of mammalian cell lines.[41] Furthermore, chemical reduction of the epoxide group in trapoxin completely abolished the inhibitory activity, suggesting that trapoxin binds covalently to the histone deacetylase via the epoxide.[42]

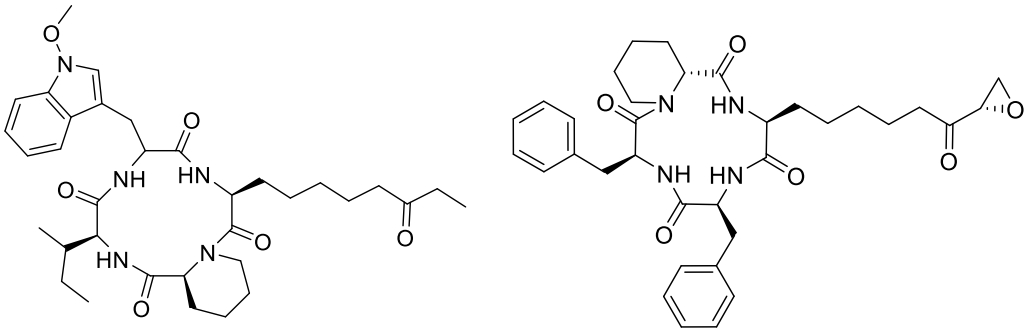

Apicidin Trapoxin

Figure 8. Examples of cyclic tetrapeptides as HDACi.

1.1.5. Oxidative stress: correlation between lipid peroxidation and cancer

The oxidative stress and resulting lipid (mainly membrane lipid) peroxidation, are involved in several biological pathways such as inflammation, atherosclerosis, neurodegenerative diseases and cancer.[43] The term “oxidative stress” is used to describe an imbalance between the systemic manifestation of reactive oxygen species (ROS) and a biological system's ability to readily detoxify the reactive intermediates or to repair the resulting damage. Base damage is mostly indirect and caused by ROS generated, *e.g.* superoxide anion ($O_2^{-\bullet}$), perhydroxyl radical ($HO_2^{\bullet}$), hydroxyl radical($^{\bullet}OH$) and hydrogen peroxide (H_2O_2).[44]

ROS are reactive chemical species containing oxygen present in our organism: they are generated as by-products of cellular metabolism, primarily in the mitochondria and include free radicals and other species such as singlet oxygen ($^1O_2$), hypochlorous acid (HOCl), and peroxynitrite ($ONOO^-$).[44] The production of ROS occurs during the oxidative phosphorylation, mechanism whose free energy that accompanies the electrons transfer along the respiratory chain is coupled to the formation of ATP by phosphorylation of ADP, through chemosmotic coupling. During the electron transport process, a radical species, the superoxide anion $O_2^{-\bullet}$, can be generated. To prevent the damage from ROS, this radical can subsequently undergo dismutation by the antioxidant enzyme superoxide dismutase (SOD), located in the mitochondria and the cytosol, which renders it inactive thanks to the conversion to hydrogen peroxide. Hydroxyl radical can be produced, through the Fenton reaction and the Haber-Weiss reaction (**Scheme 1**) starting from hydrogen peroxide and metal species.[45]

Fenton reaction:

$$Fe^{2+} + H_2O_2 \longrightarrow Fe^{3+} + OH^{\bullet} + OH^-$$

$$Fe^{3+} + H_2O_2 \longrightarrow Fe^{2+} + OOH^{\bullet} + H^+$$

Haber-Weiss reaction:

$$Fe^{3+} + O_2^{-\bullet} \longrightarrow Fe^{2+} + O_2$$

$$Fe^{2+} + H_2O_2 \longrightarrow Fe^{3+} + OH^{\bullet} + OH^-$$

Scheme 1. Fenton and Haber-Weiss reactions.

The radical generated is the most active and dangerous radical for the cell because it is able to penetrate through the membranes.[46]

Other enzymes regulate the stability of cell correlated to production of ROS, such as catalase and glutathione peroxidase. These enzymes, present in our organism, catalyze the decomposition of hydrogen peroxide to water and oxygen.[47] However, also non-ezymatic molecules, *e.g.* vitamin E, vitamin C, β-carotene, polyphenolic antioxidants like flavonoids, that can be assumed through food in everyday life, can prevent the formation of radical species.[48]

In recent years, it has become evident that cancer cells have increased levels of ROS compared with normal cells. For example, leukaemia cells isolated from blood samples from patients with chronic lymphocytic leukaemia showed increased ROS production compared with normal lymphocytes.[49]

A limited increase of production of ROS can promote cell proliferation and differentiation, whereas excessive amounts of ROS can cause oxidative damage. Therefore, it is essential to preserve the homeostasis of ROS for normal cell growth and survival.[50] An increase in ROS is associated with

abnormal cancer cell growth and reflects a disruption of redox homeostasis due either to an elevation of ROS production.[51]

Indeed, the levels of ROS-scavenging enzymes such as SOD and glutathione peroxidase have been shown to be altered in cancer cells, suggesting aberrant regulation of redox homeostasis.[52]

Furthermore, the radicals produced by oxidative stress can cause damages to membrane lipids, causing so-called lipid peroxidation (shown in **Scheme 2**).[53] This process conduces to formation of hydroperoxides and numerous secondary products, dependent on polyunsaturated fatty acids (PUFA).[43] The process consists of three major steps: initiation, propagation and termination. The initiation phase consists in the extraction of an allyl hydrogen radical, from an unsaturated fatty acid (RH) with formation of a lipid radical (R•). Oxygen is added to the product of initiation reaction (R•), giving rise to a peroxidic radical (ROO•). The latter can extract a hydrogen radical from another fatty acid forming the hydroperoxide (ROOH) of the original acid and generating a new radical (R•) which starts the propagation stage. Radical propagation ends when two radicals combine together to form a non-radical product.

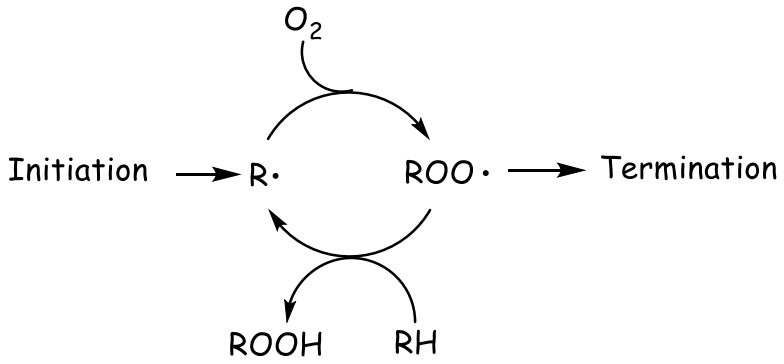

Scheme 2. Phases of lipid peroxidation.

The lipid peroxidation and the subsequent breakage of lipids with the formation of reactive compounds can lead to changes in the permeability and fluidity of the membrane lipid bilayer and can dramatically alter cell integrity.[54] This event is correlated to decrease in the phospholipid/protein ratio and increase in the cholesterol/phospholipid ratio, both in plasma and intracellular membranes. In fact, many studies on hepatocellular carcinoma showed as the increase in tumor growth rate decreased the content of phospholipids and the degree of unsaturation, regardless of the prooxidant stimulus.[52]

Although an increase of oxidative stress has been demonstrated in the majority of cancer types, the concentration of lipid peroxidation products in cancer cells is yet a matter of debate. However, since these compounds are present in lower quantities in tumor lines, it has been hypothesized that they

could play an important role in the control of cell proliferation.[43] They are divided in two categories: primary products of lipid peroxidation, mainly lipid hydroperoxides (LOOH), and secondary products, among whose 4-hydroxynonenal (HNE) is the most intensively studied since it is a highly electrophilic molecule that easily reacts with low-molecular-weight compounds, such as glutathione, with proteins and, at higher concentration, with DNA, blocking the -SH groups of DNA polymerases during cell proliferation.[55,56] Finally, the lipid peroxidation causes not only the decrease of production of PUFA, but also peroxides and hydroperoxides, involving in abnormal cell proliferation and rise up of tumor.[57]

1.1.6. Hydroxystearic acids

Lipid peroxidation products have been isolated, studied and analyzed in the control of cell proliferation.[58] Among these, two monohydroxy fatty acids, 9- and 10-hydroxystearic acids (9- and 10-HSA) showed cytotoxic effects against different cancer cell lines.[59] In particular it was evidenced both in a murine line, derived from Lewis lung cancer with high metastatic potential (C108),[60] and in the human cancer cell line HT-29, deriving from colon adenocarcinoma,[58] as the content of these two molecules is inversely proportional to the degree of cell density. Further studies were performed in normal cells of embryonic intestinal epithelium I-407, where the content of the two fatty acids increases proportionally to the degree of cell density.[61]

The effects of an exogenous administration of an equimolar mixture of the two positional isomers, at different concentration (5-100 μM), were studied considering the possible role of 9- and 10-HSA in control of cell growth.

An antiproliferative effect dose- and time- dependent was showed in cancer cell lines HT-29 and C108, starting from 20 μM, whereas it was underlined a cytotoxic effect at concentration >100 μM.[58,60] In contrast, the normal cell line I-407 showed cytotoxic effect at concentration above 150 μM.[61]

Then, the effects of two hydroxy fatty acids (administered separately) on the cell cycle were studied and it emerged that 9-HSA causes antiproliferative effect against cancer cells but no effect on normal cells, whereas 10-HSA has cytotoxic effect. In HT-29 and I-407, the administration of 9-HSA causes a block of cell cycle in G0/G1 phase with a decrease in S; instead in C108, it inhibits the cell proliferation in G2/M phase.[62]

Further studies evidenced that the main target of 9-HSA is HDAC1, with an inhibition enzyme activity of about 66.4% *in vitro*. This effect is induced by direct activation of the $p21^{WAF1}$, by-passying p53, causing a proliferative arrest of cell cycle.[24]

Through molecular docking, it was showed the binding mode of 9-HSA and the importance of the configuration of the chiral center in 9-position towards HDAC1. The carboxylic group of the fatty acid is able to chelate the zinc ion into the pocket of the enzyme (shown in **Figure 9**), in a similar way to that of TSA.[24]

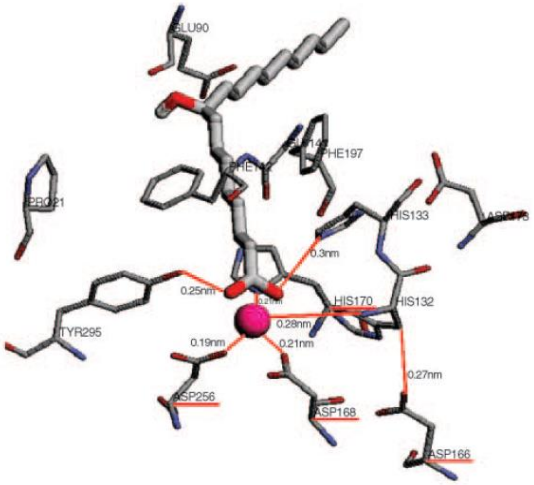

Figure 9. Molecular docking between HDAC1 and 9-HSA.

The binding energy predicted for the two enantiomers was found to be -8.45 and -1.97 kcal/mol for *R*- and *S*- isomers, respectively, suggesting that the interaction with the *R* enantiomer is more stable than that with the S enantiomer.[24]

Further studies on (*R*)- and (*S*)-9-HSA, synthesized and separately administered to HT29 cells confirmed the "in silico" predictions. Both enantiomers inhibit the enzymatic activity of HDAC1, HDAC2 and HDAC3, with a more marked effect for HDAC1, showing a greater inhibition by the R isomer than the S one (81% vs 51%). Biological tests showed an increase in the level of acetylation of histone H4 and protein p21, with a decrease in the expression of the cyclin D1 for both enantiomers. The *R* isomer showed a greater antiproliferative effect against HT-29 cells than the *S* isomer, inducing a cell cycle arrest in the G0/G1 phase.[63]

1.2. Synthesis of 9-HSA derivatives and their anticancer activity against HT-29 cancer cells[64]

As reported in the introduction of this chapter, 9-HSA is able to inhibit the cell proliferation in different cancer cell lines, without to attack the healthy cells, interacting selectively towards HDAC1. Based on the previous studies, we decided to investigate on the biological effects of 9-HSA derivatives focusing attention on the effect of the substituent in 9-position and that of the free carboxylic group that it has been predicted to play a key role in coordinating the zinc ion present in the enzymatic pocket of HDAC1 similarly to what occurs with Vorinostat. For this purpose, novel (*R*)-9-hydroxystearic acid derivatives were synthesized and their biological effect tested on HT29 cell line.

1.2.1. Results and discussion

Enantiopure (*R*)-9-HSA is easily accessible within the natural chiral pool since its precursor (*S*)-dimorphecholic acid is one of the main components of *Dimorphoteca sinuata* L. seeds. The natural availability of (*S*)-dimorphecholic acid provides a green and efficient way to obtain 9-HSA derivatives with the C-9 chiral carbon atom in enantiopure form, avoiding laborious synthetic methods. Thus we started the study preparing methyl (*R*)-9-hydroxystearate [**(*R*)-1**].

The first step is the extraction of triglycerides from seeds in a $CHCl_3$/MeOH mixture, followed by transmethylation with NaOMe at 0°C to give methyl esters of oil fatty acids, including methyl (*S*)-dimorphecolate (**Scheme 3**). Subsequently, the methyl-(*R*)-9-hydroxystearate **(*R*)-1** was isolated after hydrogenation over Adam's catalyst in Parr hydrogenator.

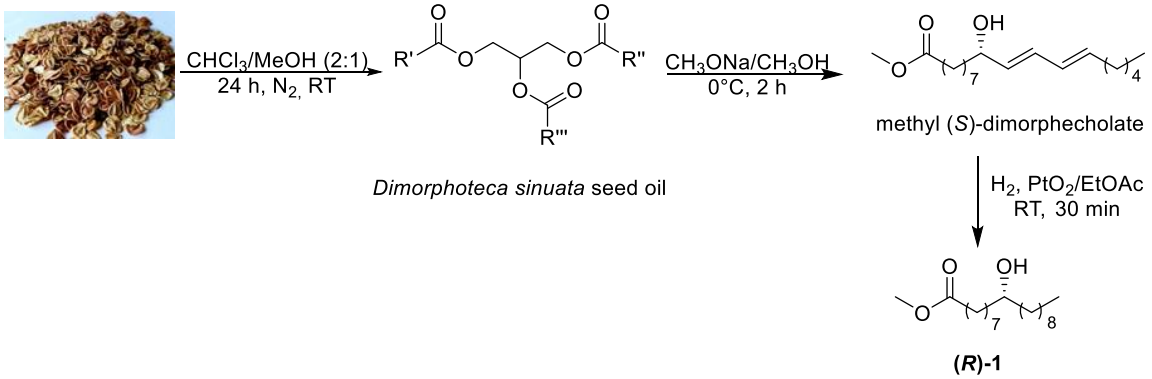

Scheme 3. Synthesis of **(*R*)-1** starting from *Dimorphoteca sinuata* seeds.

From **(*R*)-1**, it was possible to obtain 9-HSA derivatives with different substituents in C-9 position of aliphatic chain, through several synthetic routes, summarized in **Scheme 4**.

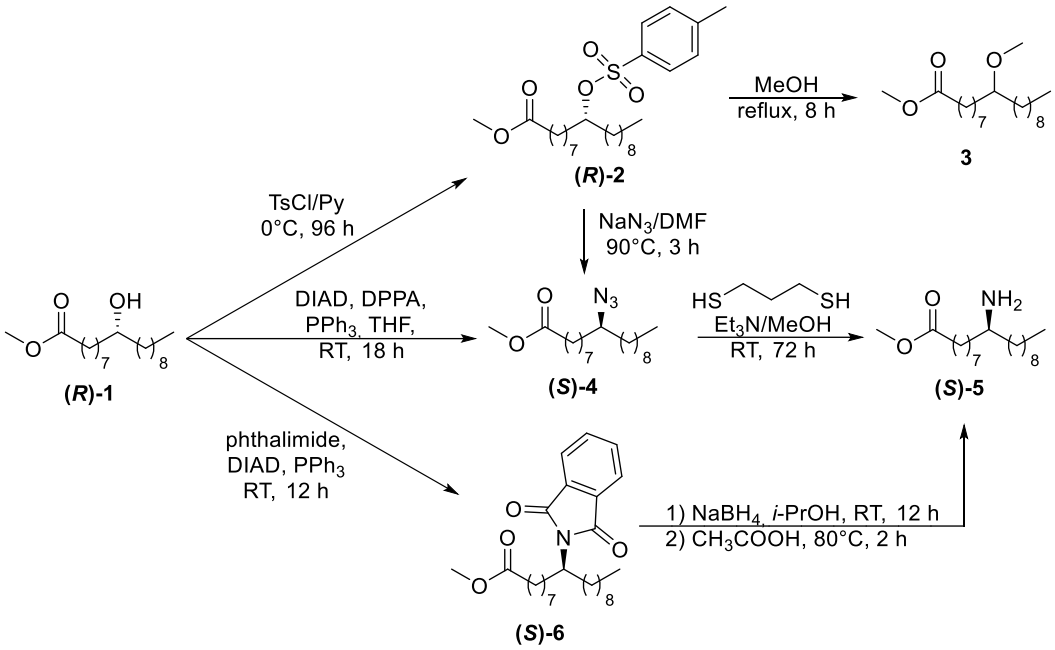

Scheme 4. Synthesis of HSA derivatives.

The tosylation of the hydroxy group of compound **(*R*)-1** leads to formation of compound **(*R*)-2**, subsequently treated with refluxing methanol to obtain the methyl ether **3**. From the tosyl derivative **(*R*)-2** the azide **(*S*)-4** was obtained through a S_N2 mechanism with NaN_3 in DMF at 90 °C. Due to diffculties of the work-up and purification steps of azidation reaction, we decided to obtain the compound **(*S*)-4** treating **(*R*)-1** with diphenylphosphoryl azide (DPPA) under Mitsunobu conditions. The last step was the reduction of azide **(*S*)-4** to aliphatic amine **(*S*)-5**. At first we tried with the Baley's method treating the azide with 1,3-propandithiol and Et_3N but this method suffered an hard work-up. After the separation of the amine from by-products through immobilization on the Dowex resin and subsequent release with triethylamine, a further treatment by liquid-liquid extraction was required and the desired amine was recovered in 13% yield. This enforced us to find an alternative synthetic route: Mitsunobu reaction between **(*R*)-1** and phthalimide followed by reduction of **(*S*)-6** with $NaBH_4$ and acetic acid giving the amine **(*S*)-5** in 36% overall yield from **(*R*)-1**.

Hence, preliminary biological tests of **(*R*)-1** and **(*S*)-5**, where they showed distinct anticancer activity, prompted us to prepare the opposite enantiomers to compare the biological activity. To prepare **(*S*)-1**, the first step was the inversion of the chiral center configuration of **(*R*)-1** through Mitsunobu

reaction, followed by the treatment with methanolic KOH and esterification with BF_3/MeOH (**Scheme 5**).

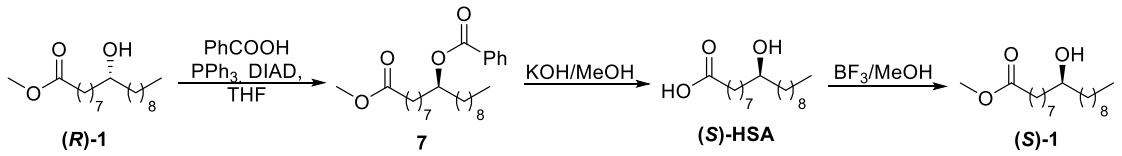

Scheme 5. Synthesis of **(*S*)-1**.

Once obtained **(*S*)-1**, the amine **(*R*)-5** was obtained through a Mitsunobu reaction with phthalimide followed by reduction (shown in **Scheme 6**).

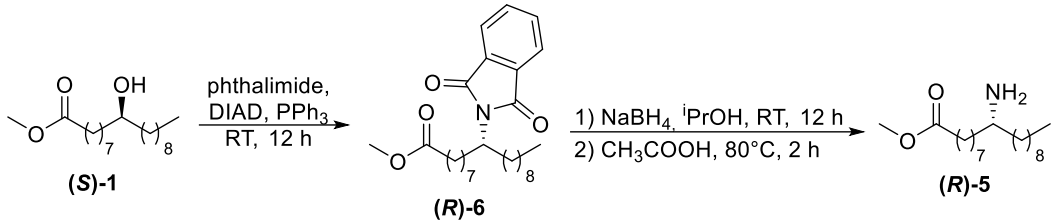

Scheme 6. Synthesis of **(*R*)-5**.

The enantiopurity degree of **(*S*)-1** was measured by reacting it with (*R*)-(–)-*O*-acetylmandelic acid: a diastereomeric ratio > 5/95 between the (*R,R*) and (*S,R*) diastereomers was calculated from the ^{1}H-NMR spectrum of the crude reaction mixture. Analogously, the **(*R*)-5** enantiopurity degree was evaluated as a 10/90 diastereomeric ratio, by analysing the ^{1}H-NMR spectrum of the crude reaction with the acyl chloride of (*S*)-*O*-acetylmandelic acid.

Biological tests

In order to gain informations on the biological effects of groups bound at the C-9 of HSA derivatives, preliminary biological tests on IC_{50} values for compounds **(*R*)-1**, **(*R*)-2**, **3**, and **(*S*)-4**, **(*S*)-5** were carried out.

From MMT test, only the methyl ester **(*R*)-1** and the amine derivative **(*S*)-5** showed biological activity. The absence of significant activity in the case of compounds functionalized on C-9 with groups not able to make hydrogen bonds might be considered as a strong indication of the importance of the presence of a group bearing hydrogen atoms bound to a heteroatom on this position. The results obtained with **(*R*)-1** and **(*S*)-5** encouraged us to also synthesize the corresponding enantiomers in order to compare their biological effects.

The IC_{50} growth inhibitory concentration *in vitro* was determined for **(*R*)-1**, **(*S*)-1**, **(*R*)-5** and **(*S*)-5**, incubating the HT29 with increasing concentrations of the compounds for 24 h.

The values obtained are 49 ± 1.3 µM for **(*R*)-1**, 51 ± 1.1 µM for **(*S*)-1**, 57 ± 2.1 µM for **(*R*)-5** and 43 ± 4.5 µM for **(*S*)-5** (**Figure 10**).

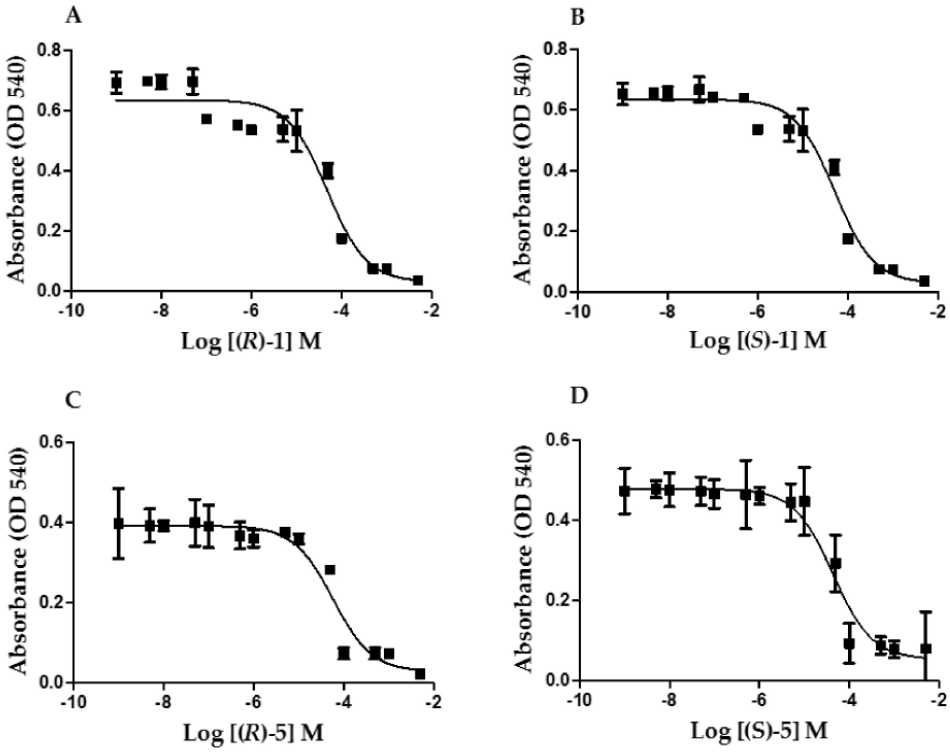

Figure 10. Dose response curves of HT29 cells viability after treatment with different concentrations of (**A**) **(*R*)-1**, of (**B**) **(*S*)-1**, of (**C**) **(*R*)-5** and (**D**) **(*S*)-5**.

The results for the **(*R*)-1** and **(*S*)-1** treatment show a significantly greater effect for the (*R*)-enantiomer (Panel A, **Figure 11**), recalling the already reported behavior of the two enantiomers of 9-hydroxystearic acid. Instead the cell proliferation for **(*R*)-5** and **(*S*)-5** is strongly reduced after 24 h, and after 48 h and 72 h of treatment, the cell numbers still diminished, indicating a continuous cytotoxic effect (Panel B, **Figure 11**).

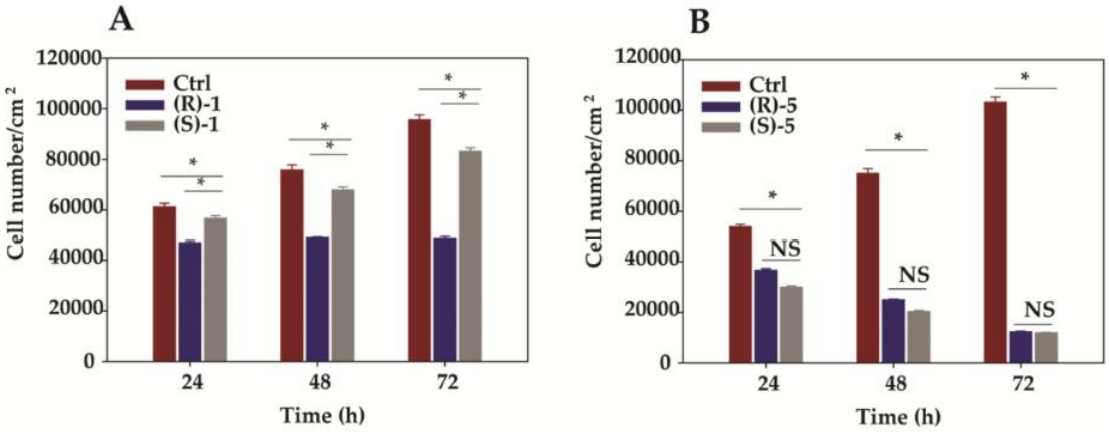

Figure 11. Cell proliferation effects. (A) Antiproliferative effect of **(*R*)-1** and **(*S*)-1** on HT29 at 24, 48, and 72 h of treatment as compared with the control. (B) Antiproliferative effect of **(*R*)-5** or **(*S*)-5** in the same experimental conditions.

Flow cytometric investigations were performed in order to associate the anticancer activity of **(*R*)-1** with the interference on the cell cycle of cultured cells. The **Figure 12** shows DNA profiles under the exposure of the compound after 48 h. Data resulted in an increase during the G0/G1 phase (80.18 ± 0.7% versus 73.91 ± 0.9%), and a decrease in the S (13.18 ± 0.5% versus 17.97 ± 0.2%) and G2/M phases (6.64 ± 0.2%versus 8.12 ± 0.1%), revealing a cell cycle arrest.

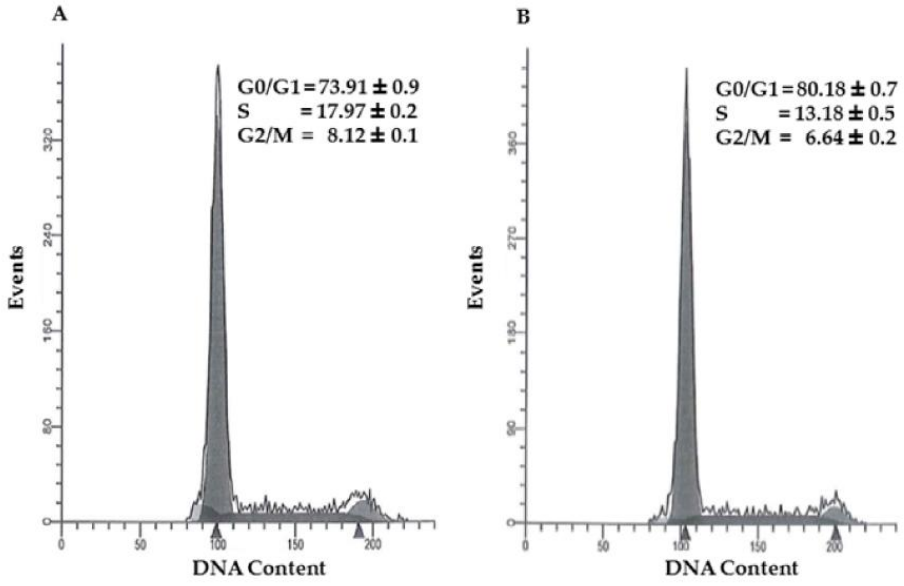

Figure 12. Effect of **(*R*)-1** on cell cycle. The cells were incubated for 48 h with the vehicle (A) or with 49 µM of **(*R*)-1** (B).

1.2.2. Conclusions

Novel 9-HSA derivatives, bearing a methyl ester group instead of the free carboxylic one and different substituents on C-9, have been synthesized to evaluate the effect of the change of substituents and also of the carboxy group on the antiproliferative activity of HT-29 human colon cancer cells.

The presence of an ester [**(*R*)-2**], an ether (***3***) or an azide [**(*S*)-4**] group on C-9 did not show a considerable anticancer activity on HT-29 cells. Instead, the presence of amino group [**(*R*)-5** or its enantiomer **(*S*)-5**] showed antiproliferative activity against colon cancer cell line, but revealed high cytotoxicity after 48 and 72 h of the treatment. The data collected showed the importance, for the biological activity, of a group bound to the C-9 able to make hydrogen bond.

Moreover, an antiproliferative effect has been observed for the methyl esters of 9-HSA, **(*R*)-1** and **(*S*)-1**. In particular, **(*R*)-1** showed to be more active than **(*S*)-1** enantiomer, revealing an accumulation of cells in the G0/G1 phase.

1.2.3. Experimental section

Dimorphotheca sinuata L. seeds were bought from Galassi Sementi Srl (Gambettola, FC, Italy). The reagents used, unless stated otherwise, were purchased from Sigma-Aldrich (Milan, Italy). For flash chromatography (FC), silica gel 0.037–0.063 mm (Merck KGaA, Darmstadt, Germany) was used as the stationary phase. Thin layer chromatography (TLC) was carried out on silica gel 60 (Fluka Analytical, Buchs, Switzerland) and the spots were revealed, depending on the compound to be analyzed, using UV light, and an aqueous solution of $(NH_4)_6MoO_{24}$ (2.5%) and $(NH_4)_4Ce(SO_4)_4$ (4%) in 10% H_2SO_4, a solution of ninhydrin 0.013 M in *n*-butanol/acetic acid, or a basic solution of potassium permanganate. Anhydrous THF was freshly distilled over sodium using benzophenone as indicator. Pyridine, trimethylamine and methanol were dried by standard methods. The hydrogenation was carried out on a Parr hydrogenator model 3911EKX at a hydrogen gas pressure of approximately 40 psi. The nuclear magnetic resonance spectra (^{1}H-NMR ^{13}C-NMR,) were recorded at 25°C on Varian spectrometers Gemini 300, Mercury 400, or Inova 600 (Varian, Palo Alto, CA, USA). The signal multiplicities were established by DEPT-135 experiments. The chemical shifts (δ) are reported in ppm relative to the solvent ($CDCl_3$, d = 7.27 and 77.0 ppm for ^{1}H and ^{13}C-NMR, respectively). Gas chromatography–mass spectrometry analysis was performed using a Hewlett-Packard HP 6890 gas chromatograph (Hewlett-Packard, Ramsey, MN, USA) directly interfaced with a mass selective detector Agilent 5973 Network (Agilent Technology, Santa Clara, CA, USA). Gas chromatograph is directly interfaced with a mass selective detector (injection temperature: 250°C; oven temperature was programmed as follows: 60°C for 2 min, increased up to 260°C at the rate of 20°/min, followed by 260°C for 20 min; the carrier gas was helium, used at a flow rate of 1 mL; the transfer line temperature was 280°C; the ionization was obtained by electron impact (EI); the acquisition range was 50–500 m/z). Mass spectra were recorded at an ionisation voltage of 70 eV in the EI mode. The ESI-MS spectra were recorded using aWaters 2Q 4000 instrument (Waters Corporation, Milford, MA, USA). The melting points were measured on a Büchi apparatus (Stone, Stas, UK) and were not corrected. The Fourier transform infrared (FT-IR) spectra of the organic compounds were recorded using a Perkin-Elmer FT-IR MOD 1600 spectrophotometer (Norwalk, CT, USA).

Synthesis of Methyl (*R*)-9-hydroxyoctadecanoate [(*R*)-1]

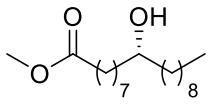

(*R*)-1

Dimorphotheca sinuata L. seeds (12.0 g) were ground and suspended in a $CHCl_3$/MeOH mixture (2:1 v/v, 200 mL) and the mixture was kept under nitrogen atmosphere, in the dark, and stirred for 24 h. After filtration and washing of the solid with $CHCl_3$ (3 x 20 mL), 20 mL of 0.1 M HCl and 0.1 M NaCl aqueous solution was added to

the green solution. After extraction with $CHCl_3$ (3 x 15 mL), the combined organic layers were dried over anhydrous $MgSO_4$. After filtration and solvent removal in vacuo at 30°C, 4.0 g of residue was recovered. The crude yellow oil was dissolved in CH_3OH (40 mL) under nitrogen atmosphere and the solution was kept at 0°C by immersion in an external water/ice bath. Then, CH_3ONa (2.16 g) was added and the mixture was magnetically stirred at 0°C for 2 h. The mixture was acidified to pH 4.0 and extracted with n-hexane (3 x 20 mL). The combined organic layers were dried over anhydrous $MgSO_4$. After filtration, the solvent was removed under reduced pressure and the residue (2.2 g) dissolved in 10 mL of ethyl acetate and transferred into the hydrogenation vessel. A catalytic amount of PtO_2 (Adam's catalyst) was added and the mixture was subjected to hydrogenation (40 psi H_2 pressure). The reaction course was monitored by ^{1}H-NMR spectroscopy. Usually, the hydrogenation is complete after approximately 40 min. The mixture was then filtered over celite and the solution concentrated under vacuum. Flash chromatography (eluent: petroleum ether/diethyl ether 7/3) of the residue gave methyl (*R*)-9-hydroxyoctadecanoate **(*R*)-1** as a white solid (0.74 g), m.p.: 50–51°C. ^{1}H-NMR (600 MHz, $CDCl_3$, 25°C): δ = 3.67 (s, 3 H, OCH_3), 3.61–3.55 (m, 1 H, CHOH), 2.30 (t, 2 H, *J* = 7.6 Hz, CH_2COO), 1.62 (quint, 2 H, *J* = 7.4 Hz, CH_2CH_2COO), 1.48–1.21 (m, 27 H, incl. OH), 0.88 (t, 3 H, *J* = 7.0 Hz, CH_3). ^{13}C-NMR (100.6 MHz, $CDCl_3$, 25°C) δ = 174.1, 71.7, 51.3, 37.4, 37.3, 33.9, 31.8, 29.6, 29.56, 29.5, 29.4, 29.2, 29.1, 28.9, 25.5, 25.4, 24.8, 22.6, 14.05. IR ($CHCl_3$): 3427, 1728 cm^{-1}. MS (EI, *m/z*) (%): 283 (M^+ -OCH_3, 2), 264 (4), 187(45), 159 (11), 158 (53), 155 (100), 129 (6), 115 (18), 109 (14), 87 (50), 74 (33), 69 (18), 55 (31).

Synthesis of Methyl (*R*)-9-(tosyloxy)octadecanoate [**(*R*)-2**]

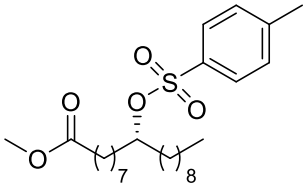

(*R*)-2

Methyl (*R*)-9-Hydroxyoctadecanoate (0.190 g, 0.60 mmol), 0.607 g (3.18 mmol) of TsCl and 10 mL of anhydrous pyridine were kept at 0°C for 1 h then at 4°C. The reaction was monitored by TLC (*n*-hexane/EtOAc 1:1, R_f = 0.54) and, when it was complete (after approximately 5 days), it was quenched with water (40 mL). The mixture was extracted with Et_2O and the combined organic layers were acidified with HCl 1 M. The organic layer was dried over anhydrous $MgSO_4$, filtered and concentrated under reduced pressure. Compound **(*R*)-2** was obtained as colorless oil in 70% yield. ^{1}H-NMR (300 MHz, $CDCl_3$, 25°C): δ = 0.87 (t, *J* = 6.9 Hz, 3 H, CH_3), 1.13–1.30 (m, 26 H, $(CH_2)_{13}$), 1.55 (m, 2 H, $CH_2CH_2COOCH_3$), 2.27 (t, *J* = 7.56 Hz, 2 H, CH_2COOCH_3), 2.42 (s, 3 H, $PhCH_3$), 3.65 (s, 3 H, $COOCH_3$), 4.52 (q, *J* = 6.1 Hz, 1 H $CHOSO_2$), 7.31(d, 2 H, *J* = 4 Hz, phenyl), 7.77 (d, *J* = 4.4 Hz, 2 H, phenyl). ^{13}C-NMR (75 MHz, $CDCl_3$, 25°C): δ = 174.3, 144.3, 134.8, 129.6, 127.7, 84.5, 51.4, 34.1 (two signals overlapped), 34.0, 31.9, 29.43,

29.38, 29.3 (two signals overlapped), 29.1, 29.0, 28.9, 24.8, 24.7, 24.6, 22.6, 21.6, 14.1. ESI-MS (*m/z*): 481 $[M + Na]^+$, 469 $[M + H]^+$.

Synthesis of Methyl 9-MethoxyOctadecanoate (**3**)

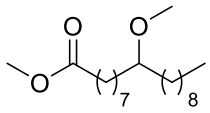

3

Compound **(*R*)-2** (0.167 g, 0.357 mmol) was dissolved in CH_3OH (5 mL) and the solution was refluxed for 7 h. After removal of the solvent under reduced pressure, brine (20 mL) was added and the mixture was extracted with Et_2O (4 x 20 mL). The combined organic layers were dried over anhydrous $MgSO_4$. After filtration and concentration, the residue was purified by FC (eluent: *n*-hexane/CH_2Cl_2 from 6:4 to 1:1 to 3:7 to 2:8 until CH_2Cl_2). Pure methyl 9-methoxyoctadecanoate **3** was obtained in 55% (0.064 g, 0.195 mmol). ^{1}H-NMR (300 MHz, $CDCl_3$, 25°C): δ = 0.86 (t, *J* = 6.9 Hz, 3 H, CH_3), 1.24–1.32 (m, 26 H, $(CH_2)_{13}$), 1.60 (m, 2 H, $CH_2CH_2COOCH_3$), 2.29 (t, *J* = 7.49 Hz, 2 H, CH_2COOCH_3), 3.10 (m, 1 H, $CHOCH_3$), 3.30 (s, 3 H, $CHOCH_3$), 3.65 (s, 3 H, $COOCH_3$). ^{13}C-NMR (150.80 MHz, $CDCl_3$, 25°C): δ = 174.3, 80.9, 56.3, 51.4, 34.1, 33.42, 33.41, 31.9, 29.9, 29.66, 29.65, 29.58, 29.3, 29.2, 29.1, 25.3, 25.26, 24.9, 22.7, 14.1. MS (EI, *m/z*) (%): 327 (M^+ -1, 0.5) 297 (3), 264 (14), 222 (6), 201 (100), 171 (50), 137 (29), 123 (8), 109 (19), 97 (43), 83 (72), 69 (57), 55 (83).

Synthesis of Methyl (*S*)-9-azidooctadecanoate [**(*S*)-4**]

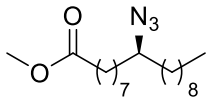

(*S*)-4

Method 1: compounds **(*R*)-2** (0.147 g, 0.314 mmol), NaN_3 (0.102 g, 1.57 mmol), and DMF (10 mL) were heated at reflux for 3 h. The mixture was treated once with brine (20 mL) then extracted with Et_2O (3 ± 15 mL), then two folds with water (30 mL and 50 mL) and each time extracted with Et_2O (3 ± 15 mL), finally with brine (20 mL) then extracted with Et_2O (3 ± 15 mL). Each time the organic layer was dried over anhydrous $MgSO_4$ and filtered. The absence of DMF was checked. The combined organic layers were concentrated and the residue chromatographed on silica gel (eluent: 7:3 *n*-hexane/EtOAc). Compound **(*S*)-4** (0.064 g, 58%) was recovered as colorless oil. ^{1}H-NMR (300 MHz, $CDCl_3$, 25°C): δ = 0.88 (t, *J* = 6.6 Hz, 3 H, CH_3), 1.24–1.33 (m, 26 H, $(CH_2)_{13}$), 1.61 (m, 2 H, $CH_2CH_2COOCH_3$), 2.30 (t, *J* = 7.9 Hz, 2 H, CH_2COOCH_3), 3.21(q, *J* = 6.1 Hz, 1 H, CHN_3), 3.65 (s, 3 H, $COOCH_3$). ^{13}C-NMR (150.80 MHz, $CDCl_3$, 25°C): δ =174.3, 63.1, 51.4, 34.4, 34.3, 34.0, 31.9, 30.3, 29.5, 29.4, 29.3, 29.2, 29.1, 29.0, 26.1, 26.0, 24.9, 22.6, 14.1; IR-Neat (cm^{-1}): 2928.0, 2856.0, 2361.2, 2098.7, 1742.6, 1465.4, 1257.5, 1171.1; ESI-MS (*m/z*): 352 $[M + Na]^+$, 340 $[M + H]^+$.

Method 2: compound **(*R*)-1** (0.230 g, 0.732 mmol) was dissolved in anhydrous THF (7.5 mL) and under nitrogen atmosphere. PPh_3 (0.398 g, 1.52 mmol) and DIAD 94% (300 µL, 1.52 mmol) were

added and the yellow mixture was stirred. After a few minutes, DPPA 97% (330 µL, 1.52 mmol) was added. The solution became cloudy and after 18 h, had come clear. The crude was subjected to FC (eluent: *n*-hexane/EtOAc 9:1) and pure **(*S*)-4** (0.190 g, 77%) was recovered.

Synthesis of Methyl (*S*)-9-aminooctadecanoate [**(*S*)-5**]

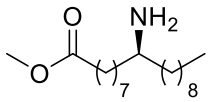

(*S*)-5

Compound **(*R*)-1** (0.222 g, 0.70 mmol) was dissolved in anhydrous THF (8.0 mL) in a flame dried apparatus immersed in an ice-bath and kept under nitrogen atmosphere. PPh_3 (0.103 g, 0.70 mmol) and phthalimide (0.103 g, 0.70 mmol) were added. Through a funnel, DIAD (0.2 mL, 0.70 mmol) in 2.0 mL of THF was added dropwise. After 12 h, the reaction appeared complete (TLC: petroleum light/diethyl ether 6:4). The reaction mixture was concentrated. FC on silica gel (light petroleum/diethyl ether: 20:1) of the residue gave 0.280 g (0.63 mmol, 90% yield) of the intermediate (9S)-9-(1,3-dioxo-1,3-dihydro-2H-isoindol-2-yl) octadecanoate [**(*S*)-6**] as a colorless oil: ^{1}H-NMR (400 MHz, $CDCl_3$, 25°C), δ = 7.83–7.79 (m, 2 H), 7.71–7.68 (m, 2 H), 4.26–4.06 (m, 1 H), 3.63 (s, 3 H, OCH_3), 2.25 (t, *J* = 7.43 Hz, 2 H), 2.11–1.97 (m, 2 H), 1.74–1.61 (m, 2 H), 1.61–1.49 (m, 2 H), 1.32–1.14 (m, 22 H), 0.84 (t, *J* = 6.97 Hz, 3 H, CH_3). ^{13}C-NMR (100 MHz, $CDCl_3$, 25°C), δ = 174.2, 168.8, 133.8, 131.8, 123.0, 52.2, 51.4, 34.0, 32.5, 32.4, 31.8, 29.45, 29.43, 29.23, 29.21, 29.04 (2 signals overlapped), 29.0, 26.6, 26.5, 24.8, 22.6, 14.1. ESI-MS (*m/z*): 444 $[M + H]^+$.

Sodium borohydride (0.06 g, 1.6 mmol) in 2-propanol (3.0 mL) was added to a solution of the compound **(*S*)-6** (0.131 g, 0.29 mmol) and the mixture was magnetically stirred at room temperature for 12 h. Glacial acetic acid (0.3 mL) was added and the mixture was heated at 80°C for 2 h. After concentration, water (5 mL), and then saturated aqueous solution of $NaHCO_3$ (5 mL) were added. After extraction with ethyl acetate (3 ± 10 mL), the combined organic layer was dried over anhydrous magnesium sulfate. After filtration and removal of the solvent under reduced pressure, the crude was subjected to FC (eluent: CH_2Cl_2/CH_3OH 10/1), the spots being evidenced with ninhydrin stain. Compound **(*S*)-5** (0.027 g, 0.09 mmol) was obtained in a 30% yield. An alternative method was as follows: Hydrazine hydrate (0.16 mL, 3.2 mmol) was added to a solution of compound **(*S*)-6** (0.280 g, 0.63 mmol) in ethanol (5 mL) and the mixture was heated and refluxed for 3 h. The formation of a white solid was observed. After cooling, 1 M HCl was added until pH = 6. Then, the solution was filtered on a Buchner funnel. The mixture was treated with saturated solution of $NaHCO_3$ until reaching pH ~ 9 and then it was extracted with CH_2Cl_2 (4 ± 10 mL) and dried over anhydrous $MgSO_4$. After filtration and removal of the solvent under reduced pressure, the light yellow oil was subjected to FC (eluent: CH_2Cl_2/CH_3OH 10/1), obtaining the product **(*S*)-5** in 28% yield: ^{1}H-NMR (400 MHz,

$CDCl_3$, 25°C): δ = 0.88 (t, *J* = 6.9 Hz, 3 H, CH_3), 1.24–1.32 (m, 26 H, $(CH_2)_{13}$), 1.58–1.65 (m, 2 H, $CH_2CH_2COOCH_3$), 2.29 (t, *J* = 7.7 Hz, 2 H, CH_2COOCH_3), 3.13 (m, 1 H, $CHNH_2$), 3.66 (s, 3 H, $COOCH_3$), 8.30 (br.s, 2 H, NH_2). ^{13}C-NMR (100 MHz $CDCl_3$, 25°C): δ = 174.2, 51.6, 51.4, 35.92, 35.86, 34.0, 31.9, 29.63, 29.55 (two signals overlapped), 29.4, 29.3, 29.12, 29.06, 25.8, 25.7, 24.9, 22.6, 14.1. MS (*m/z*): 282 (5), 267(1), 250(1), 207(3), 186(100), 156(99), 109(4), 97(2), 83(4), 70(5), 56(11). ESI-MS (*m/z*): 336 $[M + Na]^+$, 314 $[M + H]^+$; IR (cm^{-1}): 3423.5, 2950.0, 2870.0, 1710, 1635.8.

The synthesis of **(*R*)-5** was carried out with the same procedure starting from **(*S*)-1**.

Cell Culture and Treatments

The human colon cancer cell line HT29 was obtained from American Type Culture Collection (Manassas, VA, USA). The cells were cultured in RPMI 1640 medium (Labtek Eurobio, Milan, Italy), supplemented with 10% FCS (Euroclone, Milan, Italy) and 2 mM l-glutamine (Sigma-Aldrich, Milan, Italy), at 37°C and 5% CO_2 atmosphere. These conditions were used in all cell incubation steps for the experiments described below. **(*R*)-1**, **(*S*)-1**, **(*R*)-5** and **(*S*)-5** were dissolved in ethanol to obtain a 33 mM stock solution then diluted in culture medium to obtain the required concentrations. The cells were plated at a density of 1.0 x 104 cells/well in 6-well culture plates (Orange Scientific, Braine-l'Alleud, Belgium). Twenty-four hours after plating, **(*R*)-1** or **(*S*)-1** were added to a final concentration of 49 µM or 51 µM for each drug, and incubated for 24, 48, and 72 h. Moreover, HT29 cells were seeded onto 6-well plates, and after 24 h, they were treated with **(*R*)-5** at the concentration of 57 µM or with **(*S*)-5** at the concentration of 43 µM for 24, 48 and 72 h. The Trypan Blue exclusion dye method was used to determine the number of viable cells.

MTT Assay

To evaluate **(*R*)-1**, **(*S*)-1**, **(*R*)-5** and **(*S*)-5** activity, the cells were treated for 24 h without (control) or with concentrations between 1 nM–5 mM (1 nM, 5 nM, 10 nM, 50 nM, 100 nM, 500 nM, 1 µM, 5 µM, 10 µM, 50 µM, 100 µM, 500 µM, 1 mM and 5 mM) of the test samples. The culture medium was removed and the cells were further incubated for 2 h with 0.2 mg/mL MTT in PBS. After removal of the medium, the cells were lysed with 0.1 mL of iso-propanol. The absorbance of the solubilized formazan pellet at 540 nm was determined by Victor2, Multilabel plate reader (Perkin Elmer, MI, Italy). The IC_{50} was determined from three different experiments of the dose-response curve by using GraphPadPrism 5 (GraphPad Software, Inc., La Jolla, CA, USA) fitting a symmetrical sigmoidal shaped curve.

Cell Cycle Analysis by Flow Cytometry

The HT29 cells were seeded in 25 cm^2 flasks at a density of 2 x 10^4 cells/cm^2. The e ects on the cell cycle were studied 48 h after treatment with 49 µM **(*R*)-1**. To determine the cell cycle distribution at the end of incubation, HT29 cells were stained according to Busi et al.[23] Briefly, 1 x 10^6 cells were pelleted and resuspended in trisodium citrate 0.1%, RNAse 0.1 mg/L, Igepal 0.01%, Propidium Iodide (PI) 50 µg/L. After 30 min at 37°C in the dark, the cells were analyzed on a Coulter Epics Elite flow cytometer (Beckman Coulter) equipped with an argon ion laser tuned at 488 nm. PI fluorescence was collected on a linear scale at 600 nm and the DNA distribution was analyzed by the Modfit 5.0 software.

1.3. Effect of regioisomerism on the antiproliferative activity of hydroxystearic acids on a panel of human cancer cell lines[65]

1.3.1. Introduction

Hydroxy fatty acids and their derivatives are compounds of growing interest in many scientific areas. In industry they are widely used as lubricants,[65,66] surfactants,[67,68] plasticizers,[69] additives in coatings and paintings,[70,71] components of detergents, cosmetics,[72,73] flavours,[74] and foods.[75,76] In biological field, they are ubiquitous and are mainly found in triacylglycerols, membrane phospholipids, waxes, cerebrosides and other lipids.[77,78]

Among them, hydroxystearic acids (**Figure 13**) have been widely studied from long time, especially 12-hydroxystearic acid (12-HSA), also due to its easy accessibility being it produced starting from castor oil. In the past, some positional homologues of hydroxystearic acids (namely 2-HSA, 7-HSA, 8-HSA, 9-HSA, 10-HSA, and 12-HSA) have been object of our studies in material,[79,80] organic chemistry,[81,82] and mostly in biological field.[64,83,84]

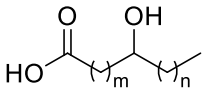

	m	n
5-HSA:	3	12
7-HSA:	5	10
8-HSA:	6	9
9-HSA:	7	8
10-HSA:	8	7
11-HSA:	9	6
12-HSA:	10	5

Figure 13. Hydroxy stearic acids considered in the present chapter.

Recently, a study on the effect of some regioisomeric hydroxystearic acids as peroxisomal proliferator-activated receptor agonists to increase the anti-ageing potential of retinoids has been published.[85] Moreover, inhibitory activities of 7-HSA and 9-HSA on A549, Caco-2, and SF268 human cancer cell lines have been reported.[86]

It has to be noticed the growing attention dedicated by scientists to fatty acyl esters of hydroxy fatty acids (FAHFA), a new class of endogenous mammalian lipids with important effects on metabolism (e.g. anti-diabetic and anti-inflammatory effects).[87,88] In these compounds, hydroxy stearic acids, mostly 5-HSA, 7-HSA, and 9-HSA, are esterified with palmitic acid (PAHSA) or other long-chain fatty acids.

Based on the above and taking into account the already known importance of both, the carboxy- and the hydroxyl- group in inducing the antiproliferative activity of 9-HSA,[64] we planned to investigate

the influence of the position of the hydroxy group along the stearic chain on the viability of a panel of cancer cell lines.

Among all positional isomers of the hydroxystearic acid (HSA), we decided to synthesize and investigate those shown in **Figure 13**, bearing the hydroxy group both on even and odd carbon atom. To the best of our knowledge, this is the first study on the anticancer activity of 5-HSA, 8-HSA and 11-HSA. In this screening study, we opted, as the synthetic method, for a simple chemical route able to afford quickly, the intended products in high amounts, starting from commercially available precursors. For the sake of comparison, the outcomes of the synthesis are racemic mixtures and due attention will be exerted when comparing the antiproliferative activity with that reported in literature, it known for the pure enantiomeric species, owing to the relevance of stereochemistry on the biological activity of hydroxyacids.[89]

1.3.2. Results and discussion

The synthesis of the homologous series of racemic 5-HSA (**12a**), 7-HSA (**12b**), 8-HSA (**12c**), 9-HSA (**12d**) and 10-HSA (**12e**) was carried out as shown in **Scheme 7**, starting from different points of the synthetic pathway depending on the commercial availability of the intermediates. Ketoderivatives **10c** and **10d**, precursors of 8-HSA and 9-HSA, respectively, have been obtained by addition at low temperature of the appropriate Grignard reagent to the acyl chloride **9c** (commercially available) and **9d**, respectively. The latter was prepared from the azelaic acid monomethyl ester **8d** and thionyl chloride. Compounds **10c** and **10d**, together with commercially available **10a**, **10b**, and **10e** were subjected to reduction of the keto group followed by hydrolysis of the esters functionality to give final compounds **12a–e**. 12-HSA (**12g**) is commercially available.

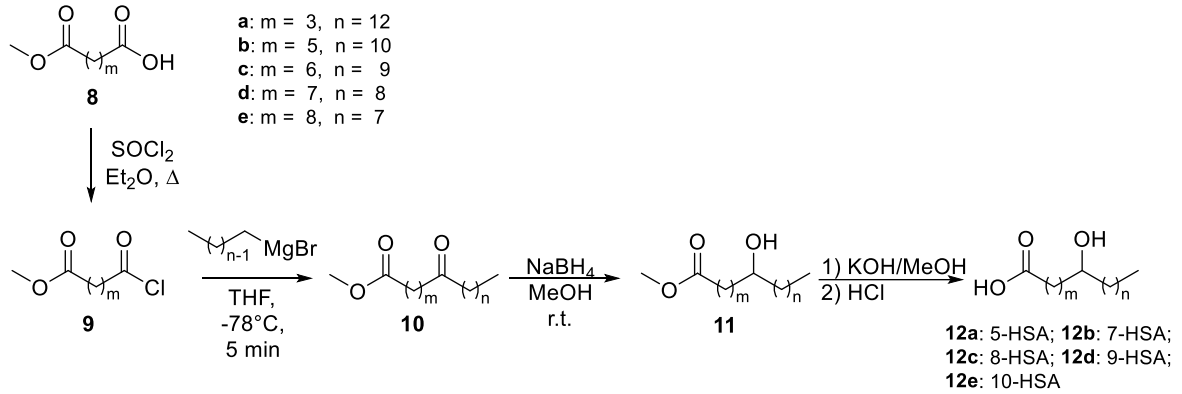

Scheme 7. Synthetic route for the synthesis of HSA derivatives **12a-e**.

A different and novel procedure was developed for the synthesis of 11-HSA (**12f**). As shown in **Scheme 8**, cross metathesis (CM) reaction[90] between 1-decen-3-ol **13**[91] and oleic acid **14** (1 : 3 respectively), carried out under microwaves irradiation at 63 °C, for 30 min, with Grubbs Catalyst® M51 afforded a complex mixture of CM products[92] from which the unsaturated hydroxyacid **15**[93] in 20% yield was isolated by flash chromatography. After hydrogenation of compound **15** by an H-Cube system (ThalesNano Inc., cartridge containing 5% Pt/C) continuously producing H_2 gas in small aliquots by electrolytic decomposition of H_2O,[94] the desired 11-HSA (**12f**) was obtained in 47% yield.

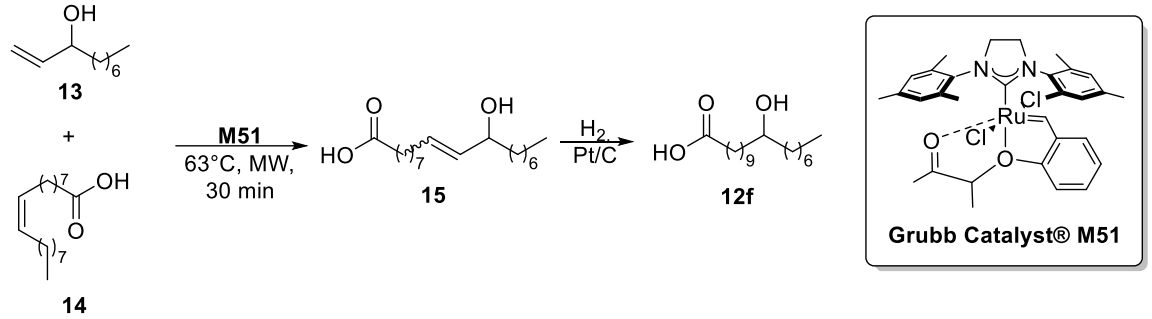

Scheme 8. Cross metathesis reaction to obtain 11-HSA.

Biological test

In order to gain informations on the biological effects of the position of the hydroxy group linked to C-5, -7, -8, -9, -10, -11 position of HSA, preliminary biological tests were carried out against a panel of human cancer cells derived from: colon (CaCo2 and HT29), intestine (I407), cervical (HeLa), breast (MCF7), prostate (PC3), and neuroblastoma cancer (NLF).

In vitro growth inhibitory concentration was determined by incubating the cells with increasing concentrations (0.01–250 μM) of the compounds for 24 h.

Dose response curves of different cancer cell viability after treatment with different concentrations of 5-,7-,8-,9-,10- and 11-HSA are reported below.

CACO 2

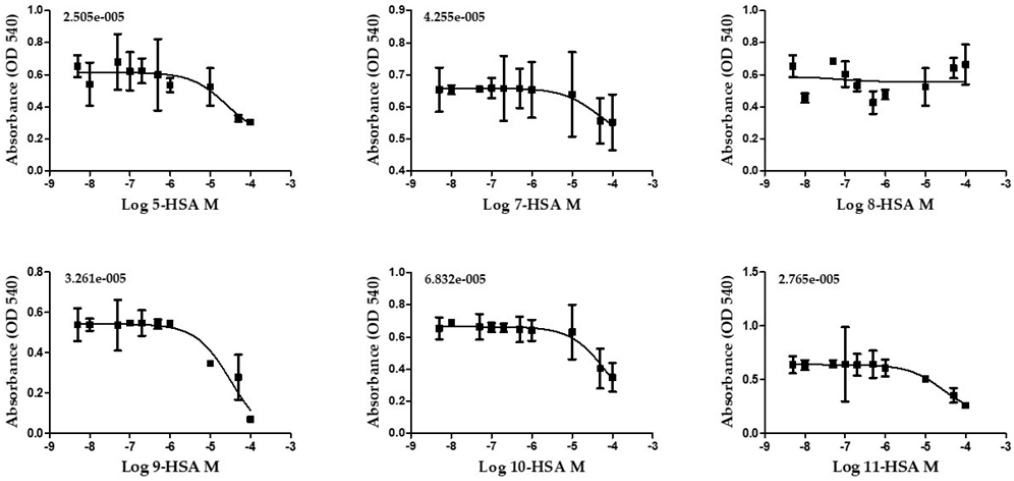

HT29

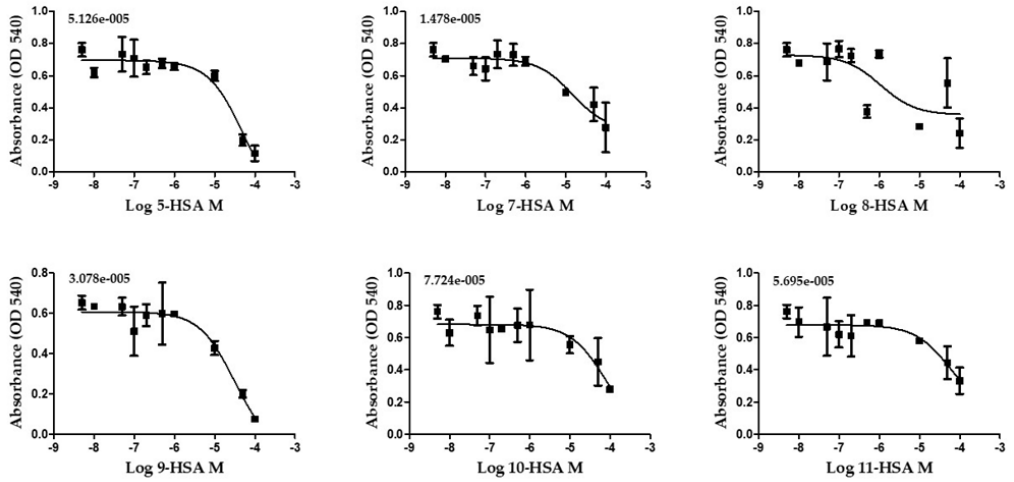

I407

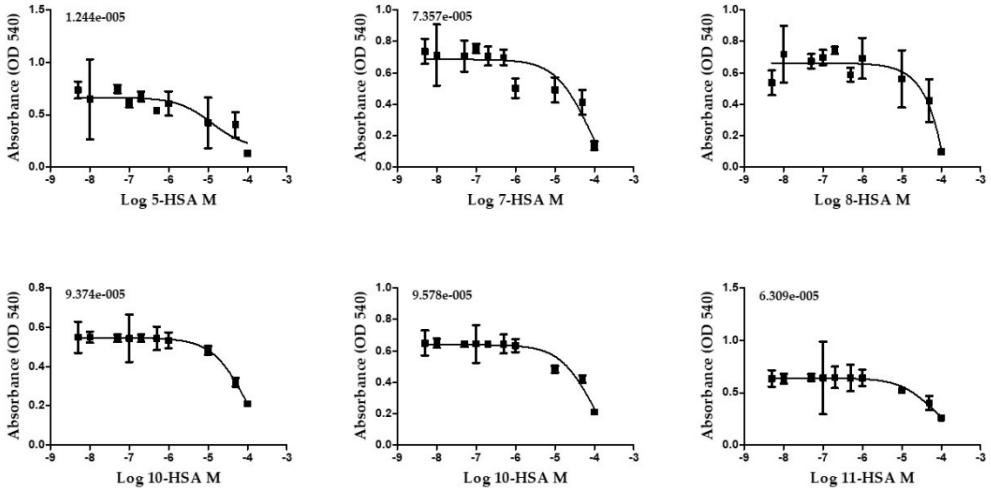

HeLa

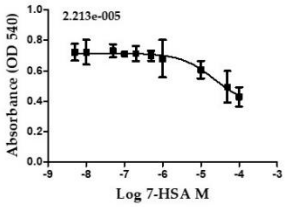

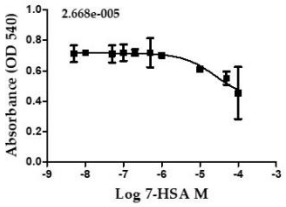

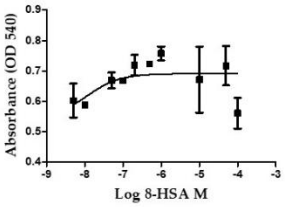

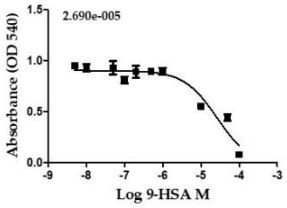

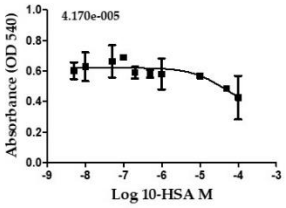

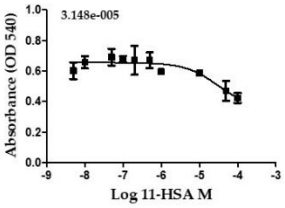

MCF7

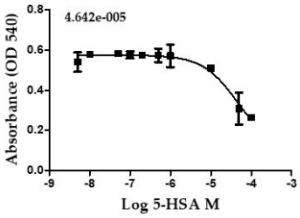

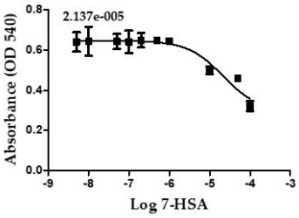

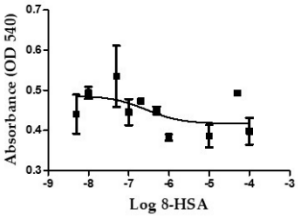

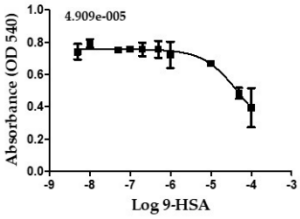

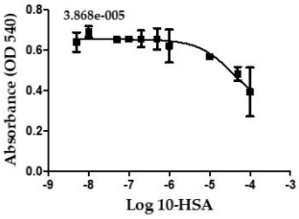

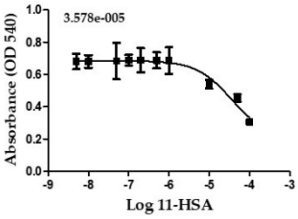

PC3

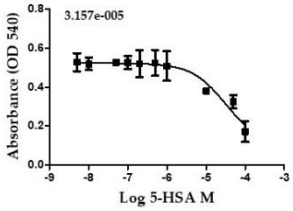

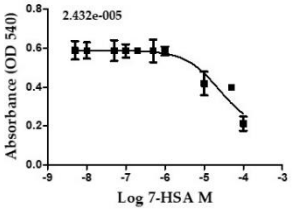

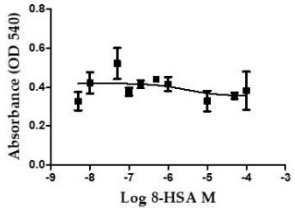

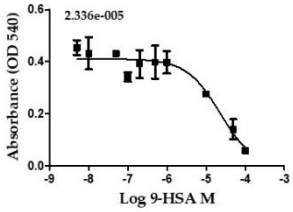

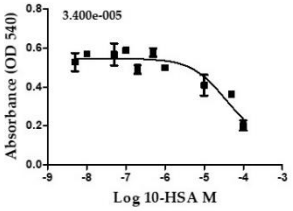

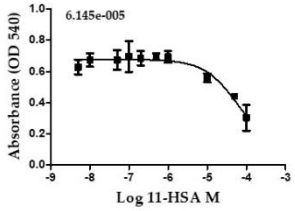

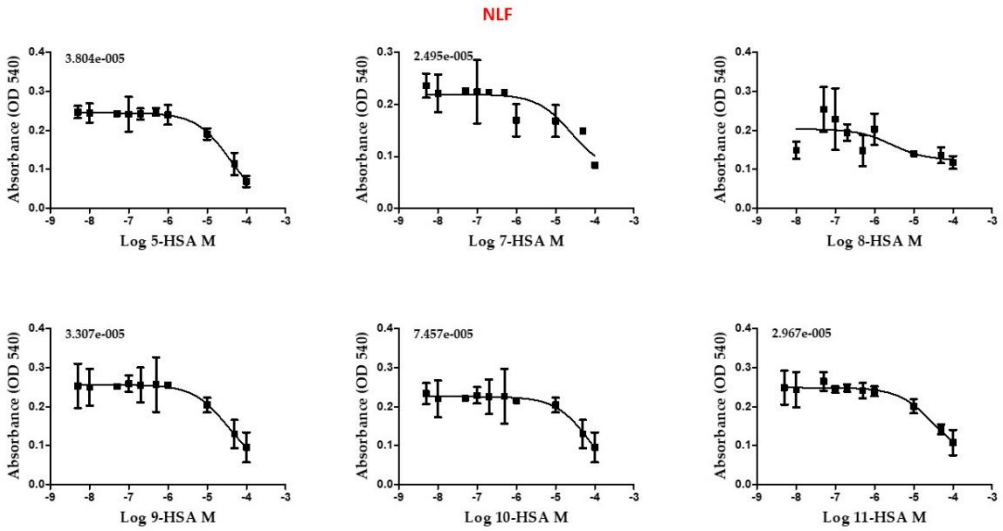

Figure 14. Dose response curves of different cancer cell viability after treatment with different concentrations of 5-,7-,8-,9-,10- and 11-HSA.

Data obtained from cell growth assays were elaborated to assess the concentration of each compound required for 50% inhibition of cell viability (IC_{50}) and the results are summarized in **Table 1**.

Table 1. IC_{50} values of HSA derivatives against different human cancer cell lines.

	CaCo2 (R square)	**HT29 (R square)**	**I407 (R square)**	**HeLa (R square)**	**MCF7 (R square)**	**PC3 (R square)**	**NLF (R square)**
5-HSA	25 µM (0.8889)	51.3 µM (0.9575)	12 µM (0.8315)	22.1 µM (0.9886)	46.4 µM (0.9820)	31.6 µM (0.9516)	38.5 µM (0.9971)
7-HSA	42 µM (0.9731)	15 µM (0.9255)	74 µM (0.8437)	27 µM (0.9703)	21.4 µM (0.9447)	24.3 µM (0.9183)	24.9 µM (0.8366)
8-HSA	> 100 µM	> 100 µM	> 100 µM	> 100 µM	> 100 µM	> 100 µM	> 100 µM
9-HSA	33 µM (0.9472)	31 µM (0.9635)	94 µM (0.9995)	27 µM (0.9321)	49 µM (0.9866)	24 µM (0.9499)	33 µM (0.9960)
10-HSA	68 µM (0.9730)	77 µM (0.9048)	96 µM (0.9470)	41 µM (0.8073)	38.7 µM (0.9599)	34 µM (0.8826)	75 µM (0.9887)
11-HSA	27.6 µM (0.9944)	56.9 µM (0.8918)	63 µM (0.9848)	31.5 µM (0.8981)	35.8 µM (0.9681)	61.4 µM (0.9610)	29.7 µM (0.9841)

The table shows as the biological activity is influenced by the position of hydroxy group on the long carbon chain in every cancer cell line tested. In particular the hydroxystearic acids characterized by the hydroxy group on odd carbons (5-, 7-, 9- and 11-HSA) are more active than the HSAs with the hydroxy group on even carbons (8- and 10-HSA). Moreover, 8-HSA resulted to be not active in every

cancer cell line tested. Based on these results, and already known inactivity of this compounds *versus* HT29 cells, tests on biological activity of 12-HSA on other considered cell lines have been postponed.

1.3.3. Conclusions

A series of regioisomers of HSA was prepared following two different synthetic routes.

Grignard addition at low temperature to the appropriate precursor bearing both acyl chloride and methyl ester functions with formation of a methyl ketostearate, reduction of the keto group to hydroxyl group and hydrolysis of the ester functionality have been the key-steps of the synthetic pathway to obtain the regioisomeric HSA derivatives **12a-e**.

Instead, a crossmetathesis reaction between the alcohol **13** and oleic acid **14**, followed by hydrogenation over Adam's catalyst, allowed to obtain 11-HSA.

The biological effect of the position of the hydroxy group along the chain of HSAs **12a-f** was investigated on a panel of human cancer cell lines. MTT test showed that the position of hydroxy group influences the biological activity. In particular, regioisomers with the hydroxy group bound to odd carbons (**12a,b,d,f**) resulted more active than those bearing the hydroxy group on even carbons (**12c,e**).

Flow cytometric investigations will be performed in order to associate the anticancer activity of different regioisomers of HSA with the interference on the cell cycle of cultured cells.

1.3.4. Experimental section

The nuclear magnetic resonance spectra (^{1}H-NMR and ^{13}C-NMR) were recorded on the Varian spectrometers Mercury 400 and 400-MR (Varian, Palo Alto, CA) both operating at 400 MHz for proton. Frequencies are reported in Hz and the chemical shifts were referenced to the solvent ($CDCl_3$, δ =7.27 and 77.0 ppm for ^{1}H and ^{13}C-NMR, respectively). Signal multiplicities were established by DEPT-135 experiments. ESI-MS spectra have been recorded using a Waters 2Q 4000 instrument (Waters Corporation, Milford, MA, USA). Melting points were measured on a Büchi apparatus (Stone, Staffs, UK) and are not corrected. For flash chromatography (FC) silica gel 0.037-0.063 mm (Merck KGaA, Darmstadt, Germany) was used as stationary phase. Thin layer chromatography (TLC) was carried out on silica gel 60 (Fluka Analytical, Buchs, Switzerland) and the spots were revealed using an aqueous solution of $(NH_4)_6MoO_{24}$ (2.5%) and $(NH_4)_4Ce(SO_4)_4$ (4%) in 10% H_2SO_4. Microwave irradiations were performed by an Anton Paar Monowave 400 (Anton Paar GmbH Graz, Austria) instrument. Continuous hydrogenation was performed with an H-cube Mini-Plus Thales-Nano system (Thalesnano Inc. Budapest, H) using a cartridge containing 5% Pt/C, 15 bar inlet pressure, 1 mL/min flow rate, 25°C temperature, 30 bar H_2 pressure, 2 runs of a 0.01 M solution of compound **15** in ethanol. Nonanedioic acid 1-methyl ester (**8d**), methyl 8-chloro-8-oxooctanoate (**9c**), methyl 5-oxooctadecanoate (**10a**), methyl 7-oxooctadecanoate (**10b**), methyl 10-oxooctadecanoate (**10e**), *n*-decylmagnesium bromide (1.0 M in diethyl ether), thionyl chloride, Grubbs Catalyst® M51, and 12-HSA (12g) were purchased from Sigma-Aldrich (Milan, Italy). 1-Decen-3-ol **13** was obtained by vinylation of *n*-octanal with vinyl magnesium bromide according to the literature.[91]

7-Hydroxyoctadecanoic acid (**12b**), 8-hydroxyoctadecanoic acid (**12c**), 9-hydroxyoctadecanoic acid (**12d**) and 10-hydroxyoctadecanoic acid (**12e**) were prepared according to the procedure[81,84] shown in **Scheme 7** and their chemico-physical data agree with those reported there.

Synthesis of methyl 5-hydroxyoctadecanoate (**11a**).

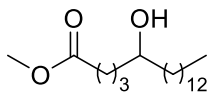

11a

Sodium borohydride (0.152 g, 4.0 mmol) was added portion-wise to a solution of methyl 5-oxooctadecanoate **10a** (0.625 g, 2.0 mmol)) in methanol (20 mL) and the mixture was stirred at room temperature. The reaction progress was monitored by TLC (light petroleum/diethyl ether: 7/3). Once verified the absence of the starting keto derivative, the reaction mixture was treated with water (5 mL) and extracted with ethyl acetate (3 x 10 mL). After extraction with brine, the collected organic layers were dried over anhydrous $MgSO_4$ and filtered. The solvent was removed 'in vacuo' and after purification by flash chromatography of the residue,

pure **11a** (0.520 g, 1.66 mmol, 83%) was obtained. Characterization data of compound **11a** agree with those reported in the literature.[95]

Synthesis of 5-hydroxyoctadecanoic acid (5-HSA, **12a**).

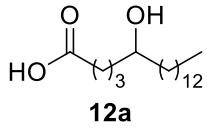

12a

Methyl 5-hydroxyoctadecanoate **11a** (0.450 g, 1.43 mmol) was dissolved (with a slight warming in 25 mL of a solution of KOH in methanol (10% w/v) and stirred for 2h at room temperature. The reaction was monitored by TLC (eluent: petroleum ether/diethyl ether 7/3). The solvent was completely removed under vacuum and the light yellow solid was dissolved in water and acidified with HCl 6 M until precipitation of the acid as a white solid. This mixture was extracted with ethyl acetate (3 x 20 mL) and the organic layers were dried over anhydrous $MgSO_4$. After filtration, the solvent was removed under vacuum. The white residue was recrystallized from methanol to give pure **12a** (0.300 g, 1 mmol, 70% yield). White solid, m.p.: 80.6-81.8 °C, ^{1}H-NMR (400 MHz, $CDCl_3$, 25 °C) δ (ppm): 3.65-3.57 (m, 1H), 2.40 (t, *J*=7.4 Hz, 2H), 1.88-1.76 (m, 1H), 1.76-1.64 (m, 1H), 1.59-1.36 (m, 4H), 1.36-1.20 (m, 24H), 0.88 (t, *J*=6.9 Hz, 3H); ^{13}C-NMR (100 MHz, $CDCl_3$, 25 °C) δ (ppm): 178.0, 71.6, 37.5, 36.5, 33.6, 31.9, 29.68, 29.66, 29.65, 29.64 (2 signals overlapped), 29.60, 29.59, 29.3, 25.6, 22.7, 20.8, 14.1; ESI-MS (m/z): 301 $[M+H]^+$, 323 $[M+Na]^+$, 339 $[M+K]^+$.

Synthesis of 11-hydroxy-9-octadecenoic acid (**15**)

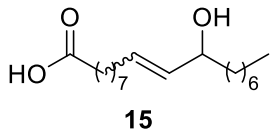

15

In a G10 vial for Anton Paar Monowave 400 instrument, 1-decen-3-ol **14** (0.165 g, 1.06 mmol), oleic acid **15** (0.895 g, 3.17 mmol) and Grubbs Catalyst® M51 (6.93 mg, 0.01 mmol) dissolved in 1 mL of DCM were added. The temperature was set to 63°C, and the mixture was irradiated for 30 min under stirring. The brown crude reaction mixture was immediately purified by flash chromatography (ethyl acetate/light petroleum, gradient from 5% up to 14% and adding 0.5 ml of glacial acetic acid every 100 mL of eluent), compound **15** (0.063 g, 0.21 mmol) was isolated in 20% yield. R_f = 0.42 light petroleum/ethyl acetate 80:20 + 1 mL of glacial acetic acid every 100 mL. Characterization data of compound **15** agree with those reported in the literature.[93]

Synthesis of 11-hydroxyoctadecanoic acid (11-HSA, **12f**).

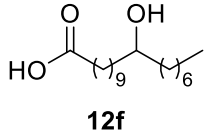

12f

Compound **15** (0.045 g, 0.15 mmol) was dissolved in 15 mL of ethanol and the solution was hydrogenated with an H-cube Mini-Plus Thales-Nano system using a cartridge containing 5% Pt/C, 15 bar inlet pressure, 1 mL/min flow rate, 25°C

temperature, 30 bar H_2 pressure, 2 runs. After evaporation of the solvent, the crude reaction mixture was dissolved in ethyl acetate and extracted with a phosphate buffer solution at pH = 7.4 in order to remove octadecanedioic acid. The organic phase was dried on anhydrous Na_2SO_4 and evaporated to afford **12f** (0.020 g, 0.07 mmol, 47% yield). m.p.: 68.3-68.6 °C; ^{1}H-NMR (400 MHz, $CDCl_3$, 25°C) δ (ppm): 3.59 (bs, 1H, H-11), 2.7-2.2 (bs, 2H, OH), 2.35 (t, *J* = 7.5 Hz, 2H), 1.69 – 1.57 (m, 2H), 1.36 (m, 26H), 0.88 (t, *J* = 6.9 Hz, 3H); ^{13}C-NMR (100 MHz, $CDCl_3$, 25°C) δ (ppm): 179.32, 72.10, 37.42, 37.38, 33.94, 31.82, 29.65, 29.59, 29.46, 29.28 (2 signals overlapped), 29.14, 28.99, 25.63, 25.57, 24.64, 22.64, 14.08. ESI-MS (m/e): 301 $[M + H]^+$, 323 $[M + Na]^+$, 339 $[M + K]^+$.

Cell culture and treatments

The human colorectal adenocarcinoma (CaCo2), human colorectal adenocarcinoma (HT29), normal human intestinal (I407), human cervical cancer (HeLa), human breast cancer (MCF7), human Caucasian prostate adenocarcinoma (PC3) and human neuroblastoma (NLF) cell lines were purchased from American Type Culture Collection (ATCC, Manassas, VA). Cells were cultured in RPMI 1640 medium (Labtek Eurobio, Milan, Italy), supplemented with 10% FCS (Euroclone, Milano, Italy) and 2mM L-glutamine (Sigma-Aldrich, Milano, Italy), at 37 °C, and a 5% CO_2 atmosphere. The compounds were dissolved in ethanol in a 30-40 Mm stock solution. In cell treatments, the final ethanol concentration never exceeded 0.2%.

MTT assay

Cells were seeded at 1.5×10^4 cells/well in a 96-well culture plastic plate (Sarsted, Milan, Italy), and after 24 h of growth were exposed to increasing concentrations of **5-HSA, or 7-HSA, or 8-HSA, or 10-HSA, or 11-HSA** (from 0.010 μM to 500 μM) solubilized in RPMI 1640 medium. MTT assay was performed as follows: after 24 h of treatment, the culture medium was replaced with 0.1 mL of 3-(4,5-dimethylthiazolyl-2)-2,5-diphenyltetrazolium bromide (MTT, Sigma-Aldrich) dissolved in PBS at the concentration of 0.2 mg/mL, and samples were incubated for 2 h at 37°C. The absorbance at 570 nm was measured using a multiwell plate reader (Tecan, Männedorf, CH), and data were analyzed by Prism GraphPad software, and expressed as IC50 μM.

Quantitative phase image (QPI) microscopy

In brief, the CaCo2, HT29, I407, HeLa, MCF7, PC3 and NLF were seeded in a 96-well plate (Corning) at 4 x 10^3 per well. After 24 hours cells were treated with **5-HSA, or 7-HSA, or 8-HSA, or 10-HSA, or 11-HSA** at 50 μM in six replicates and then QPI imaging was performed using the

Livecyte microscope (Phase Focus). The images were acquired every 60 mins for 3 days using a 10x objective (0.25 NA), at 37°C and 5% CO_2. Data were analyzed using the Cell Analysis Toolbox software (Phase Focus) to evaluate confluence and doubling times.

1.4. Magnetic nanoparticles coated with a (*R*)-9-HSA derivative: synthesis and characterization of a novel material suitable for biomedical applications[96]

1.4.1. Introduction

Magnetic nanoparticles (MNPs) have attracted increasing interest due to their versatility in a wide number of applicative fields, such as removal of toxic elements from industrial wastes,[97,98] magnetic resonance imaging (MRI) techniques for cancer diagnosis, and cancer therapy.[99,100] Imaging-diagnostic systems based on Positron Emission Tomography (PET) and MRI in a single diagnostic device PET/MRI requires a continuous effort on advanced materials, instrumentation studies and quality control.[101,102] The main advantage of using MNPs in biomedical field lies in the possibility to drive the drug to the target by an external magnetic field. Nanometer-sized particles of iron oxide allow to combine cancer therapy with their in vivo degradation into non-toxic iron ions.[98] Actually MNPs with superparamagnetic (SPM) behavior have demonstrated to be suitable in anticancer drug delivery field.[103,104]

In this context magnetite is a promising candidate as drug delivery medium. The preparation of magnetite suitable for drug release purposes, must take into account different parameters, including the size optimization and surface properties. Indeed particles with diameter lower than 10 nm are, most of the time, rapidly removed from the body while particles larger than 200 nm are retained by the spleen. Thus, the optimal dimension to fulfill the therapy requirements ranges between 10 to 100 nm.[105,106]

The need to control by magnetic fields the MNPs, requires that they are in a SPM state and the range 10-100 nm of the magnetite is often monodomain,[107] so it behaves as a superparamagnetic material as a function of temperature, size and magnetic interactions. MNPs can be derivatized by coating the iron oxide core surface with organic or inorganic molecules through a chemical bond thus obtaining magnetically controlled drug carrier for locoregional cancer treatment.

Despite the biological effect of 9-hydroxystearic acid (9-HSA), already discussed in the previous chapters, its use shows some limitations, due to the extremely poor water solubility and the need to administer relatively high doses in order to have a pharmacological effect. Recently we focused our efforts on the development of efficient delivering modes of (*R*)-9-HSA, and we were able to load it in biocompatible keratin nanoparticles[108] and to insert it in hydroxyapatite nanocrystals[109] for possible applications in bone cancer.

Now, in order to find a versatile method to target the action of (*R*)-9-HSA towards local treatment sites, and considering that the anchoring amido group, as well as the ester group, may be '*in situ*'

hydrolyzed by endogenous cellular lipases and amidases permitting the release of the organic molecule, we planned to coat (*R*)-9-HSA to MNPs through (3-aminopropyl)triethoxysilane ($NH_2(CH_2)_3Si(OC_2H_5)_3$ (APTES), owing to its ability to combine with biomolecules, drugs and metals.[110] Herein is reported the synthesis and the structural and magnetic characterization of the obtained material.

1.4.2. Results and discussion

To functionalize magnetite nanoparticles with (*R*)-9-HSA through the (3-aminopropyl) triethoxysilane (APTES) linker, we followed the procedure shown in **Scheme 9**. First, we planned to prepare amide derivative between APTES and (*R*)-9-HSA, then to anchor the amide to magnetite exploiting the reaction between the silyl group and the magnetite hydroxy groups (**Scheme 9**). The formation of an amide may be easily obtained by reaction between an amine and an acyl chloride; but in current case, the presence on (*R*)-9-HSA of the hydroxy group in C-9 might make difficult the step of preparation of the acyl chloride of (*R*)-9-HSA. Thus, to avoid undesired side reactions, the hydroxy group was protected as acetate prior the formation of the acyl chloride.

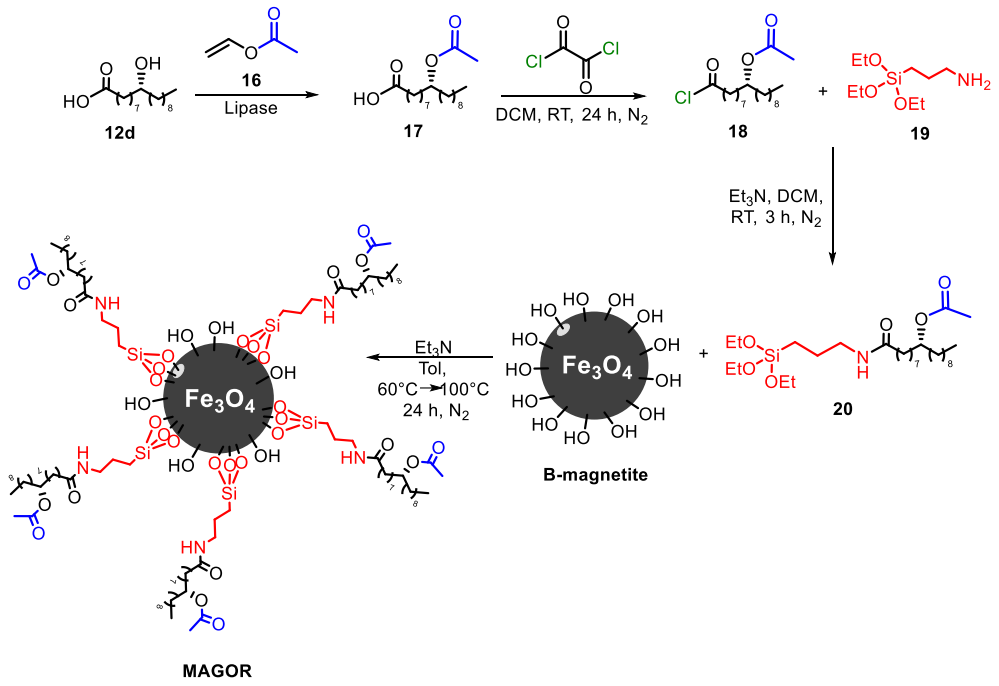

Scheme 9. Synthesis of MNPs (MAGOR) coated with a (*R*)-9-acetoxy-hydroxystearic acid.

As shown in **Scheme 9**, (*R*)-9-HSA **16** was enzymatically transformed into (*R*)-9-acetoxy-HSA **17** by a lipase, then treated with oxalyl chloride affording the corresponding acyl chloride **18**. The latter was reacted with APTES **19** under Schotten-Baumann type conditions to give the amide **20**.

The reaction course was monitored through ^{1}H-NMR spectroscopy; once the reaction resulted to be complete, the crude **20** was reacted with magnetite nanoparticles (**B-magnetite**), in turn prepared via co-precipitation of iron sulphate salts in basic media. The IR spectrum of the novel final material (**MAGOR**) was compared with that of B-magnetite and showed bands at 2927.7 cm^{-1}, due to aliphatic CH bonds, 1735.2 and 1031.7 cm^{-1} belonging to the ester group, and 1659.8 cm^{-1}, typical of the amide group, thus confirming the successful derivatization with the organic compound **20**.

The XRD patterns of **B-magnetite** and **MAGOR** showed that **MAGOR** is composed of magnetite as unique crystalline phase and that the crystallinity of starting magnetite is maintained after the functionalization with the organic moiety.

For quantification of the organic material associated to inorganic magnetite in **MAGOR**, TGA analyses were performed both on **B-magnetite** (**Figure 17a**) and on **MAGOR** (**Figure 17b**). The two thermogravimetric profiles differ because of complete decomposition of the organic moiety between 150 and 600 °C (**Figure 17**). Evaluation of the difference between the total weight loss of **MAGOR** and that of **B-magnetite** allowed us to determine organic moiety content, which amounts to ~ 9 wt%.

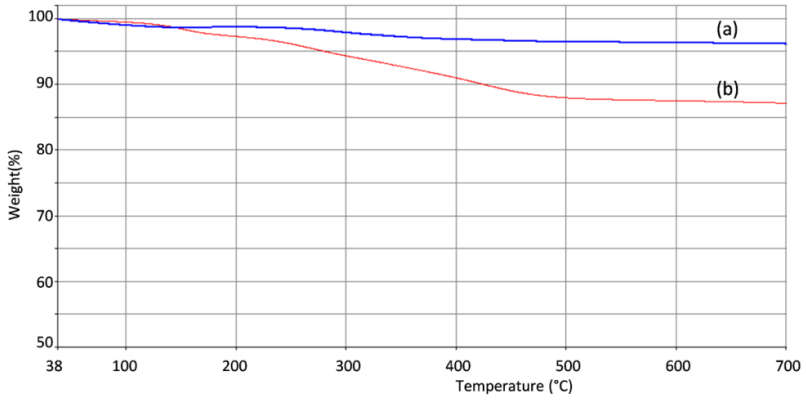

Figure 17. TGA plots of (a) B-magnetite nanoparticles used as starting supporting material and (b) MAGOR nanoparticles.

TEM observations

Transmission electron microscopy (TEM) observations were performed to further investigate the MNPs structure. Both **B-magnetite** and functionalized **MAGOR** were investigated. In particular, **Figure 18a** shows a general view of **B-magnetite**. The MNPs appear widely size-distributed and disorderly arranged on the carbon film of the TEM grid. The shape of the particles is approximately spherical with diameter ranging from 10 to 40 nm. It must be stressed that although the particle size is inhomogeneous, their diameters are fully comprised inside the interval recommended for drug delivery particles (between 10 to 100 nm). Selected area electron diffraction (SAED) measurements

were performed to investigate the crystallinity and composition of the MNPs. **Figure 18b** is the SAED pattern of the particles visible in **Figure 18a**. It is composed of well-defined diffraction rings, which indicate the random orientation of the particles and their good crystallinity degree. The diffraction rings in the SAED pattern correspond to the following interplanar distances: d1=(0.483 ± 0.003) nm, d2=(0.296 ± 0.003) nm, d3=(0.253 ± 0.002) nm, d4=(0.210 ± 0.002) nm, d5=(0.171 ± 0.002) nm, d6=(0.161 ± 0.001) nm and d7= (0.149 ± 0.001) nm. These values are in good agreement with diffraction data reported for magnetite (ICDD card n. 19-0629: d1(111); d2(220); d3(311); d4(400); d5(422); d6(511) and d7(440)). It is important to note that the upload of the organic material does not influence size, composition and crystallinity of the magnetic nanoparticles.

High-resolution transmission electron microscopy (HRTEM) observations reveal that the MNPs are single crystals and so the mean dimension of crystalline domains obtained by XRD (~17 nm), coincides with the average size of the MNPs. In particular, **Figures 18c** and **18d** show the inner structure of two typical nanoparticles. The atomic plans are clearly visible and extend with continuity from one side to the other of the particles. In more detail, **Figure 18c** shows an as-build MNP while **Figure 18d** shows a MNP covered with the organic moiety (MAGOR). Actually, looking at the exterior of this last nanoparticle, it is possible to observe an amorphous layer (red lines) that can be associated to the organic coating of the particle surface. The same layer is not revealed on the as-build MNPs surface and the visible "orange peel" contrast at the exterior of the particle of Figure 3c is due to the amorphous carbon film over the TEM grid.

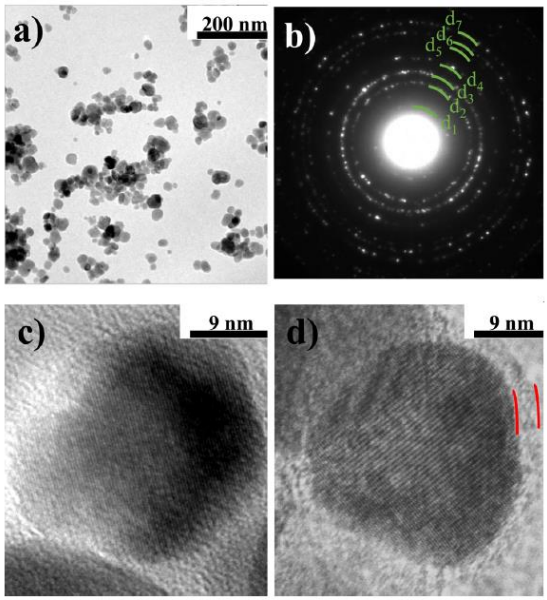

Figure 18. TEM observations. a): general view of the B-magnetite nanoparticles; b): SAED pattern of the particles visible in **Figure 18a**; c): inner structure of a B-magnetite nanoparticle; d): inner structure of a MAGOR nanoparticles.

1.4.3. Conclusions

A novel nanomaterial bearing a 9-hydroxystearic acid derivative bound for the first time to magnetite nanoparticles was synthesized. The organic coating was made through a synthetic route in which APTES played a key role as bidentate linker between (*R*)-9-acetoxystearic acid and nanomagnetite. (*R*)-9-HSA was bound to APTES via Schotten-Baumann type reaction after protection as 9-acetoxy derivative. MNPs prior (**B-magnetite**) and after the coating (**MAGOR**) were characterized by suitable and complementary techniques. XRD, TGA, TEM and HRTEM on **B-magnetite** and **MAGOR** indicated that the upload of the organic material does not influence size, composition and crystallinity of the magnetic NPs. The magnetic characterization remarks the suitability of the **MAGOR** nanoparticles for drug delivery because of the dimension inside the range 10 nm < d < 100 nm.

Thus the novel material possesses properties suitable for future biological studies on the magnetically-guided delivery of (*R*)-9-HSA.

1.4.4. Experimental section

Iron(III) pentahydrate sulphate ($Fe_2(SO_4)_3 \cdot 5H_2O$, 97%), ammonia (NH_3, 28−30 wt %, d = 0.9 g/cm3), diethyl ether, ethyl acetate, dichloromethane, toluene, ethanol (95%), vinyl acetate, and lipase acrylic resin from Candida antarctica 10,000 U/g (Novozyme 435) were purchased from Sigma-Aldrich. $CDCl_3$ was from Euriso-top (Saint-Aubin, France), iron(II) heptahydrate sulphate ($Fe_2SO_4 \cdot 7H_2O$, 95%) and triethylamine (TEA, 99%) were from Carlo Erba (Italy), and oxalyl chloride was from Alfa Aesar, Thermo Fisher Scientific (Karlsruhe, Germany). Ultrapure UPP water used for magnetite synthesis was obtained with a Milli-Q plus system (Millipore Co., resistivity 18MΩcm). (*R*)-9-Hydroxystearic acid was synthesized from *Dimorphotheca sinuata L.* seeds. CH_2Cl_2 was dried by distillation over P_4O_{10} and stored under an argon atmosphere. Toluene was dehydrated by distillation under nitrogen on Na/K amalgam and stored under nitrogen on 4 Å molecular sieves. The NMR spectra (^1H, ^{13}C, DEPT) were recorded on Varian spectrometers Gemini 300, Mercury 400 and Inova 600 (Varian, Palo Alto, USA). The frequencies are given in Hz, and the chemical shift is given in ppm using the chemical shift of the solvent $CDCl_3$ as the reference (7.26 and 77.0 ppm for ^1H and ^{13}C NMR, respectively). IR spectra were recorded using a Fourier transform spectrophotometer PerkinElmer FT-IR spectrometer Spectrum Two in the 4000−500 cm^{-1} wavelength range, using a NaCl cell for liquid samples, whereas the spectra of solid samples were recorded using an Universal ATR accessory. ESI-MS spectra were recorded on a mass spectrometry WATERS 2Q 4000. The pH-measures were carried out on a AMEL334-B, calibrated with standard solutions at pH = 7 and pH = 9. They were performed using a PerkinElmer TGA-7 with a heating ramp from 37 to 700 °C at a rate of 10 °C/min, under air flux. Powder X-ray diffractometry was carried out using a Panalytical X'Pert Pro (Cu Kα radiation, λ = 0.154 nm, 40 mA, 40 kV). The peak broadening was used to evaluate the crystal size (τ_{hkl}), which was calculated from the width at half maximum intensity ($\beta_{1/2}$) using the Scherrer equation. For crystal size calculation, the most intense reflection for magnetite was taken into consideration, that is, peak (311). Magnetic and TEM measurements were performed by the research group of Prof. Daniele Rinaldi of the Department of Materials, Environmental Sciences and Urban Planning, Università Politecnica delle Marche, 60131 Ancona, Italy.

Transmission Electron Microscopy

The size and inner structure of the NPs were investigated by TEM techniques using a Philips CM200 microscope operating at 200 kV and equipped with a LaB6 filament. For TEM observations, a small quantity of NPs was dispersed in ethanol and subjected to ultrasonic agitation for approximately one

min. A drop of the suspension was deposited on a commercial TEM grid covered with a thin carbon film; finally, the grid is kept in air until complete evaporation of the ethanol.

Synthesis of the Organic Coating

Synthesis of (*R*)-9-Acetoxyoctadecanoic Acid (17).

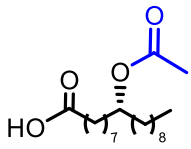

17

To a mixture of (*R*)-9-hydroxystearic acid (0.60 g, 2.0 mmol) and vinyl acetate (10 mL), diethyl ether was added until dissolution of the solid (about 20 mL). Novozyme 435 (0.630 g) was added, and the mixture was stirred at 30 °C for 5 days. The suspension was filtered through a Gooch funnel, and the enzyme was washed with diethyl ether and ethyl acetate. Evaporation of the combined organic phases afforded acetylated product **17** (0.66 g, 1.9 mmol, 97% yield). ^{1}H-NMR (600 MHz, $CDCl_3$, 25°C): δ, ppm: 4.85 (qt, *J* = 5.8 Hz, 1H, CHO), 4.51-2.45 (br.s., 1H, COOH), 2.34 (t, *J* = 7.4 Hz, 2H, CH_2COOH), 2.04 (s, 3H, CH_3CO), 1.63 (qt, *J* = 7.3 Hz, 2H, CH_2CH_2COOH), 1.55−1.45 (m, 4H), 1.37−1.20 (m, 22H, remaining CH_2 chain), 0.88 (t, *J* = 6.9 Hz, 3H, CH_3); ^{13}C-NMR (150 MHz, $CDCl_3$, 25°C): δ, ppm: 179.6, 171.0, 74.4, 34.1, 34.03, 33.9, 31.8, 29.5 (2 signals overlapped), 29.26 (2 signals overlapped), 29.1, 28.9, 25.20, 25.19, 24.6, 22.7, 21.3, 14.1; ESI-MS^{+} (*m/z*): 365 $[M + Na]^{+}$, 381 $[M + K]^{+}$; ESIMS^{-}(*m/z*): 341 $[M-H]^{-}$; IR (ν, cm^{-1}): 3428, 2958, 2925, 2856, 1735, 1705, 1646, 1462, 1373, 1242, 1027.

Synthesis of (*R*)-1-Chloro-1-oxooctadecan-9-yl Acetate (18)

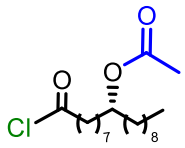

18

Into a three-necked round-bottom flask and under an argon atmosphere, (*R*)-9-acetoxyoctadecanoic acid **17** (300 mg, 0.88 mmol) was dissolved in anhydrous CH_2Cl_2 (10 mL). Oxalyl chloride (0.077 mL, 0.88 mmol) was added to the solution, and the mixture was stirred for 24 h at room temperature. The reaction course was monitored by ^{1}H-NMR spectroscopy. When it resulted complete, the solvent was removed and the oil obtained was used without purification. ^{1}H-NMR (400 MHz, $CDCl_3$, 25°C): δ, ppm: 4.85 (qt, *J* = 5.9 Hz, 1H, CHO), 2.88 (t, *J* = 7.3 Hz, 2H, CH_2COOH), 2.04 (s, 3H, CH_3CO), 1.70 (qt, *J* = 7.4 Hz, 2H, CH_2CH_2COOH), 1.55−1.45 (m, 4 H), 1.39−1.19 (m, 22 H), 0.88 (t, *J* = 7.0 Hz, 3H, CH_3); ^{13}C NMR (100 MHz, $CDCl_3$, 25°C): δ, ppm: 173.8, 171.0, 74.3, 53.4, 47.1, 34.1, 34.0, 31.9, 29.5 (2 signals overlapped), 29.3, 29.2, 28.9, 28.3, 25.3, 25.2, 25.0, 22.7, 21.3, 14.1; IR (ν, cm^{-1}, neat): 2928, 2858, 1791, 1721, 1378, 1266, 1019.

Synthesis of (*R*)-1-Oxo-1-((3-(triethoxysilyl)propyl)-amino)octadecan-9-yl Acetate (20)

Triethylamine (0.122 mL, 0.88 mmol) and APTES (0.20 mL, 0.88 mmol) were added to a solution of **18** (0.88 mmol) in CH_2Cl_2 (10 mL), and the mixture was stirred for 3 h at room temperature. The reaction was monitored by ^{1}H-NMR spectroscopy until it resulted complete. The solvent was removed under inert atmosphere to avoid exposure to air, the solvent was removed, and the residue was used without purification. ^{1}H-NMR (600 MHz, $CDCl_3$, 25°C): δ, ppm: 4.76 (qt, *J* = 6.03 Hz, 1H, CHO), 3.73 (q, *J* = 7.1 Hz, 6H, CH_2OSi), 3.16 (q, *J* = 6.4 Hz, 2H, CH_2NH), 2.08 (t, *J* = 7.6 Hz, 2H, CH_2COOH), 1.90 (s, 3H, CH_3CO), 1.57−1.46 (m, 2 H), 1.47−1.37 (m, 4 H), 1.22−1.10 (m + t, 24H + 9H, aliphatic chain + CH_3CH_2OSi), 0.77 (t, *J* = 7.0 Hz, 3H, CH_3), 0.53 (t, *J* = 8.1 Hz, 2H, CH_2Si); ^{13}C-NMR (150 Hz, $CDCl_3$, 25°C): δ, ppm: 172.9, 170.8, 74.2, 58.2, 45.6, 41.6, 36.6, 33.92, 33.87, 31.7, 29.3 (2 signals overlapped), 29.10, 29.08, 29.01 25.6, 25.11, 25.06, 22.7, 22.5, 21.1, 18.1, 13.9, 8.5; ESI-MS$^+$ (*m/z*): 568 $[M + Na]^+$, 584 $[M + K]^+$; IR (ν, cm^{-1}, neat): 3448, 2930, 2859, 2416, 2248, 2212, 1717, 1662, 1520, 1465, 1387, 1371, 1261, 1103, 1077.

20

Preparation of Bare Magnetite (Fe_3O_4) Nanoparticles (B-Magnetite).

The synthesis of bare magnetite nanoparticles was carried out following a previous protocol. Into a three-necked round-bottom flask, $FeSO_4 \cdot 7H_2O$ (2.788 g, 10 mmol) and $Fe_2(SO_4)_3 \cdot 5H_2O$ (5.131 g, 10 mmol) were dissolved in 100 mL of water Milli-Q purity grade, and the solution was degassed with three vacuum/nitrogen purging cycles. An excess of ammonia (13.0 mL, 200 mmol) was added dropwise monitoring the pH of the mixture until to pH = 10.4. The black suspension was stirred for 2 h at 60 °C and cooled and allowed to stand. MNPs were separated from the supernatant solution using an external magnetic bar and thoroughly washed with water and ethanol, dried at 60 °C, and kept under vacuum for 12 h at 50 °C. The final product (2.220 g, 96% yield) was stored under an argon atmosphere.

B-magnetite

Functionalization of B-Magnetite with 20.

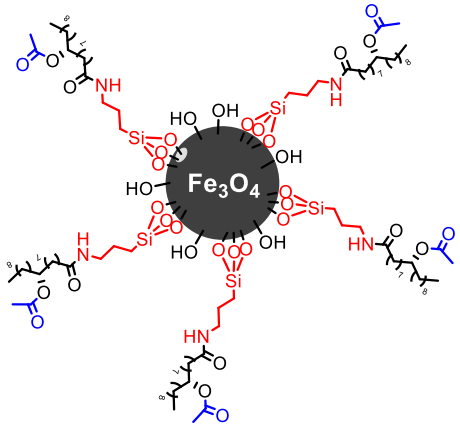

Dry toluene (10 mL), MNPs (B-magnetite, 205 mg, 0.88 mmol), and Et_3N (10 µL, 0.072 mmol) were added to the crude amide **20** (0.88 mmol). The suspension was vigorously stirred for 24 h at 60 °C and then maintained at 100 °C for 1 h. The solvent was removed using Magnetic bar's technique described for the synthesis of MNPs, and then, the product was washed with dry toluene. (*R*)-1-Oxo-1-((3-(triethoxysilyl)-propyl)amino)octadecan-9-ylacetate-coated MNPs, hereinafter indicated as **MAGOR**, were first dried in an oven for 12 h (70 °C) and then kept under vacuum for 12 h. IR analysis confirmed the presence of characteristic bands of organic groups: IR (ν, cm^{-1}): 2930.4, 1735.2, 1659.8, 1478.8, 1121.4 and 1031.7.

References

[1]Amaldi, F.; Benedetti, P.; Pesole, G.; Plevani, P. *Biologia Molecolare*, Ambrosiana, 2011.
[2] Rubin, H. *Science*, **2001**, *21*, 2477-2478.
[3] Bird, A. *Nature*, **2007**, *447*, 396-398.
[4] Lengauer, C.; Issa, J.P. *Mol. Med. Today*, **1998**, *4*, 102.
[5] Jones, PA, Laird, P.W. *Nat. Genet.*, **1999**, *21*, 163.
[6] Fire, A. *Nature*, **1998**, *391*, 806.
[7] Takai, D.; Jones, P.A. *Proc. Natl Acad. Sci. USA*, **2002**, *99*, 3740-3745.
[8] Bernstein, B.E.; Meissner, A.; Lander, E.S. *Cell*, **2007**, *128*, 669-681.
[9] Suzuki, M.M.; Bird, A. *Nat Rev Genet*,. **2008**, *9(6)*, 465-76.
[10] Bilian, J.; Yajun, L.; Robertson, K.D. *Genes & Cancer*, **2011**, *2(6)*, 607-617.
[11] Beckers, T.; Burkhardt, C.; Wieland, H.; Gimmnich, P.; Ciossek, T.; Maier, T.; Sanders, K. *Int. J. Cancer*. **2007**, *121(5)*, 1138.
[12] Bolden, J.E.; Peart, M.J,; Johnstone, R.W. *Nat. Rev. Drug Discov.* **2006**, *5(9)*, 769.
[13] Bannister, A.J.; Zegerman, P.; Partridge, J.F. *Nature*, **2001**, *410*, 120.
[14] Wagner, J.M.; Björn, H.; Lübbert, M.; Jung, M. *Clin. Epigen.*, **2010**, *1*, 117-136.
[15] Weichert, W.; Roske, A.; Niesporek, S.; Noske, A.; Buckendahl, A. C.; Dietel, M.; Gekeler, V.; Boehm, M.; Beckers, T.; Denkert, C. *Clin. Cancer Res.*, **2008**, *14*, 1669–1677.
[16] Wilson, A.J.; Byun, D.S.; Popova, N.; Murray, L. B.; L'Italien, K.; Sowa, Y.; Arango, D.; Velcich, A.; Augenlicht, L. H.; Mariadson, J. M. *J. Biol. Chem.*, **2006**, *281*, 13548–13558.
[17] Bhaskara, S.; Chyla, B.J.; Amann, J.M.; Knutson, S. K.; Cortez, D.; Sun, Z. W.; Hiebert, S. W. *Mol. Cell.*, **2008**, *30*, 61–72.
[18] Wilson, A.J.; Byun, D.S.; Nasser, S.; Murray, L. B.; Ayyanar, K.; Arango, D.; Figueroa, M.; Melnick, A.; Kao, G. D.; Augenlicht, L. H.; Mariadson, J. M. *Mol. Biol. Cell.*, **2008**, *19*, 4062– 4075.
[19] Mottet, D.; Bellahcene, A.; Pirotte, S.; Waltregny, D.; Deroanne, C.; Lamour, V.; Lidereau, R.; Castronovo, V. *Circ. Res.*, **2007**, *101*, 1237–1246.
[20] Moller, C.; Leutz, A. *Curr. Opin. Genet. Dev*., **2001**, *11*, 167.
[21] Jones, P.A.; Baylin, S.B. *Nat. Rev. Genet.*, **2002**, *3*, 415.
[22] Kramer, O.H.; Gottlicher, M.; Heinzel, T. *Trends Endocrinol. Metab.*, **2001**, *12*, 294.
[23] Marks, P.A.; Richon, V.M.; Breslow, R. *Curr. Opin. Oncol.*, **2001**, *13*, 477.
[24] Calonghi, N.; Cappadone, C.; Pagnotta, E.; Boga, C.; Bertucci, C.; Fiori, J.; Tasco, G.; Casadio, R.; Masotti, L. J. Lipid Res., 2005, 46, 1596-1603.
[25] Richon, V.M.; Sandhoff, T. W.; Rifkind, R. A.; Marks, P. A. *Proc. Nat. Acad. Sci. USA*, **2000**, *97*,10014–10019.
[26] Butler, L.M.; Zhou, X.; Xu, W.S. *Proc. Natl. Acad. Sci. USA*, **2002**, *99*, 11700.
[27] Bradner, J.E.; West, N., Grachan, M. L.; Greenberg, E. F.; Haggarty, S. J.; Warnow, T.; Mazitschek, R. *Nat. Chem. Biol.*, **2010**, *6*, 238–243.
[28] Bertrand, P. *Eur. J. Med, Chem.*, **2010**, *45*, 2095-2116.
[29] Rocchi, P.; Tonelli, R.; Camerin, C.; Purgato, S.; Fronza, R.; Bianucci, F.; Guerra, F.; Pession, A.; Ferreri, A.M. *Oncol. Rep.*, **2005**, *13 (6)*, 1139-1144.
[30] Göttlicher, M.; Minucci, S.; Zhu, P.; Kramer, O. H.; Schimpf, A.; Giovara, S.; Sleeman, J. P.; Lo Coco, F.; Nervi, C.; Pelicci, P. G.; Heinzel, T. *EMBO J.*, **2001**, *20*, 6969–6978.
[31] Villar-Garea, A.; Esteller, M. *Int. J. Cancer*, **2004**, *112*, 171-178.
[32] Rao, J.; Bhattacharya, D.; Banerjee, B.; Sarin, A.; Shivashankar, G.V. *Biochem. Biophys. Res. Commun.*, **2007**, *363*, 263-268.
[33] Duvic, M. Expert *Rev. Hematol.*, **2008**, *2 (5)*, 39-43.
[34] Xu, W.S.; Parmigiani, R.B.; Marks, P.A. *Oncogene*, **2007**, *26*, 5541-5552.
[35] Beckers, T.; Burkhardt, C.; Wieland, H.; Gimmnich, P.; Ciossek, T.; Maier, T.; Sanders, K. *Int. J. Cancer*, **2007**, *121 (5)*, 1138-1148.
[36] Bressi, J.C.; Jennings, A. J.; Skene, R.; Wu, Y.; Melkus, R.; De Jong, R.; O'Connell, S.; Grimshaw, C. E.; Navre, M.; Gangloff, A. R. *Bioorg. Med. Chem. Lett.*, **2010**, *20*, 3142–3145.
[37] Saito; A.; Yamashita, T.; Mariko, Y.; Nosaka, Y.; Tsuchiya, K.; Ando, T.; Suzuki, T.; Tsuruo, T.; Nakanishi, O. *Proc Natl Acad Sci USA*, **1999**, *96 (8)*, 4592-4597.
[38] Hess-Stump, H.; Brackera, T. U.; Hendersonb, D.; Politz, O. *Int. J. Biochem. Cell Biol.*, **2007**, *39*, 1388–1405.
[39] Kwon, S.H.; Ahn, S.H.; Kim, Y.K.; Bae, G.; Yoon, J.W.; Hong S.; Lee, H.Y.; Lee, Y.; Lee, H.; Han, J. *J. Biol, Chem.*, **2002**, *277 (3)*, 2073-2080.
[40] Ueda, T.; Takai, N.; Nishida, M.; Nasu, K.; Narahara, H. *Int. J. Mol. Med.*, **2007**, *19 (2)*, 301-308.
[41] Kijima, M; Yoshida, M.; Sugita, K.; Horinouchi, S.; Beppu, T. *J. Biol. Chem.*, **1993**, *268 (30)*, 22429-22435

[42] Porter, N.J.; Christianson, D.W. *ACS Chem. Biol.*, **2017**, *12*, 2281-2286.
[43] Barrera, G. *ISRN Oncol.*, **2012**, *2012*, 137289.
[44] Lu, J. M.; Lin, P. H.; Yao, Q.; Chen, C. *J. Cell. Mol. Med.*, **2010**, *14 (4)*, 840–860.
[45] Klaunig, J. E.; Kamendulis, L. M. Ann. *Rev. Pharmacol. Toxicol.*, **2004**, *44*, 239-267.
[46] Dix, T. A.; Aikens, J. *Chem. Res. Toxicol.*, **1993**, *6 (1)*, 2–18.
[47] Weisiger, R.A.; Fridovich, I. *J. Biol. Chem.*, **1973**, *248*, 10, 3582–3592.
[48] Droge, W. *Physiol. Rev.*, **2002**, *82 (1)*, 47–95.
[49] Zhou, Y.; Hileman, E.O.; Plunkett, W.; Keating, M.J.; Huang, P. *Blood*, **2003**, *101 (10)*, 4098–4104.
[50] Boonstra, J.; Post, J. A. *Gene*, **2004**, *337*, 1–13.
[51] Seema, K.; Anil, K.B.; Murali, M.G.; Shailender, G.; RamaRao, M. *Biomark Insights*, **2018**, *13*, 1-9.
[52] Masotti, L.; Casali, E.; Galeotti, T. *Free Radical Biol. Med.*, **1988**, *4*, 377-386.
[53] Comporti, M. *Molec. Aspects. Med.*, **1993**, *14*, 199-207.
[54] Pamplona, R. *Biochim. Biophys. Acta*, **2008**, *10*, 1249-1262.
[55] Barrera, G.; Pizzimenti, S.; Dianzani, M.U. *Mol. Asp. Med.*, **2008**, *29 (1)*, 1–8.
[56] Pizzimenti, S.; Toaldo, C.; Pettazzoni, P.; Dianzani, M.U.; Barrera, G. *Cancers*, **2010**, *2 (2)*, 338–363.
[57] Klaunig, J. E.; Kamendulis, L. M. Ann. *Rev. Pharmacol. Toxicol.*, **2004**, *44*, 239-267.
[58] Calonghi, N.; Cappadone, C.; Pagnotta, E.; Farruggia, G.; Buontempo, F.; Boga, C.; Brusa, G.L.; Santucci, M.A.; Masotti, L. *Biochem. Biophys. Res. Commun.*, **2004**, *314*, 138-142.
[59] Bertucci, C.; Hudaib, M.; Boga, C.; Calonghi, N.; Cappadone, C.; Masotti, L. *Rapid Commun. Mass Spectrom.*, **2002**, *16*, 859–864.
[60] Cavalli, G.; Casali, E.; Spisni, A.; Masotti, L. *Biochem. Biophys. Res. Commun.*, **1991**, *178 (3)*, 1260-1265.
[61] Gesmundo, N.; Casali, E.; Farruggia, G.; Spisni, A.; Masotti, L. *Biochem. Mol. Biol. Int.*, **1994**, *33*, 705-712.
[62] Casali, E.; Cavalli, G.; Spisni, A.; Masotti, L. *Recent Adv. Cell. Molec. Biol.*, **1992**, *6*, 245-250.
[63] Parolin, C.; Calonghi, N.; Presta, E.; Boga, C.; Caruana, P.; Naldi, M.; Andrisano, V.; Masotti, L.; Sartor, G. *Biochim. Biophys. Acta*, **2012**, *1821*, 1334-1340.
[64] Calonghi, N.; Boga, C.; Telese, D.; Bordoni, S.; Sartor, G.; Torsello, C.; Micheletti, G. *Molecules*, **2019**, *24*, 3714, 1-16.
[65] A) McDermott, G. N. *Miscellaneous oil and fat products in Bailey's industrial oil and fat products*, Swern D. Ed., John Wiley &Sons: New York, 1982. B) Calonghi, N.; Boga, C.; Nitti, P.; Telese, D.; Bordoni, S.; Farruggia, G.; Asaro, F.; Grandi, M.; Zalambani, C.; Micheletti, G. *Molecules*, **2022**, *27*, 2396.
[66] Teeter, H. M.; Gast, L. E.; Bell, E. W.; Cowan, J. C. *Ind. Engin. Chem.*, **1953**, *45*, 1777–1779.
[67] Pryde, E. H.; Princen, L. H.; Mukherjiee, K. D. *New sources of fats and oils*, American oil Chemists Society: Champaign, 1981.
[68] Svensson, M. *Surfactants Based on Natural Fatty Acids, in Surfactants from Renewable Resources* Kjellin M. and Johansson I., Eds., John Wiley & Sons: Chichester, UK, 2010.
[69] Petrović, Z. S.; Cvetković, I.; Hong, D.; Wan, X.; Zhang, W.; Abraham, T.; Malsam, J. *J. Appl. Pol. Sci.*, **2008**, *108*, 1184–1190.
[70] Marrion, A.; Marrion, A.R. *Binders for conventional coatings in The Chemistry and Physics of Coatings*, Marrion, Alistair R. Ed., RCS Publ. 2004, 1, pp. 96–150.
[71] Naughton, F. C. *J. Am. Oil Chem. Soc.*, **1974**, *51*, 65–71.
[72] Drovetskaya, T. V.; Yu, W. H.; Diantonio, E. F.; Jordan, S. L.; *Hair styling and conditioning personal care films*, US Pat No. US 2010/0247459 A1, 2010.
[73] Grissett, G. A.; Keenan, D. M.; Macedo, F. A.; Williams, D. R. *Fibrous toilette article* US Pat No. US 10/938,384, 2008.
[74] Schwab, W.; Davidovich-Rikanati, R.; Lewinsohn, E. *Plant J.*, **2008**, *54*, 712–732.
[75] *Nutraceutical and Specialty Lipids and their Co-Products* Shahidi, F., Ed., CRC Press 2006.
[76] Toro-Vazquez, Jorge F.; Morales-Rueda, J. *Food Biophys.*, **2010**, *5*, 193–202.
[77] Gunstone, F. D. *Fatty acid and lipid chemistry*, Springer Verlag: Berlin, 1996.
[78] Fulco, A. *J. Lipid Res.*, **1983**, *22*, 133–160.
[79] Asaro, F.; Boga, C.; De Zorzi, R.; Geremia, S.; Gigli, L.; Nitti, P.; Semeraro, S. *Int. J. Mol.Sci.*, **2020**, *21*, 8124.
[80] Cristofolini, L.; Fontana, M. P.; Boga, C.; Konovalov, O. *Langmuir*, **2005**, *21*, 11213-11219.
[81] Ebert, C.; Felluga, F.; Forzato, C.; Foscato, M.; Gardossi, L.; Nitti, P.; Pitacco, G.; Boga, C.; Caruana, P.; Micheletti, G.; Calonghi, N.; Masotti, L. *J. Molec. Catal. B: Enzymatic*, **2012**, *83*, 38– 45.
[82] Boga, C.; Drioli, S.; Forzato, C.; Micheletti, G.; Nitti, P.; Prati, F. *Synlett*, **2016**, *27*, 1354–1358.
[83] Harwood, J.; Russell, N. *Lipids in Plants and Microbes*, Allen and Unwin: London, 1984.
[84] Bertucci, C.; Hudaib, M.; Boga, C.; Calonghi, N.; Cappadone, C.; Masotti, L. *Rapid Commun. Mass Spectr.*, **2002**, *16*, 859-864.
[85] Rawlings A. V.; Wandeler, E.; Bendik, I.; Fuchs, P.; Monneuse, J.-M.; Imfeld, D.; Schütz, R. *Int. J. Cosmet Sci.*, **2021**, *43*, 619–626.

[86] Kokotou, M. G.; Kokotos, A. C.; Gkikas, D.; Mountanea, O. G.; Mantzourani, C.; Almutairi, A.; Lei, X.; Ramanadham, S.; Politis, P. K.; Kokotos, G. *J. Med. Chem.*, **2020**, *63*, 12666-12681.
[87] Wood, P. L. *Metabolites*, **2020**, *10*, 512.
[88] Brejchova, K.; Balas, L.; Paluchova, V.; Brezinova, M.; Durand, T.; Kuda, O. *Progr.Lipid Res.*, **2020**, *79*, 101053.
[89] Nelson, A.T.; Kolar, M.J.; Chu, Q.; Syed, I.; Kahn, B.B.; Saghatelian, A.; Siegel, D. *J. Am. Chem. Soc.*, **2017**, *139*, 4943–4947.
[90] Asaro, F.; Drioli, S.; Forzato, C.; Nitti, P. *ChemistrySelect*, **2018**, *3*, 13372–13376.
[91] Satyanarayana, S.; Reddy, B.V.S.; Narender, R. *Tetrahedron Lett.*, **2014**, *55*, 6027–6029.
[92] Rybak, A.; Meier, M. A. R. *Green Chem.*, **2007**, *9*, 1356–1361.
[93] Zha, S.; Kuwano, K.; Shibahara, T.; Ishibashi, F. *Fitoterapia*, **2020**, *145*, 104639.
[94] Hsieh, C.-T.; Ötvös, S. B.; Wu, Y.-C.; Mándity, I. M.; Chang, F.-R.; Fülöp, F. *ChemPlusChem*, **2015**, *80*, 859–864.
[95] Bergstrŏm, S.; Aulin Erdtman, G.; Rolander, B.; Stenhagen, E.; Östling., S. *Acta Chem. Scand.*, **1952**, *6*, 1157–1174.
[96] Micheletti, G.; Boga, C.; Telese, D.; Cassani, M.C.; Boanini, E.; Nitti, P.; Ballarin, B.; Ghirri, A.; Barucca, G.; Rinaldi, D. *ACS Omega*, **2020**, *5*, 12707-12715.
[97] Ngomsik, A.-F.; Bee, A.; Draye, M.; Cote, G.; Cabuil, V. *C. R. Chim.*, **2005**, *8*, 963−970.
[98] Saharan, P.; Chaudhary, G. R.; Mehta, S. K.; Umar, A. *J. Nanosci. Nanotechnol.*, **2014**, *14*, 627−643.
[99] Chenthamara, D.; Subramaniam, S.; Ramakrishnan, S. G.; Krishnaswamy, S.; Essa, M. M.; Lin, F.-H.; Qoronfleh, M. W. *Biomater. Res.*, **2019**, *23*, 20.
[100] Gobbo, O. L.; Sjaastad, K.; Radomski, M. W.; Volkov, Y.; Prina-Mello, A. *Theranostics*, **2015**, *5*, 1249−1263.
[101] Montalto, L.; Paone, N.; Scalise, L.; Rinaldi, D. A *Rev. Sci. Instrum.*, **2015**, *86*, 063102.
[102] Scalise, L.; Rinaldi, D.; Davì, F.; Paone, N. *Nucl. Instrum. Methods Phys. Res., Sect. A*, **2011**, *654*, 122−126.
[103] Rinaldi, D.; Ciriaco, A.; Lebeau, M.; Paone, N. *Nucl. Instrum. Methods Phys. Res., Sect. A*, **2010**, *615*, 254−258.
[104] Arruebo, M.; Fernández-Pacheco, R.; Ibarra, M. R.; Santamaría, J. *Nano Today*, **2007**, *2*, 22−32.
[105] Wang, X.; Zhang, R.; Wu, C.; Dai, Y.; Song, M.; Gutmann, S.; Gao, F.; Lv, G.; Li, J.; Li, X.; Guan, Z.; Fu, D.; Chen, B. *J. Biomed. Mater. Res., Part A*, **2007**, *80*, 852−860.
[106] Ehsani, M. H.; Esmaeili, S.; Aghazadeh, M.; Kameli, P.; Karimzadeh, I. *J. Supercond. Novel Magn.*, **2019**, *32*, 2021−2030.
[107] Gupta, A. K.; Gupta, M. *Biomaterials*, **2005**, *26*, 3995−4021.
[108] Busi, A.; Aluigi, A.; Guerrini, A.; Boga, C.; Sartor, G.; Calonghi, N.; Sotgiu, G.; Posati, T.; Corticelli, F.; Fiori, J.; Varchi, G.; Ferroni, C. *Mol. Pharm.*, **2019**, *16*, 931−942.
[109] Boanini, E.; Torricelli, P.; Boga, C.; Micheletti, G.; Cassani, M.C.; Fini, M.; Bigi, A. *Langmuir*, **2016**, *32*, 188−194.
[110] Yamaura, M.; Camilo, R. L.; Sampaio, L. C.; Macêdo, M. A.; Nakamura, M.; Toma, H. E. *J. Magn Mater.*, **2004**, *279*, 210−217.

Chapter II: Synthesis and biological evaluation of novel hybrids between aza-heterocycles and azelaic acid moiety[111]

2.1. Introduction

Aza-heterocycles belong to a well-known class of compounds of wide interest in several applied fields, *i.e.* material, agrochemical and medicinal chemistry. A large variety of biological activities are being described for these privileged scaffolds, such as antibacterial, antitubercular, antiviral, antimalarial, anticancer, anti-inflammatory, antithrombics, anticoagulants, antidepressants *etc*.. [112,113,114,115]

Among aza-heterocycles, pyridine is one of the simplest, isolated by Thomas Anderson in 1851 through high-temperature heating of animal bones.[116] However the chemical structure of pyridine was proposed only two decades later by Wilhelm Korner and James Dewar in 1871. They suggested that the structure of pyridine is derived from benzene by substituting one C-H unit with a nitrogen atom.

One of the oldest methods of synthesis[117] of this simple aromatic azine is the condensation between glutaconaldehyde and ammonium acetate, used as ammonia precursor (**Scheme 10**).

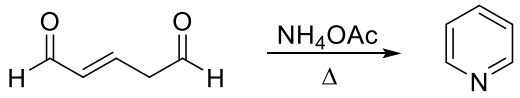

Scheme 10. Synthesis of pyridine from glutaconaldehyde and ammonium acetate.

Because of the difficult access to the glutaconaldehyde, reactions in presence of transition metal catalysts are preferred to synthesize the pyridine ring[117] (**Scheme 11**).

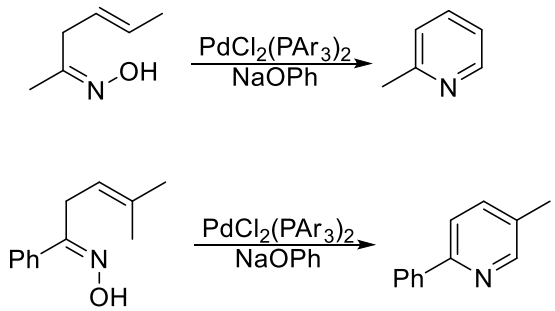

Scheme 11. Synthesis of pyridine ring with metal catalysts.

However the general and major synthesis of pyridine derivatives was described by Arthur Rudolf Hantzsch in 1881[117] (**Scheme 12**).

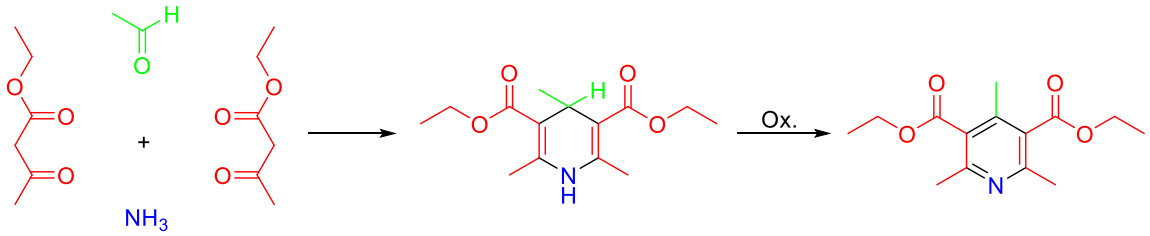

Scheme 12. The Hantzsch synthesis to obtain pyridine derivatives.

The Hantzsch synthesis is carried out between a β-ketoester, an aldehyde and ammonia, or its salt as nitrogen donor, using a 2:1:1 mixture. At first, a hydrogenated pyridine is obtained, which is oxidized to the corresponding pyridine derivative using nitric acid or bromine.

The structure of pyridine is similar to benzene's one with six π-electrons delocalized on the molecule with just one difference. One carbon atom is replaced with a nitrogen atom with an ion pair on a sp^2 orbital. The other important element that has to be considered is the electronegativity of the nitrogen atom, higher than that of the carbon. Consequently the HOMO of the pyridine is lower in energy, localizing the electron density on itself, and turning the aromatic ring in a worse nucleophile.

Given its structure, pyridine is subject to three different types of reactivity, summarized in **Figure 19**: electrophilic substitution, nucleophilic substitution, and oxidation/protonation/alkylation at the nitrogen atom.

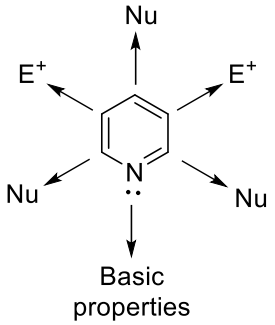

Figure 19. Reactivity sites of pyridine ring.

Because of the decreased electron density in the aromatic system, electrophilic substitutions are inhibited in pyridine and its derivatives with respect to benzene. Substitutions can occur in drastic conditions at the 3-position, which is the less deactivated position on the ring and is, therefore, more susceptible to an electrophilic attack.

In contrast to benzene, pyridine efficiently supports several nucleophilic substitutions. These reactions include substitutions with elimination of a hydride ion and elimination-additions with formation of an intermediate aryne configuration, and usually proceed at the 2- or 4-position.

N-oxidation of pyridine occurs at nitrogen to give pyridine-*N*-oxide. The oxidation can be achieved with peracids as shown in the following **Scheme 13**:

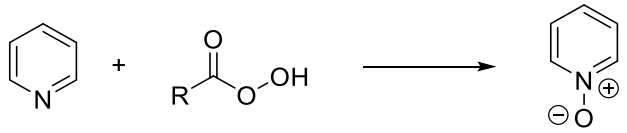

Scheme 13. *N*-oxidation of pyridine.

Some electrophilic substitutions on the pyridine ring are usefully carried out using pyridine-*N*-oxide followed by deoxygenation. *N*-oxidation suppresses further reactions at nitrogen atom and promotes substitution at the 2- and 4-positions; then the oxygen atom can be removed using zinc dust.

Moreover, the lone pair of the nitrogen atom of pyridine does not overlap with the aromatic π-system, consequently pyridine is basic (Lewis base); protonation of pyridine gives pyridinium cation with a pKa value equal to 5.2. Pyridine also can react with alkyl halides giving the corresponding salts.

The replacement of a carbon atom on pyridine ring with a further nitrogen atom gives 1,2-diazines, 1,3-diazines and 1,4-diazines, whose ancestors are pyridazine, pyrimidine, and pyrazine, respectively (**Figure 20**).

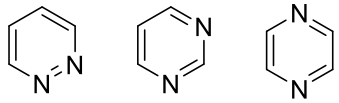

Figure 20. Basilar of diazine rings.

In particular, I will focus on the last two heterocyclic ring systems in this chapter of my PhD thesis.

The synthesis of pyrimidine is not that common to other classes of heterocyclic derivatives. In fact three different schemes exist to synthesize this aza-heterocyclic ring as shown in **Figure 21**:

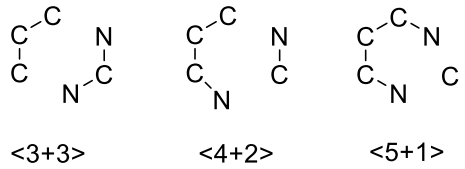

Figure 21. Possible approaches for the formation of pyrimidine ring.

The main method used is the cyclization <3+3> type between a β-dicarbonyl compound (or an equivalent C-C-C system) and an amidine (or an equivalent N-C-N system). Moreover, depending on the reagent used, the presence of functional groups on the aromatic ring is determined: the fragment N-C-N establishes the type of substituent in 2-position (**Scheme 14).**

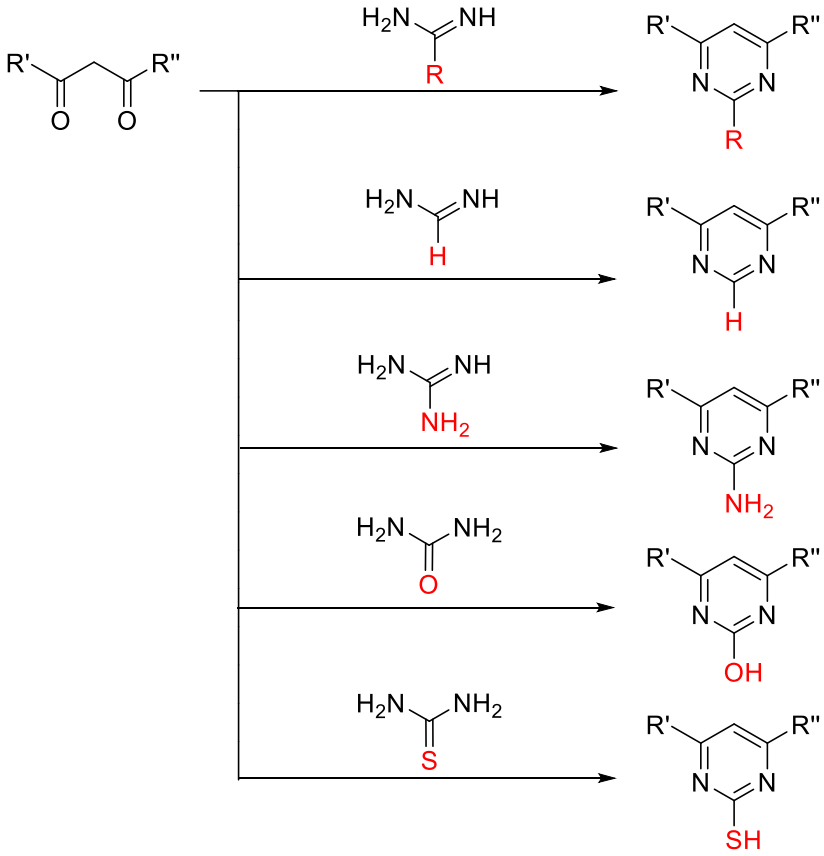

Scheme 14. Ring-closure reaction to obtain the 2-substituted pyrimidine ring.

Because of the decreased basicity (pK_a=1.3)[118] compared to that of the pyridine (pK_a=5.2),[118] electrophilic substitutions on pyrimidine ring are less favourite. Protonation or alkylation takes place at only one of the ring nitrogen atoms, whereas *N*-oxidation takes divergent pathways, depending on the presence of strong acids (**Scheme 15**).[119] Although the pyrimidine ring seems to be more susceptible to reactions such as hydrolysis, ring

opening and decomposition under *N*-oxidation conditions,[120] it is possible to obtain the pyrimidine *N*-oxide (**22a-c**) or the corresponding pyrimidinone (**23a-c**).

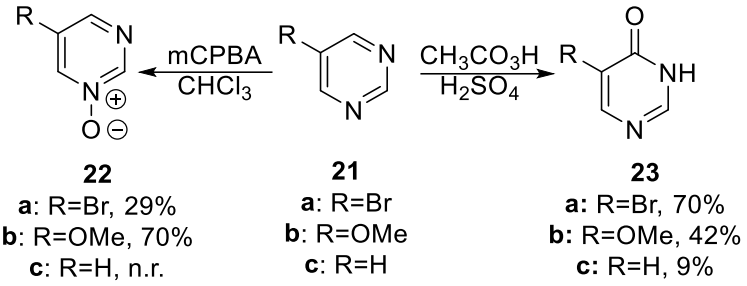

Scheme 15. Oxidation reactions of pyrimidine ring.

The electron-donor effect of the methoxy group increases the yield of *N*-oxide as compared with 5-bromopyrimidine. While the pyrimidine without substituents is much less stable and it is susceptible to ring opening and fragmentation.[67]

Electrophilic *C*-substitutions of pyrimidine occur at the 5-position, the least electron-poor. Nitration, halogenation, sulfonation, formylation, hydroxymethylation and aminomethylation have been observed with substituted pyrimidines.

Nucleophilic *C*-substitutions occur at 2-,4- and 6-position but there are only few examples. Amination and hydroxylation have been observed in substituted pyrimidines.

The classical route for the synthesis of pyrazines is the direct condensation reaction between 1,2-diketones and 1,2-diamines (**Scheme 16**), although with poor yields.[121]

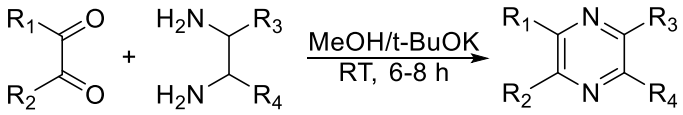

Scheme 16. Synthesis of pyrazine ring by condensation.

Also the reaction of diamines with diols in vapor phase in presence of granular alumina is diffuse to obtain pyrazine derivatives (**Scheme 17**).[122]

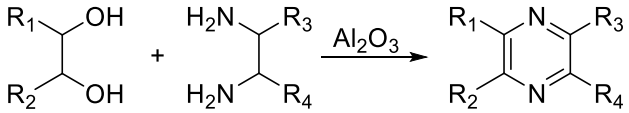

Scheme 17. Synthesis of pyrazine derivatives starting from diols and 1,2-diamines.

Over the years, catalytic methods have been developed: systems such as copper-chromium, copper-zinc-chromium, zinc-phosphoric acid-manganese and silver are also patented as

catalysts for the synthesis of 2-methylpyrazine from ethylen diamine and propylene glycol (**Scheme 18**).[123]

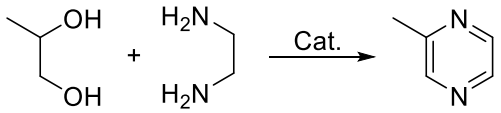

Scheme 18. Synthesis of pyrazine ring catalyzed by metals.

Among bicyclic aza-heterocycles, indole is by far one the most popular scaffolds in nature. This organic compound is characterized by a pyrrole fused to benzene ring.

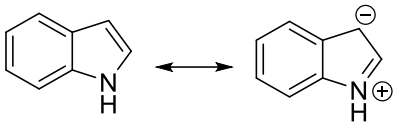

Figure 22. Resonance forms of indole nucleus.

As shown in **Figure 22**, the 3-position of indole is very reactive towards electrophiles; on the contrary, the 2-position is less reactive.

In general indoles are poor bases, with a $pK_a \approx 21$ in water,[118] and their acidity increases when an electron withdrawing group is present in 3-position.[124]

N-deprotonation is easily achieved by using a strong base and the resulting anion reacts quickly with electrophiles to provide *N*-alkylated derivatives.

Fischer's synthesis was the first method to obtain indoles starting from arylhydrazine and ketones (or aldehydes) in acidic environment[125] (**Scheme 19**):

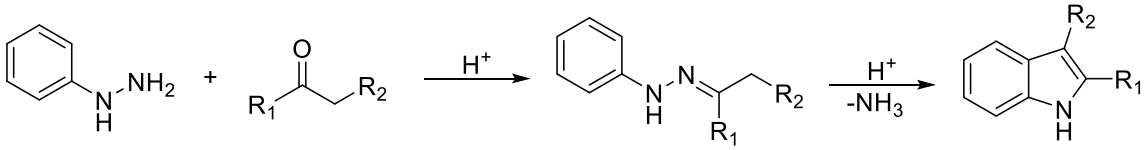

Scheme 19. Synthesis of indole derivatives by Fischer.

Instead, Madelung's synthesis provides a base-catalyzed intramolecular cyclization of *N*-phenylamides at high temperature[126] (**Scheme 20**):

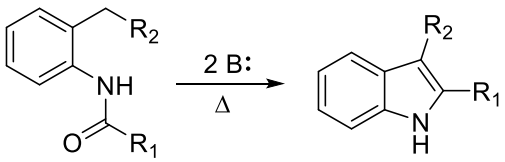

Scheme 20. Synthesis of indole derivatives by Madelung.

It is possible to obtain indoles with substituents in 2- and 3- position through the Bartoli reaction,[127] starting from *ortho*-substituted nitrobenzene and vinyl Grignard reagents (**Scheme 21**):

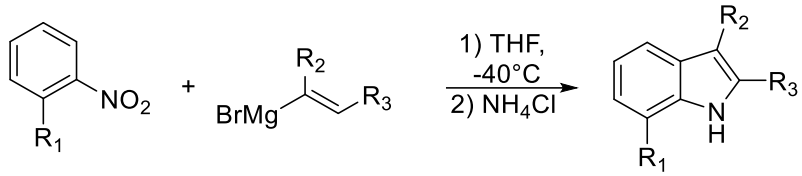

Scheme 21. Bartoli's reaction to obtain indole derivatives.

Kobayashi K. *et al.*[128] founded a versatile synthesis of indole derivatives based on the selective *ortho*-lithiation of *o*-akylphenyl isocyanides with subsequent intramolecular ring closure with lithium 2,2,6,6-tetramethylpiperidide (LTMP) as shown in **Scheme 22**:

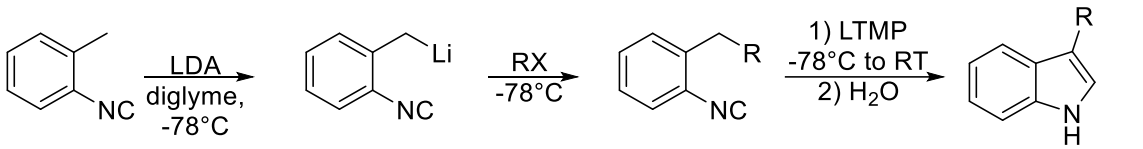

R= CH_3, 95%
R= *n*-C_4H_9, 85%
R= *i*-C_4H_9, 78%

Scheme 22. Synthesis of indole derivatives by Kobayashi.

The above aza-heterocycles are the basic structure of many natural products of biological interest: most of them were found in plants, microorganisms, marine organisms, animals, insects and the key-core structure of nucleotides and coenzymes. Moreover, some of them play an important role as pharmaceutical drugs, including anticancer agents.

The ability of 1,3-diazinic compounds to interact with biological systems is intrinsic in their nature, due to their high availability in nature. Some examples are nucleobases, also called nitrogenous bases that form nucleotides of DNA (deoxyribonucleic acid) and RNA (ribonucleic acid), essential macromolecules for living organisms. The five major bases in nucleic acids, whose structures are shown in **Figure 23**, are adenine (A), cytosine (C), guanine (G), thymine (T) and uracil (U). Cytosine, thymine and uracil are derived of pyrimidine and then called pyrimidine bases; instead adenine and guanine have a structure derived from purine and then called purine bases.

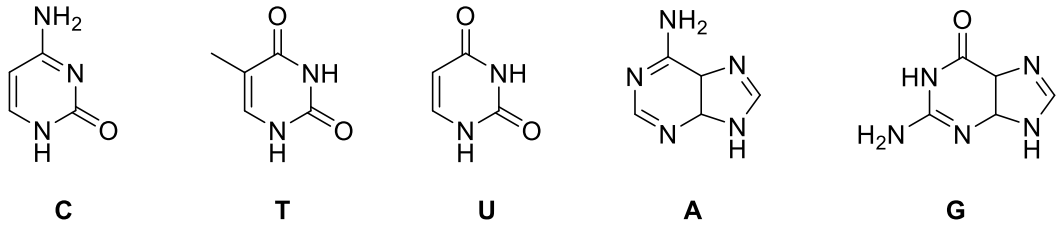

Figure 23. Nucleobases: Cytosine (C), thymine (T), uracil (U), adenine (A), guanine (G).

Other examples of diazinic compounds present in nature are B1 and B2 vitamins (**Figure 24**), also called aneurine and riboflavin respectively. Aneurine is a colorless compound, characterized by an aminopyrimidine and a thiazolium ring, linked by a methylene bridge. It is possible to find it in some food sources like whole grain and legumes. Instead, riboflavin is a heterocyclic compound obtained starting from flavin, linked to a ribitol chain. This compound, involved in many metabolic ways, including cellular respiration, is present in eggs, green vegetables, milk, meat, mushrooms and almonds.

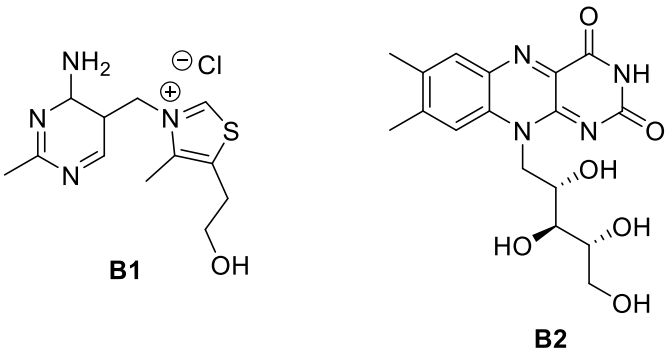

Figure 24. Chemical structure of B1 and B2 vitamins.

A series of heteroamines, characterized by a purinium skeleton (thus containing pyrimidine ring), have been isolated from *Heterostemma brownii Hayata* (Asclepiadaceae), a plant used against different tumors in Taipei.[129] Among them, heteromine A and B (**Figure 25**) showed a biological activity as antimicrobials and anticancer agents.[130]

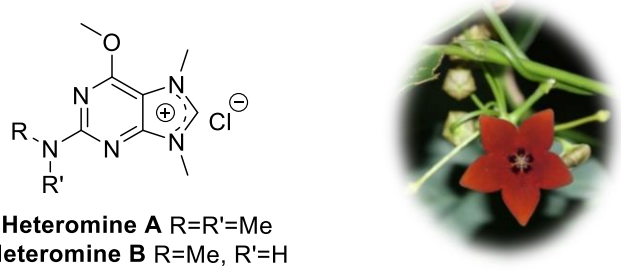

Figure 25. Heteroamines with biological activity.

Other diazinic substrates have been particularly useful in biological field for their activity against several types of cancers. Among them, Mocetinostat, also known as MGCD0103 (**Figure 26**), is one of the new class I selective HDAC inhibitors,[131] undergoing clinical trials for treatment of various types of cancer, including follicular lymphoma, Hodgkin's lymphoma and acute myeloid leukemia (AML).[132] Pracinostat, shown in **Figure 26**, is an oral HDACi with good tolerability in patients,[133] which is currently in clinical development for the treatment of solid tumors as well as myelodysplastic syndrome, AML and myelofibrosis.[134] Imatinib (**Figure 26**), approved by FDA and sold as Glaveec®, is a tyrosine kinase inhibitor used for chronic myeloid leukemia (CML) and acute lymphocytic leukemia (ALL), chronic eosinophilic leukemia (CEL), gastrointestinal stromal tumors (GIST), hypereosinophilic syndrome (HES), systemic mastocytosis, and myelodysplastic syndrome.[135,136] Berzosertib (VE-822) which structure is shown in **Figure 26**, is an ATR kinase inhibitor invented by Vertex and licensed to Merck. It prevents ATR-mediated signaling in the ATR-checkpoint kinase 1 (Chk1) signaling pathway, inducing apoptosis in solid tumors such as lung, pancreatic and ovarian cancer.[137,138,139]

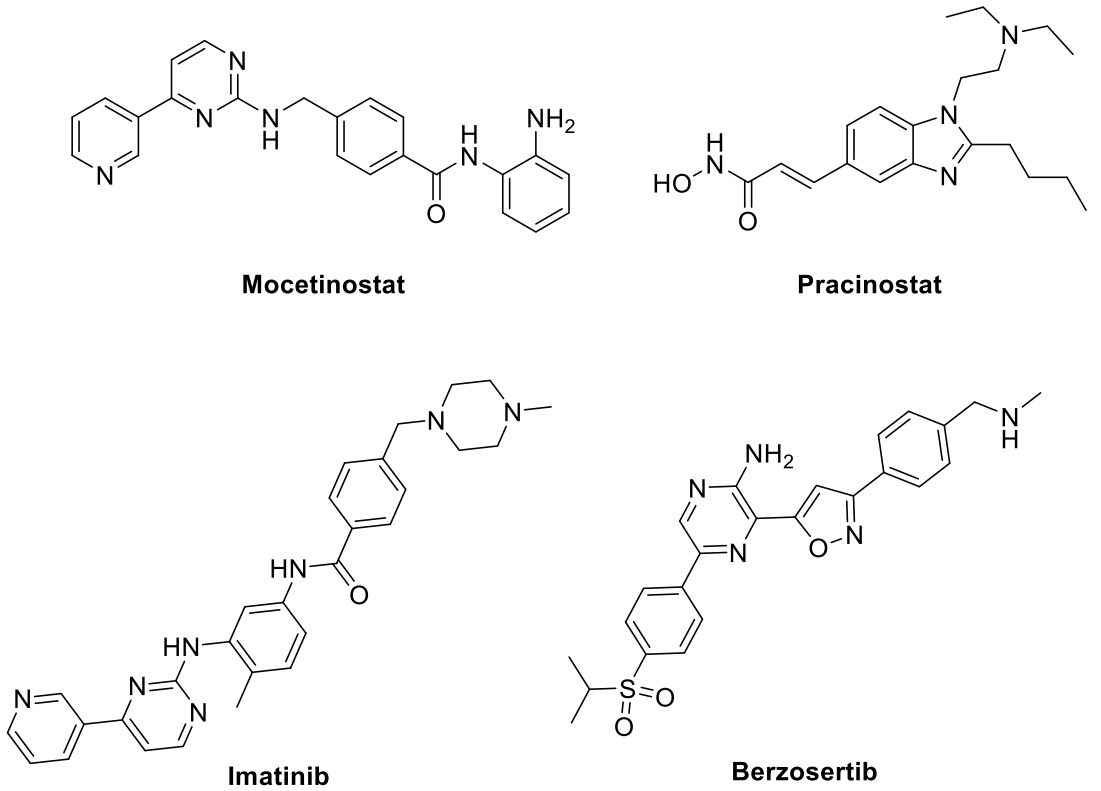

Figure 26. Diazinic derivatives with anticancer activity.

Moreover, serotonin, tryptophan and melatonin (**Figure 27**) are important indole derivatives, present in our body. Serotonin is an amine neurotransmitter synthesized mainly by serotoninergic neurons in the central nervous system, known to be involved in many bodily functions, ranging from regulating mood to digesting food. Serotonin is synthesized at endogenous level starting from L-tryptophan, an essential α-amino acid. It is involved in the biosynthesis of proteins and it must be assumed from the diet since our body is not able to produce it. Melatonin instead is a hormone released by the pineal gland and it has been associated with control of the sleep–wake cycle, through its action on the hypothalamus.

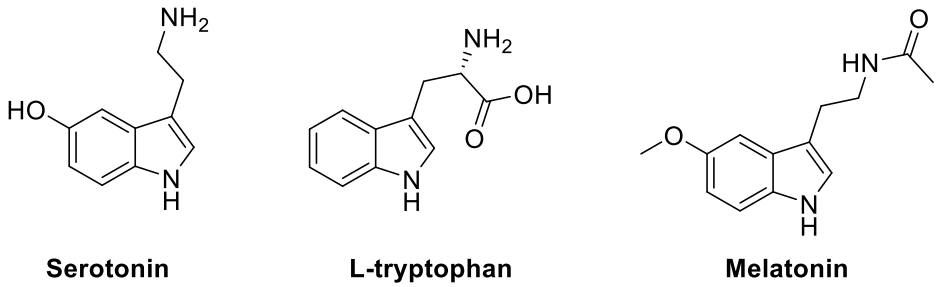

Figure 27. Indole derivatives with biological activity.

The indole scaffold is found also in marine organisms such as ostracods and deep-sea fish. In these animals in fact is present the so-called vargulin (shown in **Figure 28**), a light-emitting compound that generates bioluminescence. In particular vargulin is oxidized by the Vargula luciferase to produce blue light at 462 nm.[140]

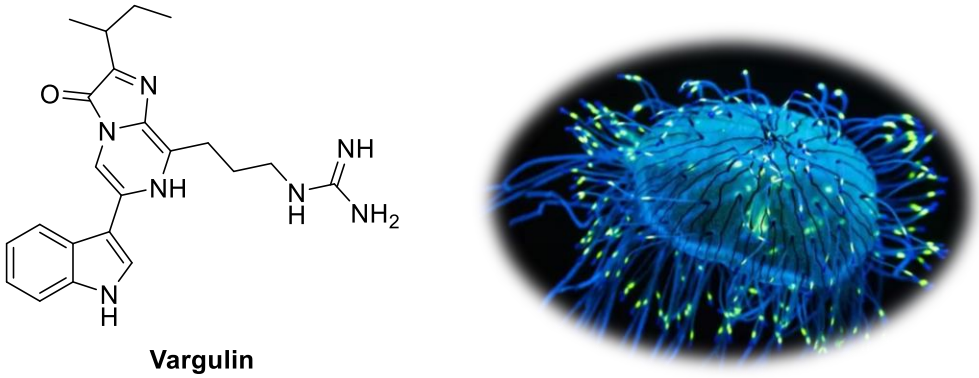

Figure 28. Vargulin, a natural indole derivative present in marine organisms.

Indole nucleus is present also in some natural alkaloids, such as ergotamin, vinblastine and armalin (**Figure 29**), extracted from vinca, ergot and syrian ruta respectively, that have been shown to be particularly active on the human organism. In particular, ergotamin is used as an active ingredient in the treatment of migraine; vinblastine is used against several

cancers, including Hodgkin's lymphoma, lung, breast and testicles cancer; armalina is a central nervous system stimulant and a reversible inhibitor of MAO-A (RIMA).

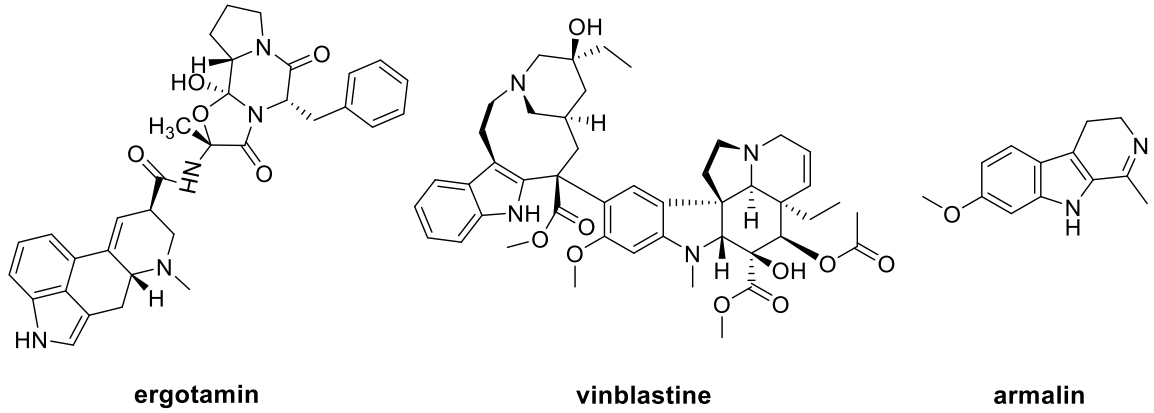

Figure 29. Chemical structure of some natural indole-containing alkaloids.

Indole is also a fundamental pharmacophoric scaffold for the interaction with different protein systems. Its importance is confirmed by the high number of biologically active drugs containing its skeleton.

Some examples are sumatriptan, rizatriptan and zolmitriptan (shown in **Figure 30**), used for the treatment of migraine. These compounds belong to the class of tryptans, drugs characterized by a tryptamine nucleus which biological activity is attributed to interaction with serotonin receptors. In particular, they act as agonists of receptors 5-HT_{1B} and 5-HT_{1D}, predominantly distributed in the central nervous system and responsible for regulating many physiological activities.[141,142]

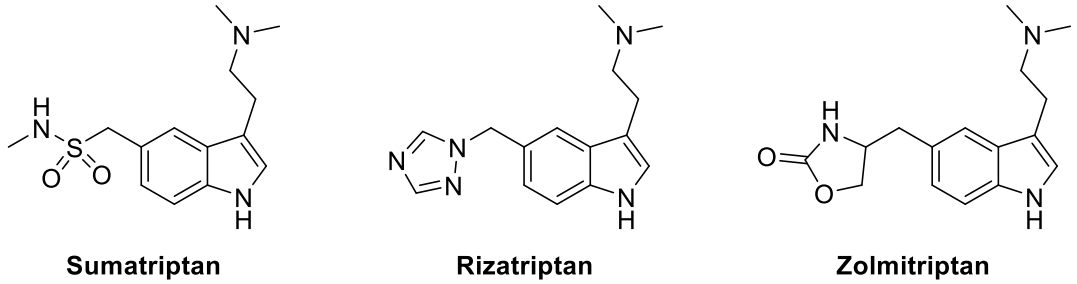

Figure 30. Tryptamine-based biologically active drugs.

A further example of indole derivative is Panobinostat (shown in **Figure 31**), a drug approved by FDA in 2015, sold by Novartis and used in combination with Bortezomib and Dexamethasone for the treatment of multiple myeloma. This molecule is an orally administered hydroxamic acid, which acts as no-selective HDACi, since it has shown preclinical activity in all four classes of HDACs.[143]

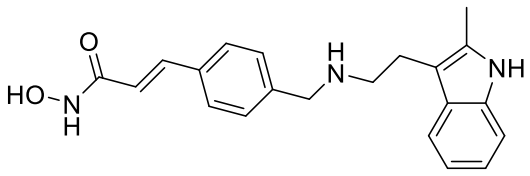

Panobinostat

Figure 31. Structure of Panobinostat used for the treatment of multiple myeloma.

The aim of this part of my PhD work was to synthesize new hybrid compounds containing aza-heterocycles and azelaic acid moiety.

The choice to bind some aza-heterocycles to azelaic acid is due to a series of circumstances. Our research group synthesized several hybrid systems with the azelayl scaffold bound to the 2-aminobenzothiazolyl moiety as shown in **Scheme 23**, which have shown an anticancer activity against the human cancer cell line HT-29 and some of them behaved as HDACi.[144]

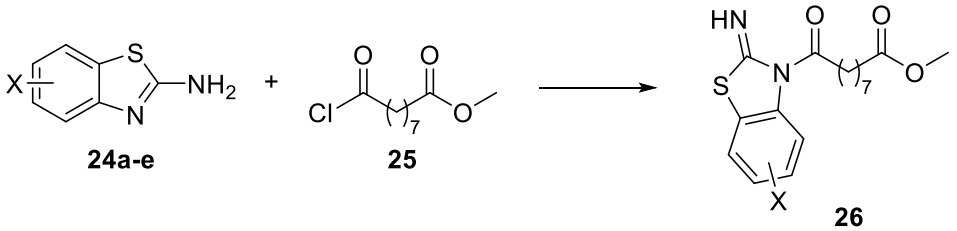

24a-e **25** **26**

a. X=H,
b. X=4-OMe,
c. X=6-OEt,
d. X=6-Me
e. X=6-Cl

Scheme 23. Synthesis of hybrids bearing benzothiazole and azelayl moieties.

To bind the benzothiazolyl group to the $–(CH_2)_7COOMe$ chain through an amide bond was inspired by the analogy of these structural hybrids with the structure of some HDACi, such as Vorinostat and 9-hydroxystearic acid (9-HSA), described in the previous chapter. In particular the long carbon chain constitutes a moiety of the endogenous cellular lipid 9-HSA with antiproliferative activity against cancer cells; 9-HSA, as well as his methyl ester, acts as a HDACi; and finally the total structure of the designed compounds is analogous to the well-known Vorinostat molecule. Based on the above considerations, we planned to synthesize similar novel derivatives with an azelayl scaffold bound through an amide bond to pyridine, 1,3-diazine, benzimidazole, benzotriazole and indole moieties. Moreover, the biological activity of these novel compounds was investigated on different cell lines, and

the more active ones were subjected to further experiments to analyze the effect on cell proliferation and histone acetylation.

2.2. Results and discussion

The novel heterocyclic derivatives were synthesized through a Schotten Bauman type reaction between the acyl chloride **25**, obtained reacting by the mono methyl ester of azelaic acid (**27)** with oxalyl chloride, and several nucleophiles. From aminopyridines **28a-c**, aminopyrimidines **28d-f**, benzimidazole **28g**, benzotriazole **28h** and indole **28i** the related derivatives **29a-i** shown in **Table 2** were obtained.

Table 2. Synthesis of aza-heterocycles derivatives **29a-i** bearing the azelayl moiety.

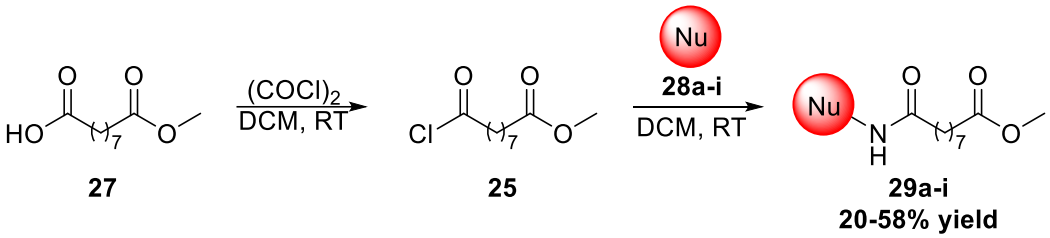

Entry	Nucleophile	Product	Yield[a]
1	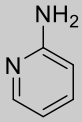 **28a**	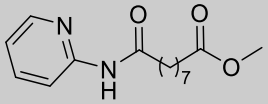 **29a**	39%
2	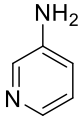 **28b**	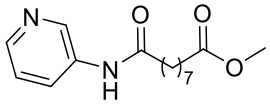 **29b**	55%
3	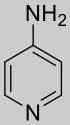 **28c**	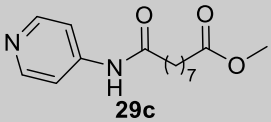 **29c**	42%
4	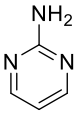 **28d**	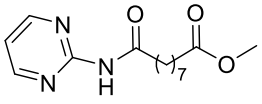 **29d**	32%
5	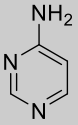 **28e**	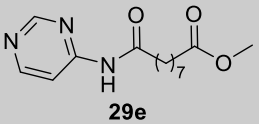 **29e**	40%
6	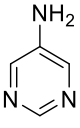 **28f**	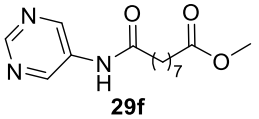 **29f**	26%

7	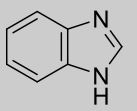	**28g**	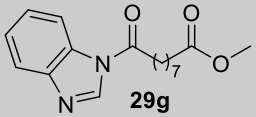 **29g**	50%
8	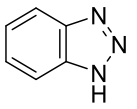	**28h**	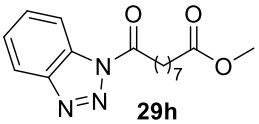 **29h**	20%
9	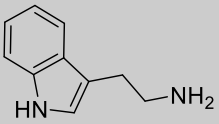	**28i**	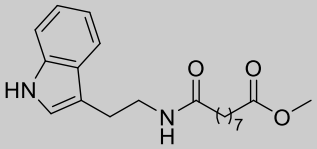 **29i**	58%

[a] Yields of pure product after FC.

The reactions between **25** and the aza-heterocycles **28a-i** were carried out in anhydrous dichloromethane in 1:2 relative molar ratio to neutralize the hydrochloric acid formed *in situ*. The reactions were performed under nitrogen atmosphere to avoid the hydrolysis of the acyl chloride **25** and checked through ^{1}H-NMR analysis to verify the disappearance of the acyl chloride. The yields, ranging from 20% to 58%, have not been optimized, and in some cases the mono methyl azelate (**27**) was recovered, likely due to a certain amount of hydrolyzed acyl chloride before the amidation reaction.

Concerning the reaction with 2-aminopyrimidine (**Table 2**, entry 4), the product **30**, formed from the double attack of acyl chloride **25** to amino group of **28d**, was also isolated (**Scheme 24**).

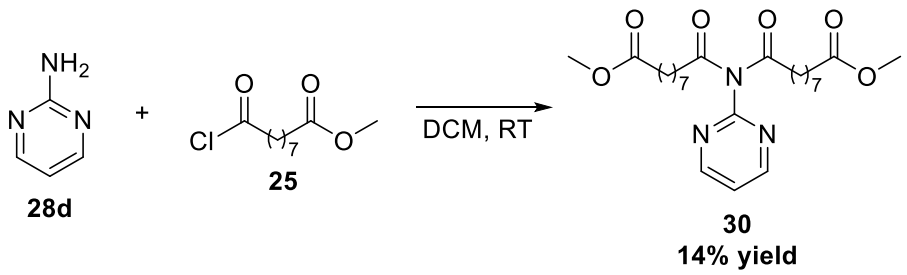

Scheme 24. Double attack of acyl chloride **25** on **28d** producing the derivative **30**.

This might be due to the stronger basicity of 2-aminopyrimidine respect to that of the other regioisomers, as supported by comparing the pK_a values of 2-aminopyrimidine and 4-aminopyrimidine (20.5 and 18.4 respectively).[145] All products obtained were purified through flash chromatrography and fully characterized. In cases 1,4 and 5, the structure was confirmed by nuclear Overhauser effect (NOE) NMR experiments, which indicate the formation of an exocyclic amide bond (**Table 2**).

Finally, only the triptamine derivative **29i** (**Table 2**, entry 9) was subjected to selective hydrolysis with LiOH (**Scheme 25**), getting the compound **31**, to compare its biological activity with that of the corresponding methyl ester **29i**.

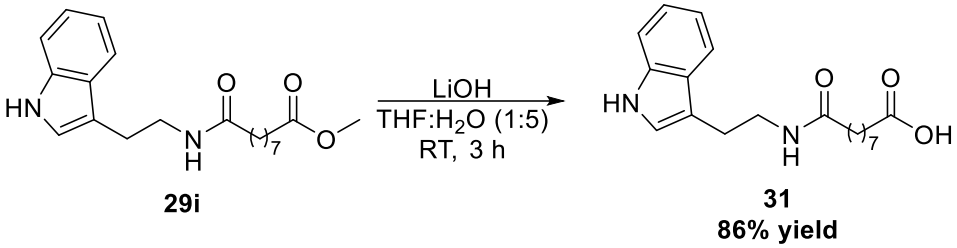

29i **31** **86% yield**

Scheme 25. Ester hydrolysis of the indole derivative **29i**.

In order to gain information on the activity of all compounds synthesized, biological tests were carried out on different cell lines by the research group of Prof. Natalia Calonghi of the Department of Pharmacy and Biotechnology of the University of Bologna. The biological activity of products **29a-h** and **30** was tested against U2OS (human osteosarcoma), HT29 (human colon adenocarcinoma), PC3 (human prostatic carcinoma), IGROV1 (human ovarian carcinoma), and HDFa (normal human adult fibroblast) cell lines. Instead, the biological activity of indole derivatives **29i** and **31** was tested against HT29, U2OS, IGROV1 and A431 (epidermoid carcinoma) cell lines.

Biological test

To investigate whether the novel compounds synthesized have a biological effect, *in vitro* preclinical assays were performed. Data obtained, listed in **Table 3**, were elaborated to assess the concentration of each compound required for 50% inhibition of cell viability (IC_{50}). Each value was calculated using Prism, fitted by means of sigmoidal fit.

Table 3. Half maximal inhibitory concentration (IC_{50}) of compounds in different cell lines after 48 h of treatment. The substrates are dissolved in DMSO 60 mM. (n.a. = not active).

Entry	Compound	U2OS	HDFa	HT29	PC3	IGROV1
1	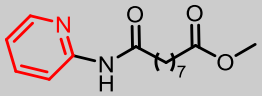 **29a**	>100 µM	n.a.	>100 µM	n.a.	n.a.
2	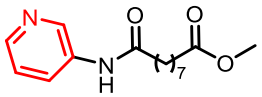 **29b**	>100 µM	n.a.	>100 µM	n.a.	n.a.

3	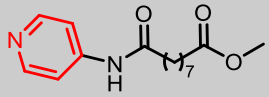 **29c**	>100 µM	n.a.	n.a.	n.a.	n.a.
4	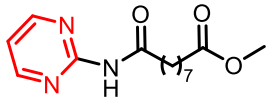 **29d**	50 µM	n.a.	n.a.	n.a.	n.a.
5	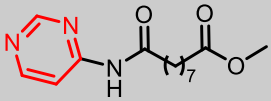 **29e**	>100 µM	n.a.	n.a.	n.a.	>100 µM
6	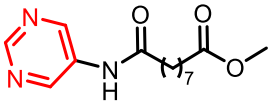 **29f**	n.a.	n.a.	>100 µM	>100 µM	>100 µM
7	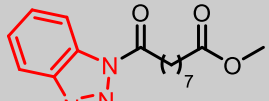 **29g**	n.a.	n.a.	n.a.	n.a.	>100 µM
8	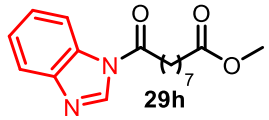 **29h**	50 µM	n.a.	>100 µM	>100 µM	n.a.
9	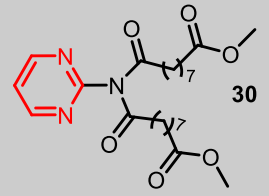 **30**	35 µM	n.a.	>100 µM	n.a.	n.a.

Among tumor cell lines, only U2OS was sensitive to compounds **29d**, **29h** and **30**. The well-known anticancer agents such as cisplatin, doxorubicin, and 5-fluorouracile, show an IC_{50} of 1.67 µM, 0.5 µM, and 0.3 µM, respectively in the U2OS cell line[146,147] but they suffer some disadvantages. They interfer with DNA repair mechanisms, inducing death in cancer and normal cells, and frequently they induce multidrug resistance. Our compounds show higher IC_{50}, but without to induce cytotoxic effects on normal cells.

Moreover, additional studies on the most active compounds against U2OS were performed: the effect on cell proliferation and the effect on histone acetylation.

The effect of these three substrates on DNA profiles of cultured cells were examinated by flow cytometry. As shown in **Figure 32**, compound **29d** and **29h** caused a slight accumulation in the synthesis (S) phase, instead compound **30** induced an increase in the gap 0/gap 1 (G0/G1) fraction, with concomitant decrease in the G2/mitosis (M) phase.

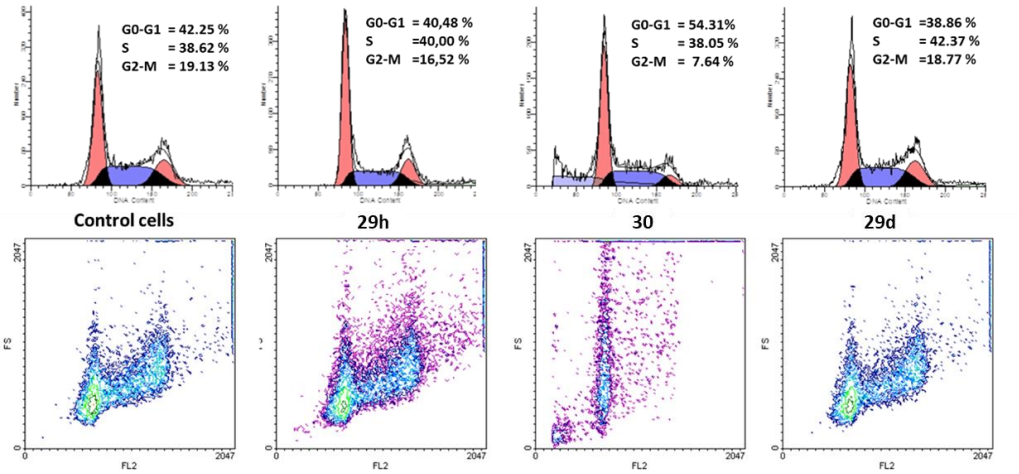

Figure 32. Flow cytometric assays of U2OS cells treated with compounds **29d**, **29h** and **30**.

To identify acetylated histones, the nuclear cell lysates were analyzed by Western blot using a 15% polyacrylamide gel electrophoresis. After electrophoresis, the proteins were transferred to a nitrocellulose membrane and then immunoblotted with an anti-acetyl lysine monoclonal antibody. As shown in **Figure 33**, the antibody could detect the accumulation of acetylated proteins induced in U2OS cells by treatment with compounds **29d**, **29h** and **30**. Differences in the density of bands are thought to reflect differences in protein acetylation levels. Histone acetylation signals were quantified by densitometry and normalized on histone H1. Histones H2/H3 acetylation increased by 28% upon treatment with **30** for 6 h with no effect on H4 acetylation, whereas compound **29h** induced hyperacetylation by 30% on histone H4 only. Interestingly, compound **29d** caused a post-transcriptional modification of both H2/H3 and H4 histones, increasing acetylation by 89% and 22%, respectively.

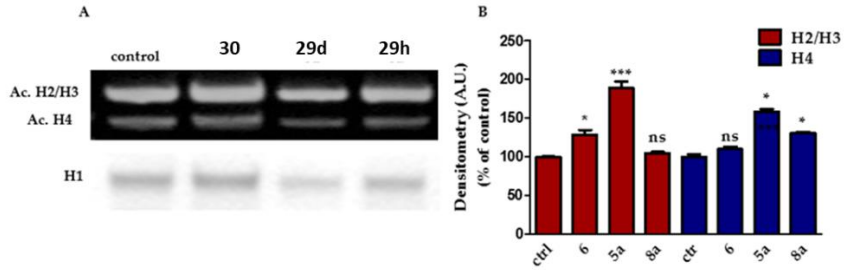

Figure 33. Effect of compounds **29d**, **29h** and **30** on histone acetylation levels. (A) Cell nuclear extracts were prepared and subjected to Western blot analysis for acetylated (Ac) histones H2/H3 and H4. Histone H1 was used as loading control. A representative experiment is shown, which was repeated three times. (B) Densitometric analysis of the bands (mean ± SD; n = 3) is shown. * $p \leq 0.05$, *** $p \leq 0.01$ vs. control.

These effects induced by the above compounds on histone acetylation are not associated with events involved in apoptotic death. The analysis of the nucleus labeling with Hoechst 33,342 showed indeed no morphological alterations typical of apoptotic cell death (**Figure 34**). However, the compounds induced a state of nuclear alteration, as shown in **Figure 34**, where it is possible to see how the compounds **29d** and **29h** caused a dim staining of nuclei, while compound **30** induced an increase in nuclear size.

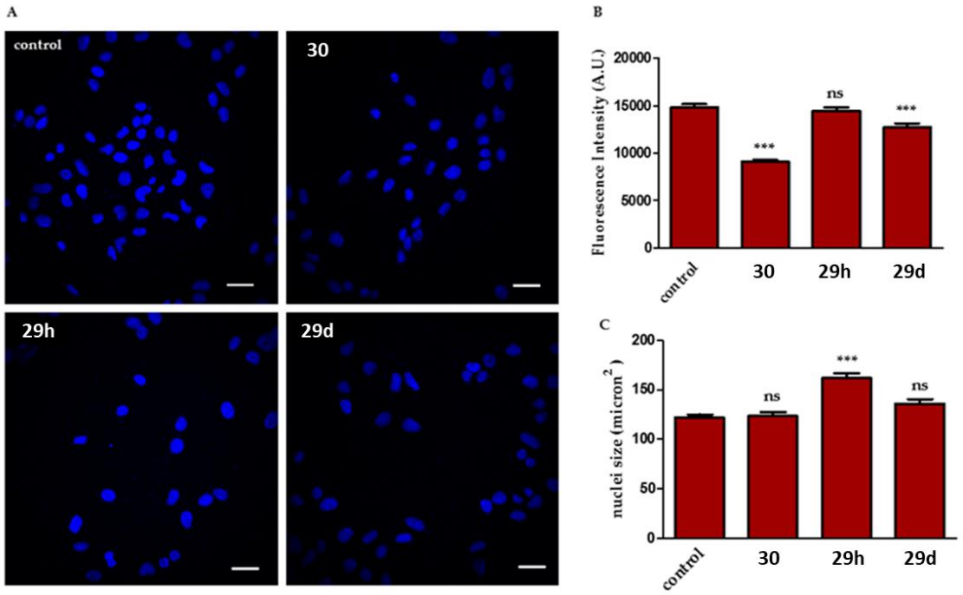

Figure 34. Confocal microscopy of Hoechst 33,342 nuclear staining in control and treated U2OS cells. (A) U2OS cells were treated with compounds **29d**, **29h** or **30** for 24 h, and then stained with Hoechst 33,342. Representative images are shown (scale bar = 20 μm). (B) Image densitometry measured using ImageJ (*** $p < 0.01$ with respect to control). (C) Cell size was estimated by Hoechst 33,342 staining by image densitometry using ImageJ (*** $p < 0.01$ with respect to control).

For indole derivatives, biological tests were carried out slightly different from other compounds synthesized for temporal reasons. *In vitro* growth inhibitory concentration was determined by incubating the cells with increasing concentrations (0.01–250 μM) of the compounds for 24 h. The data are collected in **Table 4**.

Table 4. IC_{50} of compounds in different cell lines after 24 h of treatment.

Entry	Compound	A431	HT29	IGROV1	U2OS
1	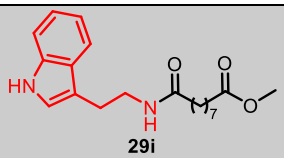 **29i**	303.8 µM	5.9 nM	289 µM	222 µM
2	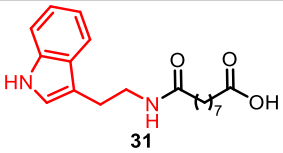 **31**	7.16 nM	96.5 nM	1.47 nM	468 nM

The indole derivatives showed a good activity: in particular compound **31** shows an activity at nanomolar concentration on all cancer cell lines tested. However, colon cancer is more sensitive to methyl ester derivative **29i**; while the acid derivative **31** is more active against the other cell lines than the corresponding methyl ester.

2.3. Conclusions

Novel structural hybrids between aza-heterocycles and azelayl scaffold were synthesized and their effect was investigated towards several tumor cell lines. Among them, only osteosarcoma U2OS cells have shown to be highly sensible to compounds **29d**, **29h** and **30**. Interestingly no compounds synthesized (listed in **Table 3**) induced cytotoxicity in the normal fibroblast cell line. The treatment of U2OS cells with **29d** and **29h** induced an accumulation in the S cell cycle phase, while compound **30** caused an increase in the G0/G1 fraction with a decrease in the G2/Mphase. These changes were associated with a post-transcriptional modification of both H2/H3 and H4 histones.

Tryptamine derivatives **29i** and its free acid form **31** showed a good biological activity towards all cancer cell lines tested. Since their structures recall those of compounds behaving as HDAC inhibitors, additional biological studies will be performed to investigate their effect on cell cycle and histone acetylation.

2.4. Experimental section

The reagents used, unless stated otherwise, were purchased from Sigma-Aldrich (Milan). CH_2Cl_2 was anhydrified by distillation over P_4O_{10}. Chromatographic purifications (FC) were carried out on glass columns packed with silica gel (Merck grade 9385, 230–400 mesh particle size, 60 Å pore size) at medium pressure. Thin layer chromatography (TLC) was performed on silica gel 60 F254 coated aluminium foils (Fluka). The spots related to azelaic acid were revealed using a bromocresol green solution (6% in ethanol).

The nuclear magnetic resonance spectra were recorded at 25 °C on Varian spectrometers Gemini 300, Mercury 400 or Inova 600 operating at 400 or 600 MHz (for ^{1}H NMR) and 100 or 150 MHz (for ^{13}C NMR), respectively. Signal multiplicities were established by DEPT-135 experiments. Chemical shifts were measured in δ (ppm) with reference to the solvent (δ= 7.26 ppm and 77.00 ppm for $CDCl_3$, δ= 1.96 ppm and 118.26 ppm for CD_3CN for ^{1}H and ^{13}C NMR, respectively). *J* values are given in Hz. ESI-MS and ESI-HRMS spectra have been recorded using a Waters ZQ 4000 and Xevo instrument, respectively. Melting points were measured on a Büchi 535 apparatus and are uncorrected.

Synthesis of methyl 9-chloro-9-oxononanoate (**25**)

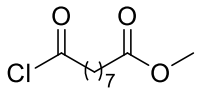

25

9-Methoxy-9-oxononanoic acid **27** (commercially available, 1.12 mL, 5.87 mmol) was introduced in a dried three-necked round bottom flask (equipped with a dropping funnel and kept under nitrogen atmosphere) and dissolved in 45 mL of anhydrous CH_2Cl_2. Oxalyl chloride (0.53 mL, 6.26 mmol) diluted in 5 mL of anhydrous CH_2Cl_2 was introduced in the funnel and added dropwise to the magnetically stirred solution over 10 min. The reaction was monitored through ^{1}H NMR spectroscopy. When the signals of the starting acid disappeared, the solvent was removed under reduced pressure, having care to avoid contact with moisture, and the residue was dissolved in anhydrous CH_2Cl_2, in amount calculated in order to obtain a 0.5 M solution of acyl chloride **25**. The chemical-physical data of compound **25** agreed with those reported in the literature.[84]

General procedure for the synthesis of compounds 29a-i

In a dried apparatus and under nitrogen atmosphere, to a magnetically stirred solution containing 0.001 mol of heterocyclic compound (selected within the **28a-i** series) dissolved in 5 mL of anhydrous CH_2Cl_2, 1.0 mL of a 0.5 M solution of **25** in CH_2Cl_2 (0.0005 mol)

was added. The reaction course was monitored by ^{1}H NMR spectroscopy until the acyl chloride signals disappeared. Then, water (10 mL) was added and the mixture was extracted with dichloromethane (3 x 10 mL). The organic layer was dried over anhydrous $MgSO_4$ and filtered. After removal of the solvent under reduced pressure, the product was purified by column chromatography on silica gel or by bulb-to-bulb distillation (0.01 mmHg).

Methyl 9-oxo-9-(pyridin-2-ylamino)nonanoate (**29a**).

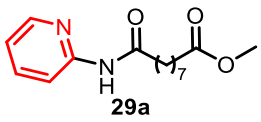

29a

Purified by FC (ethyl acetate/dichloromethane 40/60). White solid; 0.054g (39%); m.p. 59-60 °C; ^{1}H-NMR (600 MHz, $CDCl_3$, 25°C), δ (ppm): 8.43 (br. s, 1 H, NH), 8.25 (d, J = 5.2 Hz, 1 H, CH), 8.21 (d, J = 8.3 Hz, 1 H, CH), 7.69 (dt, J_1 = 7.2 Hz, J_2 = 1.7 Hz, 1H, CH), 7.02 (dd, J_1 = 7.1 Hz, J_2 = 5.1 Hz, 1 H, CH), 3.65 (s, 3 H, $COOCH_3$), 2.37 (t, J = 7.6 Hz, 2 H, CH_2CON), 2.28 (t, J = 7.6 Hz, 2 H, CH_2COOCH_3), 1.71 (quint., J = 7.5 Hz, 2 H, CH_2CH_2CON), 1.60 (quint, J = 7.1 Hz, 2 H, $CH_2CH_2COOCH_3$), 1.39–1.27 (m, 6 H, CH_2); ^{13}C-NMR (150 MHz, $CDCl_3$, 25°C) δ (ppm): 174.2, 171.8, 151.5, 147.6, 138.4, 119.6, 114.1, 51.4, 37.6, 34.0, 28.94, 28.9, 28.8, 25.2, 24.8; ESI-MS (*m/z*): 313 $[M + Cl]^-$; ESI-HRMS$^+$ (*m/z*): calculated for $C_{15}H_{22}N_2NaO_3^+$: 301.1523, found: 301.1528

Methyl 9-oxo-9-(pyridin-3-ylamino)nonanoate (**29b**).

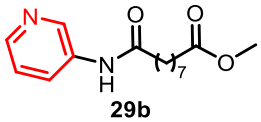

29b

Purified by FC (ethyl acetate/dichloromethane 40/60). White solid; 0.076g (55%); m.p. 75.5-77.7 °C; ^{1}H-NMR (600 MHz, $CDCl_3$, 25°C) δ (ppm): 8.80 (br.s, 1 H, NH); 8.58 (d, J = 2.3 Hz, 1 H, CH); 8.26 (d, J = 4.5 Hz, 1 H, CH); 8.20 (d, J = 8.1 Hz, 1 H, CH); 7.23 (dd, J_1 = 8.2 Hz, J_2 = 4.6 Hz, 1 H, CH); 3.63 (s, 3 H, $COOCH_3$); 2.35 (t, J = 7.8 Hz, 2 H, CH_2CON); 2.26 (t, J = 7.8 Hz, 2 H, CH_2COOCH_3); 1.67 (quint., J = 7.3 Hz, 2 H, CH_2CH_2CON); 1.56 (quint., J = 7.3 Hz, 2 H, $CH_2CH_2COOCH_3$); 1.34-1.23 (m, 6 H, CH_2); ^{13}C-NMR (150 MHz, $CDCl_3$, 25°C) δ (ppm): 174.4, 172.4, 144.3, 140.7, 135.5, 127.4, 123.8, 51.4, 37.2, 33.9, 28.8, 28.76, 28.72, 25.2, 24.7; ESI-MS (*m/z*): 279 $[M+H]^+$, 301 $[M+Na]^+$; ESI-HRMS$^+$ (*m/z*): calculated for $C_{15}H_{22}N_2NaO_3^+$: 301.1523, found: 301.1528.

Methyl 9-oxo-9-(pyridin-4-ylamino)nonanoate (**29c**).

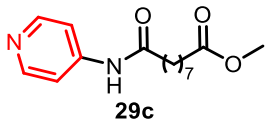

29c

Purified by FC (methanol/ethyl acetate 5/95). White solid; 0.059g (42%); m.p. 83-85 °C; ^{1}H-NMR (600 MHz, $CDCl_3$, 25°C) δ (ppm): 8.91 (s, 1 H, NH), 8.43 (d, *J* = 5.1 Hz, 2 H, CH), 7.56 (d, *J* = 5.1 Hz, 2 H, CH), 3.64 (s, 3 H, $COOCH_3$), 2.35 (t, *J* = 7.6 Hz, 2 H, CH_2CON), 2.28 (t, *J* = 7.6 Hz, 2 H, CH_2COOCH_3), 1.67 (quint., *J* = 7.4 Hz, 2 H, CH_2CH_2CON), 1.57 (quint., *J* = 7.4 Hz, 2 H, $CH_2CH_2COOCH_3$), 1.35-1.25 (m, 6 H, CH_2); ^{13}C-NMR (150 MHz, $CDCl_3$, 25°C) δ (ppm): 174.4, 172.7, 149.9, 146.0, 113.7, 51.5, 37.5, 33.9, 28.8, 28.77, 28.73, 25.1, 24.7; ESI-MS (*m/z*): 277 $[M-H]^-$, 313 $[M+Cl]^-$; ESI-HRMS$^+$ (*m/z*): calculated for $C_{15}H_{22}N_2NaO_3^+$: 301.1523, found: 301.1528.

Methyl 9-oxo-9-(pyrimidin-2-ylamino)nonanoate (**29d**).

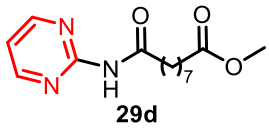

29d

Purified by FC (methanol/ethyl acetate 5/95). White solid; yield 0.067g (32%); m.p. 86.2-87.3 °C; ^{1}H-NMR (400 MHz, $CDCl_3$, 25°C) δ (ppm): 9.55 (br.s, 1 H, NH), 8.61 (d, *J* = 4.9 Hz, 2 H, CH), 6.97 (7, *J* = 4.9 Hz, 1 H, CH), 3.62 (s, 3 H, $COOCH_3$), 2.73 (t, *J* = 7.4 Hz, 2 H, CH_2CON), 2.26 (t, *J* = 7.6 Hz, 2 H, CH_2COOCH_3), 1.70 (quint., *J* = 7.3 Hz, 2 H, CH_2CH_2CON), 1.59 (quint., *J* = 7.0 Hz, 2 H, $CH_2CH_2COOCH_3$), 1.45-1.2 (m, 6H, CH_2); ^{13}C-NMR (100 MHz, $CDCl_3$, 25°C) δ (ppm): 174.2, 173.7, 158.2, 157.6, 115.9, 51.3, 37.3, 33.9, 28.93, 28.90, 28.8, 24.8 (two signals overlapped); ESI-MS (*m/z*): 280 $[M+H]^+$, 302 $[M+Na]^+$, 318 $[M+K]^+$; ESI-HRMS$^+$ (*m/z*): calculated for $C_{14}H_{21}N_3NaO_3^+$: 302.1475, found: 302.1481.

Methyl 9-oxo-9-(pyrimidin-4-ylamino)nonanoate (**29e**).

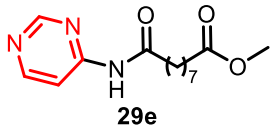

29e

Purified by FC (methanol/ethyl acetate 5/95). White solid; 0.056g (40%); m.p. 92.0-94.2 °C; ^{1}H-NMR (600 MHz, $CDCl_3$, 25°C) δ (ppm): 8.84 (s, 1 H, CH), 8.62 (d, *J* = 5.7 Hz, 1 H, CH), 8.18 (dd, J_1 = 5.9 Hz, J_2 = 1.2 Hz, 1 H, CH), 8.13 (br.s, 1 H, NH), 3.66 (s, 3 H, $COOCH_3$), 2.42 (t, *J* = 7.5 Hz, 2 H, CH_2CON), 2.30 (t, *J* = 7.2 Hz, 2 H, CH_2COOCH_3), 1.72 (quint., *J* = 7.2 Hz, 2 H, CH_2CH_2CON), 1.62 (quint., *J* = 7.1 Hz, 2 H, $CH_2CH_2COOCH_3$), 1.42-1.24 (m, 6 H, CH_2); ^{13}C-NMR (150 MHz, $CDCl_3$, 25°C) δ (ppm): 174.2, 172.5, 158.4, 158.2, 156.9, 110.2, 51.5, 37.7, 34.0, 28.9, 28.8, 24.9, 24.8; ESI-MS (*m/z*): 280 $[M+H]^+$, 302 $[M+Na]^+$, 318 $[M+K]^+$; ESI-HRMS$^+$ (*m/z*): calculated for $C_{14}H_{21}N_3NaO_3^+$: 302.1475, found: 302.1481.

Methyl 9-oxo-9-(pyrimidin-5-ylamino)nonanoate (**29f**).

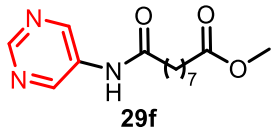

29f

Purified by FC (methanol/ethyl acetate 5/95). Orange solid; 0.036g (26%); m.p. 78.6-80.2 °C; ^{1}H-NMR (600 MHz, $CDCl_3$, 25°C) δ (ppm) 9.29 (s, 2 H, CH), 8.98 (s, 1 H, CH), 8.63 (br. s, 1 H, NH), 3.66 (s, 3 H, $COOCH_3$), 2.47 (t, *J* = 7.6 Hz, 2 H, CH_2CON), 2.31 (t, *J* = 7.3 Hz, 2 H, CH_2COOCH_3), 1.74 (quint., *J* = 7.4 Hz, 2 H, CH_2CH_2CON), 1.62 (quint., *J* = 7.4 Hz, 2 H, $CH_2CH_2COOCH_3$), 1.42-1.28 (m, 6 H, CH_2); ^{13}C-NMR (150 MHz, $CDCl_3$, 25°C) δ (ppm): 174.4, 172.5, 150.7, 147.2, 134.8, 51.5, 37.1, 34.0, 28.7, 25.0, 24.7; ESI-MS (*m/z*): 280 $[M+H]^+$, 302 $[M+Na]^+$, 318 $[M+K]^+$; ESI-HRMS$^+$ (*m/z*): calculated for $C_{14}H_{21}N_3NaO_3^+$: 302.1475, found: 302.1481.

Dimethyl 9,9'-(pyrimidin-2-ylazanediyl)bis(9-oxononanoate) (**30**).

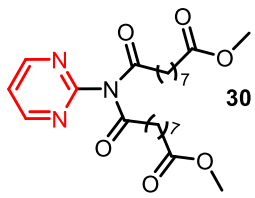

30

Purified by FC (methanol/ethyl acetate 5/95). Colourless liquid; 0.016g (14%); ^{1}H-NMR (600 MHz, $CDCl_3$, 25°C) δ (ppm): 8.81 (d, *J* = 4.7 Hz, 2 H, CH), 7.33 (t, *J* = 4.8 Hz, 1 H, CH), 3.59 (s, 6 H, $COOCH_3$), 2.47 (t, *J* = 7.4 Hz, 4 H, CH_2CON), 2.22 (t, *J* = 7.6 Hz, 4 H, CH_2COOCH_3), 1.60-1.48 (m, 8 H, $CH_2CH_2COOCH_3$), 1.29-1.18 (m, 12 H, CH_2), ^{13}C-NMR (150 MHz, $CDCl_3$, 25°C) δ (ppm): 175.0, 174.0, 159.3, 120.3, 51.2, 37.9, 33.8, 28.75, 28.70, 28.66, 28.60, 24.6, 24.0; ESI-MS (*m/z*): 498 $[M+Cl]^-$; ESI-HRMS$^+$ (*m/z*): calculated for $C_{24}H_{37}N_3NaO_6^+$: 486.2575, found: 486.2580.

Methyl 9-(1*H*-benzo[d]imidazol-1-yl)-9-oxononanoate (**29g**).

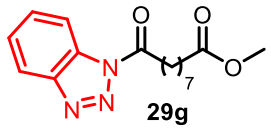

29g

Purified by bulb-to-bulb distillation at 150 °C and 0.1 mmHg. White solid; 0.032g (20%); m.p: 55.5-57.2 °C; ^{1}H-NMR (600 MHz, $CDCl_3$, 25°C) δ (ppm): 8.28 (d, *J* = 8.3 Hz, 1 H, CH), 8.10 (d, *J* = 8.0 Hz, 1 H, CH), 7.64 (t, *J* = 7.8 Hz, 1 H, CH), 7.49 (t, *J* = 7.8 Hz, 1 H, CH), 3.65 (s, 3 H, $COOCH_3$), 3.40 (t, *J* = 7.4 Hz, 2 H, CH_2CON), 2.30 (t, *J* = 7.6 Hz, 2 H, CH_2COOCH_3), 1.89 (quint., *J* = 7.8 Hz, 2 H, CH_2CH_2CON), 1.63 (quint., *J* = 7.5 Hz, 2 H, $CH_2CH_2COOCH_3$), 1.48 (quint., *J* = 7.7 Hz, 2 H, CH_2), 1.42-1.32 (m, 4 H, CH_2); ^{13}C-NMR (150 MHz, $CDCl_3$, 25°C) δ (ppm) 174.1, 172.5, 146.1, 131.1, 130.3, 126.0, 120.1, 114.4, 51.4, 35.4, 34.0, 28.9, 28.8, 24.8, 24.3; ESI-MS (*m/z*): 304 $[M+H]^+$, 326 $[M+Na]^+$.

Methyl 9-(1*H*-benzo[d][1,2,3]triazol-1-yl)-9-oxononanoate (**29h**).

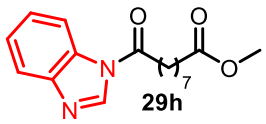

Purified by bulb-to-bulb distillation at 150 °C and 0.1 mmHg. White solid; 0.075g (50%); m.p. 83.0-84.3 °C; ^{1}H-NMR (600 MHz, $CDCl_3$, 25°C) δ (ppm): 8.40 (s, 1 H, CH), 8.25 (d, *J* = 7.9 Hz, 1 H, CH), 7.80 (d, *J* = 7.0 Hz, 1 H, CH), 7.43 (dt, J_1 = 8.5 Hz, J_2 = 1.2 Hz, 1 H, CH), 7.40 (dt, J_1 = 9.3 Hz, J_2 = 1.6 Hz, 1 H, CH), 3.67 (s, 3 H, $COOCH_3$), 3.00 (t, *J* = 7.4 Hz, 2 H, CH_2CON), 2.32 (t, *J* = 7.3 Hz, 2 H, CH_2COOCH_3), 1.88 (quint., *J* = 7.8 Hz, 2 H, CH_2CH_2CON), 1.64 (quint., *J* = 7.8 Hz, 2 H, $CH_2CH_2COOCH_3$), 1.47 (quint., *J* = 7.7 Hz, 2 H, CH_2), 1.43-1.32 (m, 4 H, CH_2); ^{13}C-NMR (150 MHz, $CDCl_3$, 25°C) δ (ppm): 174.2, 170.3, 143.9, 140.9, 131.5, 125.9, 125.0, 120.5, 115.6, 51.5, 35.9, 34.0, 28.9, 28.86, 28.84, 24.8, 24.2; ESI-MS (*m/z*): 303 $[M+H]^+$, 325 $[M+Na]^+$; ESI-HRMS$^+$ (*m/z*): Calculated for $C_{16}H_{21}N_3NaO_3^+$: 325.1523, Found: 325,1528.

Methyl 9-((2-(1*H*-indol-3-yl)ethyl)amino)-9-oxononanoate (**29i**)

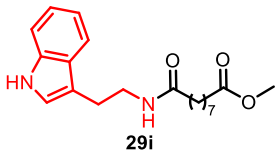

In a dried apparatus and under nitrogen atmosphere, tryptamine **28i** (160 mg, 1 mmol) was added to a magnetically stirred solution of crude freshly prepared compound **25** (0.3205g, 2 mmol). After 3 h at room temperature, ^{1}H-NMR analysis of a sample revealed disappearance of the signals belonging to **28i**. After removal of the solvent in vacuo and purification through FC (dichloromethane/methanol 95/5) 0.1995g (0.58 mmol, 58%) of pure **29i** was obtained as a light brown solid: m.p.:56.5–58.0 °C; ^{1}H-NMR (400 MHz, $CDCl_3$, 25°C) δ, ppm = 8.60 (s, 1 H, NH), 7.59 (d, *J* = 7.8 Hz, 1 H), 7.37 (d, *J* = 8.1 Hz, 1 H), 7.19 (t, *J* = 7.0 Hz, 1 H), 7.11 (t, *J* = 7.2 Hz, 1 H), 7.00 (s, 1 H), 5.65 (br.s, 1 H, NH), 3.67 (s, 3 H), 3.59 (q, *J* = 6.4 Hz, 2 H, CH_2CH_2NH), 2.97 (t, *J* = 6.4 Hz, 2 H), 2.29 (t, *J* = 7.3 Hz, 2 H, CH_2COOCH_3), 2.08 (t, *J* = 7.3 Hz, 2 H), 1.65–1.50 (m, 4 H), 1.26 (br.s, 6 H); ^{13}C-NMR (100 MHz, $CDCl_3$, 25°C) δ, ppm = 174.4, 173.5, 136.4, 127.3, 122.1 (CH), 122.0 (CH), 119.3 (CH), 118.5 (CH), 112.6, 111.3 (CH), 51.5 (CH_3), 39.7 (CH_2), 36.5 (CH_2), 34.0 (CH_2), 28.9 (CH_2, 2 signals overlapped), 28.8 (CH_2), 25.6 (CH_2), 25.2 (CH_2), 24.7 (CH_2); ATR-IR: (cm^{-1}): 3390, 3272, 1730, 1633, 737; ESI-MS (*m/z*): 345 $[M+H]^+$, 367 $[M+Na]^+$, 383 $[M+K]^+$; ESI-HRMS$^+$ (*m/z*): for $C_{20}H_{28}N_2NaO_3^+$ Calc. 367.19976, found 367.1998.

Synthesis of 9-((2-(1*H*-Indol-3-yl)ethyl)amino)-9-oxononanoic Acid (31)

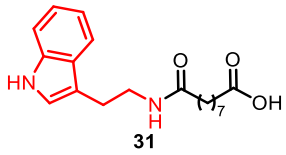

31

$LiOH \cdot H_2O$ (25 mg, 0.6 mmol) was added to a solution of compound **29i** (0.172 g, 0.5 mmol) in 25 mL of a 20% v/v solution of THF in H_2O and the mixture was stirred at room temperature for 3 h. After acidification with 10% aq. HCl, EtOAc and H_2O were added to the mixture. The extracted organic layer was dried over anhydrous $MgSO_4$ and concentrated and pure compound **31** was recovered in 86% yield (142 mg, 0.41 mmol) as pale grey solid: m.p.: 88.0–91.4 °C; ^{1}H-NMR (300 MHz, $CDCl_3$, 25°C) δ, ppm = 9.00-8.00 (br.s., 1 H, COOH), 8.42 (br.s, 1 H, NH), 7.58 (d, *J* = 7.8 Hz, 1 H), 7.37 (d, *J* = 7.8 Hz, 1 H), 7.19 (dt, J_1 = 7.8 Hz, J_2 = 1.2 Hz, 1 H), 7.11 (dt, J_1 = 7.8 Hz, J_2 = 1.2 Hz, 1 H), 7.01 (d, *J* = 1.9 Hz, 1 H), 5.63 (br.s, 1 H, NH), 3.60 (q, *J* = 6.2 Hz, 2 H), 2.96 (t, *J* = 7.0 Hz, 2 H), 2.38–2.28 (m, 4 H), 2.09 (t, *J* = 6.2, 2 H) 1.69–1.48 (m, 6 H), 1.39–1.29 (br.s, 2 H); ^{13}C-NMR (75 MHz, $CDCl_3$, 25°C) δ, ppm = 179.0, 173.5, 173.4, 127.3, 122.2 (CH), 122.1 (CH), 119.4 (CH), 118.6 (CH), 112.7, 111.3 (CH), 39.6 (CH_2), 36.7 (CH_2), 33.9 (CH_2), 30.3 (CH_2), 28.8 (CH_2), 28.7 (CH_2), 25.5 (CH_2), 25.2 (CH_2), 24.6 (CH_2); ^{1}H-NMR (600 MHz, CD_3CN, 25°C) δ, ppm = 9.17 (br.s, 1 H, NH), 7.59 (d, *J* = 8.0 Hz, 1 H), 7.40 (d, *J* = 8.2 Hz, 1 H), 7.14 (t, *J* = 8.2 Hz, 1 H), 7.09 (d, *J* = 1.6 Hz, 1 H), 7.06 (t, *J* = 8.0 Hz, 1 H), 6.53 (br.s, 1 H, NH), 5.80-3.70 (br.s., 1 H, COOH), 3.46 (q, *J* = 7.0 Hz, 2 H), 2.91 (t, *J* = 7.2 Hz, 2 H), 2.27 (t, *J* = 7.6, 2 H), 2.09 (t, *J* = 7.7 Hz, 2H), 1.60–1.48 (m, 4 H) 1.34–1.20 (m, 6 H); ^{13}C-NMR (150 MHz, CD_3CN, 25°C) δ, ppm = 175.4, 174.1, 137.5, 128.5, 123.5 (CH), 122.3 (CH), 119.7 (CH), 119.4 (CH), 113.4, 112.2 (CH), 40.5 (CH_2), 36.8 (CH_2), 34.2 (CH_2), 29.60 (CH_2), 29.58 (CH_2), 29.54 (CH_2), 26.4 (CH_2), 26.0 (CH_2), 25.5 (CH_2); ATR-IR: (cm^{-1}): 3388, 3269, 1710, 1631; ESI-MS (*m/z*): 331 $[M+H]^+$, 353 $[M+Na]^+$, 369 $[M+K]^+$; ESI-HRMS (*m/z*): for $C_{19}H_{26}N_2NaO_3^+$ Calc. 353.18411, found 353.1841.

Cell culture

The human prostate cancer (PC3), human colon cancer (HT29), human bone osteosarcoma (U2OS), normal human adult fibroblast (HDFa) cell lines were purchased from American Type Culture Collection (ATCC, Manassas, VA); the human ovarian cancer cell line (IGROV1) has been kindly provided by Istituto Nazionale Tumori (IRCCS, Milano, Italy). Cells were cultured in RPMI 1640 medium (Labtek Eurobio, Milan, Italy), supplemented with 10% FCS (Euroclone, Milano, Italy) and 2mM L-glutamine (Sigma-Aldrich, Milano, Italy), at 37 °C and 5% CO_2 atmosphere. The compounds were dissolved in DMSO in a

60mM stock solution. In cell treatments, the final DMSO concentration never exceeded 0,1%.

MTT assay

U2OS were seeded at 1.5 × 10^4 cells/well in a 96-well culture plastic plate (Orange Scientific, Braine-l'Alleud, Belgium) and after 24 h of growth, cells were exposed for additional 48 h to increasing concentrations of compounds (0.1 μM and 500 μM) solubilized in RPMI 1640 medium. On the day of measurement, the culture medium was replaced with 0.1 mL of 3-(4,5-dimethylthiazolyl-2)-2,5-diphenyltetrazolium bromide (MTT, Sigma-Aldrich) dissolved in PBS at the concentration of 0.2 mg/mL, and samples were incubated for 2 h at 37°C. To dissolve the blue-violet formazan salt crystals formed, 0.1 mL of isopropyl alcohol was added to each well and incubated for 20 min. The absorbance at 570 nm was measured using a multiwell plate reader (Wallac Victor2, PerkinElmer), viability was compared with that of untreated cells, used as controls.

Cell cycles

For cell cycle assay U2OS cells were treated for 24 h with 35 μM of compound **30**, or 50 μM of **29d**, or 50 μM of **29h**, detached with 0.11% trypsin 0.02% ethylenediaminetetraacetic acid (EDTA), washed in PBS, and centrifuged. The pellet was resuspended in 0.01% Nonidet P-40 (Sigma-Aldrich, S.Louis, MO), 10 μg/mL RNase (Sigma-Aldrich), 0.1% sodium citrate, and 50 μg/mL propidium iodide (PI), for 30 min at room temperature in the dark. PI fluorescence and Forward Scatter (FS) signals were analysed by using a Beckman Coulter Epics XL-MCL flow cytometer. DNA distribution in the cell cycle was analysed by the MODFIT 5.0 software. Being the signal collected by a multichannel analyser, the mean of the FS distribution is expressed as mean channel.

Histones extraction, SDS-PAGE and Western Blot

U2OS were cultured with **29d**, or **30**, or **29h**, for 6 h, and the histone fraction was immediately extracted. Cells were harvested using 0.11% trypsin and 0.02% EDTA, washed twice with 10 mM sodium butyrate (NaBu) in PBS, and nuclei were isolated according to Amellem et al..[148] The nuclear pellet was suspended in 0.1 ml of ice-cold water using a Vortex mixer, and concentrated H_2SO_4 was added to the suspension to give a final concentration of 0.4 N. After incubation at 4 C for 1 h, the suspension was centrifuged for

5 min at 14,000 g, and the supernatant was taken and mixed with 1 ml of acetone. After overnight incubation at -20°C, the coagulate material was collected by microcentrifugation and air-dried, and proteins were quantified using a protein assay kit (Bio-Rad, Hercules, CA). Histones were analyzed as previously described.[64] Briefly, histones were resolved by 15% SDS–PAGE and immunoblotted with anti-acetylated lysine antibody (Cell Signaling Technology, Beverly, MA), and detection of immunoreactive bands was performed with a secondary antibody conjugated with horseradish peroxidase and developed with an enhanced chemiluminescence (ECL) system, developed with the enhanced chemiluminescence system Clarity Western (Bio-Rad, Hercules, CA), and quantification was done by Fluor-S Max MultiImager (Bio-Rad). Histone acetylation signals were quantified by densitometry and normalized on histone H1.

Hoechst 33342 staining

Nuclear morphology was assayed using a specific dye Hoechst 33342. U2OS treated cells were washed, fixed and then stained with 1µM Hoechst 33342 for 15min. Samples were embedded in Mowiol and analyzed using a Nikon C1s confocal laser-scanning microscope, equipped with a Nikon PlanApo 40X, 1.4-NA oil immersion lens. Images were quantified by ImageJ software.

References

[111] Micheletti, G.; Calonghi, N.; Farruggia, G.; Strocchi, E.; Palmacci, V.; Telese, D.; Bordoni, S.; Frisco, G.; Boga, C. Molecules, **2020**, *25*, 404, 1-17.

[112] Brunton, L.; Knollmann, B.; Hilal-Dandan, R.*Goodman & Gilman's the Pharnacological basis of Therapeutics*,13th ed.; McGraw-Hill: New York, NY, USA, 2013; ISBN 13 97812595847.

[113] Pozharskii, A.F.; Soldatenkov, A.T.; Katritzky, A.R. Chemistry, Biochemistry and Applications; Wiley-VCH: Weinheim, Germany, **2011**; ISBN 978-0-470-71411-9.

[114] Neha, D.A.R.; Kumar, R.; Kumar, V. *Curr. Org. Synth*, **2018**, *15*, 321–340.

[115] Chourasiya, S.S.; Kathuria, D.; Wani, A.A.; Bharatam, P.V. *Org. Biomol. Chem.*, **2019**, *17*, 8486–8521.

[116] Kalaria, P.N.; Karad, S.C.; Raval, D.K.A. *Eur. J. Med. Chem.*, **2018**, *158*, 917–936.

[117] a) Pagani, G.A.; Abbotto, A. *Chimica etrociclica*, **1995**, Piccin Nuova Libraria S.p.A.-Padova, 387-398; b) Hantzsch, A.*Chem. Berichte*.**1881**, *14*, 1637–1638.

[118] Baran, R. *Essentials of heterocyclic chemistry I*, handbook.

[119] Kress, T.J. *J. Org. Chem.*, **1985**, *50*, 3073-3076.

[120] Javanovic, M.V. *Can. J. Chem.*, **1984**, *62*, 1176.

[121] Pradhan, B.P.; Ghosh, P. *Ind. J. Chem.*, **1993**, *32B*, 590-591.

[122] Ghosh, P.; Mandal, A. *Green Chem. Lett. Rev.*, **2012**, *5 (2)*, 127-134.

[123] Higashio, Y.; Shoji, T. *Appl Catal. A-Gen*, **2004**, *260*, 251-259.

[124] Hinman, R.L.; Lang, J. *J. Am. Chem. Soc.*, **1964**, *86*, 18, 3796–3806.

[125] Fischer, E.; Jourdan, F. *Ber.*, **1883**, *16*, 2241.

[126] Madelung, W. *Ber.*, **1912**, *45*, 1128-1134.

[127] Bartoli, G.; Palmieri, G.; Bosco, M.; Dalpozzo, R. *Tetrahedron. Lett.*, **1989**, *30*, 2129-2132.

[128] Ito, Y.; Kobayashi, K.; Saegusa, T. *J. Am. Chem. Soc.*, **1977**, *99 (10)*, 3532-3534.

[129] Lin, Y.L.; Huang, R.L.; Chang, C.M.; Kuo, Y.H. *J. Nat. Prod.*, **1997**, *60*, 982–985.

[130] Roggen, H.; Charnock, C.; Gundersen, L. *Tetrahedron*, **2009**, *65*, 5199-5203.

[131] Fournel, M.; Bonfils, C.; Hou, Y.; Yan, P.; Trachy Bourget M.C.; Kalita, A. *Mol Cancer Ther*, **2008**, *7*, 759–768.

[132] Zwergel, C.; Stazi, G.; Valente, S.; Mai, A. *J. Clin. Epigen.*, **2016**, *2*, 1–15.

[133] Razak, A.; Hotte, S.H.; Siu,, L.L.; Chen, E.X.; Hirte, H.W.; Powers, J. *Br J Cancer*, **2011**, *104*, 756–762.

[134] Novotny-Diermayr, V.; Hart, S.; Goh, K.C.; Cheong, A.; Ong, L.; Hentze, H.; Pasha, M.K.; Jayaraman, R.; Ethirajulu, K.; Wood, J.M. *Blood Cancer J.*, **2012**, *2*, 1-10.

[135] Moen, M.D.; McKeage, K.; Plosker, G.L.; Siddiqui, M.A. *Drugs*, **2007**, *67*, 299–320.

[136] Siddiqui, M.A.; Scott, L.J. *Drugs*, **2007**, *67*, 805–820.

[137] Konstantinopoulos P.A.; Cheng, S.; Wahner Hendrickson, A.E.; Penson, R.T.; Schumer, S.T.; Doyle, L. A.; Lee, E.K.; Kohn, E.C; Duska, L.R.; Crispens, M.A.; Olawaiye, A.B.; Winer, I.S.; Barroilhet, L.M.; Fu, S.; McHale, M.T.; Schilder, R.J.; Färkkilä, A.; Chowdhury, D.; Curtis, J.; Quinn, R.S.; Bowes, B.; D'Andrea, A.D.; Shapiro, G.I.; Matulonis, U.A. *Lancet Oncol.*, **2020**, *21(7)*, 957-968.

[138] Hall, A.B.; Newsome, D.; Wang, Y.; Boucher, D.M.; Eustace, B.; Gu, Y.; Hare, B.; Johnson, M.A.; Li, H.; Milton, S.; Murphy, C.E.; Takemoto, D.; Tolman, C.; Wood, M.; Charlton, P.; Charrier, J.; Furey, B.; Golec, J.; Reaper, P.M.; Pollard, J.R. *Oncotarget*, **2014**, *5*, 5674-5685.

[139] Ni, F.; Tang H.; Wang, C.; Wang, Z.; Yu, F.; Chen, B.; Sun, L. *Cancer Manag. Res.*, **2019**, *11*, 8391-8405.

[140] Thompson, E.M.; Nagata, S.; Tsuji, F.I. *Proc. Natl. Acad. Sci. USA*, **1989**, *86*, 6567-6571.

[141] Chadha, N.; Silakari, O. *Eur. J. Med. Chem.*, **2017**, *134*, 159-184.

[142] Tepper, S.; Rapoport, A. M.; Sheftell, F.D. *Arch. Neurol.*, **2002**, *59*, 1084-1088.

[143] Eleutherakis-Papaiakovou, E.; Kanellias, N.; Kastritis, E.; Gavriatopoulou, M.; Terpos, E.; Dimopoulos, M.A. *J. Oncol.*, **2020**, *2020*, 1-11.

[144] Boga, C.; Micheletti, G.; Orlando, I.; Strocchi, E.; Vitali, B.; Verardi, L.; Sartor, G.; Calonghi, N. *Curr. Org. Chem.*, **2018**, *22(16)*, 1649-1660.

[145] Harris, M.G.; Stewart, R. *Can. J. Chem.*, **1977**, *55*, 3800-3806.

[146] Jiang, K.; Zhang, J.; Ji, M.; Gai, P.; Lv, Q. *J. BUON*, **2019**, *24*, 1706–1711.

[147] Shin, S.H.; Choi, Y.J.; Lee, H.; Han-Soo Kim, H.-S.; Seo, S.W. *Tumor Biol.*, **2016**, *37*, 1591–1598.

[148] Amellem, O.; Stokke, T.; Sandvik, J.A.; Pettersen, E.O. *Exp. Cell Res.*, **1996**, *227*, 106–115.

Chapter III: Potential CDC20 inhibitors: Synthesis and biological evaluation of Apcin analogues

3.1. Introduction

The progression of the cell cycle relies on the periodic fluctuations of the activities of cyclin-dependent kinases (CDKs). Activation of CDK1 is required for the execution of some events during mitosis whereas inactivation of CDK1 is a prerequisite for the exit from mitosis. An important mechanism for the inactivation of CDK1 is the degradation of its positive regulatory subunits, mitotic cyclins A and B, through the ubiquitin-proteasome pathway. In addition, the same ubiquitin-dependent degradation that degrades mitotic cyclins is also responsible for the degradation of an anaphase inhibitor called APC/C. This inhibitor is a ubiquitin ligase composed of 19 subunits and it is the major driving force controlling the cell cycle process, especially in M and G1 phases. APC/C targets are differentially regulated throughout the cell cycle by two mutually exclusive activator proteins, CDC20 and CDH1, a CDC20 homologue protein. These proteins target the APC/C to specific sets of substrates at different times in the cell cycle.[149]

The cell-division cycle is characterized by a series of processes that are coordinated by core cell cycle regulatory proteins. The molecular understanding of the cell cycle began when Lee Hartwell and coworkers isolated Cell Division Cycle (CDC) mutants of *S. cerevisiae* that failed to execute or complete key cell-cycle events, such as DNA replication or mitosis.[149] Among the original Hartwell mutant collection there were the CDC20 mutants that arrest cell division in mitosis and fail to initiate anaphase and chromosome segregation. Molecular cloning of the CDC20 gene revealed that it encodes a protein related to the β subunit of trimeric G proteins.[149] Both CDC20 and Gβ contain seven WD40 repeats that form a seven-bladed β propeller structure ideally suited for mediating protein-protein interactions (**Figure 35**).

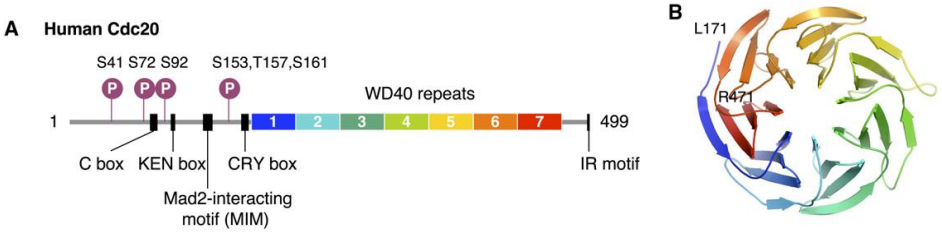

Figure 35. (A): Domain structure of CDC20. (B): Structure model of the WD40 domain of human CDC20.[149]

However, the biochemical functions of CDC20 remained obscure until the discovery of the anaphase-promoting complex/cyclosome (APC/C).[150]

Hence, the *S. cerevisiae* CDC20 mutants fail to initiate anaphase, suggesting that CDC20 might be required for the activation of APC/C at the metaphase-anaphase transition. This finding suggests that the CDC20/CDH1 family of proteins serves as substrate-specific activator of APC/C. Thus, CDC20 activates APC/C predominantly in mitosis when CDK activities are high whereas CDH1 mainly interacts with APC/C in telophase/G1 when CDK activities are low.

These two mediators appear to have opposite effects in the process of carcinogenesis, in particular CDH1 has a function as a suppressor of carcinogenesis while CDC20 reveals a pro-oncogenic function. It is deduced the importance of CDC20 as target for the treatment of human cancer, where the expression of this protein is increased towards healthy cells.

The research of compounds able to inhibit the interaction between APC/C and CDC20 has strongly emerged gaining a great deal of interest in recent years as useful tool for the design of CDC20 inhibitors, providing a therapeutic window in multiple human malignancies.

Recently it was discovered a new molecule called Apcin (APC inhibitor) which binds to CDC20, inhibiting the anaphase promoting complex.[150]

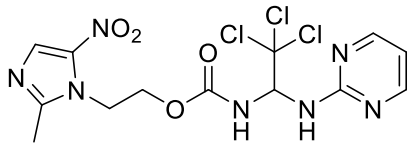

Apcin

Figure 36. Chemical structure of Apcin.

Analysis of the crystal structure of the Apcin-CDC20 complex suggests that Apcin occupies the D-box-binding pocket on the side face of the WD40-domain (**Figure 37**).[96] The binding mode of Apcin is consistent with the structure-activity relationship, as the pyrimidine ring and aminal nitrogens make hydrogen bonds with backbone atoms from D177. The hydrophobic trichloromethyl group is buried in the pocket occupied by leucine of the D-box.

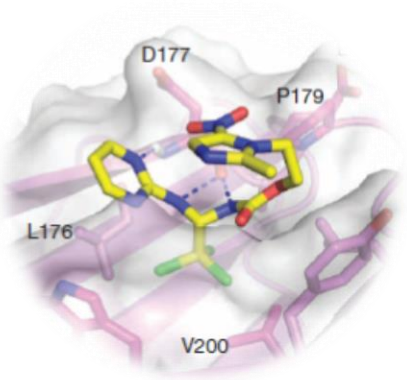

Figure 37. Apcin binds to the D-box binding site of CDC20.[96]

It was demonstrated that this novel cell-permeable molecule shows biological activity towards some human cancer cell lines.[151] For example, it is able to induce metaphase arrest and apoptosis in two multiple myeloma cell lines, LP-1 and RPMI-8226.[152] Moreover, the activity increases significantly, compared to single treatments, when Apcin is combined with proTAME,[96] a prodrug which binds to the APC and prevents its activation by CDC20. This synergic effect suggests that targeting several weak protein-protein interactions could be a good strategy to block protein complexes such as the APC/C. In addition, Apcin inhibits osteosarcoma cell growth inducing apoptosis on MG-63 and U2OS cells in a time- and dose-dependent manner, indicating that this molecule could have the therapeutic potential for the osteosarcoma treatment.[153]

Another CDC20 inhibitor is Withaferin A (WA), a steroidal lactone derived from *Acnistus arborescens* with anticancer activity towards several solid and hematological cancer cell lines.[154]

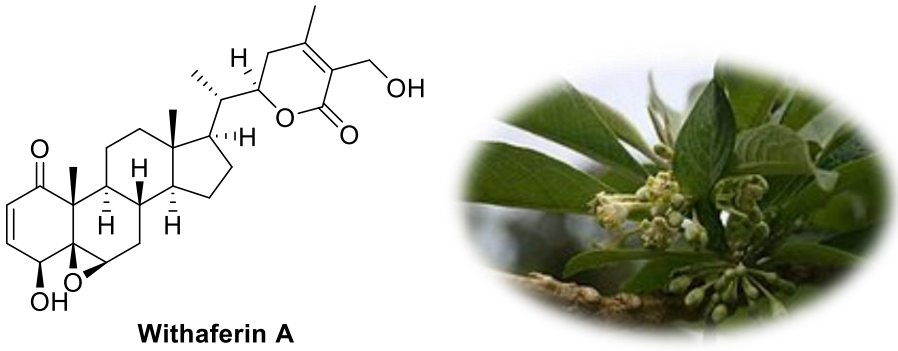

Figure 38. Chemical structure of WA and *Acnistus arborescens*.

This bioactive compound exhibits its biological activity through enhanced degradation of CDC20, inducing apoptosis and cell cycle arrest at G2/M checkpoint in different acute

leukemia cell lines[155-156] and in primary acute myeloid leukemia (AML) cells.[157] Given that it has been reported that both Withaferin A and Apcin are able to suppress CDC20 activity, Apcin could be considered a promising candidate against AML.

In fact, it is upregulated across several cancer types, including aneuploid compared with euploid acute myeloid leukemia.[158]

Studies on structure-activity relationship of apcin revealed the importance of trichloromethyl and aminopyrimidyl group on the biological activity (**Figure 39**).[96] The replacement of the pyrimidine moiety with a pyridine group (apcin-P) reduced activity slightly, but the replacement with a morpholino group (apcin-M) eliminated activity. In contrast, elimination of the nitro-imidazole moiety (apcin-A) had little effect.[150]

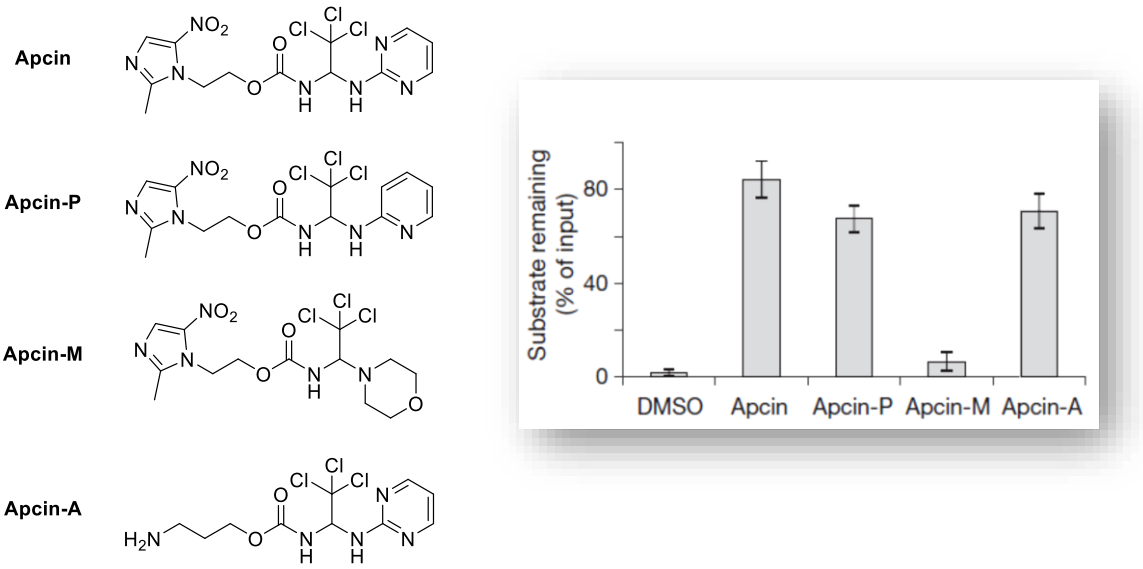

Figure 39. Structure of Apcin and its derivatives and related effects (200 μM) on proteolysis of an *N*-terminal fragment of cyclin B1 (cycB1-NT) in mitotic Xenopus egg extract.[150]

Structural modifications both on pyrimidine and imidazole moiety improves considerably the biological activity compared with that of Apcin. Zhuon Chen and coworkers designed and synthesized a series of 2,2,2-trichloro-1-carbamate derivatives as CDC20 inhibitors,[159] among which the most active compound (**Figure 40**) induced apoptosis in MCF-7 (breast cancer), A375 (melanoma), HepG2 (hepatocellular carcinoma), and Hela (cervical cancer) cell lines.

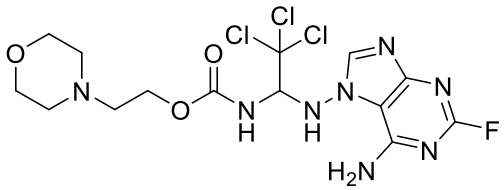

Figure 40. CDC20 inhibitor with anticancer activity.

Furthermore, it had approximately the same binding affinity with Apcin in Surface Plasmon Resonance (SPR) assays, suggesting that another mechanism of action, different from that discussed above, might exist.

In this context, I focused attention on benzothiazoles, a class of versatile fused heterocycles with extensive pharmaceutical applications. In recent decades, the benzothiazole nucleus has been considered as a promising pharmacophore owing its presence in anticonvulsant,[160] antihelmintic,[161] neuroprotective,[162] antiglutamate,[163] antimalarial,[164] antitubercular,[165] antimicrobial,[166] anti-inflammatory[167] and anticancer agents.[168-169]

For example, this motif is present in Riluzole and Phortress (**Figure 41**).

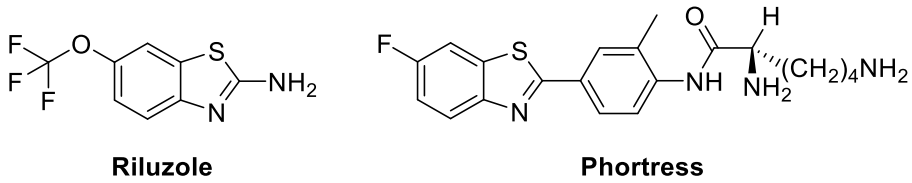

Figure 41. Benzothiazole derivatives with biological activity.

Riluzole is a drug approved by FDA for the treatment of amyotrophic lateral sclerosis (ALS), a neurodegenerative disease that involves the progressive loss of central and peripheral motor neurons. It is a glutamate receptor antagonist acting by blocking voltage-dependent sodium channels, thus decreasing the amount of glutamate released by the presynaptic termination.[170]

Phortress is a prodrug in clinical phase I to treat the ovarian and breast cancer, which acts *via* binding to Arylhydrocarbon Receptor (AhR), inducing expression of CYP1A1, a cytochrome P450 isoform, followed by the formation of adducts in DNA.[171]

Based on the above, we designed, synthesized and characterized novel Apcin analogues, containing heterocyclic moieties found in many compounds of biological activity but maintaining the 1,1,1-thrichloroethyl core, essential for the biological activity. Moreover, the novel compounds were subjected to biological activity evaluation towards a panel of solid and hematological cancer cell lines.

3.2. Results and discussion

At first, we planned the synthesis of compounds **33** and **34**, bearing both tryptamine and trichloromethyl moieties (**Scheme 26**). Tryptamine (**28i**) was treated with HCl 37% and potassium cyanate to give the ureido derivative **32**, which, after reaction with chloral hydrate, led to the formation, depending on the experimental conditions used, of the derivatives **33** or **34** in 50% and 93% yield respectively.

After obtaining compound **35** by chlorination of **34** with $SOCl_2$, we tried to functionalize it by nucleophilic substitution with 2-aminopyrimidine (**28d**) under different conditions summarized in **Table 5**. Initially, compound **35** was dissolved in CH_3CN and reacted with 2-aminopyrimidine in the presence of Et_3N under reflux conditions for 12 hours. After preparative TLC on silica gel, compound **36** was isolated in 7% yield. It should be noted that the yield obtained is similar to that reported in the literature for the synthesis of Apcin.[96] We tried to improve the yield, carring out the reaction in the same conditions but under microwaves irradiation (300 W) at 85°C for 2 hours or using dioxane as solvent and 2 equivalents of 2-aminopyrimidine, the final product has not been detected in both experiments.

Moreover, the compound **34** was treated directly with 2-aminopyrimidine both under Mitsunobu conditions and in presence of $CsOH{\cdot}H_2O$ under microwaves irradiation (300 W) at 90°C for 2 hours but the desired product has not been detected either in this case.

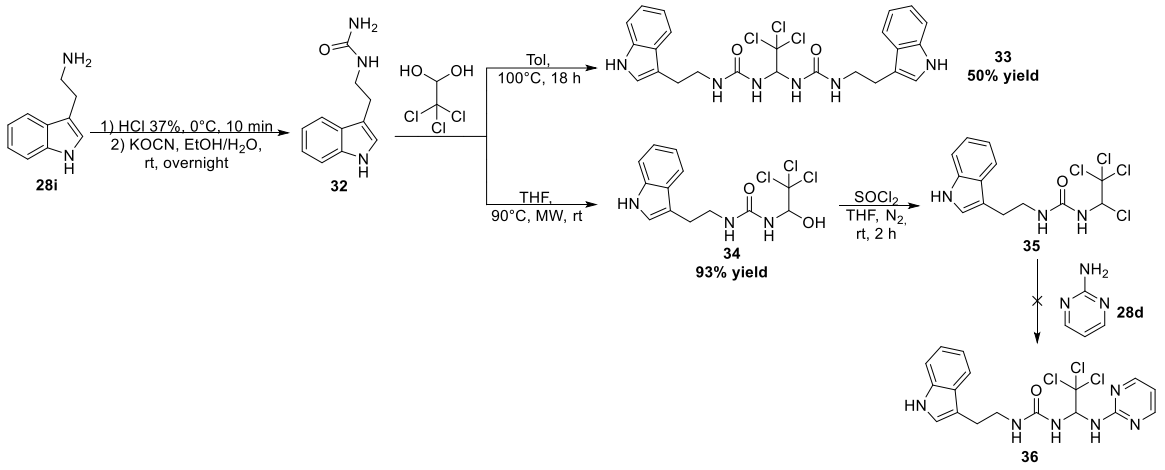

Scheme 26. Synthetic pathway to obtain **33**, **34** and **36**.

Table 5. Reaction conditions to obtain **36** starting from **35** and 2-aminopyrimidine.

Entry	Solvent	Base	Temperature	Time	Yield
1	MeCN	Et_3N	85°C reflux	12 h	7%
2	MeCN	Et_3N	85°C MW	2 h	n.d.
3	Dioxane	/	80°C	18 h	n.d.

Given the difficulties encountered to obtain **36**, we focused our efforts to synthesize 2,2,2-trichloro-*N*-(pyrimidin-2-yl)ethane-1,1-diaminyl derivatives **39-43** bearing benzothiazole (**39a-e**), indole (**40**, **41**), benzofurazan (**42a,b**) and pyrimidine (**43**) moieties bound to 2-aminopyrimidine through 1,1,1-trichloroethyl unit. The multistep synthetic procedure adopted is shown in **Scheme 27**.

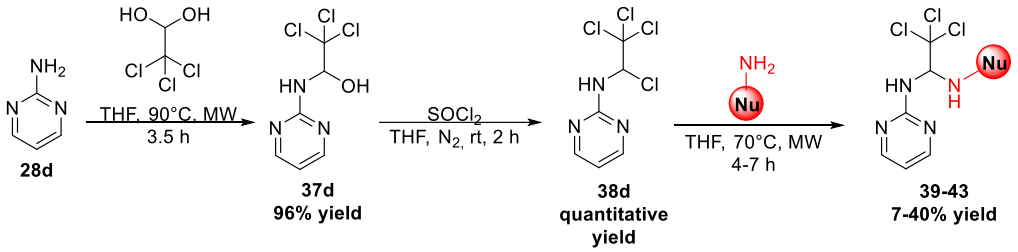

Apcin analogues obtained:

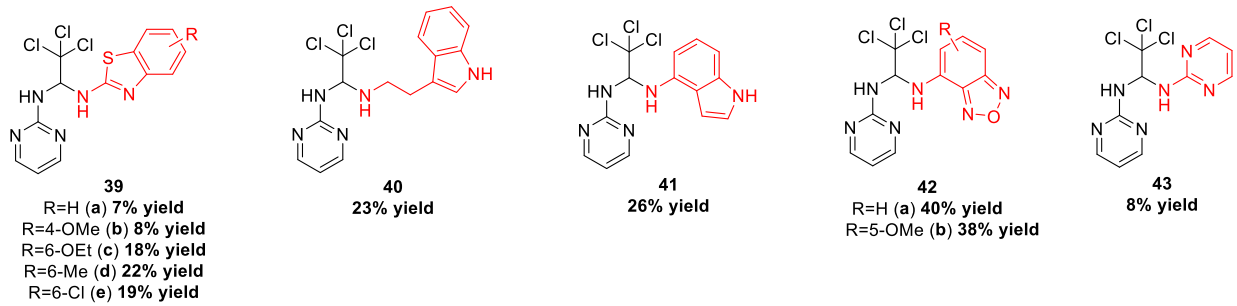

Scheme 27. Synthetic pathway to obtain compounds **39-43**.

2-Aminopyrimidine (**28d**) was reacted with chloral hydrate in THF under microwaves irradiation giving the hemiaminal **37d** in 96% yield. After reaction with $SOCl_2$ under nitrogen flow in order to remove gaseous products produced during the reaction, the crude chloride **38d** was then reacted with 2 equivalents of the amino nucleophile under microwaves conditions. The novel compounds were recovered, after chromatography on neutral alumina or silica gel, with purity > 99% even if in low yield in some cases (see experimental). The reason of the low yield might be due to the decomposition of the product during the purification step. We tried also the reaction between the chloride **38d** and ureido derivative **32** but no product was detected, probably because of the low nucleophilicity of the amide nitrogen atom of compound **32**.

Compounds **33**, **34**, **37d**, **39a-e**, **40** and **42a,b** were administered to a panel of cancer cell lines (see **Table 6** and data discussed in the next paragraph). Given that most of them, especially those bearing the aminobenzothiazolyl moiety, showed interesting biological activity, we decided to synthesize other novel Apcin analogues (shown in **Scheme 28**) maintaining both the trichloroethyl (in green) and benzothiazole (in red) group, already present in **39a-e**, and replacing the 2-aminopyrimidine moiety with a different amino aza-heterocycle (in blue), in order to investigate the influence on the biological activity of the latter and of the position on its ring of the amino group bound to the trichloroethyl group.

For this purpose, hemieminals **37a-c**, **37e-f** and **37l** were obtained starting from the corresponding precursors (*i.e.* aminopyridines **28a-c**, aminopyrimidines **28e,f** and aminopyrazine **28l**) and chloral hydrate in THF under microwaves irradiation (or reflux conditions in $CHCl_3$ depending on the solubility of the starting material **28**). Because of the low stability of **37c** and **37f**, only chlorides **38a-b**, **38e** and **38l**, obtained through chlorination reaction with $SOCl_2$ have been reacted with 2-aminobenzothiazoles **24a-e**. The final pyrazine derivative was not obtained, probably because of the low reactivity of **38l** towards the benzothiazole derivatives. The other final compounds **44a,d-e**, **45a,c-e** and **46a-d**, have been obtained after reaction times ranging from 4-7 h (depending on the benzothiazole derivative used), in low amount and in mixture with the symmetric compounds **47**. Attempts to gain higher yields by increasing the reaction time caused higher amount of bis(benzothiazolyl) derivatives **47c-e**.

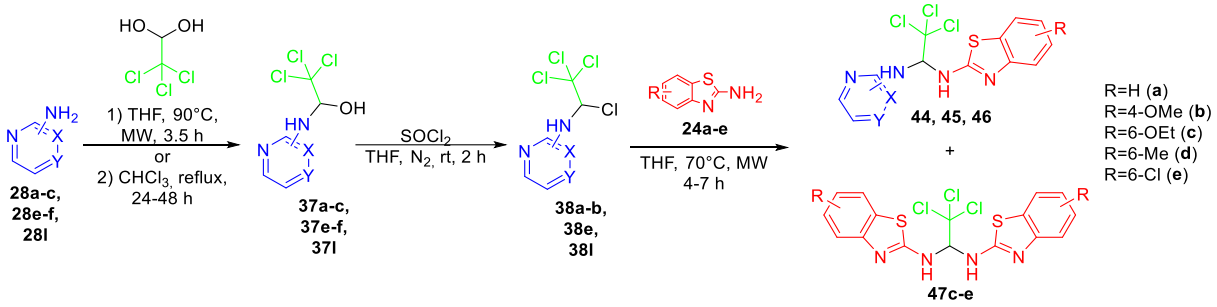

Aza-Heterocycles used:

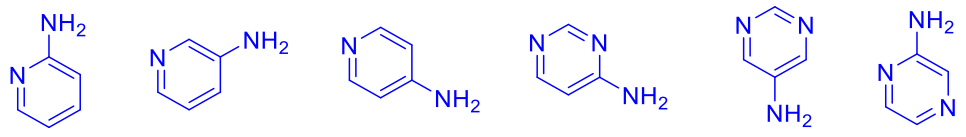

28a **28b** **28c** **28e** **28f** **28l**

Apcin analogues obtained:

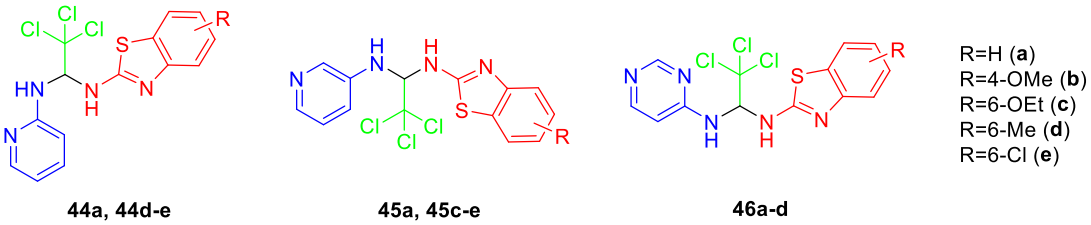

Scheme 28. Synthetic pathway to obtain Apcin analogues bearing 2-aminobenzothiazole and other amino aza-heterocyclic moieties.

Biological tests

In order to gain information on the anticancer activity of the compounds synthesized, preliminary biological tests were carried out on a panel of human solid cancer cell lines, derived from skin (A431), ovarian (IGROV1), cervix (HeLa), colon (HT29), breast (MCF7) and bone cancer (U2OS). *In vitro* growth inhibitory concentration was determined by incubating the cells with increasing concentrations (0.01–250 μM) of the compounds for 24 h. Data obtained from cell growth assays were elaborated to assess the concentration of each compound required for 50% inhibition of cell viability (IC_{50}) and the results are shown in **Table 6**.

Table 6. IC_{50} values of some synthesized compounds administered to solid cancer cell lines. n.a.: not active.

	A431	IGROV1	HeLa	HT29	MCF7	U2OS
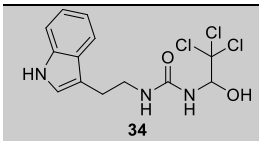 **34**	n.a.	>250 μM	/	11.5 nM	/	22.54 μM
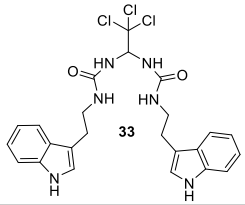 **33**	n.a.	n.a.	/	212 μM	/	n.a.
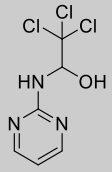 **37d**	n.a.	n.a.	/	n.a.	/	0.383 μM

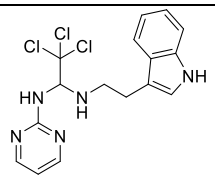 **40**	n.a.	n.a.	/	n.a.	/	235 μM
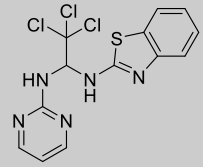 **39a**	/	/	n.a.	31.8 nM	8.1 nM	5.4 nM
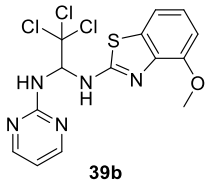 **39b**	/	/	3.5 μM	n.a.	n.a.	6.5 nM
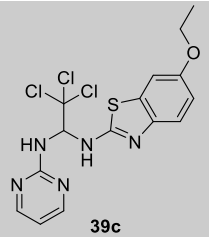 **39c**	/	/	n.a.	500 nM	10.2 nM	8.6 nM
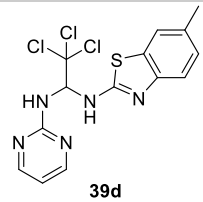 **39d**	/	/	342 nM	n.a.	24 nM	n.a.
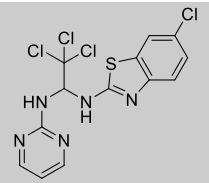 **39e**	/	/	53.6 nM	500 nM	112 nM	6.6 nM
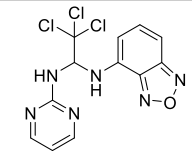 **42a**	/	/	n.a.	164.8 nM	n.a.	n.a.
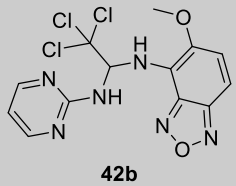 **42b**	/	/	51.1 nM	n.a.	12.9 nM	1.7 nM

All the tested compounds showed biological activity, however it is possible to observe striking differences in the structure-activity relationships towards cancer cell lines tested. In general, the benzothiazole and benzofurazan derivatives showed a greater effect than

tryptamine derivatives, with exception for **34** in HT29 cell line. Moreover, the nature of the substituents on the benzothiazole and benzofurazan ring seems to influence the biological activity. Because the molecular target is still unknown, it is difficult now to make further considerations but this point will be developed in the next step of this research.

Due to lack of time it has not been possible to insert in this thesis the data about the biological effect of compounds **44-47**, since they are object of investigation by biologists.

The good results obtained on solid cancer cell lines (**Table 6**), induced us to test the benzothiazole derivatives **39a-e** on five leukemia cell lines, including 3 models of acute myeloid leukemia (KG1, MV4-11, OCI-AML3) and 2 of acute lymphoblastic leukemia (HAL-01, NALM-6, **Figure 42**). The products **39a-e** are labelled in this section as **M1** (R=6-Me, **39d**), **M2** (R=6-Cl, **39e**), **M3** (R=4-OMe, **39b**), **M4** (R=6-OEt, **39c**) and **M5** (R=H, **39a**). *In vitro* growth inhibitory concentration was determined by incubating the cells with increasing concentrations of the benzothiazole derivatives for 48 h.

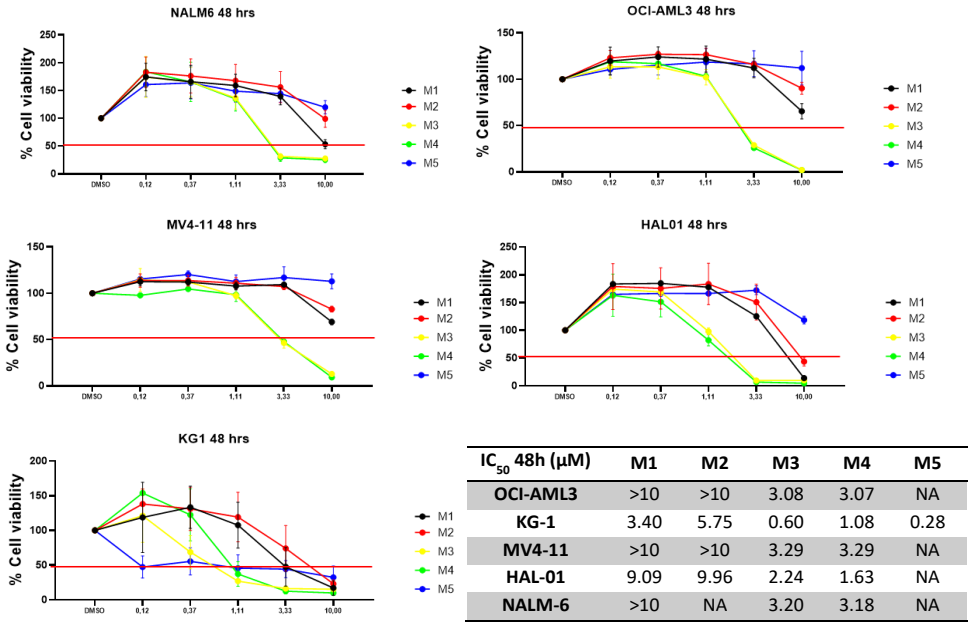

IC_{50} 48h (µM)	M1	M2	M3	M4	M5
OCI-AML3	>10	>10	3.08	3.07	NA
KG-1	3.40	5.75	0.60	1.08	0.28
MV4-11	>10	>10	3.29	3.29	NA
HAL-01	9.09	9.96	2.24	1.63	NA
NALM-6	>10	NA	3.20	3.18	NA

Figure 42. MTT assays of benzothiazole derivatives **M1-M5** on leukemia cell lines.

Data obtained from cell growth assays showed that the compounds **M3** and **M4** have a higher cytotoxic effect than other ones in every cancer cell line, already at low concentrations. Moreover, in KG1 cell line each compound showed greater activity than Apcin.[96]

The most active compounds **M3** and **M4** were subject to further studies. At first, the effect on cell cycle was examined on the same hematological cell lines after 24 hours by flow cytometry (**Figure 43**).

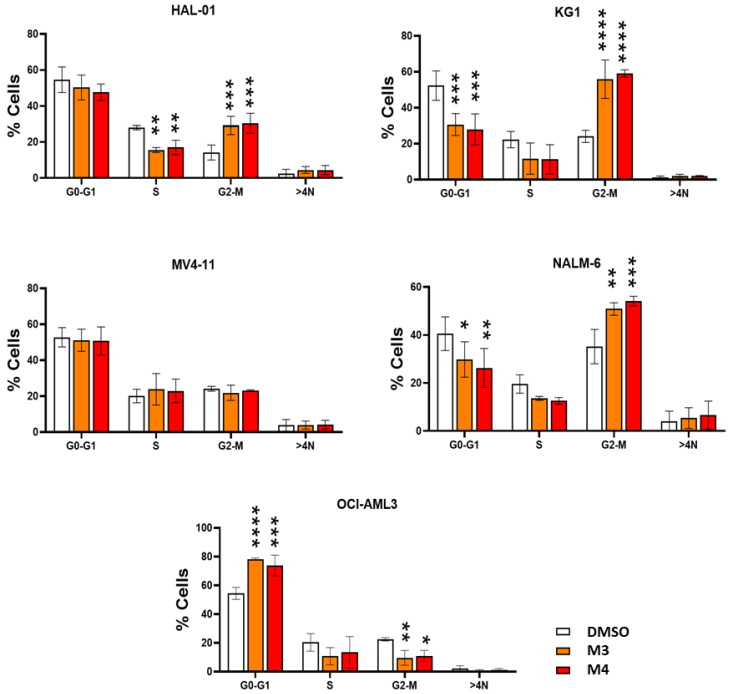

Figure 43. Effects on cell cycle of **M3** and **M4** on hematological cancer cell lines.

The compounds **M3** and **M4** induced an increase in G2-M phase and a slight decrease in S and G0/G1 phases in 3 out of 5 cell lines (KG1, HAL-01, NALM-6). Conversely, OCI-AML3 cells showed an arrest in G0-G1 phase and no effects on cell cycle were observed in MV4-11.

We then analyzed apoptotic cells by Annexin V staining of **M3**- and **M4**-treated cells at 5 µM after 24 hours (**Figure 44**). In flow cytometry, annexin V is commonly used to detect apoptotic cells by its ability to bind to phosphatidylserine, a marker of apoptosis.

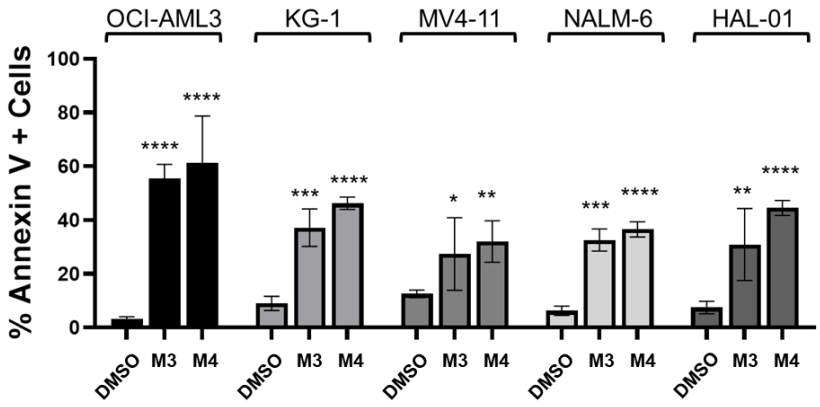

Figure 44. Flow cytometry analysis of annenxin V to detect apoptotic cells in presence of **M3** and **M4** after 24 hours.

The data show that compounds **M3** and **M4** have an apoptotic effect on all leukemia cell lines: in particular **M4** is slightly more active than **M3** and OCI-AML3 cells were the most sensitive cells to apoptosis induction.

Morphological analysis confirmed the induction of cell death in the treated cells (**Figure 45**).

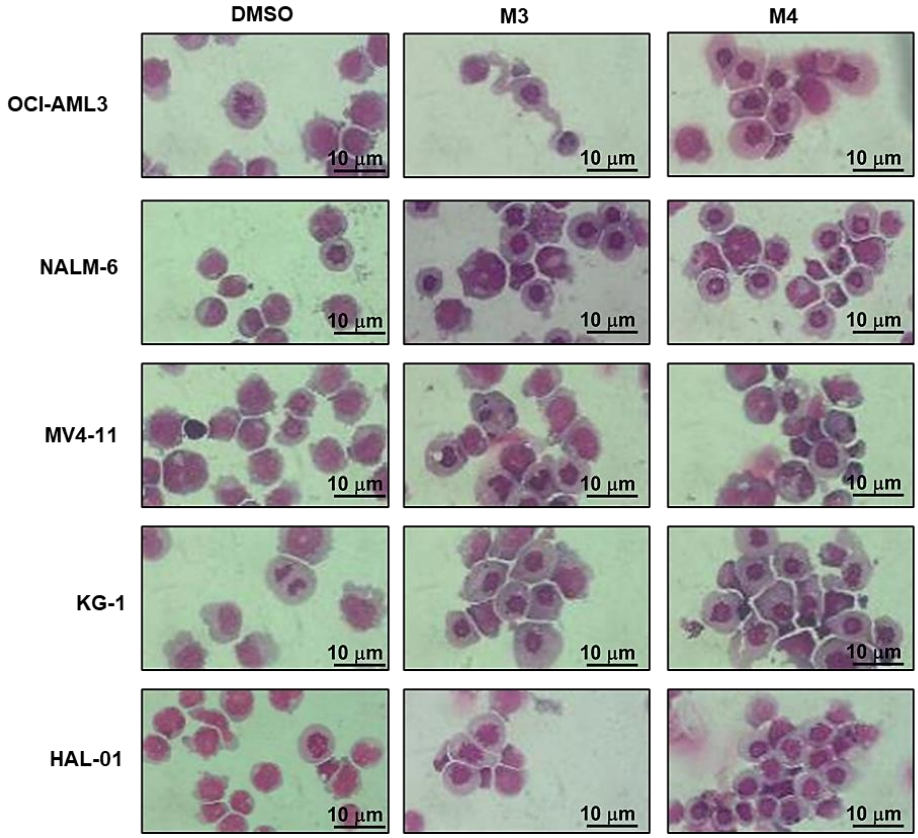

Figure 45. Microscope analysis of hematological cancer cell lines of leukemia after the treatment with **M3** and **M4**.

Notably, OCI-AML3 cell line showed some protrusions in response of the treatment of **M3** specifically in mitotic cells after 18 hours. We thus plan to investigate this effect thorugh immunofluorence.

3.3. Conclusions

Several novel Apcin analogues characterized by the indole, benzofurazan and benzothiazole moieties, connected to amino pyridinyl- and pyrimidyl- ring through a 1,1,1-trichloroethyl group have been synthesized and fully characterized.

Biological tests showed the importance of the presence of both the trichloroethyl- and pyrimidinyl- moieties, confirming the effectiveness against acute leukemia models, while showed a modest and selective activity in solid cancers. Administration of benzothiazole and benzofurazan derivatives gave antiproliferative activity, at nanomolar concentration, against cervical, colon, breast and bone cancer cell lines. Moreover, the benzothiazole derivatives showed to be more active than Apcin after 48 hours on KG-1 cell line, sensible to AML. The effect of the benzothiazole derivatives, **M3** and **M4**, on the cell cycle was examined, inducing an increase in G2-M phase and a slight decrease in S and G0/G1 phases in KG1, HAL-01 and NALM-6 cell lines. The analysis with Annexin V showed that the benzothiazole derivative **M4** is more active than **M3** in every leukemia cell line tested.

Our forward plans will be to find a new synthetic strategy to improve the yields of final compounds. Molecular docking studies will be performed to find the molecular target of compounds synthesized. Finally immunofluorescence analyses are performing to investigate the interaction between the molecules synthesized and the mitotic cells affected by AML.

3.4. Experimental section

The reagents used, unless stated otherwise, were purchased from Sigma-Aldrich (Milan, Italy). CH_2Cl_2 was dried by distillation over P_4O_{10}. Anhydrous THF was freshy distilled over sodium with benzophenone as indicator. Chromatographic purifications (FC) were carried out on glass columns packed with silica gel Geduran Si 60, 0.063–0.200 mm, (Sigma-Aldrich, Milan, Italy) or neutral alumina (Brockmann Grade 58 angstroms, Alfa Aesar, Kandel Germany) at medium pressure. Thin-layer chromatography (TLC) was performed on silica gel 60 F254-coated aluminum foils (Fluka) or neutral alumina coated plates (Polygram Alox N/UV254, Macherey-Nagel, Oensingen, Switzerland). The nuclear magnetic resonance spectra were recorded at 25°C on Varian spectrometers Mercury 400 or Inova 600 operating at 400 or 600 MHz (for ^{1}H-NMR) and 100 or 150 MHz (for ^{13}C-NMR), respectively. Signal multiplicities were established by DEPT-135 experiments. Chemical shifts were measured in δ (ppm) with reference to the solvent (DMSO-d_6: δ = 2.50 ppm for ^{1}H-NMR and δ = 39.5 for ^{13}C NMR; CD_3OD: δ = 3.34 ppm for ^{1}H NMR and δ = 49.03 ppm for ^{13}C-NMR). J-values are given in Hz. Electrospray ionization (ESI)-MS spectra and ESI high-resolution HRMS spectra were recorded using Waters ZQ 4000 and Xevo instrument, respectively (Waters Corporation, Milford, MA, USA). IR spectra were recorded using a Fourier transform spectrophotometer PerkinElmer FT-IR spectrometer Spectrum Two in the 4000-400 cm^{-1} wavelength range, using an Universal ATR accessory (Perkin Elmer,Waltham, MA, USA). Melting points (m.p.) were measured on a Büchi 535 apparatus and are uncorrected. Bulb to bulb distillation was carried out using a Buchi GKR-50 apparatus (Büchi Flawil, Switzerland). Reactions under microwave irradiation were carried out using a Milestone Start Synth (Milestone Inc, Shelton, CT, USA) apparatus at 300W. Characterization data for known compounds agree with those reported in the literature.

Cell culture

Biological tests were carried out on solid cancer cell lines by the research group of Prof. Natalia Calonghi of the Department of Pharmacy and Biotechnology of the University of Bologna. Tests on leukemia cell lines have been made by the research teams of Prof. Giovanni Martinelli and Dr. Giorgia Simonetti at the Department of Experimental, Diagnostic and Specialty Medicine, University of Bologna and Institute of Hematology and

Medical Oncology “L. and A. Seràgnoli”, Bologna, and at IRCCS Istituto Romagnolo per lo Studio dei Tumori "Dino Amadori" - IRST S.r.l., Meldola (FC), Italy.

The squamous carcinoma (A431), human colon cancer (HT29), human bone osteosarcoma (U2OS), human cervical cancer (HeLa), and human breast cancer (MCF7) cell lines were purchased from American Type Culture Collection (ATCC, Manassas, VA). The human ovarian cancer cell line (IGROV1) has been kindly provided by Istituto Nazionale Tumori (IRCCS, Milan, Italy).

The B-cell acute lymphoblastic leukemia (NALM-6, HAL-01, REH) and acute myeloid leukemia (MV-4-11, OCI-AML3 and KG1) cell lines were purchased from The Leibniz Institute DSMZ German Collection of Microorganisms and Cell Cultures GmbH (Braunschweig, Germany). OCI-AML3 cells were cultured in α-MEM supplemented with 20% heat-inactivated fetal bovine serum (Thermo Fisher Scientific, Waltham, MA, USA). The other cell lines were cultured in RPMI 1640 medium (Labtek Eurobio, Milan, Italy), supplemented with 10% heat-inactivated fetal bovine serum (All mediums were additioned of 100 U/mL penicillin, 100 g/mL streptomycin (GE Healthcare, Chicago, IL, USA) and 2mM L-glutamine (Sigma-Aldrich, Milan, Italy), at 37°C and 5% CO_2 atmosphere. The compounds were dissolved in DMSO (Sigma-Aldrich, Milan, Italy).

Cell viability assay

To evaluate the compounds activity, the cells were treated for 24 h (for solid cancer cell lines) or 48 h (for leukemia cell lines) with vehicle (DMSO, as control) or with the test compounds at concentrations between 0.01 µM and 250 µM (for solid cancer cell lines) and between 0.12 µM and 10 µM (for leukemia cell lines). Cell growth was assessed by the luminescence-based RealTime-Glo MT Cell Viability Assay (Promega, Madison, WI, USA) or the colorimetric 3-(4,5-dimethylthiazolyl-2)-2,5-diphenyltetrazolium bromide assay (MTT, Sigma-Aldrich, Milan, Italy). RealTime-Glo MT Cell Viability Assay was performed according to manufacturer instructions and luminescence was quantified by using GloMax 96 Microplate Luminometer (Promega, Madison, WI, USA). As for MTT assays, the culture medium was removed and cells incubated with 0.1 mL of MTT dissolved in PBS at the concentration of 0.2 mg/mL following Micheletti et.al. [16]. The absorbance at 570 nm was measured using a multiwell plate reader (Tecan, Männedorf, Switzerland). The IC50 was determined from the dose-response curve by using Graph Pad software v.6.0.

Cell cycle analysis

Leukemia cell lines were harvested, fixed with 70% ice-cold ethanol and stained using the PI staining mix (BD Biosciences, Franklin Lakes, NJ, USA). Flow cytometric analysis was performed on a BD FACSCanto II instrument (BD Biosciences, Franklin Lakes, NJ, USA) and cell cycle profile analysis was performed using ModFiT software (Verity Software House, ME, USA).

Apoptosis detection

Leukemia cells were stained with Annexin V (eBioscience™ Annexin V Apoptosis Detection Kit FITC, Thermo Fisher Scientific) according to the manufacturer's instructions. The percentage of Annexin V^+ cells was determined on a FACS analyzer BD FACSCanto II (BD Biosciences) by assaying a minimum of 10,000 cells.

Morphological analyses

Morphological changes induced by the tested compounds were evaluated after 24 h of treatment. Cells were seeded at 0.5 X 10^6 cells/mL in a 6 wells plate and treated with or without M3 and M4 compounds (10μM). After 21 h of treatment, cells were seeded on poly-D-lysine-coated coverslips for additional 3 h. After that, cells attached to the coverslips were washed in PBS, air-dried for 20 minutes and stained with May-Grunwald-Giemsa staining solution. Images were acquired on a ZEISS Axioscope 5 microscope at 50X magnification.

Synthesis of 1-(2-(1*H*-Indol-3-yl)ethyl)urea (**32**)

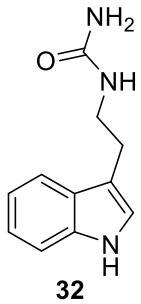

32

Tryptamine **28i** (2 g, 0.0125 mol) was introduced in a round bottom flask immersed in a water/ice bath. After 5 min, 37% aq. HCl (1.24 mL, 0.015 mol) was added and the mixture was magnetically stirred for 10 min. Ethanol (10 mL) was added and the system was immersed in an oil bath and heated at reflux for 5 min. To the solution, allowed to stand until to reach the room temperature, a solution of KOCN (1.21 g, 0.015 mol) in H_2O (10 mL) was added. The resulting mixture was stirred at room temperature overnight then concentrated in vacuo. The residue was purified by flash column chromatography on silica gel (eluent: 8/2 DCM/MeOH) to afford compound **32** (70% yield) as a pale yellow solid whose chemico physical data are in agreement with those reported in the literature.[118] m.p.: 140.5–142.0

°C (Lit.[172] 140–142 °C); Below we report the ^{1}H-NMR spectrum, never published in CD_3OD: ^{1}H-NMR (400 MHz, CD_3OD), δ (ppm): 7.56 (dt, *J* = 8.0 Hz, *J*= 1.0 Hz, 1 H), 7.32 (dt, *J* = 8.0 Hz, *J*= 0.9 Hz, 1 H), 7.08 (ddd, *J* = 8.0 Hz, *J* = 7.1 Hz *J* = 1.3 Hz 1 H), 7.07 (br.s., 1 H), 6.9 (ddd, *J* = 8.0 Hz, *J* = 7.1 Hz, *J* = 1.1 Hz 1 H), 3.41 (t, *J* = 7.25 Hz, 2 H, NCH_2), 2.92 (t, *J* = 7.25 Hz, 2 H, CH_2).

Synthesis of 1-(2-(1*H*-Indol-3-yl)ethyl)-3-(2,2,2-trichloro-1-(3-(2-(3a,7a-dihydro-1*H* indol-3-yl)ethyl)ureido)ethyl)urea (**33**)

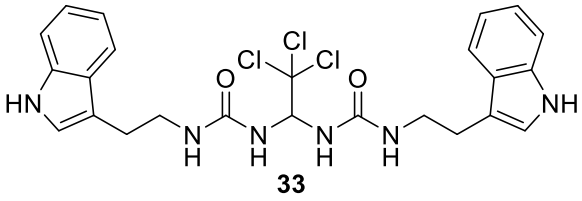

33

In a three necked round bottomed flask, partially immersed in an oil bath and equipped with a reflux condenser and a magnetic bar, chloral hydrate (0.17 g, 1.03 mmol) was introduced under argon atmosphere. The system was heated at 100°C until melting of chloral hydrate, then compound **32** (0.200 g, 0.984 mmol) and after 1 h anhydrous toluene (2 mL) were added and the reaction was stirred at 100°C overnight and then allowed to cool to room temperature. After adding 10 mL of ethyl acetate the mixture was filtered under vacuum and the obtained solid was washed with methanol to obtain compound **33** (132 mg, 0.246 mmol, 50%) as a grey solid: m.p.: 208–210°C; ^{1}H-NMR (400 MHz, DMSO-d_6, 25°C), δ (ppm): 10.81 (s, 2 H, NH indole), 7.55 (d, *J* = 7.8 Hz, 2 H), 7.33 (d, *J* = 8.1 Hz, 2 H), 7.14 (d, *J* = 2.4 Hz, 2 H, CHNH), 7.06 (ddd, *J* = 8.1 Hz, *J* = 7.0 Hz, *J* = 1.2 Hz, 2 H), 6.97 (ddd, *J* = 7.8 Hz, *J* = 7.0 Hz, *J* = 1.0 Hz, 2 H), 6.78 (d, *J* = 9.5 Hz, 2 H, $NHCHCCl_3$), 6.33 (t, *J* = 9.5 Hz, 1 H, $CHCCl_3$), 6.25 (t, *J* = 5.6 Hz, 2 H, $NHCH_2$), 2.81 (td J_1 = 6.9 Hz, J_2 = 2.71 Hz, 4 H, CH_2CH_2N), (a signal is overlapped to that of water); ^{13}C-NMR (100 MHz, DMSO-d6, 25°C), δ, ppm = 155.9, 136.3, 127.2, 122.7 (CH), 120.9 (CH), 118.4 (CH), 118.2 (CH), 111.7, 111.3 (CH), 103.8, 67.6 (CH), 40.2 (CH2), 25.8 (CH2); ATR-IR: (cm^{-1}): 3386, 3329, 3286, 1637, 1558, 740; ESI-MS^+ (m/z): 535 $[M + H]^+$ 557 $[M + Na]^+$, 575 $[M + K]^+$; ESI-$HRMS^+$ (*m/z*): for $C_{24}H_{25}Cl_3N_6NaO_2^+$ Calc. 557.10023, found 557.1002.

Synthesis of 1-(2-(Indolin-3-yl)ethyl)-3-(2,2,2-trichloro-1-hydroxyethyl)urea (**34**)

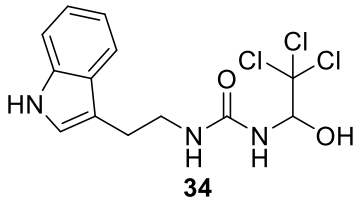

34

A solution of compound **32** (0.5 g, 2.46 mmol) in THF (20 mL) was introduced in a vessel for MW experiments equipped with a heating plate and a magnetic bar. Chloral hydrate (0.85 g, 5.14 mmol) was added to the solution and the mixture was heated at 90°C for 2 h under MW irradiation (300 W). After cooling and removal of the solvent in vacuo, the crude residue was subjected to FC on silica gel (eluent: ethyl acetate) to afford compound **34** (0.80 g, 2.28 mmol, 93% yield) as ocher solid: m.p.: 138–140°C; ^{1}H-NMR (600 MHz, DMSO-d_6, 25°C), δ (ppm): 10.82 (s, 1 H, NH indole), 7.55 (d, *J* = 7.8 Hz, 1H), 7.35 (d, *J* = 7.3 Hz, 1H), 7.14 (d, *J* = 1.7 Hz, 1H), 7.07 (t, *J* = 7.8 Hz, 1H), 6.98 (t, *J* = 7.3 Hz, 1H), 6.78 (d, *J* = 9.6 Hz, 1H), 6.35 (t, *J* = 5.6 Hz, 1H), 5.63 (t, *J* = 9.6 Hz, 1H), 3.37 (m, 2H), 2.83 (m, 2H), (A very broad signal is overlapped to that at 7.35 ppm); ^{13}C-NMR (150 MHz, CD_3OD, 25°C), ppm = 156.3 (C), 136.3 (C), 127.2 (C), 122.8 (CH), 120.9 (CH), 118.4 (CH), 118.2 (CH), 111.7 (C), 111.3 (CH), 103.3 (C), 81.9 (CH), 39.8 (CH2), 25.8 (CH2); ATR-IR: (cm^{-1}): 3401, 1658, 1558, 1074, 737; ESI-MS$^+$ (m/z): 350 $[M + H]^+$, 372 $[M + Na]^+$; ESI-HRMS$^+$ (m/z): for $C_{13}H_{14}Cl_3N_3NaO_2^+$ Calc. 372.00493, found 372.0049.

Synthesis of 2,2,2-Trichloro-1-(pyrimidin-2-ylamino)ethan-1-ol (**37d**)

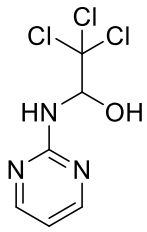

37d

A solution of 2-aminopyrimidine **28d** (1 g, 10.5 mmol) and chloral hydrate (1.73 g, 10.5 mmol) in THF (20 mL) was introduced in a wessel for MW experiments equipped with a heating plate and a magnetic bar. The mixture was heated at 90°C for 3.5 h under MW irradiation (300 W) then allowed to stand at room temperature. The solvent was removed in vacuo and the residue was subjected to bulb-to-bulb distillation (90°C, 0.01 mmHg, 3 h). Pure compound **37d** was recovered as white solid in the initial bulb (2.44 g, 10.12 mmol, 96% yield). m.p.:166.5–168.0°C (Lit.[173] 167–169 °C); ^{1}H-NMR (600 MHz, DMSO-d_6, 25°C), δ (ppm): 8.40 (d, *J* = 4.8 Hz, 2 H), 7.50 (m, 2 H, NH+OH), 6.79 (t, *J* = 4.8 Hz, 1 H), 6.20 (dd J_1 = 9.7 Hz, J_2 = 5.9 Hz, 1 H, $CHCCl_3$); ^{13}C-NMR (150 MHz, DMSO-d_6, 25°C), δ, ppm = 160.9, 158.1 (CH), 112.4 (CH), 103.1, 82.5 (CH); ATR-IR: (cm^{-1}): 3300, 1576, 1074, 794; ESI-MS$^+$ (m/z): 242 $[M + H]^+$, 264 $[M + Na]^+$; ESI-HRMS$^+$ (*m/z*): for $C_6H_7Cl_3N_3O^+$ Calc. 241.96547, found 241.9655.

Synthesis of *N*-(1,2,2,2-tetrachloroethyl)pyrimidin-2-amine (38d)

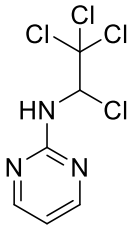

38d

In a flame-dried apparatus, equipped with a reflux condenser, dropping funnel and kept under inert atmosphere, a solution of compound **37d** (241 mg, 1 mmol) in anhydrous THF (20 mL) was added. A solution of $SOCl_2$ (73 µL, 1 mmol) in anhydrous THF (2 mL) was put in the dropping funnel and slowly added (dropwise in 20 min.). During and after the addition of $SOCl_2$, nitrogen was bubbled into the solution in order to remove the gaseous by-products. The reaction course was monitored through ^{1}H-NMR spectroscopy. When the conversion resulted quantitative, the solvent was removed and the white solid **38d** obtained was characterized and used without further purification. m.p.: 116.3–118.8 °C; ^{1}H-NMR (300 MHz, DMSO-d_6, 25°C), δ (ppm): 8.45 (d, *J* = 4.6 Hz, 2 H), 7.74 (d, *J* = 9.5 Hz, 1 H, NH), 6.84 (t, *J* = 4.6 Hz, 1 H), 6.21 (d, *J* = 9.5 Hz, 1 H, $CHCCl_3$); ^{13}C-NMR (150 MHz, DMSO-d_6, 25°C), δ, ppm = 160.2, 158.0 (CH), 112.4 (CH), 102.9, 82.4 (CH); GC-MS (m/z): 189 (18, M-70), 154 (100, M-105), 119 (10, M-140), 79 (20); ESI-MS$^-$ (*m/z*): 224 [M - Cl]$^-$.

Synthesis of *N*-(benzo[d]thiazol-2-yl)-2,2,2-trichloro-*N'*-(pyrimidin-2-yl)ethane-1,1-diamine (39a)

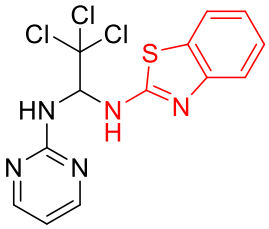

39a

2-Aminobenzothiazole **24a** (150 mg, 1.0 mmol) in anhydrous THF (5 mL) was added to a solution of compound **38d** (130 mg, 0.5 mmol) in anhydrous THF (5 mL). The reaction mixture was heated under reflux condition overnight. After removal of the solvent, the crude was subjected to FC on silica gel disactivated with Et_3N (eluent: 1/1 EtOAc/MeOH). The residue was further subjected to bulb-to-bulb distillation (60°C, 0.01 mmHg, 2 h). Pure compound **39a** was recovered as brown solid in the initial bulb (13 mg, 0.035 mmol, 7% yield). m.p.: 153-155°C; ^{1}H-NMR (600 MHz, DMSO-d_6, 25 °C), δ (ppm): 8.87 (d, *J* = 8.9 Hz, 1 H, NH), 8.44 (d, *J* = 4.6 Hz, 2 H), 7.86 (d, *J* = 9.4 Hz, 1 H, NH), 7.73 (d, *J* = 7.6 Hz, 1 H), 7.47 (d, *J* = 8.2 Hz, 1 H), 7.33 (t, *J* = 8.9 Hz, 1 H, $CHCCl_3$), 7.26 (t, *J* = 7.2 Hz, 1 H), 7.08 (t, *J* = 7.2 Hz, 1 H), 6.81 (t, *J* = 4.6 Hz, 1 H); ^{13}C-NMR (150 MHz, DMSO-d_6, 25°C), δ, ppm = 164.9, 160.8, 158.1 (CH), 151.3, 130.8, 125.6 (CH), 121.8 (CH), 121.1 (CH), 118.8 (CH), 112.5 (CH), 102.2, 71.2 (CH); ESI-MS$^+$ (*m/z*): 374 [M+H]$^+$, 396 [M+Na]$^+$.

Synthesis of 2,2,2-trichloro-N-(4-methoxybenzo[d]thiazol-2-yl)-*N'*-(pyrimidin-2-yl)ethane-1,1-diamine (39b)

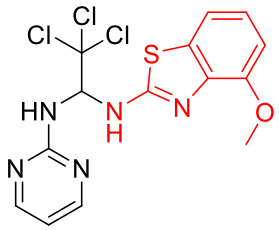

39b

4-Methoxybenzo[d]thiazol-2-amine **24b** (270 mg, 1.5 mmol) in anhydrous THF (5 mL) was added to a solution of compound **38d** (195 mg, 0.75 mmol) in anhydrous THF (5 mL). The mixture was heated at 70°C for 2 h under MW irradiation (300 W) then allowed to stand at room temperature. After removal of the solvent, the crude was subjected to FC on silica gel disactivated with Et_3N (eluent: 7/3 EtOAc/*n*-hexane). The residue was further subjected to bulb-to-bulb distillation (70°C, 0.01 mmHg, 2 h). Pure compound **39b** was recovered as light yellow solid in the initial bulb (24 mg, 0.06 mmol, 8% yield). m.p.: 108.7-110.3 °C; ^{1}H-NMR (600 MHz, DMSO-d_6, 25 °C), δ (ppm): 8.79 (d, *J* = 8.9 Hz, 1 H, NH), 8.43 (d, *J* = 4.9 Hz, 2 H), 7.82 (d, *J* = 9.4 Hz, 1 H, NH), 7.32 (dd, *J* = 7.9, 1 H), 7.28 (t, *J* = 8.9 Hz, 1 H, $CHCCl_3$), 7.04 (t, *J* = 7.9 Hz, 1 H), 6.87 (dd, *J* = 8.1, 1 H), 6.81 (t, *J* = 4.9 Hz, 1 H), 3.87 (s, 3 H); ^{13}C-NMR (150 MHz, DMSO-d_6, 25 °C), δ, ppm = 163.4, 160.8, 158.1 (CH), 150.3, 134.2, 132.0, 122.6 (CH), 113.4 (CH), 112.6 (CH), 108.7 (CH), 102.4, 71.3 (CH), 55.9 (CH_3); ESI-MS$^+$ (*m/z*): 404 $[M+H]^+$, 426 $[M+Na]^+$.

Synthesis of 2,2,2-trichloro-*N*-(6-ethoxybenzo[d]thiazol-2-yl)-*N'*-(pyrimidin-2-yl)ethane-1,1-diamine (39c)

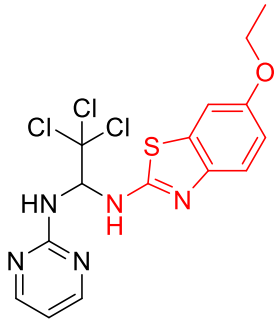

39c

6-Ethoxybenzo[d]thiazol-2-amine **24c** (194 mg, 1 mmol) in anhydrous THF (5 mL) was added to a solution of compound **38d** (130 mg, 0.5 mmol) in anhydrous THF (5 mL). The reaction mixture was heated under reflux condition overnight. After removal of the solvent, the crude was subjected to FC on silica gel disactivated with Et_3N (eluent: 2/8 EtOAc/DCM). The residue was further subjected to bulb-to-bulb distillation (60°C, 0.01 mmHg, 2 h). Pure compound **39c** was recovered as yellow solid in the initial bulb (37 mg, 0.09 mmol, 18% yield). m.p.: 166.5-168.5 °C; ^{1}H-NMR (400 MHz, DMSO-d_6, 25 °C), δ (ppm): 8.63 (d, *J* = 8.9 Hz, 1 H, NH), 8.43 (d, *J* = 4.9 Hz, 2 H), 7.80 (d, *J* = 9.5 Hz, 1 H, NH), 7.36 (t, *J* = 8.8 Hz, 1 H), 7.34 (t, *J* = 2.6 Hz, 1 H), 7.27 (t, *J* = 9.2 Hz, 1 H, $CHCCl_3$), 6.84 (dd, J_1 = 8.8, J_2 = 2.6 Hz, 1 H), 6.80 (t, *J* = 4.9 Hz, 1 H), 3.99 (q, *J* = 7.0, 2 H, CH_2), 1.30 (t, *J* = 7.00 Hz ,3 H, CH_3); ^{13}C-NMR (100 MHz, DMSO-d_6, 25 °C), δ, ppm = 163.1, 160.8, 158.1

(CH), 154.0, 145.3, 131.8, 119.2 (CH), 113.8 (CH), 112.5 (CH), 106.1 (CH), 102.4, 71.3 (CH), 63.5 (CH_2), 14.6 (CH_3); ESI-MS^+ (*m/z*): 418 $[M+H]^+$, 440 $[M+Na]^+$.

Synthesis of 2,2,2-trichloro-*N*-(6-methylbenzo[d]thiazol-2-yl)-*N'*-(pyrimidin-2-yl)ethane-1,1-diamine (**39d**)

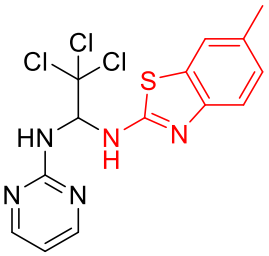

39d

6-Methylbenzo[d]thiazol-2-amine **24d** (262 mg, 1.6 mmol) was added to a solution of compound **38d** (260 mg, 1 mmol) dissolved in anhydrous THF (15 mL). The mixture was heated at 70°C for 4 h under MW irradiation (300 W) then allowed to stand at room temperature. After removal of the solvent, the mixture was dissolved in DCM and filtered on a Büchner funnel. The liquid phase was concentrated and subjected to FC on silica gel (eluent: 6/4 EtOAc/*n*-hexane). The residue was further subjected to bulb-to-bulb distillation (90°C, 0.01 mmHg, 2 h). Pure compound **39d** was recovered as white solid in the initial bulb (85 mg, 0.22 mmol, 22% yield). m.p.: 157 - 159 °C; ^{1}H-NMR (400 MHz, DMSO-d_6, 25 °C), δ (ppm): 8.74 (d, *J* = 9.0 Hz, 1 H, NH), 8.43 (d, *J* = 4.7 Hz, 2 H), 7.82 (d, *J* = 9.4 Hz, 1 H, NH), 7.53 (s, 1 H), 7.35 (d, *J* = 8.0 Hz, 1 H), 7.29 (t, *J* = 9.0 Hz, 1 H, $CHCCl_3$), 7.07 (dd, J_1 = 8.0, J_2 = 1.1 Hz, 1 H), 6.81 (t, *J* = 4.7 Hz, 1 H), 2.32 (s, 3 H); ^{13}C-NMR (100 MHz, DMSO-d6, 25 °C), δ, ppm = 164.1, 160.9, 158.1 (CH), 149.2, 131.0, 130.9, 126.7 (CH), 120.9 (CH), 118.6 (CH), 112.6 (CH), 102.4, 71.3 (CH), 20.8 (CH_3); ESI-MS^+ (m/z): 388 $[M+H]^+$, 410 $[M+Na]^+$; ESI-MS^- (m/z): 386 $[M-H]^-$.

Synthesis of 2,2,2-trichloro-*N*-(6-chlorobenzo[d]thiazol-2-yl)-*N'*-(pyrimidin-2-yl)ethane-1,1-diamine (**39e**)

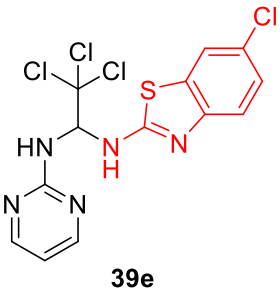

39e

6-Chlorobenzo[d]thiazol-2-amine **24e** (294 mg, 1.6 mmol) was added to a solution of compound **38d** (260 mg, 1 mmol) dissolved in anhydrous THF (15 mL). The mixture was heated at 70°C for 4 h under MW irradiation (300 W) then allowed to stand at room temperature. After removal of the solvent, the mixture was dissolved in DCM and filtered on a Büchner funnel. The liquid phase was concentrated and subjected to FC on silica gel (eluent: 7/3 DCM/EtOAc). The residue was further subjected to bulb-to-bulb distillation (90°C, 0.01 mmHg, 2 h). Pure compound **39e** was recovered as white solid in the initial bulb (77 mg, 0.19 mmol, 19%

yield). m.p.: 158 - 160 °C; ^{1}H-NMR (600 MHz, DMSO-d$_6$, 25 °C), δ (ppm): 9.01 (d, *J* = 9.1 Hz, 1 H, NH), 8.44 (d, *J* = 4.8 Hz, 2 H), 7.97 (d, *J* = 9.6 Hz, 1 H, NH), 7.86 (s, *J* =1.9 Hz, 1 H), 7.44 (d, *J* = 8.8 Hz, 1 H), 7.32 (t, *J* = 9.2 Hz, 1 H), 7.07 (dd, J_1 = 8.6, J_2 = 1.9 Hz, 1 H), 6.80 (t, *J* = 4.6 Hz, 1 H); ^{13}C-NMR (150 MHz, DMSO-d$_6$, 25 °C), δ, ppm = 165.7, 160.9, 158.1 (CH), 150.2, 132.6, 125.8 (CH), 125.6, 120.8 (CH), 119.8 (CH), 112.6 (CH), 102.1, 71.3 (CH); ESI-MS$^-$ (*m/z*): 406 [M-H]$^-$.

Synthesis of 2,2,2-Trichloro-*N*-(2-(3a,7a-dihydro-*1H*-indol-3-yl)ethyl)-*N0*-(pyrimidin-2-yl)ethane-1,1-diamine (40)

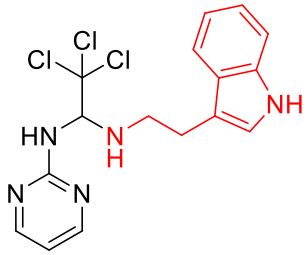

40

Tryptamine **28i** (0.200 g, 1.25 mmol) in anhydrous THF (5 mL) was added to a solution of compound **38d** (0.120 mg, 0.5 mmol) in anhydrous THF (5 mL). The reaction mixture was heated at 50°C overnight. After removal of the solvent, the crude was subjected to FC on neutral alumina (changing gradient eluent from n-hexane/ethyl acetate 1/1 until pure ethyl acetate) and 44.2 mg (0.115 mmol, 23% yield) of pure compound **40**, as waxy brown solid was obtained. m.p.: 132.5–134.5 °C; ^{1}H-NMR (400 MHz, DMSO-d$_6$, 25 °C), δ (ppm): 10.76 (br. s, 1 H, NH indole), 8.37 (d, *J* = 4.7 Hz, 2 H), 7.56 (d, *J* = 9.1 Hz, 1 H), 7.39 (d, *J* = 7.8 Hz, 1 H), 7.30 (dt, J_1 = 8.0, J_2 = 0.8 Hz, 1 H), 7.11 (d, *J* = 2.3 Hz, 1 H), 7.03 (ddd, *J* = 8.0 Hz, *J* = 7.0 Hz, *J* = 1.2 Hz, 1 H), 6.91 (ddd, *J* = 7.8 Hz, *J* = 7.0 Hz, *J* = 1.0 Hz, 1 H), 6.73 (t, *J* = 4.7 Hz, 1 H), 5.70 (dd, J_1 = 10.8, J_2 = 9.1 Hz, 1 H, $CHCCl_3$), 3.04–2.76 (m, 4 H); ^{13}C-NMR (100 MHz, DMSO-d$_6$, 25 °C), δ, ppm = 162.0, 158.1 (CH), 157.9, 136.1, 127.1 (CH), 122.6 (CH), 120.8 (CH), 118.1 (CH), 111.9, 111.8 (CH), 111.3 (CH), 103.8, 76.3 (CH), 47.3 (CH2), 25.5 (CH2); ATR-IR: (cm^{-1}): 3411, 3221, 1584, 1444, 1415, 798, 784, 740; ESI-MS$^+$ (*m/z*): 384 [M + H]$^+$, 406 [M+Na]$^+$, 424 [M+K]$^+$; ESI-HRMS$^+$ (*m/z*): for $C_{16}H_{16}Cl_3N_5Na^+$ Calc. 406.03690, found 406.0369.

Synthesis of 2,2,2-trichloro-*N*-(1H-indol-4-yl)-*N'*-(pyrimidin-2-yl)ethane-1,1-diamine (41)

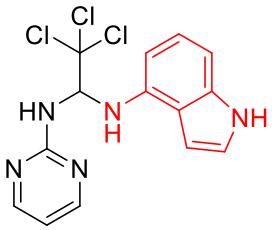

41

1H-indol-4-amine (264 mg, 2 mmol) was added to a solution of compound **38d** (260 mg, 1 mmol) dissolved in anhydrous THF (15 mL). The mixture was heated at 70°C for 4 h under MW irradiation (300 W) then allowed to stand at room temperature. After removal of the solvent, the mixture was dissolved in DCM and filtered on a Büchner funnel. The liquid phase was concentrated and subjected to FC on silica gel (eluent: 6/4 *n*-hexane/EtOAc). Pure compound **41** was recovered as white solid (92 mg, 0.26 mmol, 26% yield). m.p.: >80 °C decomposition; ^{1}H-NMR (400 MHz, DMSO-d$_6$, 25 °C), δ (ppm): 11.0 (s, 1 H, NH), 8.44 (d, *J* = 4.0 Hz, 2 H), 7.79 (d, *J* = 8.8 Hz, 1 H, NH), 7.22 (t, *J* = 2.9 Hz, 1 H), 6.88 (t, *J* = 8.4 Hz, 1 H), 6.83 (d, *J* = 7.9 Hz, 1 H), 6.77 (t, *J* = 5.2 Hz, 1 H), 6.66 (t, *J* = 9.6 Hz, 1 H, $CHCCl_3$), 6.51 (t, *J* = 2.5 Hz, 1 H), 6.40 (d, *J* = 7.6 Hz, 1 H), 5.66 (d, *J* = 10.0 Hz, 1H, NH); ^{13}C-NMR (100 MHz, DMSO-d$_6$, 25 °C), δ, ppm = 161.1, 138.1, 136.6, 123.2 (CH), 122.0 (CH), 117.4, 112.2 (CH), 104.0, 103.1 (CH), 100.1 (CH), 97.9 (CH), 72.0 (CH); ESI-MS$^+$ (m/z): 358 $[M+H]^+$, 380 $[M+Na]^+$; ESI-MS$^-$ (*m/z*): 356 $[M-H]^-$.

Synthesis of *N*-(benzo[c][1,2,5]oxadiazol-4-yl)-2,2,2-trichloro-*N'*-(pyrimidin-2-yl)ethane-1,1-diamine (42a)

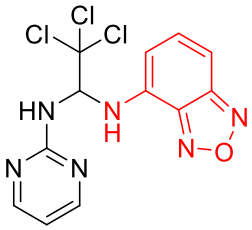

42a

Benzo[c][1,2,5]oxadiazol-4-amine (270 mg, 2 mmol) was added to a solution of compound **38d** (260 mg, 1 mmol) dissolved in anhydrous THF (15 mL). The mixture was heated at 70°C for 4 h under MW irradiation (300 W) then allowed to stand at room temperature. After removal of the solvent, the mixture was dissolved in DCM and filtered on a Büchner funnel. The liquid phase was concentrated and subjected to FC on silica gel (eluent: 7/3 DCM/*n*-hexane). Pure compound **42a** was recovered as yellow-brown solid (143 mg, 0.40 mmol, 40% yield). m.p.: >155 °C decomposition; ^{1}H-NMR (400 MHz, DMSO-d$_6$, 25 °C), δ (ppm): 8.40 (d, *J* = 4.9 Hz, 2H), 7.74 (d, *J* = 9.0 Hz, 1H), 7.41 (dd, J_1 = 8.9 Hz, J_2 = 7.4 Hz, 1H), 7.24 (d, *J* = 9.0 Hz, 1H), 7.12 (d, *J* = 9.7 Hz, 1H), 6.91 (t, *J* = 9.3 Hz, 1H), 6.80 (t, *J* = 4.9 Hz, 1H), 6.67 (d, *J* = 7.4 Hz, 1H); ^{13}C-NMR (100 MHz, DMSO-d$_6$, 25 °C), δ, ppm = 160.9 (C), 158.5 (CH), 149.8

(C), 144.5 (C), 134.8 (CH), 134.1 (C), 113.0 (CH), 105.5 (CH), 103.9 (CH), 103.0 (C), 71.3 (CH); ESI-MS$^-$ (*m/z*): 357 [M-H]$^-$.

Synthesis of 2,2,2-trichloro-*N*-(5-methoxybenzo[c][1,2,5]oxadiazol-4-yl)-*N'*-(pyrimidin-2-yl)ethane-1,1-diamine (42b)

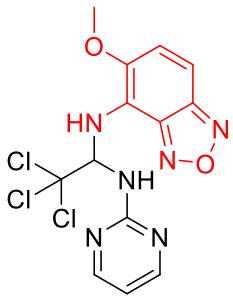

42b

5-Methoxybenzo[c][1,2,5]oxadiazol-4-amine (330 mg, 2 mmol) was added to a solution of compound **38d** (260 mg, 1 mmol) dissolved in anhydrous THF (15 mL). The mixture was heated at 70°C for 4 h under MW irradiation (300 W) then allowed to stand at room temperature. After removal of the solvent, the mixture was dissolved in DCM and filtered on a Büchner funnel. The liquid phase was concentrated and subjected to FC on silica gel (eluent: 1/1 *n*-hexane/EtOAc). Pure compound **42b** was recovered as yellow-brown solid (147 mg, 0.38 mmol, 38% yield). m.p.: >158 °C decomposition; ^{1}H-NMR (400 MHz, DMSO-d$_6$, 25 °C), δ (ppm): 8.38 (d, *J* = 4.7 Hz, 2H), 8.04 (d, *J* = 9.0 Hz, 1H), 7.72 (dd, J_1 = 10.5 Hz, J_2 = 9.0 Hz, 1H), 7.63 (d, *J* = 9.6 Hz, 1H), 7.41 (d, *J* = 9.6 Hz, 1H), 6.73 (t, *J* = 4.7 Hz, 1H), 6.32 (d, *J* = 10.5 Hz, 1H), 3.95 (s, 3H); ^{13}C-NMR (100 MHz, DMSO-d$_6$, 25 °C), δ, ppm = 160.8 (C), 158.1 (CH), 147.3 (C), 143.8 (C), 141.5 (C), 125.6 (CH), 119.5 (C), 112.4 (CH), 104.7 (CH), 104.3 (C), 72.1 (CH), 57.9 (CH_3); ESI-MS$^-$ (*m/z*): 388 [M-H]$^-$.

Synthesis of 2,2,2-trichloro-*N*,*N'*-di(pyrimidin-2-yl)ethane-1,1-diamine (43)

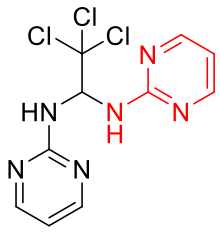

43

Pyrimidin-2-amine **28d** (190 mg, 2 mmol) was added to a solution of **38d** (260 mg, 1 mmol) dissolved in anhydrous THF (15 mL). The mixture was heated at 70°C for 4 h under MW irradiation (300 W) then allowed to stand at room temperature. After removal of the solvent, the crude was subjected to FC on silica gel (eluent: 1/1 *n*-hexane/EtOAc). Pure compound **43** was recovered as white solid (24 mg, 0.075 mmol, 8% yield). m.p.: 215-217 °C dec.; ^{1}H-NMR (600 MHz, DMSO-d$_6$, 25 °C), δ (ppm): 8.41 (d, *J*= 4.8 Hz, 2H), 7.42-7.35 (m, 6H), 6.79 (t, *J*= 4.9 Hz, 1H); ^{13}C-NMR (150 MHz, DMSO-d6, 25 °C), δ, ppm = 160.7, 158.2 (CH), 112.6 (CH), 103.7, 68.8 (CH); ESI-MS$^-$ (*m/z*): 388 [M-H]$^-$.

Synthesis of hemieminals 37a-b, 37e and 37l. General Procedure:

A solution of the amino aza-heterocycle precursor (1 eq) in anhydrous THF (0.5 M) was introduced in a vessel for MW experiments equipped with a heating plate and a magnetic bar. Chloral hydrate (1 eq) was added to the solution and the mixture was heated at 90°C for 3.5 h under MW irradiation (300 W) then allowed to stand at room temperature. After removal of the solvent, the crude was purified through bulb-to-bulb distillation or crystallization when it was necessary.

2,2,2-Trichloro-1-(pyridin-2-ylamino)ethan-1-ol (**37a**)

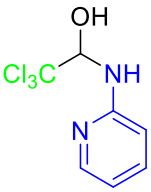

37a

The above general procedure was applied to pyridin-2-amine **28a** (1 g, 10.6 mmol) and chloral hydrate (1.75 g, 10.6 mmol). The residue was subjected to bulb-to-bulb distillation (75 °C, 0.01 mmHg, 3 h). Pure compound **37a** was recovered as light yellow solid in the initial bulb (2.37 g, 9.83 mmol, 93% yield). m.p.: 108-110°C; ^{1}H-NMR (300 MHz, DMSO-d$_6$, 25 °C), δ (ppm): 8.04 (d, *J*= 4.6 Hz, 1H), 7.46 (dt, J_1= 2.1 Hz, J_2= 8.4 Hz, 1H), 7.34 (d, *J*=6.0 Hz, 1H), 7.19 (d, *J*= 9.7 Hz, 1H), 6.78 (d, *J*= 8.8 Hz, 1H), 6.64 (t, *J*= 6.5 Hz, 1H), 6.30 (dd, J_1=9.7 Hz, J_2= 6.0 Hz, 1H); ^{13}C-NMR (100 MHz, DMSO-d$_6$, 25 °C), δ, ppm = 156.8, 147.0, 137.2, 113.8, 109.7, 103.7, 81.7; ESI-MS$^+$ (*m/z*): 243 [M+H]$^+$, 265 [M+Na]$^+$.

2,2,2-Trichloro-1-(pyridin-3-ylamino)ethan-1-ol (**37b**)

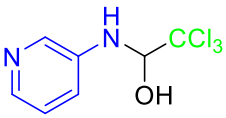

37b

The above general procedure was applied to pyridin-3-amine **28b** (1.5 g, 15.95 mmol) and chloral hydrate (2.63 g, 15.95 mmol). The reaction provided the pure compound **37b** as pink solid (3.47 g, 14.45 mmol, 90% yield). m.p.: 148-150°C; ^{1}H-NMR (400 MHz, DMSO-d$_6$, 25 °C), δ (ppm): 8.28 (d, *J*=2.8 Hz, 1H), 7.91 (dd, J_1= 4.9 Hz, J_2= 1.6, 1H), 7.38 (d, *J*=5.8 Hz, 1H), 7.28-7.32 (m, 1H), 7.14 (dd, J_1= 8.4 Hz, J_2= 4.8 Hz, 1H), 6.46 (d, *J*=9.6, 1H), 5.49 (dd, J_1= 9.4 Hz, J_2= 5.5 Hz, 1H); ^{13}C-NMR (100 MHz, DMSO-d$_6$, 25 °C), δ, ppm = 142.2, 139.1, 136.8, 123.5, 119.8, 103.5, 85.1; ESI-MS$^+$ (*m/z*): 243 [M+H]$^+$, 265 [M+Na]$^+$.

2,2,2-Trichloro-1-(pyrimidin-4-ylamino)ethan-1-ol (**37e**)

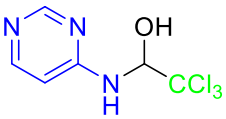

37e

The above general procedure was applied to pyrimidin-4-amine **28e** (260 mg, 2.73 mmol) and chloral hydrate (451 mg, 2.73 mmol). The reaction provided the pure compound **37e** as white solid (641 mg, 2.66

mmol, 97% yield). m.p.: 163-165°C; ^{1}H-NMR (400 MHz, DMSO-d$_6$, 25 °C), δ (ppm): 8.52-8.54 (m, 1H), 8.18 (d, *J*= 5.9 Hz, 1H), 8.13 (d, *J*= 9.6 Hz, 1H), 7.67 (d, *J*= 5.9 Hz, 1H), 6.79 (dd, J_1= 5.9 Hz, J_2= 1.2 Hz, 1H), 6.30 (dd, J_1= 9.4 Hz, J_2= 5.8 Hz, 1H); ^{13}C-NMR (100 MHz, DMSO-d$_6$, 25 °C), δ, ppm = 161.0, 157.8, 155.2, 106.7, 102.8, 80.8; ESI-MS$^+$ (*m/z*): 244 $[M+H]^+$.

2,2,2-Trichloro-1-(pyrazin-2-ylamino)ethan-1-ol (**37l**)

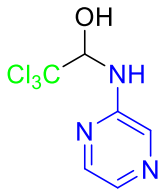

37l

The above general procedure was applied to pyrazin-2-amine **28l** (1 g, 10.5 mmol) and chloral hydrate (1.73 g, 10.5 mmol). The residue was subjected to crystallization from MeOH providing the pure compound **37l** as white solid (2.29 g, 9.5 mmol, 90% yield). m.p.: 147-149°C; ^{1}H-NMR (400 MHz, DMSO-d$_6$, 25 °C), δ (ppm): 8.21 (s, 1H), 8.04 (s, 1H), 7.85 (s, 1H), 7.81 (d, *J*=9.9 Hz, 1H), 7.57 (d, *J*=6.1 Hz, 1H), 6.18 (dd, J_1= 8.8 Hz, J_2= 6.1 Hz, 1H); ^{13}C-NMR (100 MHz, DMSO-d$_6$, 25 °C), δ, ppm = 153.3, 141.2, 133.9, 133.6, 103.2, 81.5; ESI-MS$^-$ (*m/z*): 242 $[M-H]^-$; ESI-MS$^+$ (*m/z*): 244 $[M+H]^+$.

Synthesis of chlorides 38a,b,e,l. General procedure:

In a flame-dried three necked round bottomed flask, equipped with a reflux condenser and magnetic bar, and kept under inert atmosphere, a solution of hemiaminal **37** (1 eq) in anhydrous THF (0.1 M) was added. $SOCl_2$ (1 eq) was added dropwise. During and after the addition of $SOCl_2$, nitrogen was bubbled into the solution in order to remove the gaseous by-products. The reaction course was monitored through ^{1}H-NMR spectroscopy. When the conversion resulted quantitative, the solution was used directly without further purification for the next step.

***N*-(1,2,2,2-tetrachloroethyl)pyridin-2-amine** (**38a**)

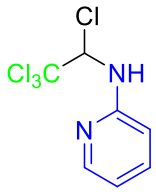

38a

The above general procedure was applied to hemiaminal **37a** (480 mg, 2 mmol) and $SOCl_2$ (160 µL, 2 mmol). White solid. m.p.: 181-184°C; ^{1}H-NMR (400 MHz, DMSO-d$_6$, 25 °C), δ (ppm): 9.20 (d, J= 9.1 Hz, 1H), 8.14, (d, *J*= 6.3 Hz, 1H), 8.08 (ddd, J_1= 8.9 Hz, J_2= 7.2 hz, J_3= 1.7 Hz, 1H), 7.47 (d, *J*= 9.2 Hz, 1H), 7.07 (ddd, J_1= 7.1 Hz, J_2= 6.2 Hz, J_3= 0.9 Hz, 1H), 6.29 (d, *J*= 8.9 Hz, 1H); ^{13}C-NMR (150 MHz, DMSO-d$_6$, 25 °C), δ, ppm = 162.1, 153.9, 113.5, 106.7, 105.8, 101.6, 82.9; ESI-MS$^+$ (*m/z*): 255, 257, 259 [M – Cl + H + OMe]$^+$.

***N*-(1,2,2,2-tetrachloroethyl)pyridin-3-amine (38b)**

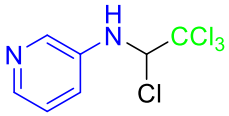

38b

The above general procedure was applied to hemiaminal **37b** (480 mg, 2 mmol) and $SOCl_2$ (160 µL, 2 mmol). Yellow solid. m.p.: 107-110°C; ^{1}H-NMR (300 MHz, DMSO-d_6, 25 °C), δ (ppm): 8.54 (d, *J*= 2.7 Hz, 1H), 8.21 (d, *J*= 5.1 Hz, 1H), 8.13 (dd, J_1=8.6 Hz, J_2=1.5 Hz, 1H), 7.87-7.79 (m, 1H), 7.76 (d, *J*= 9.2 Hz, 1H), 5.80 (d, *J*= 9.1 Hz, 1H); ^{13}C-NMR (150 MHz, DMSO-d_6, 25 °C), δ, ppm =.145.5, 129.7, 128.9, 127.3, 125.7, 102.7, 84.1; ESI-MS$^+$ (*m/z*): 255, 257, 259 $[M - Cl + H + OMe]^+$.

***N*-(1,2,2,2-tetrachloroethyl)pyrimidin-4-amine (38e)**

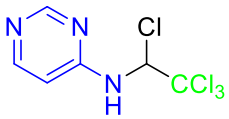

38e

The above general procedure was applied to hemiaminal **37e** (480 mg, 2 mmol) and $SOCl_2$ (160 µL, 2 mmol). White solid. m.p.: 173-175°C; ^{1}H-NMR (600 MHz, DMSO-d_6, 25 °C), δ (ppm): 10.03 (d, *J*= 8.5 Hz, 1H), 8.99 (s, 1H), 8.40 (d, *J*= 7.2 Hz, 1H), 7.11 (d, *J*= 6.7 Hz, 1H), 6.33 (d, *J*=8.4 Hz, 1H); ^{13}C-NMR (150 MHz, DMSO-d_6, 25 °C), δ, ppm = 162.9, 152.0, 143.8, 106.5, 101.5, 81.4; ESI-MS$^+$ (*m/z*): 256, 258, 260 $[M - Cl + H + OMe]^+$.

***N*-(1,2,2,2-tetrachloroethyl)pyrazin-2-amine (38l)**

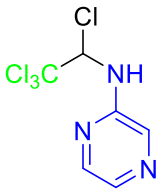

38l

The above general procedure was applied to hemiaminal **37l** (480 mg, 2 mmol) and $SOCl_2$ (160 µL, 2 mmol). Yellow solid. m.p.: 89-91°C; ^{1}H-NMR (300 MHz, DMSO-d_6, 25 °C), δ (ppm): 8.26 (d, *J*= 1.7 Hz, 1H), 8.17 (dd, J_1= 2.9 Hz, J_2= 1.2 Hz, 1H), 8.07 (d, *J*= 9.4 Hz, 1H), 7.91 (d, *J*= 2.9 Hz, 1H), 6.20 (d, *J*= 8.4 Hz, 1H); ^{13}C-NMR (100 MHz, DMSO-d_6, 25 °C), δ, ppm = 153.6, 142.2, 132.1, 131.3, 103.1, 81.6; ESI-MS$^+$ (*m/z*): 256, 258, 260 $[M - Cl + H + OMe]^+$.

General procedure for the synthesis of compound series 44, 45, 46 and 47

2-Aminobenzothiazole **24a-e** (2 eq) was added to a solution of the corresponding chloride **38** (1 eq) in anhydrous THF (0.16 M). The mixture was heated at 70°C for 4-7 h under MW irradiation (300 W) then allowed to stand at room temperature. After removal of the solvent, the crude was subjected to FC on silica gel. The yield of isolated compounds **44**, **45**, and **46** were not higher than 11% (see below), whereas compounds **47** were isolated in

very low yields (1-5%). When longer reaction times were adopted, a little increase of symmetric compounds **47** was detected. However, this procedure has not been optimized and this will be object of future investigations.

Synthesis of *N*-(benzo[d]thiazol-2-yl)-2,2,2-trichloro-*N'*-(pyridin-2-yl)ethane-1,1-diamine (44a)

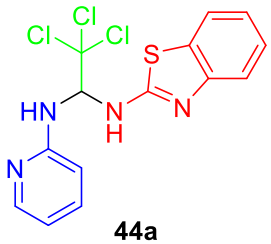

44a

General procedure was used employing the chloride **38a** (260 mg, 1 mmol) and amino benzothiazole **24a** (300 mg, 2 mmol). The reaction time was 4 hours. FC (eluent: 1/1 *n*-hexane/EtOAc) provided pure compound **44a** as white solid (40 mg, 0.11 mmol, 11% yield). m.p.: 172-174 °C dec.; ^{1}H-NMR (600 MHz, DMSO-d_6, 25 °C), δ (ppm): 8.89 (d, *J*= 7.8 Hz, 1H), 8.07 (d, *J*= 4.9 Hz, 1H), 7.71 (d, *J*= 7.8 Hz, 1H), 7.51-7.45 (m, 2H), 7.44-7.38 (m, 2H), 7.26 (t, *J*= 8.0 Hz, 1H), 7.07 (t, *J*= 7.4 Hz, 1H), 6.86 (d, *J*= 8.7 Hz, 1H), 6.65 (t, *J*= 5.7 Hz, 1H); ^{13}C-NMR (150 MHz, DMSO-d_6, 25 °C), δ, ppm = 165.0, 156.3, 151.5, 147.2, 137.3, 130.8, 125.6, 121.6, 121.1, 118.8, 114.1, 109.4, 102.8, 70.7; ESI-MS$^+$ (*m/z*): 373 $[M+H]^+$, 395 $[M+Na]^+$.

Synthesis of 2,2,2-trichloro-*N*-(6-methylbenzo[d]thiazol-2-yl)-*N'*-(pyridin-2-yl)ethane-1,1-diamine (44d)

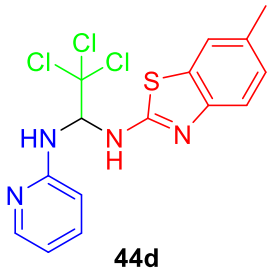

44d

General procedure was used employing the chloride **38a** (520 mg, 2 mmol) and amino benzothiazole **24d** (656 mg, 4 mmol). The reaction time was 6 hours. FC (eluent: 6/4 *n*-hexane/EtOAc) provided pure compound **44d** as white solid (5 mg, 0.01 mmol, 1% yield). m.p.: 167-170 °C dec.; ^{1}H-NMR (600 MHz, DMSO-d_6, 25 °C), δ (ppm): 8.75 (d, *J*= 8.1 Hz, 1H), 8.06 (d, *J*= 4.7 Hz, 1H), 7.51 (s, 1H), 7.47 (t, *J*= 7.6 Hz, 1H), 7.41-7.33 (m, 3H), 7.07 (d, *J*= 8.5 Hz, 1H), 6.85 (d, *J*= 8.5 Hz, 1H), 6.65 (t, *J*= 5.6 Hz, 1H), 2.33 (s, 3H); ^{13}C-NMR (150 MHz, DMSO-d_6, 25 °C), δ, ppm = 170.3, 164.3, 156.3, 149.4, 147.1, 137.3, 130.8, 126.6, 120.9, 118.4, 114.0, 109.3, 102.8, 70.7, 20.8; ESI-MS$^+$ (*m/z*): 387 $[M+H]^+$.

Synthesis of 2,2,2-trichloro-*N*-(6-chlorobenzo[d]thiazol-2-yl)-*N'*-(pyridin-2-yl)ethane-1,1-diamine (44e)

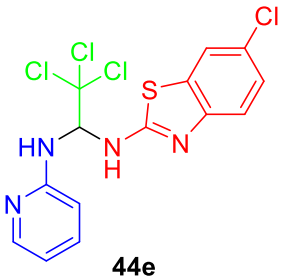

44e

General procedure was used employing the chloride **38a** (520 mg, 2 mmol) and amino benzothiazole **24e** (736 mg, 4 mmol). The reaction time was 7 hours. FC (eluent: 1/3/1 *n*-hexane/DCM/EtOAc) provided pure compound **44e** as white solid (7 mg, 0.02 mmol, 2% yield). ^{1}H-NMR (600 MHz, DMSO-d$_6$, 25 °C), δ (ppm): 9.00 (d, *J*= 8.2 Hz, 1H), 8.06 (d, *J*= 4.7 Hz, 1H), 7.85 (s, 1H), 7.52-7.45 (m, 2H), 7.44-7.36 (m, 2H), 7.26 (dd, J_1= 8.6 Hz, J_2= 2.2 Hz, 1H), 6.85 (d, *J*= 8.3 Hz, 1H), 6.65 (t, *J*= 6.1 Hz, 1H); ^{13}C-NMR (150 MHz, DMSO-d$_6$, 25 °C), δ, ppm = 165.8, 156.3, 150.4, 147.2, 137.4, 132.5, 125.8, 125.4, 120.8, 119.7, 114.1, 109.4, 102.6, 70.7; ESI-MS$^+$ (*m/z*): 407 [M+H]$^+$, 429 [M+Na]$^+$.

Synthesis of *N*-(benzo[d]thiazol-2-yl)-2,2,2-trichloro-*N'*-(pyridin-3-yl)ethane-1,1-diamine (45a)

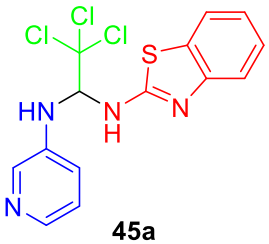

45a

General procedure was used employing the chloride **38b** (260 mg, 1 mmol) and amino benzothiazole **24a** (300 mg, 2 mmol). The reaction time was 4 hours. FC (eluent: 6/4 *n*-hexane/EtOAc) provided pure compound **45a** as white solid (30 mg, 0.08 mmol, 8% yield). m.p.: 116-118 °C; ^{1}H-NMR (600 MHz, DMSO-d$_6$, 25 °C), δ (ppm): 9.03 (d, *J*= 8.7 Hz, 1H), 8.31 (d, *J*= 2.8 Hz, 1H), 7.90 (dd, J_1=4.6 Hz, J_2= 1.2 Hz, 1H), 7.74 (d, *J*= 7.3 Hz, 1H), 7.55 (d, *J*= 8.0 Hz, 1H), 7.32 (d, *J*=8.6 Hz, 1H), 7.29 (t, *J*= 7.6 Hz, 1H), 7.17-7.13 (m, 1H), 7.10 (t, *J*= 7.5 Hz, 1H), 6.8 (d, *J*= 9.1 Hz, 1H), 6.42 (t, *J*= 8.6 Hz, 1H); ^{13}C-NMR (150 MHz, DMSO-d$_6$, 25 °C), δ, ppm = 165.4, 151.3, 141.9, 139.3, 136.5, 130.6, 125.7, 123.6, 121.8, 121.2, 119.7, 118.9, 101.3, 73.8; ESI-MS$^+$ (*m/z*): 373 [M+H]$^+$.

Synthesis of 2,2,2-trichloro-*N*-(6-ethoxybenzo[d]thiazol-2-yl)-*N'*-(pyridin-3-yl)ethane-1,1-diamine (45c

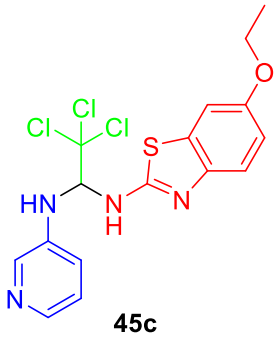

45c

General procedure was used employing the chloride **38b** (520 mg, 2 mmol) and amino benzothiazole **24c** (776 mg, 4 mmol). The reaction time was 4 hours. FC (eluent: 45/55 *n*-hexane/EtOAc) provided the product desired and a mixture of amino benzothiazole **24c** and desired product, further purified through crystallization in DCM. Pure compound **45c** was recovered as white solid (32 mg, 0.07 mmol, 4% yield). m.p.: 136-138 °C; ^{1}H-NMR (600 MHz, DMSO-d$_6$, 25 °C), δ (ppm): 8.81 (d, *J*= 8.6 Hz, 1H), 8.30 (d, *J*= 2.3 Hz, 1H), 7.9 (d, *J*= 4.6 Hz, 1H), 7.43 (d, *J*= 8.7 Hz, 1H), 7.35 (d, *J*= 1.5 Hz, 1H), 7.31 (d, *J*= 7.8 Hz, 1H), 7.16-7.12 (m, 1H), 6.87 (dd, J_1= 8.7 Hz, J_2= 1.8 Hz, 1H), 6.76 (d, *J*= 9.1 Hz, 1H), 6.36 (t, *J*= 8.9 Hz, 1H), 4.00 (q, *J*= 6.9 Hz, 2H), 1.32 (t, *J*= 7.1 Hz, 3H); ^{13}C-NMR (150 MHz, DMSO-d$_6$, 25 °C), δ, ppm = 163.3, 154.1, 145.3, 142.0, 139.3, 136.5, 131.7, 123.6, 119.7, 119.3, 113.9, 106.2, 101.4, 73.8, 63.6, 14.7; ESI-MS$^+$ (*m/z*): 439 [M+Na]$^+$.

Synthesis of 2,2,2-trichloro-*N*-(6-methylbenzo[d]thiazol-2-yl)-*N'*-(pyridin-3-yl)ethane-1,1-diamine (45d)

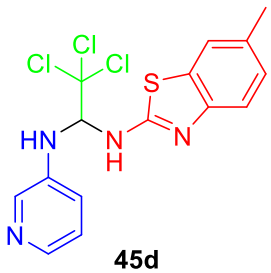

45d

General procedure was used employing the chloride **38b** (260 mg, 1 mmol) and amino benzothiazole **24d** (328 mg, 2 mmol). The reaction time was 4 hours. FC (eluent: 6/4 *n*-hexane/EtOAc) provided pure compound **45d** as white solid (25 mg, 0.06 mmol, 6% yield). m.p.: 138-140 °C; ^{1}H-NMR (600 MHz, DMSO-d$_6$, 25 °C), δ (ppm): 8.91 (d, *J*= 8.8 Hz, 1H), 8.30 (d, *J*= 2.5 Hz, 1H), 7.90 (d, *J*= 4.7 Hz, 1H), 7.53 (s, 1H), 7.42 (d, *J*= 8.4 Hz, 1H), 7.31 (d, *J*= 8.5 Hz, 1H), 7.16-7.12 (m, 1H), 7.10 (d, *J*= 7.7 Hz, 1H), 6.78 (d, *J*= 9.4 Hz, 1H), 6.39 (t, *J*= 8.9 Hz, 1H), 2.33 (s, 3H); ^{13}C-NMR (150 MHz, DMSO-d$_6$, 25 °C), δ, ppm = 164.6, 149.2, 141.9, 139.3, 136.5, 131.0, 130.7, 126.7, 123.6, 121.0, 119.7, 118.5, 101.3, 73.8, 20.8; ESI-MS$^+$ (*m/z*): 387 [M+H]$^+$.

Synthesis of 2,2,2-trichloro-*N*-(6-chlorobenzo[d]thiazol-2-yl)-*N'*-(pyridin-3-yl)ethane-1,1-diamine (**45e**)

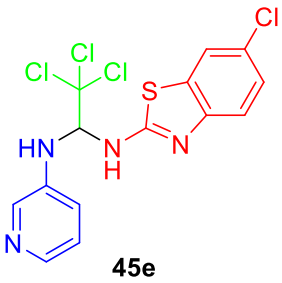

45e

General procedure was used employing the chloride **38b** (520 mg, 2 mmol) and amino benzothiazole **24e** (736 mg, 4 mmol). The reaction time was 7 hours. FC (eluent: 4/6 *n*-hexane/EtOAc) provided pure compound **45e** as white solid (8 mg, 0.02 mmol, 2% yield). m.p.: 157-159 °C; ^{1}H-NMR (600 MHz, DMSO-d_6, 25 °C), δ (ppm): 9.14 (d, *J*= 8.6 Hz, 1H), 8.29 (d, *J*= 2.8 Hz, 1H), 7.90 (dd, J_1= 4.5 Hz, J_2= 0.8 Hz, 1H), 7.87 (d, *J*= 2.1 Hz, 1H), 7.52 (d, *J*= 9.0 Hz, 1H), 7.32-7.28 (m, 2H), 7.17-7.13 (m, 1H), 6.83 (d, *J*= 9.6 Hz, 1H), 6.39 (t, *J*= 8.7 Hz, 1H); ^{13}C-NMR (150 MHz, DMSO-d_6, 25 °C), δ, ppm = 166.1, 150.2, 141.9, 139.4, 136.5, 132.4, 125.7, 123.7, 120.9, 119.9, 119.8, 104.6, 101.1, 73.9; ESI-MS$^+$ (*m/z*): 407 $[M+H]^+$, 429 $[M+Na]^+$.

Synthesis of *N*-(benzo[d]thiazol-2-yl)-2,2,2-trichloro-*N'*-(pyrimidin-4-yl)ethane-1,1-diamine (**46a**)

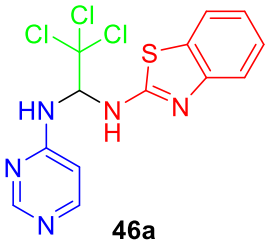

46a

General procedure was used employing the chloride **38e** (260 mg, 1 mmol) and amino benzothiazole **24a** (300 mg, 2 mmol). The reaction time was 7 hours. FC (eluent: 1/4 *n*-hexane/EtOAc) provided a mixture of amino benzothiazole **24a** and desired product, further purified on preparative TLC (eluent: 1/4 *n*-hexane/EtOAc). Pure compound **46a** was isolated as white solid (10 mg, 0.03 mmol, 3% yield). ^{1}H-NMR (600 MHz, DMSO-d_6, 25 °C), δ (ppm): 9.03 (d, *J*= 8.7 Hz, 1H), 8.59 (s, 1H), 8.34 (d, *J*= 8.7 Hz, 1H), 8.20 (d, *J*= 5.9 Hz, 1H), 7.73 (d, *J*= 7.7 Hz, 1H), 7.48 (d, *J*= 7.9 Hz, 1H), 7.46-7.42 (m, 1H), 7.26 (t, *J*= 8.0 Hz, 1H), 7.09 (t, *J*= 6.9 Hz, 1H), 6.87 (d, *J*= 6.0 Hz, 1H); ^{13}C-NMR (150 MHz, DMSO-d6, 25 °C), δ, ppm = 164.8, 160.9, 157.9, 155.3, 151.3, 130.9, 125.7, 121.8, 121.2, 118.9, 106.4, 101.8, 69.72; ESI-MS$^+$ (*m/z*): 374 $[M+H]^+$.

Synthesis of 2,2,2-trichloro-*N*-(4-methoxybenzo[d]thiazol-2-yl)-*N'*-(pyrimidin-4-yl)ethane-1,1-diamine (**46b**) DT_237

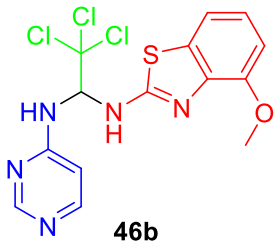

46b

General procedure was used employing the chloride **38e** (260 mg, 1 mmol) and amino benzothiazole **24b** (360 mg, 2 mmol). The reaction time was 7 hours. FC (eluent: 1/4 *n*-hexane/EtOAc) provided the product desired and a mixture of amino benzothiazole **24b** and desired product, further purified through crystallization in DCM. Pure compound **46b** was recovered as white solid (34 mg, 0.08 mmol, 8% yield). m.p.: 218-220 °C dec.; ^{1}H-NMR (600 MHz, DMSO-d$_6$, 25 °C), δ (ppm): 8.96 (d, *J*= 8.9 Hz, 1H), 8.58 (s, 1H), 8.32 (d, *J*= 8.9 Hz, 1H), 8.20 (d, *J*= 5.8 Hz, 1H), 7.40 (bt, *J*= 9.8 Hz, 1H), 7.32 (d, *J*= 8.0 Hz, 1H), 7.04 (t, *J*= 8.0 Hz, 1H), 6.88-6.85 (m, 2H), 3.87 (s, 3H); ^{13}C-NMR (150 MHz, DMSO-d$_6$, 25 °C), δ, ppm = 163.4, 160.9, 157.8, 155.3, 150.4, 140.7, 132.1, 122.6, 113.5, 108.9, 106.4, 101.9, 69.9, 55.9; ESI-MS$^+$ (*m/z*): 404 [M+H]$^+$, 426 [M+Na]$^+$.

Synthesis of 2,2,2-trichloro-*N*-(6-ethoxybenzo[d]thiazol-2-yl)-*N'*-(pyrimidin-4-yl)ethane-1,1-diamine (**46c**)

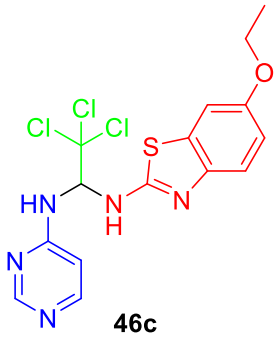

46c

General procedure was used employing the chloride **38e** (260 mg, 1 mmol) and amino benzothiazole **24c** (388 mg, 2 mmol). The reaction time was 6 hours. FC (eluent: 1/4 *n*-hexane/EtOAc) provided a mixture of amino benzothiazole **24c** and desired product, further purified on preparative TLC (eluent: 1/4 *n*-hexane/EtOAc). Pure compound **46c** was isolated as white solid (8 mg, 0.2 mmol, 2% yield). ^{1}H-NMR (600 MHz, DMSO-d$_6$, 25 °C), δ (ppm): 8.81 (d, *J*= 9.3 Hz, 1H), 8.58 (s, 1H), 8.30 (d, *J*= 9.3 Hz, 1H), 8.20 (d, *J*= 5.7 Hz, 1H), 7.43-7.33 (m, 3H), 6.87-6.83 (m, 2H), 4.00 (q, *J*= 7.1 Hz, 2H), 1.31 (t, *J*= 7.1 Hz, 3H); ^{13}C-NMR (150 MHz, DMSO-d$_6$, 25 °C), δ, ppm = 163.0, 160.9, 157.8, 155.2, 154.1, 145.3, 131.9, 119.3, 113.8, 106.1, 101.9, 69.7, 63.5, 14.7; ESI-MS$^+$ (*m/z*): 440 [M+Na]$^+$.

Synthesis of 2,2,2-Trichloro-*N*-(6-methylbenzo[d]thiazol-2-yl)-*N'*-(pyrimidin-4-yl)ethane-1,1-diamine (46d)

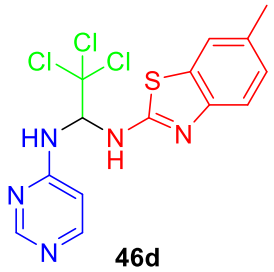

46d

General procedure was used employing the chloride **38e** (260 mg, 1 mmol) and amino benzothiazole **24d** (328 mg, 2 mmol). The reaction time was 6 hours. FC (eluent: 1/4 *n*-hexane/EtOAc) provided the product desired and a mixture of amino benzothiazole **24d** and desired product, further purified through crystallization in DCM. Pure compound **46d** was recovered as white solid (40 mg, 0.10 mmol, 10% yield). m.p.: 216-218 °C; ^{1}H-NMR (600 MHz, DMSO-d$_6$, 25 °C), δ (ppm): 8.91 (d, *J*= 9.0 Hz, 1H), 8.58 (s, 1H), 8.31 (d, *J*= 9.2 Hz, 1H), 8.20 (d, *J*= 5.9 Hz, 1H), 7.53 (s, 1H), 7.42 (bt, *J*= 10.3 Hz, 1H), 7.36 (d, *J*= 8.2 Hz, 1H), 7.07 (d, *J*= 8.2 Hz, 1H), 6.86 (d, *J*= 6.1 Hz, 1H), 2.32 (s, 3H); ^{13}C-NMR (150 MHz, DMSO-d$_6$, 25 °C), δ, ppm = 164.0, 160.9, 157.8, 155.3, 149.2, 131.0, 130.9, 126.7, 121.0, 118.6, 106.4, 101.9, 69.7, 20.8; ESI-MS$^+$ (*m/z*): 410 [M+Na]$^+$.

2,2,2-trichloro-*N*,*N'*-bis(6-ethoxybenzo[d]thiazol-2-yl)ethane-1,1-diamine (47c)

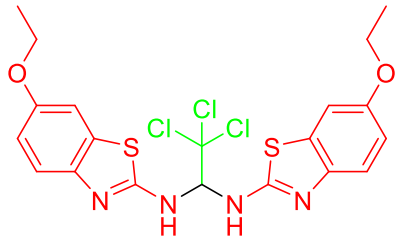

47c

White solid. m.p.: 162-164 °C; ^{1}H-NMR (600 MHz, DMSO-d$_6$, 25 °C), δ (ppm): 8.91 (d, *J*= 9.0 Hz, 2H), 7.39 (d, *J*= 8.8 Hz, 2H), 7.35 (d, *J*= 2.3 Hz, 2H), 7.16 (t, *J*= 9.0 Hz, 1H), 6.85 (dd, J_1= 8.9 Hz, J_2= 2.3 Hz, 2H), 3.99 (q, *J*= 7.2 Hz, 4H), 1.31 (t, *J*= 6.9 Hz, 6H); ^{13}C-NMR (150 MHz, DMSO-d$_6$, 25 °C), δ, ppm = 163.0, 154.1, 145.3, 132.0, 119.3, 113.8, 106.1, 101.6, 73.2, 63.5, 14.7; ESI-MS$^+$ (*m/z*): 517 [M+H]$^+$, 539 [M+Na]$^+$.

2,2,2-Trichloro-*N*,*N'*-bis(6-methylbenzo[d]thiazol-2-yl)ethane-1,1-diamine (47d)

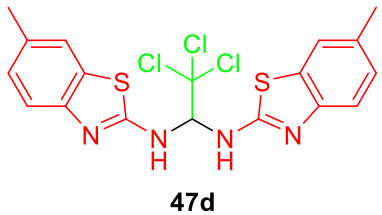

47d

White solid. ^{1}H-NMR (600 MHz, DMSO-d$_6$, 25 °C), δ (ppm): 9.03 (d, *J*= 8.6 Hz, 2H), 7.53 (s, 2H), 7.38 (d, *J*= 8.2 hz, 2H), 7.21 (t, *J*= 8.9 Hz, 1H), 7.08 (d, *J*= 8.0 Hz, 2H), 2.32 (s, 6H); ^{13}C-NMR (150 MHz, DMSO-d$_6$, 25 °C), δ, ppm = 164.1, 149.1, 131.0, 126.7, 121.0, 118.6, 104.6, 101.5, 73.2, 21.2; ESI-MS$^+$ (*m/z*): 479 [M+Na]$^+$.

2,2,2-trichloro-*N*,*N'*-bis(6-chlorobenzo[d]thiazol-2-yl)ethane-1,1-diamine (47e)

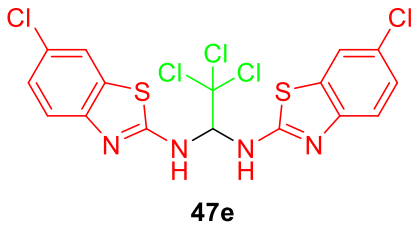

47e

Yellow solid. ^{1}H-NMR (600 MHz, DMSO-d$_6$, 25 °C), δ (ppm): 9.30 (d, *J*= 8.9 Hz, 2H), 7.88 (s, 2H), 7.49 (d, *J*= 8.9 Hz, 2H), 7.28 (dd, J_1= 8.9 Hz, J_2= 2.0 Hz, 2H), 7.22 (t, *J*= 8.7 Hz, 1H); ^{13}C-NMR (150 MHz, DMSO-d$_6$, 25 °C), δ, ppm = 165. 5, 150.1, 132.6, 125.9, 125.7, 120.9, 119.9, 101.0, 73.2; ESI-MS$^+$ (*m/z*): 519 [M+Na]$^+$.

References

[149] a) Hongtao, Y. *Molecular Cell*, **2007**, *27*, 1-16. b) Hartwell, L.H., Culotti, J., Reid, B. *Proc. Natl. Acad. Sci. USA*, **1970**, *66*, 352–359. c) Hartwell, L.H., Mortimer, R.K., Culotti, J., Culotti, M. *Genetics*, **1973**, *74*, 267–286.
[150] Sackton, K.L.; Dimova, N.; Zeng, X.; Tian, W.; Zhang, M.; Sackton, T.B.; Meaders, J.L.; Pfaff, K.L.; Sigoillot, F.D.; Yu, H. *Nature*, **2014**, *514*, 646–649.
[151] Simonetti, G.; Bruno, S.; Padella, A.; Tenti, E.; Martinelli, G. *Int. J. Cancer*, **2019**, *144*, 8–25.
[152] Lub, S.; Maes, A.; Maes, K.; De Veirman, K.; De Bruyne, E.; Menu, E.; Fostier, K.; Kassambara, A. ; Moreaux Dirk Hose, J.; Leleu, X.; King, R.W.; Vanderkerken, K.; E. Van Valckenborgh *Oncotarget*, **2015**, *7(4)*, 4062-4076.
[153] Gao, Y.; Zhang, B.; Wang, Y.; Shang , G. *Oncol. Rep.*, **2018**, *40*, 841-848.
[154] Wang, L.; Zhang, J.; Wan, L.; Zhou, X.; Wang, Z.; We, W. *Pharmacol. Ther.*, **2015**, *151*, 141-151.
[155] Oh, J.H.; Lee, T.J.; Kim, S.H.; Choi, Y.H.; Lee, S.H.; Lee, J.M.; Kim, Y.H.; Park, J.W.; Kwon, T.K. *Apoptosis*, **2008**, *13*, 1494–504.
[156] Okamoto, S.; Tsujioka, T.; Suemori, S.; Kida, J.; Kondo, T.; Tohyama, Y.; Tohyama, K. *Cancer Sci*, **2016**, *107*, 1302–1314.
[157] Oben, K.Z.; Alhakeem, S.S.; McKenna, M.K.; Brandon, J.A.; Mani, R.; Noothi, S.K.; Jinpeng, L.; Akunuru, S.; Dhar, S.K.; Singh, I.P.; Liang, Y.; Wang, C.; Abdel-Latif, A.; Stills, H.F.; St. Clair, D.K.; Geiger, H.; Muthusamy, N.; Tohyama, K.; Gupta, R.C.; Bondada, S. *Oncotarget*, **2017**, *8(44)*, 77436–52.
[158] Simonetti, G.; Padella, A.; Valle, I.F.D.; Fontana, M.C.; Fonzi, E.; Bruno, S.; Baldazzi, C.; Guadagnuolo, V.; Manfrini, M.; Ferrari, A. *Cancer*, **2018**, *125*, 712–725.
[159] Huang, P.; Le, X.; Huang. F.; Yang, J.; Yang, H.; Ma, J.; Hu, G.; Li, Q.; Chen, Z. *J. Med. Chem.*, **2020**, *63*, 4685-4700.
[160] Deng, X.Q.; Song, M.X.; Wei, C.X. *J. Med. Chem.*, **2010**, *6*, 313-320
[161] Sreenivasa, G.M.; Jayachandran, E.; Shivakumar, B. *Arch. Pharm. Res.*, **2009**, *1*, 150-157.
[162] Choi, M.M.; Kim, E.A.; Hahn, H.G. *Toxicology*, **2007**, *239*, 156-166.
[163] Jimonet, P.; Audiau, F.; Barreau, M. *J. Med. Chem.*, **1999**, *42*, 2828-2843.
[164] Bowyer, P.W.; Gunaratne, R.S.; Grainger, M. *Biochem. J.*, **2007**, *408*, 173-180.
[165] Huang, Q.; Mao, J.; Wan, B. *J. Med. Chem.*, **2009**, *52*, 6757-6767.
[166] Al-Tel, T.H.; Al-Qawasmeh, R.A.; Zaarour, R. *Eur. J. Med. Chem.*, **2011**, *46*, 1874-1881.
[167] Lee, Y.R.; Jin, G.H.; Lee, S.M. *Biochem. Biophys. Res. Comm.*, **2011**, *408*, 625-629.
[168] Kamal, A.; Srikanth, Y.V.; Naseer Ahmed Khan, M. *Bioorg. Med. Chem.*, **2011**, *23*, 7136-7150.
[169] Kamal, A.; Reddy, K.S.; Khan, M.N. *Bioorg. Med. Chem.*, **2010**, *18*, 4747-4761.
[170] Arun, P.; Moffett, J. R.; Namboodiri, A. M. *Brain Res.*, **2010**, *1334*, 25-30.
[171] Bradshaw, T.D.; Westwell, A.D. *Curr. Med. Chem.*, **2004**, *11*, 1241-1253.
[172] Aillaud, I.; Barber, D.M.; Thompson, A.L.; Dixon, D.J. *Org. Lett.*, **2013**, *15*, 2946–2949.
[173] Nelson,W.J.; Edwards, L.D.; Christian, E.J.; Jenkins, G.L. *J. Am. Pharm. Assoc.*, **1947**, *36*, 349–352.

Chapter IV: Benzofuroxan derivatives and 2-aminothiazoles: mechanistic and biological studies[174,175]

4.1. Introduction

Benzofuroxan and their derivatives belong to a class of heterocycles of wide and growing interest both in applied and in mechanistic field.[176,177] Depending on the substituents, they can be exploited in a range of applications, that can range from energetic materials[178,179] to biologically active compounds.

From the structural point of view, since from its discovery[180] the benzofuroxanyl ring has been a considerable challenge to organic chemists.[181,182] At first, benzofuroxans were thought to have the dioxime peroxide structure, then that of an o-dinitroso-system, and in 1912 the right structure was proposed[183] but only about 50 years later, NMR spectroscopy and X-ray crystallography have proved unequivocally the basic structure of benzo[1,2-c]1,2,5-oxadiazole *N*-oxide.[184,185]

Moreover, substituted benzofuroxans are source of interesting structural features. The first peculiarity is the possibility to undergo fast isomerisation between the *N*-1-oxide and *N*-3-oxide form, a transformation that is believed to occur through 1,2-dinitrosoarene as transient intermediate (pathway a, **Scheme 29**). The existence of this putative species has been supported by kinetic studies[186,187] and theoretical calculations;[188,189] spectroscopic indications of its existence were obtained by photolysis of benzofuroxan in Argon matrices at 14 K.[190] When benzofuroxan was reacted with acetonylmethyl sulfide,[191] *p*-anisyl azide and diphenyldiazomethane[192] the reaction products recovered were explained invoking the intermediacy of the 1,2-dinitrosoarene species. Terrier et al. reported the recovery and characterization of a diadduct from a Diels-Alder cycloaddition as a result of the reaction with a *o*-dinitroso species.[193] Recently, a Ruthenium complex of the 1,2-dinitrosoarene intermediate derived from the opening of the pentatomic ring of benzofuroxan has been reported.[194]

A second characteristic feature of substituted benzofuroxans is their susceptibility to undergo Boulton-Katritsky rearrangement (BKR) (pathway b, **Scheme 29**).[195,196] The BKR of 4-nitrobenzofuroxan can be considered as a prototype reaction for a class of molecular rearrangements and can compete with the *N*-1-oxide/*N*-3-oxide tautomerization; the direction of this rearrangement depends on the substituent in the 5 or 7 position.[197,198]

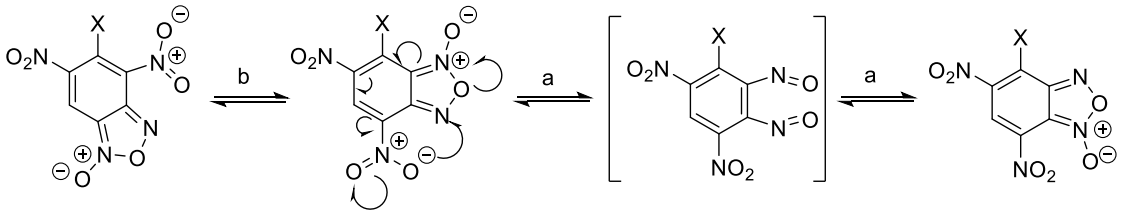

Scheme 29. Pathway a: *N*-1-oxide/*N*-3-oxide tautomerism. Pathway b: Boulton-Katritsky rearrangement.

A third peculiar aspect of benzofuroxans is their 10π-electron structure that confers them electrophilic properties. In particular, when two nitro substituents are bound to the carbocyclic ring of the benzofuroxan (or benzofurazan) or their derivatives, these compounds are so much electrophilic to be labeled as superelectrophiles.[199,200] Actually, it is well-known[201,202] that the reaction of 4,6-dinitrobenzofuroxan (DNBF), as well as 4,6-dinitrobenzofurazan (DNBZ), with a series of charged or neutral nucleophiles produces stable Meisenheimer intermediates. Recently, the coupling of DNBF or DNBZ with 1,3,5-triaminobenzene derivatives (**TABa-c**)[203] or 2-aminothiazoles[204,205] gave evidence of the zwitterionic intermediate (Wheland-Meisenheimer, **WM**) formed in these S_EAr/S_NAr aromatic substitution reactions (**WMa-h** in **Scheme 30**).

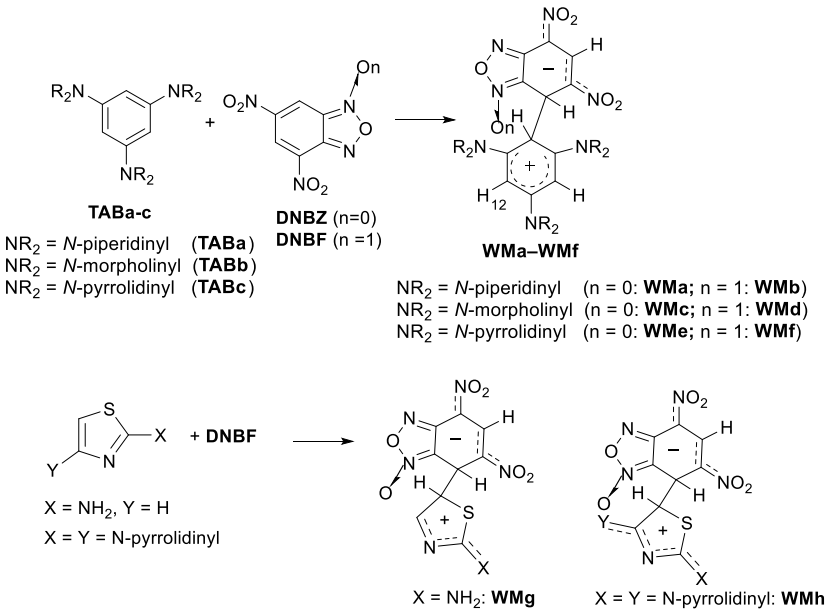

Scheme 30. Examples of **WM** intermediates detected and characterized using DNBF or DNBZ as electrophiles.

In particular, in thiazole series, the coupling between 2,4-dipyrrolidinylthiazole and DNBF produced the intermediate **WMh** (**Scheme 30**) that, owing to the high stability of the positive charge conferred to the Wheland moiety by the two pyrrolidinyl groups,[198] was stable enough to permit the first X-Ray structure of such a zwitterionic intermediates. On the other hand, 2,4-dipyrrolidinyl thiazole is a nucleophile so activated that, when reacted with other electrophiles such as aryldiazonium salts, a complicate mixture of compounds was obtained. On the contrary, 2-pyrrolidinylthiazole gave, in good yield, the corresponding azo derivatives bound in position 5 of the thiazole ring.[206]

As bioactive compounds, benzofuroxans can behave as anti-parasitic, anti-microbial, anti-fungal, immunosuppressive and anticancer agents, and have anti-aggregating and vasorelaxant activity owing to their ability to release NO under physiological conditions.[207,208]

Also 2-aminothiazoles derivatives are of great interest for pharmaceutical production, biochemistry, engineering, clinical and experimental medicine. They are used as disperse dyes in cotton industries,[209,210] and in medical field posses high anti-inflammatory, analgesic, antioxidant,[211] antiviral,[212] antimycobacterial,[213] antiplasmodial,[214] anticancer,[215] neuroprotective and anti-inflammatory properties.[216]

For example, 2-aminothiazole derivatives, such as Norsulfazolum, Phthalylsulfathiazole, Khlotazol, Nitazol, Abafungin, Cefdinir, Meloxicam (shown in **Figure 46**) are widely used in medicine and veterinary medicine as a nonsteroidal anti-inflammatory and antimicrobial agents.

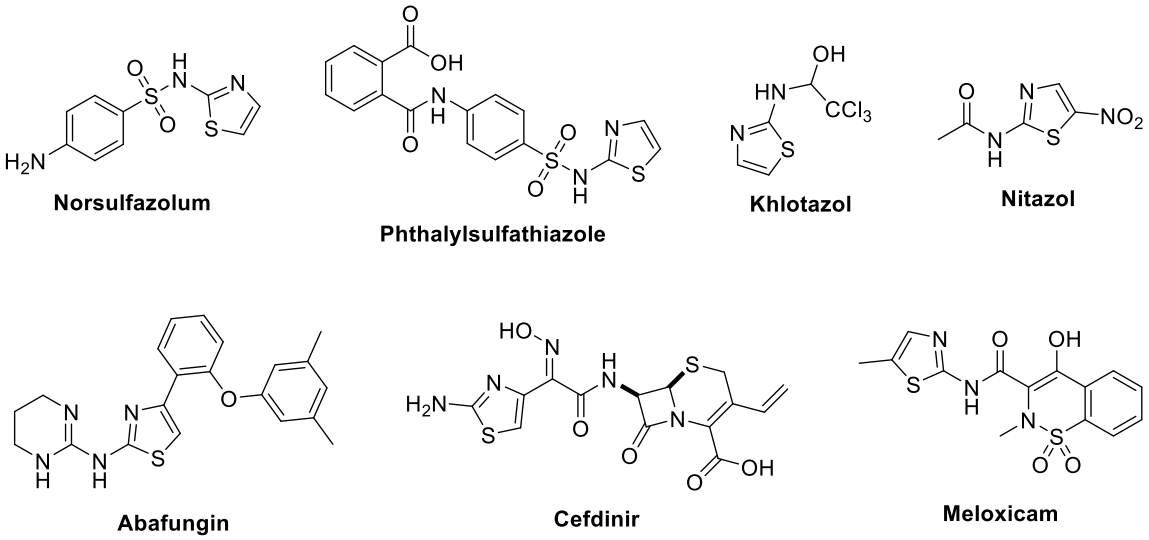

Figure 46. Drugs characterized by an aminothiazole moiety.

2-Aminothiazole molecule has three nucleophilic reaction centers (endocyclic nitrogen atom, exocyclic NH_2 group and the carbon atom in 5-position, **Figure 47**), which provide additional interest of research on this compound.

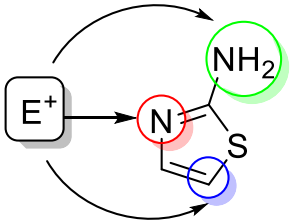

Figure 47. Three possible reactions sites of an electrophile towards 2-aminothiazole.

In this context, we designed to carry out reactions between some 2-aminothiazole derivatives and 7-chloro-4,6-dinitrobenzofuroxan (ClDNBF) or 7-chloro-4,6-dinitrobenzofurazan (ClDNBZ) to obtain novel hybrids bearing two moieties, thiazolyl- and benzofuroxanyl one. Our attention focused not only on the obtainement of reaction products, but also on the mechanistic behavior and the biological activity of the compounds synthesized.

4.2. Results and discussion

To study the mechanism of interaction between 7-chloro-4,6-dinitrobenzofuroxan (**48**) (ClDNBF) and 2-aminothiazole (**49**), a quantum-chemical study of these reactions has been carried out. Three possible ways have been considered for this S_NAr reaction: Pathway 1—attack of the electrophile on the exocyclic NH_2; Pathway 2—attack of the electrophile on the endocyclic nitrogen atom; and Pathway 3—attack on the carbon atom in position 5 of the thiazole ring (**Scheme 31**).

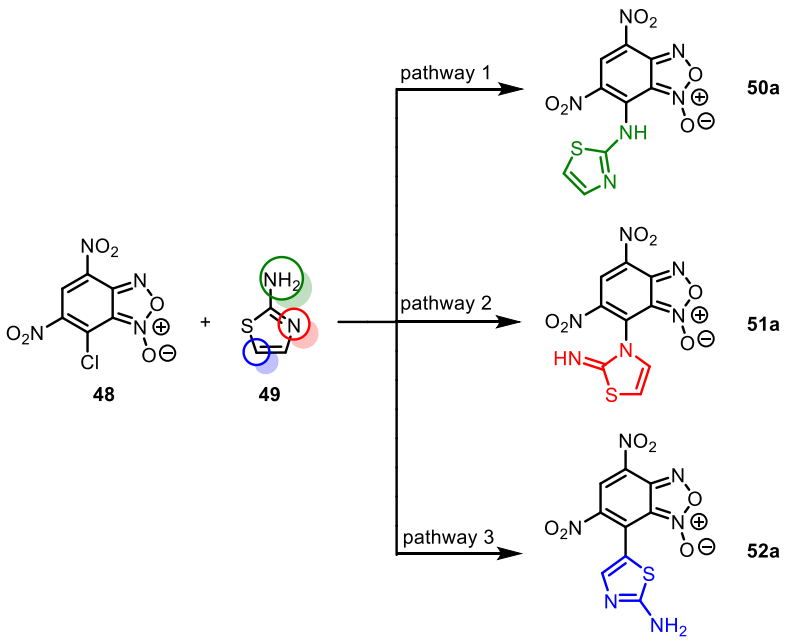

Scheme 31. Three possible reaction pathways starting from **48** and **49**.

Analysis of transition states thorugh computational studies for the three considered pathways showed the highest barrier for pathway 3, where ΔE resulted to be 18.3 kcal/mol compared to 13.2 and 12.8 for pathways 1 and 2 respectively (details in ref 175).

Pathways 1 and 2 can form different isomers both due to the N-1/N-3-oxide equilibrium and/or prototropic tautomerism in the molecule (**Table 7**). Among them, the most stable one is **50aC**; however, the energy difference between models with different locations of hydrogen (at amine/thiazole N: **50aA/50aC** and **50aB/50aD**) is less than 1 kcal/mole, suggesting the possible coexistence of both structures (**Table 7**). The preferable location of the benzofuroxan oxygen moiety is at the N1 atom that is almost by 4 kcal/mol more advantageous compared to the tautomers with an oxygen atom located at N3. Instead the products **51aA** and **51aB** that can be obtained by Pathway 2 are unfavorable (**Table 7**). Thus, the reaction will more easily proceed by kinetically close pathways 1 and 2; however, the first way is preferable, leading to much more stable thermodynamically products **50aC** and **50aA**.

Table 7. Possible tautomeric forms of benzofuroxan derivatives **50** and **51** and relative energies.

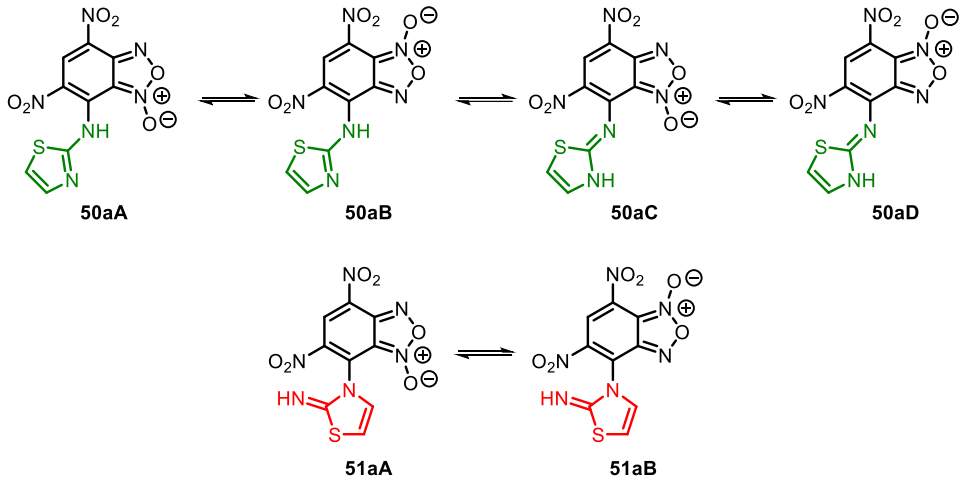

Tautomer	50aA	50aB	50aC	50aD	51aA	51aB
ΔE (Kcal/mol)	0.9	4.6	0	3.9	14.6	16.3

Once understood the mechanism between 2-aminothiazole (**49**) and ClDNBF, novel benzofuroxan derivatives were designed and synthesized. It has to be noted, however, that the above is strictly applicable to 2-aminothiazole or 2-aminothiazoles bearing a secondary amine that permits endo/exo prototropy leading to compounds as **50a** and **51a.**

4.2.1. Reactions between 7-chloro-4,6-dinitrobenzofuroxan and thiazoles 2-substituted with cyclic amino groups

As first approach, we planned to study the reaction between ClDNBF and aminothiazoles bearing cyclic secondary amines in 2-position, a situation that hinders both pathways 1 and 2 of **Scheme 31**, while make possible pathway 3.

Thus, 2-morpholinylthiazole (**55a**), 2-piperidinylthiazole (**55b**) and 2-pyrrolidinyl-thiazole (**55c**) have been synthesized at room temperature under solvent-free conditions by reacting 2-bromothiazole (**53**) with morpholine (**54a**), piperidine (**54b**), or pyrrolidine (**54c**), respectively (**Scheme 32**). Compounds **55a-c** have been obtained in 90, 95, and 98% yield after 24, 4 and 2 h, respectively; the different reaction time required to reach the indicated yields is likely due to the different nucleophilicity of the starting amines that, according to the nucleophilic scale developed by Mayr,[217,218,219] are, in acetonitrile at 20 °C, N_{Mayr} = 15.65, 17.35, and 18.64 for **54a**, **54b**, and **54c**, respectively.[220] As explained before, the selected substrates **55a-c** bear a secondary amino group bound in position 2 and this prevents the tautomeric equilibrium and the attack of ClDNBF to the exocyclic or endocylic

nitrogen atoms, permitting only formation of **56a-c** derived from the nucleophilic attack at C-5 (**Scheme 32**), a behavior previously found for the reaction of **55a-c** with aryldiazonium salts.[199]

The reaction between **55a-c** and 7-chloro-4,6-dinitrobenzofuroxan (**48**) was carried out in acetonitrile at room temperature using the reagents in a 2:1 relative molar ratio. Immediately, a blue color developed. The reaction, monitored by TLC, showed presence of a blue spot with R_F higher than that of the starting reagents. After 24h (for the combination **55a/48**), 12h (for **55b/48**), or 4 h (for **55c/48**), the crude was subjected to column chromatography on silica gel (FC) and the blue fraction was isolated.

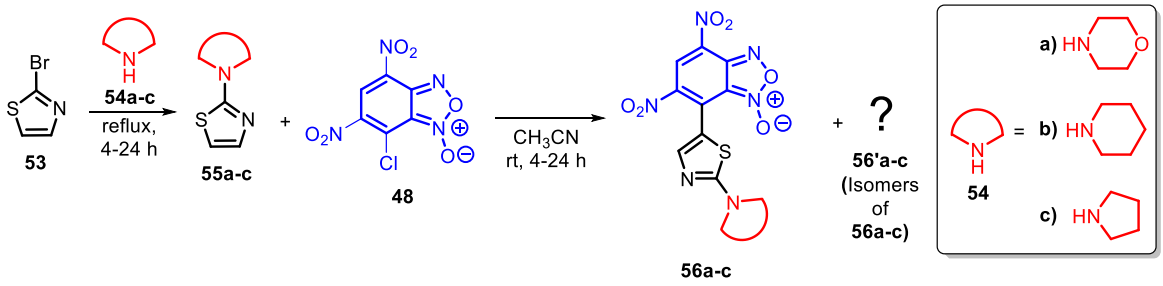

Scheme 32. Synthesis of benzofuroxan derivatives **56a-c**.

The ESI-MS of the blue solid isolated agreed with that of a product derived from the aromatic substitution between **55a–c** and **48**, but the ^{1}H- and ^{13}C-NMR spectrum showed a number of signals higher with respect to those expected for species **56a-c**. In particular, the ^{1}H-NMR spectrum in CD_3CN of the solid derived from the reaction between **55c** and **48** showed four singlets in the aromatic region, with relative integration suggesting the presence of two isomers bearing the benzofuroxan moiety bound to the C-5 of the thiazole moiety in 6/4 relative molar ratio (**Figure 48**). After many attempts to separate the two species, two blue spots were observed on the preparative TLC plate (eluent diethyl ether : petroleum light 7:3). Then, each spot was scraped and worked-up, and the organic residues were dissolved in CD_3CN and analyzed by NMR. Surprisingly, each spectrum showed presence of two compounds, as previously observed after FC, thus suggesting the occurrence of a re-equilibration phenomenon.

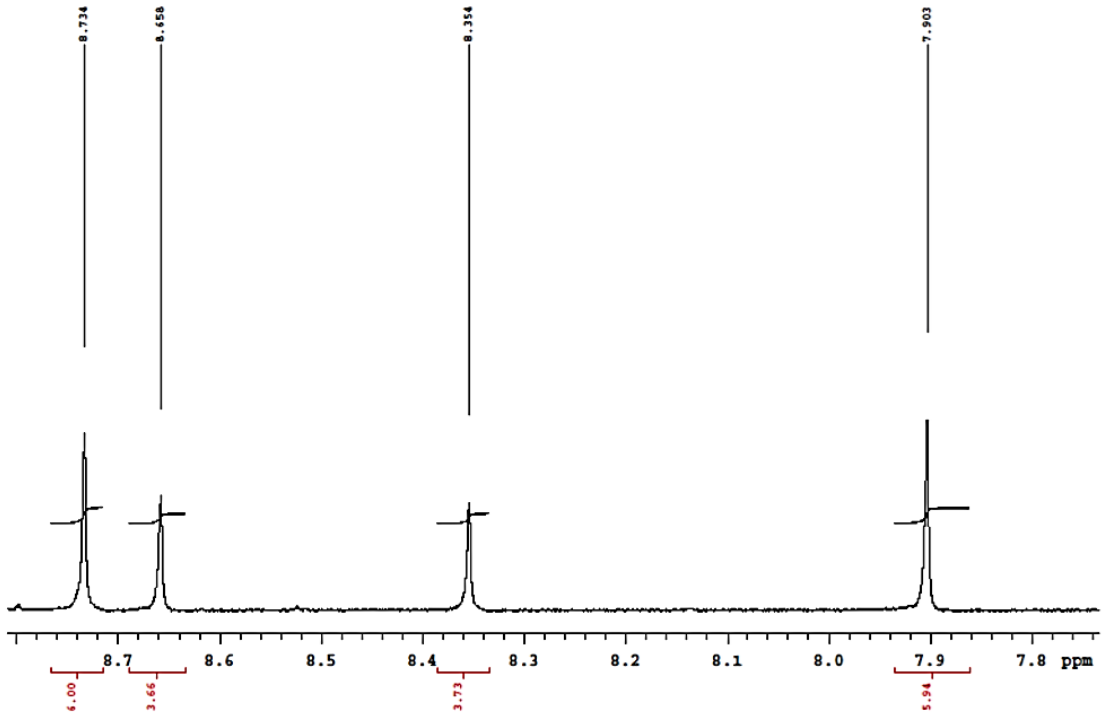

Figure 48. ^{1}H-NMR spectrum in CD_3CN (expanded view) of the reaction products obtained from **55c** and **48** indicating the presence of two species.

These findings suggested to deepen this behavior; below we report, divided in sub-headings, the steps of the investigation.

Is the isomeric ratio or the reaction outcome influenced by the solvent or the temperature?
To investigate whether the relative ratio between the two isomers could be influenced by the solvent or the temperature, we studied the behavior of the isomeric mixture derived from the combination of **55c** and **48**. The isomeric mixture, after isolation by FC, was analyzed through ^{1}H-NMR in different solvents at 25 °C. We attributed the two set of signals to the isomers A and A' without direct relation to structure **56c** of **Scheme 32**. The results are reported in **Table 8**.

Table 8. Relative ratio of the isomers[a] derived from the reaction between **55c** and **48** in different solvents.

Entry	Solvent polarity[b]	Solvent	Isomer A (%)[c]	Isomer A' (%)[c]
1	Benzene 0.111	Benzene-d_6	53	47
2	THF 0.207	Tetrahydrofuran-d_8	50	50
3	$CHCl_3$ 0.259	Chloroform-d_1	55	45
4	Acetone 0.355	Acetone-d_6	57	43
5	CH_3CN 0.460	Acetonitrile-d_3	60	40
6	DMSO 0.444	DMSO-d_6	67	33
7	CH_3OH 0.762	Methanol-d_4	59	41

[a] After isolation by FC; [b] Data from ref. [221]; [c] Calculated from the ^{1}H-NMR spectrum recorded at 25 °C.

From the relative integration of the signals of the two species it emerged that their relative ratio is always in favor of the same isomer except in THF (entry 2, **Table 8**). The most relevant difference was observed in DMSO (entry 6, **Table 8**). On going from THF to acetonitrile (entries 2-5, **Table 8**) the relative ratio seems to be slighly dependent from the solvent even if, from the data obtained, a clear correlation with the solvent polarity cannot be advanced.

In a second series of experiments the ^{1}H-NMR spectrum of the mixture A and A' at variable temperature and in different solvents was recorded. The results are reported in **Table 9**.

Table 9. Isomeric ratio of the products[a] derived from **55c** and **48** in different solvents at different temperatures.

Entry	Solvent	Temperature (°C)	Isomer A (%)[b]	Isomer A' (%)[b]
1	DMSO-d_6	25	67	33
2		35	65	35
3		50	64	36
4		70	60	40
5		80	57	43
6	CD_3CN	25	61	39
7		35	61	39
8		45	59	41
9		55	58	42
10		65	58	42
11	Acetone-d_6	25	57	43
12		0	60	40
13		-20	60	40
14		-50	60	40
15		-90	60	40

[a] After isolation by FC; [b]Calculated from the ^{1}H NMR spectrum.

In DMSO-d_6 the spectrum of the mixture was recorded from 25 °C to 80 °C (entries 1-5, **Table 9**): on raising the temperature, a gradual increase (until 15%) of the minor isomer was observed. On the contrary, no significant variation was observed both in acetonitrile from 25 °C to 40 °C (entries 6-10, **Table 9**) and in acetone from +25 °C to –90 °C (entries 11-15, **Table 9**). These findings suggest that, once the mixture of isomers is formed (by reaction in acetonitrile at room temperature), their relative ratio cannot be modified changing the temperature both in acetonitrile and in acetone, while in DMSO it seems to be slightly influenced by an increase of the temperature.

After, the reaction was carried out directly in the NMR spectroscopy tube both at room temperature and at low temperature. When reagents **55c** and **48** (in 2:1 molar ratio) were mixed at 25 °C in $CDCl_3$ or CD_3CN, the ratio between the two isomers was equal to that reported in entries 3 and 5 of **Table 8**, respectively. Surprisingly, when the reagents were mixed in DMSO-d_6, no product was formed.

In the experiments carried out at low temperature, cooled solutions of reagents **55c** and **48** in deuterated solvent were mixed in the NMR spectroscopy tube that was immediately inserted in the cooled NMR probe, and the ^{1}H-NMR spectrum was recorded at low

temperature. The reaction was monitored with time and at different temperatures. The results are reported in **Table 10**.

Table 10. Monitoring[a] of the reaction outcome between **55c** and **48** carried out in different solvents at variable temperature.[b]

Entry	Solvent	Temp (°C)	Conversion	A/A'[c]
1	**$CDCl_3$**	-48	32	43/57
2		-37	40	36/64
3		-26	50	34/66
4		-15	58	31/69
5		-4	71	41/59
6		+30	90	55/45
7		+40	93	56/44
8	**CD_3CN**	-43	36	75/25
9		-32	42	80/20
10		-21	45	85/15
11		-9	66	78/22
12		+6	74	73/27
13		+13	84	72/28
14		+24	91	62/38
15		+24 after 1 day	99	62/38
16	**Acetone-d_6**	-93[d]	7	95/5
17		-82[d]	7	93/7
18		-71[d]	8	92/8
19		-59[d]	8	95/5
20		-48[d]	11	96/4
21		-37[d]	22	96/4
22		-26[d]	35	96/4
23		-15	51	93/7
24		-15 after 10 min.	61	87/13
25		-4	71	72/28
26		-4 after 10 min.	78	63/37
27		+8[d]	86	59/41
28		+25[d]	94	58/42

[a] Monitoring of the reaction conversion and isomeric ratio of the products through ^1H NMR spectroscopy at variable temperature; [b.] Reaction carried out directly in the NMR tube by mixing, at the lowest temperature indicated in the Table, **55c** and **48** in 2:1 molar ratio. [c.] % molar ratio calculated from the NMR spectrum of the crude reaction mixture; [d.] the conversion and relative ratio values remained unchanged by recording the spectrum immediately after the change of temperature and after having kept the system for 10 min at this temperature.

The reaction was carried out in acetone-d_6 at –93 °C, in $CDCl_3$ at – 48 °C, and in CD_3CN at –43 °C. In all cases the conversion was low and the ^{1}H-NMR spectrum showed prevalence of signals of one isomer with respect to those of the other. On raising the temperature, the conversion gradually increased until to reach completeness at +25 °C; at this temperature the relative isomeric ratio was in all cases about 6/4, in agreement with results reported in **Table 8**. It has to be noted that in $CDCl_3$, once the reaction was complete, the major isomer was the opposite with respect to that formed at low temperature. In acetonitrile at -43 °C the conversion was 36% and the isomeric ratio 75/25. This ratio increased until 85/15 at -21 °C then gradually decreased until to became 62/38 at 25 °C; the conversion gradually increased by raising the temperature.

In acetone-d_6 at -93 °C, the reaction occurred with low conversion (7%) producing the two isomers in 95/5 relative % ratio. This latter remained almost unchanged from -93°C to -26 °C; within this temperature range the conversion gradually reached 35%. On raising again the temperature until 25 °C, the conversion further increased until to reach almost completeness and, contemporarily, the isomeric ratio gradually changed until to became 58/42.

In acetone-d_6 we also recorded the ^{1}H-NMR spectrum of ClDNBF from +25 °C to -93 °C in order to see if it might be possible to detect the presence of two species or of the corresponding dinitroso intermediate, but no variation was detected; this can be considered an indication that the formation of A and A' might occur during the C-C coupling.

It has to be emphasized the peculiarity of this behavior; actually, in previous studies on the C-C coupling between ClDNBF and diamino-, triamino- or trihydroxybenzene derivatives, only one product was always isolated.[195,222]

Overall, even if the behavior in acetone seems to suggest that the formation of the isomer A occurs under kinetic control conditions (being A the almost exclusive product at lowest temperatures), the partial conversion at low temperature and the contemporaneous variation of both, the conversion and the relative molar ratio of the two isomers on raising the temperature, do not permit to state if the formation of the two species A and A' depends from a kinetics or a thermodynamic control, or from both.

Finally, it is worth note that, in the ^{1}H-NMR spectra recorded when the conversion was not complete, the signals belonging to the unreacted starting aminothiazole and those of the aminothiazole salified with hydrochloric acid formed in the reaction were not distinguishable: this indicates the occurrence of an equilibrium between the two species,

i.e. protonated and not-protonated 2-aminothiazole, a behavior similar to that already observed by us in similar protonation reactions.[199]

What about the structure of the two isomers?

The unexpected finding of the formation of two isomers from the reaction between ClDNBF and aminothiazoles **55a-c** has given rise the enigma on their structure and on the mechanism of their formation. From the mechanistic point of view, it has to be considered that, in principle, the products from the reaction between **55a-c** and ClDNBF might undergo structural rearrangement through two main pathways: *N*-1/*N*-3-oxide tautomerism (pathway a, **Scheme 33**) or Boulton-Katritzky rearrangement (BKR, pathway b, **Scheme 33**). The first equilibrium is a ring open-closure via the 1,2-dinitroso intermediate that, in current case, might produce species B1 and B2 of **Scheme 33**, derived from the formal shift of the oxygen atom from *N*-1 to *N*-3.

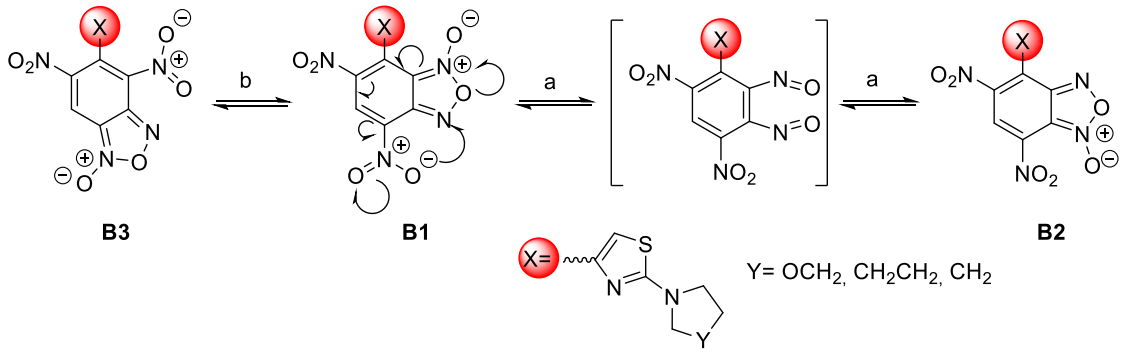

Scheme 33. Different pathways of rearrangement of benzofuroxans **56a-c**. Pathway a: *N*-1/*N*-3-oxide equilibrium. Pathway b: BKR.

The second reaction pathway, *i.e.* BKR, occurs when the benzofuroxan moiety bears a nitro group bound on the carbon atom belonging to the carbocyclic ring and adjacent to the fusion carbon, as in current case. In **Scheme 33** we indicated the occurrence of BKR on product B1 because it has been reported that **48** does not undergo BKR rearrangement.[223]

In principle, both the mechanisms might contemporarily occur but this has to be excluded given that in ^{1}H-NMR spectrum of the crude reaction mixture only presence of two novel species was detected. On the contrary, in case of occurrence of both the rearrangements, the signals of three products, B1, B2, and B3, must be detected. Therefore, we planned experiments to discriminate between the two possible pathways. Focusing attention to the possible occurrence of the N-1/N-3 oxide interconversion, we realized that the reduction of B1 and B2 from furoxan derivatives to furazans produces the same product. Thus, the

isomeric mixture **56c/56'c** (also indicated as A and A' in **Tables 8-10**, without correspondence of the structure of A or A' with **56c** in **Scheme 5**) derived from the reaction between **55c** and **48** was subjected to reduction with triphenylphosphine in xylene. Since only one compound was recovered as reduction product, the hypothesis of the occurrence of the 1-oxide/3-oxide tautomerism depicted in **Scheme 33** is strongly supported. However, it is not possible to exclude, '*a priori*', the occurrence of a preferential reduction of only one of the two species involved in the BKR rearrangement, and this, due to the equilibrium, also might give only one isomer after reduction.

To shed light on this, it was necessary to ascertain the structure of the product derived from the reduction of the mixture of A + A'. For this purpose, an authentic sample of the product that might derive from the reduction of B1 and B2, namely **59c**, was prepared in order to compare its data with those of the product obtained by reduction of the mixture **56c**+**56'c**.

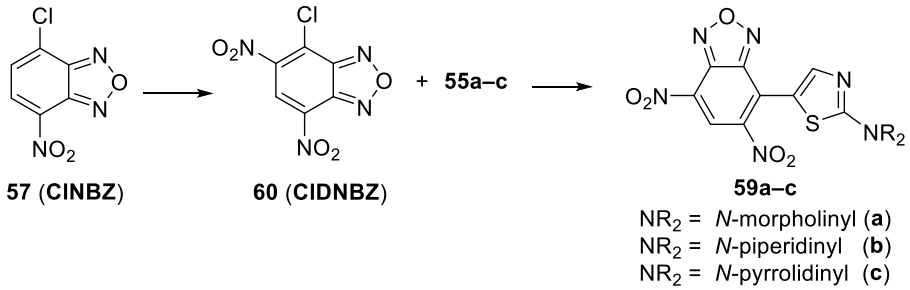

Scheme 34. Synthesis of **59a-c**.

According to the procedure shown in **Scheme 34**, 4-chloro-5,7-dinitrobenzofurazan (**60**) prepared by nitration of 4-chloro-7-nitrobenzofurazan (**57**, ClNBZ) was reacted with **55c** to give **59c**, whose chemico-physical data agreed with those of the unique compound obtained by reduction of mixture of isomers **56c** and **56'c**. Moreover, by adding a little amount of **59c** to the product obtained by reduction of the mixture of **56c** and **56'c**, an increase of its ^{1}H-NMR signals was observed. Through this procedure also **59a** and **59b** were synthesized, given that **59a-c** were unknown and possess contemporarily an electron-donor and an electron-withdrawing moiety, a feature that might be of interest in applied field.

Summarizing, the above findings permitted to exclude structure B3 in favor of a 1/3-oxide rearrangement since in this case the reduction of the furoxan ring to furazan ring produces the same product.

DFT Calculations

Focusing attention on the attribution of the NMR signals belonging to isomers A and A' to structure **56** or **56'**, and to further confirm that their structures are those derived from 1/3-oxide rearrangement, we have resorted to DFT calculations (details in ref 174). Even if, owing their different relative ratio and with the aid of *g*-HSQC experiments, we were able to distinguish ^{13}C-NMR signals of A and A', that are collected in **Table 11**, the structure of A and A' (due to the 1/3 oxide rearrangement) in solution cannot be unambiguously assigned by NMR experiments solely.

Table 11. Calculated energies for A and A' tautomers. Experimental and calculated ^{13}C chemical shifts[a]

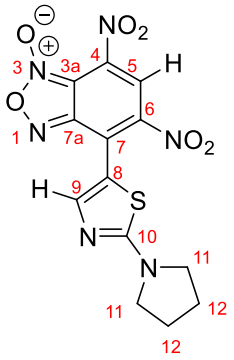

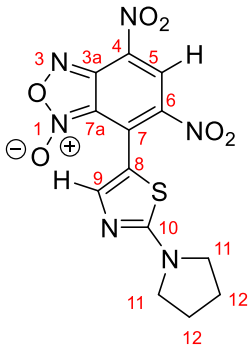

Energy (kcal/mol)	0.0		0.23	
^{13}C chem shifts	**Calc.**	**Exp.[a] (A, major isomer)**	**Calc.**	**Exp.[a] (A', minor isomer)**
C_{3a}	106.12	105.95	144.84	144.89
C_4	127.03	124.97	126.21	125.38
C_5	125.03	127.87	128.71	128.53
C_6	138.13	137.95	137.51	138.93
C_7	127.38	128.04	129.73	130.72
C_{7a}	151.20	151.26	114.73	113.43
C_8	115.67	113.83	110.92	109.06
C_9	157.53	156.57	156.59	153.85
C_{10}	171.60	172.54	173.37	172.38
C_{11}	50.64	50.76	50.97	50.76
C_{12}	27.23	25.61	27.21	25.55

[a] Data from spectra recorded at T = 25 °C in $CDCl_3$.

One of the main difficulties in studying these compounds spectrometrically resides mainly in the lack of spin markers (protons). The *g*-HSQC experiments allowed to assign with confidence only correlations with the H5 and H9 signals while other correlations are usually too weak to be used in structural elucidation. Quantum mechanical calculations of ^{13}C-NMR chemical shifts are widely used to make easier signal assignment. Thus, a joint analysis of experimental and calculated NMR ^{13}C chemical shifts was used for the assignment of the ^{13}C chemical shifts of the two tautomers. The ^{13}C theoretical chemical shifts (**Table 11**) correlate very well with the experimental data, with correlation coefficients of least-squares linear fits (R^2) close to unity (0.9995 and 0.9992 respectively for A and A'). Theoretical calculations allowed also the determination of the energy of the tautomers A and A'. The most abundant tautomer A (*N*-3-oxide) is also energetically more stable than A' (*N*-1-oxide). The energetic difference between the two tautomers is very small (0.23 kcal mol^{-1}), explaining their presence in a isomeric mixture (**Table 8**).

4.2.2. Reactions between 7-chloro-4,6-dinitrobenzofuroxan and thiazoles 2-substituted with primary or acyclic secondary amino groups

Benzofuroxan **48** was also reacted with a series of thiazoles bearing a primary (**49**) or a secondary amino group in 2-position (**61a-f**) as shown in **Scheme 35** to obtain novel compounds in order to investigate their biological activity as anticancer agents. The reaction was carried out in $CHCl_3$ at room temperature between ClDNBF and 2-aminothiazole derivatives **49** and **61a-f** in a 1:2 molar ratio (**Scheme 35**). The excess of 2-aminothiazole is used to neutralize the hydrogen chloride formed during the reaction.

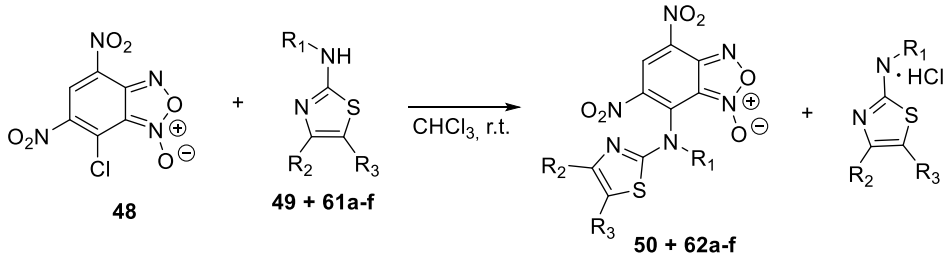

49,**50**: R_1=R_2=R_3=H
61,**62**: R_1=R_2=H, R_3= Me (**a**)
R_1=R_3=H, R_2= COOEt (**b**)
R_1=Ph, R_2=R_3=H (**c**)
R_1=Ph, R_2=H, R_3=Me (**d**)
R_1=*p*-OMePh, R_2=R_3=H (**e**)
R_1=*m*-ClPh, R_2=R_3=H (**f**)

Scheme 35. Synthesis of benzofuroxan derivatives **50** and **62a-f**.

In this case, the reaction led to the formation, in good yields, of the thermodynamically more stable product bearing the benzofuroxan moiety bound to the exocyclic nitrogen atom of the thiazole ring.

The structure of the novel compounds **50** and **62a-f** was ascertained through ^{1}H-, ^{13}C-, ^{15}N-NMR analysis and 2D-NMR techniques (COSY, HSQC and HMBC).

Biological test[175]

In order to gain information on the anticancer activity of compounds synthesized and their possible mechanism of action, preliminary biological tests were carried out.

The biological study was carried out by scientist of Institute of Organic and Physical Chemistry in Kazan Scientific Center.

The cytotoxicity was tested against human normal and cancer cell lines at 1-100 μM. concentration of synthesized compounds. The IC_{50} values obtained are summarized in **Table 12**.

The drugs tamoxifen and 5-fluorouracil, widely used in medicinal field, were used as reference substances.

Table 12. IC_{50} values of compounds synthesized against cancer and normal human cell lines.

Compound tested	Cancer cell lines			Normal cell line Chang Liver
	HeLa	HuTu 80	PANC-1	
48	94.1 μM ± 8.6	>100 μM	>100 μM	>100 μM
49	91 μM ± 8.3	>100 μM	>100 μM	>100 μM
50	61 μM ± 5.4	>100 μM	>100 μM	>100 μM
61 a	92 μM ± 7.9	>100 μM	>100 μM	>100 μM
62 a	70 μM ± 6.2	>100 μM	>100 μM	>100 μM
61 b	63.3 μM ± 5.7	>100 μM	>100 μM	95.4 μM ± 8.7
62 b	95.8 μM ± 8.4	>100 μM	>100 μM	100 μM ± 9.4
62 c	61 μM ± 5.6	>100 μM	>100 μM	86.1 μM ± 7.8
61 d	92 μM ± 8.2	>100 μM	>100 μM	>100 μM
62 d	79 μM ± 6.3	>100 μM	>100 μM	85.8 μM ± 7.4
61 e	93.8 μM ± 8.4	>100 μM	>100 μM	>100 μM
62 e	56.6 μM ± 4.7	>100 μM	>100 μM	>100 μM
Tamoxifen	28.0 μM ± 2.5	-	-	46.2 μM ± 3.5
5-Fluorouracil	62.0 μM ± 4.9	65.2 μM ± 5.5	68.3 μM ± 5.7	72.4 μM ± 6.5

As shown in **Table 12**, in relation to the M-HeLa cancer cell line, the compounds **50**, **62c** and **62d** exhibit moderate citotoxicity. Moreover the compounds **50**, **62a**, **62d** and **62e** turned out to be more active than their starting materials and **50**, **62c** and **62e** are more active than 5-fluorouracil. In relation to HuTu 80, PANC-1 and the normal cell line Chang Liver, all tested compounds did not show toxicity.

Apoptotic effect of the most active compound **62e** was studied by flow cytometry in order to establish whether the cytotoxic effect is associated with the induction of apoptosis in M-HeLa cells. As shown in **Figure 49**, apoptotic effects were observed after 24 hours of incubation of the M-HeLa cells in presence of **62e** at concentrations of 50 and 100 µM. These effects were most pronounced at the stage of early apoptosis at a concentration of 50 µM. Compound **62e** induced apoptosis in 10.73% M-HeLa cells. Increasing the concentration of **62e** to 100 µM, the number of apoptotic cells increased to 17.29%. The results suggest that the cytotoxic effect of **62e** in relation to M-HeLa cancer cells can be explained by an apoptotic pathway.

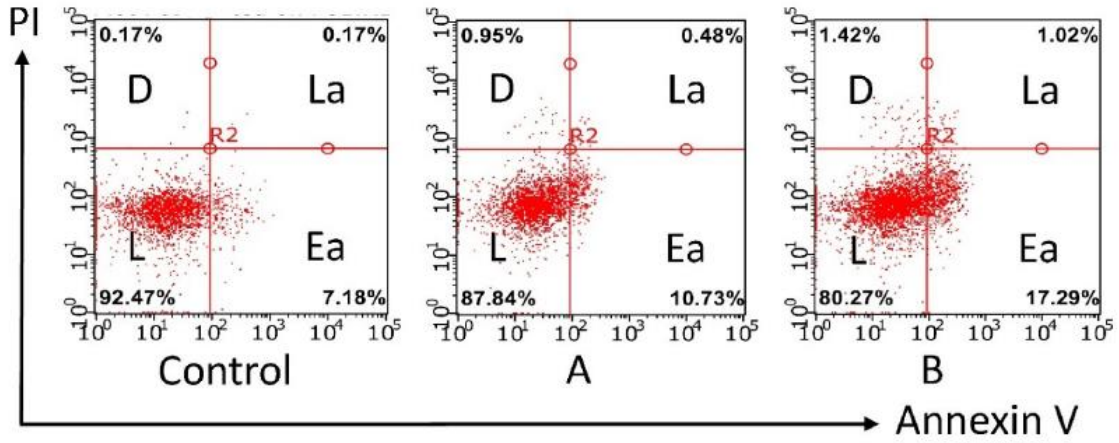

Figure 49. Apoptotic effects of **62e** on M-HeLa cells. (A) M-HeLa cells were treated with the indicated compound **62e** at concentration of 50 µM. (B) M-HeLa cells were treated with the indicated compound **62e** at a concentration of 100 µM. The values are presented as the mean ± SD (n = 3). L—living cells; D—dead cells; Ea—early apoptotic cells; La—late apoptotic cells.[175]

Afterwards the possible mechanism of the apoptosis-inducing effect of **62e** was studied. There are two main mechanisms for the induction of apoptosis: an external pathway through death receptors and an internal pathway accompanied by a interruption of the mitochondrial membrane, which leads to a decrease in its potential, a key indicator of the state of cells. The ability of the studied compounds to cause a decrease in the mitochondrial

membrane potential (ΔΨm) in the cells of the M-HeLa culture was evaluated using the compound **62e** as example. The study was carried out by flow cytometry methods using the JC-10 reagent. In normal cells with a high mitochondrial membrane potential, the dye JC-10 forms aggregates (J-aggregate producing red fluorescence) near the mitochondrial membranes. When the membrane potential, due to the stimulation of apoptosis, falls, JC-10 is distributed in the cell as a monomer (J-monomer, causing green fluorescence). The ratio between red and green fluorescence can be used to judge the onset of apoptosis. A reduction in ΔΨm was demonstrated using flow cytometry analysis (**Figure 50**). The intensity of the red fluorescence decreased with the increasing concentration of the tested compound.

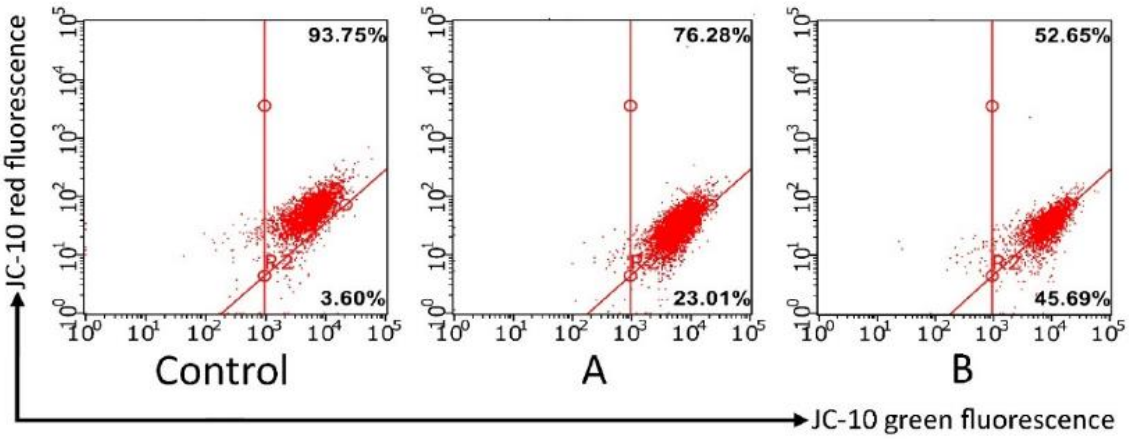

Figure 50. Flow cytometry analysis of M-HeLa cells treated with **62e**, along with the quantification of % of cells with red and green aggregates. (A) M-HeLa cells were treated with **62e** at a concentration of 50 µM. (B) M-HeLa cells were treated with **62e** at a concentration of 100 µM. [175]

The results obtained suggest that the mechanism of action of the studied compounds may be associated to the induction of apoptosis, which proceeds along the mitochondrial pathway.

4.3. Conclusions

The S_EAr/S_NAr reaction between ClDNBF and 2-aminothiazole derivatives **55a-c** gave two isomeric products bearing the benzofuroxanyl moiety bound to the C-5 carbon atom of the thiazole ring. The two isomers are formed in relative ratio dependent from the solvent and the reaction temperature, suggesting the occurrence of an equilibrium between them. The reduction of the furoxanyl ring to furazanyl and the comparison of the products obtained with those derived from the reaction between **55a-c** and 7-chloro-4,6-dinitrobenzofurazan (ClDNBZ) supported the structure of the two isomers as derived from a 1/3-oxide isomerization. DFT calculations and correlation between experimental and ^{13}C-NMR signals permitted to attribute the structure to each isomer.

When thiazoles bearing a primary or a acyclic secondary amino group in 2-position (**61a-f**) were reacted with ClDNBF, a series of novel benzofuroxans derivatives was synthesized. From this nucleophilic aromatic substitution reaction, the product thermodynamically more stable (bearing the benzofuroxan moiety bound to the exocyclic nitrogen atom of the thiazole ring) was obtained exclusively. The biological activity of the novel hybrids **50** and **62a-f** was tested *in vitro* on a panel of cancer cell lines and on one normal cell line.

M-HeLa cancer cells resulted sensible to compounds **50**, **62a**, **62d** and **62e** that not only showed an antiproliferative activity greater than that of the starting materials **48**, **49** and **61a-f**, but also they were found to be not toxic on normal cell line Chang Liver. Moreover, flow cytometry analysis showed that the mechanism of action of apoptosis induced by them could be associated to a mitochondrial pathway.

4.4. Experimental section

The ^{1}H- and ^{13}C-NMR spectra were recorded at 300, 400, 500, or 600 MHz (^{1}H-NMR) and 75, 100, 125 or 150 MHz (^{13}C-NMR), respectively. *J* values are given in Hz. Signal multiplicities were established by DEPT-135 experiments. Chemical shifts were referenced to the solvent [(δ= 7.27 and 77.0 ppm for $CDCl_3$), (δ= 1.96 and 118.26 ppm for CD_3CN), (δ= 2.05 and 30.2 ppm for CD_3COCD_3), (δ= 2.50 and 39.5 ppm for DMSO-d_6) for ^{1}H- and ^{13}C-NMR, respectively]. ESI-MS spectra were recorded using a Waters 2Q 4000 instrument. Chromatographic purifications (FC) were carried out on silica gel columns at medium pressure. TLC was carried out on aluminum coated silica gel with 254 nm fluorescence indicator (Fluka, DC-Alufolien-Kieselgel). ClNBZ was commercially available, whereas 2-pyrrolidinylthiazole (**55c**),[199] 7-Chloro-4,6-dinitrobenzofurazan (ClDNBZ, **60**),[200] and 7-Chloro-4,6-Dinitrobenzofuroxan (ClDNBF, **48**),[210] were synthesized and purified as previously described. 4,6-dinitro-7-(thiazol-2-ylamino)benzo[c][1,2,5]oxadiazole 1-oxide **56a** was prepared according to literature.[224] Where melting point are not done, this indicates that solid compounds decomposed when heated in the m.p. apparatus. Although the reactions carried out in NMR spectroscopy tube showed conversion almost quantitative, the yields in isolated products were lower, likely due to purification methods, but we did not focus our efforts on yield optimization. Computational and variable temperature NMR experimental details are reported in literature.[174,175] IR spectra were recorded in KBr or as emulsions in vaseline oil (sample concentration 0.25%) on a Bruker Vector-22 spectrometer in the range 400–4000 cm^{-1}; given are the most intense absorption bands. Gas chromatography–mass spectrometry analysis was performed using a Hewlett-Packard HP 6890 gas chromatograph (Hewlett-Packard, Ramsey, MN, USA) directly interfaced with a mass selective detector Agilent 5973 Network (Agilent Technology, Santa Clara, CA, USA). Injector temperature: 250 °C (mode: split with 50:1 splitting ratio). Column: Agilent Technology VF-WAXms, length: 30 m; diameter: 0.25 mm; film thickness: 0.25 µm. Oven temperature was programmed as follows: 60 °C for 5 min, increased up to 260 °C at the rate of 10 °C/min, followed by isotherm at 260 °C for 30 min; solvent delay time: 4.0 min. The carrier gas was helium, with an initial flow rate of 1 mL/min; transfer line temperature was 280 °C; the ionization was obtained by electron impact (EI), acquisition range 50–500 *m/z*.

General procedure for the synthesis of compounds 55a–c.

2-Bromothiazole (**53**, 0.56 mL, 6.22 mmol) was added to 5 mL of amine [morpholine (**54a**), piperidine (**54b**), pyrrolidine (**54c**)] and the mixture was kept at reflux under magnetic stirring. The conversion of **53** was monitored through TLC (eluent: diethyl ether/petroleum light 8/2; R_f = 0.45) and GC-MS. After removal under vacuum of the excess of amine, the product was purified through column chromatography on silica gel (eluent: diethyl ether/petroleum light 8/2; R_f = 0.45). The product obtained after FC sometimes appeared as viscous liquid; in this case, the residual solvent was removed by adding little amount of chloroform or dichloromethane then filtering off the liquid. Compounds **55a–c** were obtained in yield of 90 (**55a**), 95 (**55b**), and 98% (**55c**), respectively, and their data agreed with those reported in the literature.[225,226,119] They were stored in freezer and in the dark.

General procedure for the synthesis of benzofuroxan derivatives 56a-c and 56'a-c.

To a solution of ClDNBF (0.023 g, 0.088 mmol) in acetonitrile (7 mL), 0.030 g of **55a**, **55b** or 0.028 g for **55c** (0.177, 0.179, or 0.181 mmol, respectively) were added at room temperature. Immediately, the solution turned blue and was monitored by TLC (eluent: DCM/ethyl acetate 9/1). After 24, 12 and 4 h, respectively, the solvent was removed *in vacuo* and the residue subjected to FC eluting with DCM until the first blue eluate was obtained, then with the DCM/ethyl acetate 9/1. The collected fractions were concentrated and analyzed through ^{1}H-NMR, ^{13}C-NMR, and mass spectrometry. The NMR analysis indicated presence of two species. Many attempts to obtain crystals suitable for X-ray diffraction analysis failed. The mixture was subjected to preparative TLC and the two separated blue spots were scraped but, once each was dissolved in CD_3CN to be analyzed, the ^{1}H-NMR revealed presence of a mixture of two compounds in relative ratio equal to that found prior to separation. Thus, below we report the physico-chemical data of the mixture of isomers. In particular, when, from the ^{1}H-NMR spectrum, it was evident that the two species were present in different amount, we indicated as Maj or Min the signals of the isomer present in major or minor amount, respectively. On the basis of the analysis derived from experimental data/DFT calculations, below we report the names of the isomers attributing structure A' to **56c** and A to **56'c**, and assuming analogous behaviour also for cases **a** and **b**.

7-(2-Morpholinothiazol-5-yl)-4,6-dinitrobenzo[c][1,2,5]oxadiazole 1-oxide (**56a**) and **4-(2-morpholinothiazol-5-yl)-5,7-dinitrobenzo[c][1,2,5]oxadiazole 1-oxide** (**56'a**).

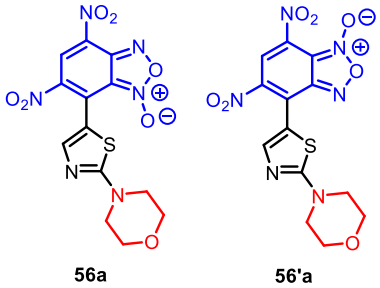

Dark blue solid, 0.008 g, 24% yield; ^{1}H-NMR (300 MHz, CD_3CN, 25° C, isomeric Maj (**56'a**)/Min (**56a**) ratio = 67 : 33) δ (ppm): 8.73 (s, 1H, Maj), 8.47 (s, 1H, Min), 8.32 (s, 1H, Min), 7.71 (s, 1H, Maj), 3.85–3.75 (m, 8H, Maj + Min), 3.67–3.59 (m, 8H, Maj + Min); ^{1}H-NMR (400 MHz, $CDCl_3$, 25°C, isomeric Maj/Min ratio = 50 : 50) δ (ppm): 8.69 (s, 1H), 8.65 (s, 1H), 8.24 (s, 1H), 7.79 (s, 1H), 3.89–3.84 (m, 8H), 3.78–3.74 (m, 4H), 3.71–3.67 (m, 4H); ^{13}C-NMR: (150 MHz, $CDCl_3$, 25°C) δ (ppm, selected data): 176.0, 175.9, 154.9 (CH), 152.1 (CH), 151.1, 144.6, 139.5, 132.4, 127.9 (CH), 125.0, 124.6, 124.2 (CH), 113.5, 113.3, 108.6, 105.8, 66.0 (OCH_2), 65.9 (OCH_2), 48.9 (NCH_2), 48.8 (NCH_2); ESI-MS (m/z): 393 (M - H)$^{-}$; HRMS (ESI^{+}) *m/z*: [M + H]$^{+}$ calcd for $C_{13}H_{11}N_6O_7S^{+}$: 395.0404; found: 393.0412.

4,6-Dinitro-7-(2-(piperidin-1-yl)thiazol-5-yl)benzo[c][1,2,5] oxadiazole 1-oxide (**56b**) and **5,7-dinitro-4-(2-(piperidin-1-yl) thiazol-5-yl)benzo[c][1,2,5]oxadiazole 1-oxide** (**56'b**).

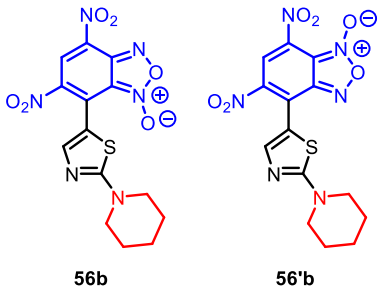

Night blue solid, 0.010 g, 29% yield. ^{1}H-NMR: (600 MHz, $CDCl_3$, 25°C, isomeric Maj (**56'b**)/Min (**56b**) ratio = 56 : 44) δ (ppm): 8.79 (s, 1H, Maj), 8.71 (s, 1H, Min), 8.29 (s, 1H, Maj), 7.94 (s, 1H, Min), 3.80–3.73 (m, 4H, Min), 3.73–3.68 (m, 4H, Maj), 1.83–1.73 (m, 12H, Maj + Min); ^{13}C-NMR: (150 MHz, $CDCl_3$, 25°C) δ (ppm): 176.1, 175.8, 157.1 (CH), 155.1 (CH), 151.3, 145.0, 138.6, 138.0, 130.4, 128.7 (CH), 127.9, 125.4, 125.0, 124.9 (CH), 113.8, 113.3, 109.4, 105.9, 50.5 (NCH_2, 2 signals overlapped), 25.4 (NCH_2CH_2), 23.8 ($NCH_2CH_2CH_2$), 23.7 ($NCH_2CH_2CH_2$); HRMS (ESI^{+}) *m/z*: [M + H]$^{+}$ calcd for $C_{14}H_{13}N_6O_6S^{+}$: 393.0612; found: 393.0632.

4,6-Dinitro-7-(2-(pyrrolidin-1-yl)thiazol-5-yl)benzo[c][1,2,5] oxadiazole 1-oxide (**56c**) and **4-(2-morpholinothiazol-5-yl)-5,7-dinitrobenzo[c][1,2,5]oxadiazole 1-oxide** (**56'c**).

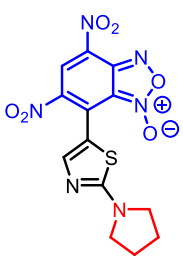

56c

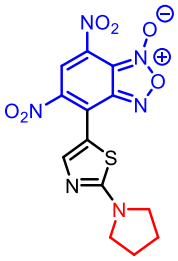

56'c

Brilliant dark green shiny, 0.019 g, 57% yield. ^{1}H-NMR: (400 MHz, $CDCl_3$, 25°C, isomeric Maj (**56'c**, or A)/Min (**56c**, or A') ratio = 59 : 41) δ (ppm): 8.81 (s, 1H, Maj), 8.71 (s, 1H, Min), 8.28 (s, 1H, Maj), 7.96 (s, 1H, Min), 4.00–3.35 (m, 8H, Maj + Min), 2.27–2.03 (m, 8H, Maj + Min); ^{1}H-NMR: (300 MHz, CD_3CN, 25°C, isomeric Maj/Min ratio = 56 : 44) δ (ppm): 8.73 (s, 1H, Maj), 8.66 (s, 1H, Min), 8.35 (s, 1H, Min), 7.90 (s, 1H, Maj), 3.72–3.33 (m, 8H, Maj + Min), 2.14–1.94 (m, 8H, Maj + Min); ^{13}C-NMR: (150.8 MHz, $CDCl_3$, 25°C) δ (ppm): 172.8, 172.7, 156.8 (CH), 154.9 (CH), 151.3, 145.0, 138.6, 137.9, 130.3, 128.6 (CH), 127.9, 125.6, 125.0, 124.9 (CH), 113.9, 113.3, 109.2, 106.0, 50.6 (NCH_2, 2 broad signals overlapped), 29.7 (NCH_2CH_2), 25.6 (NCH_2CH_2); HRMS (ESI^+) *m/z*: $[M + H]^+$ calcd for $C_{13}H_{11}N_6O_6S^+$: 379.0455; found: 379.0466.

General procedure for the synthesis of 7-(2-dialkylaminothiazol)-4,6-dinitrobenzo[c][1,2,5]oxadiazoles 59a-c

To a solution of ClDNBZ (0.018 g, 0.074 mmol) in acetonitrile (9 mL) 0.028 g of **55a** (or **55b**, or **55c**) (0.165, 0.167, 0.182 mmol, respectively) were added. Immediately after the reagents mixture, the colour of the solution turned blue. The mixture was kept at room temperature under magnetic stirring, and the conversion was monitored through TLC analysis (eluent: DCM). After 4 h, 3 h and 2 h, for the reaction with **55a**, **55b**, or **55c**, respectively, the solvent was removed in vacuo and the crude residue was purified by FC eluting with DCM obtaining pure substitution compounds **59a–c**. Compound **59c** was obtained also from reduction of the isomeric mixture **56c**/**56'c** with $P(Ph)_3$ in xylene using the procedure already reported of reduction of benzofuroxans to benzofurazans.[227]

4-(2-Morpholinothiazol-5-yl)-5,7-dinitrobenzo[c][1,2,5]oxadiazole (**59a**).

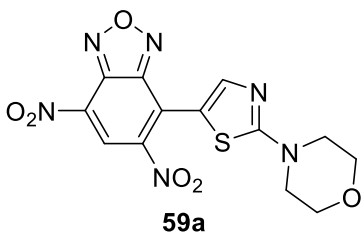

59a

Dark blue solid, 0.007 g, 25% yield. ^{1}H-NMR: (600 MHz, CD_3CN, 25°C) δ (ppm): 8.80 (s, 1H), 8.78 (s, 1H), 3.83–3.80 (m, 4H), 3.77–3.73 (m, 4H); ^{13}C-NMR: (150 MHz, CD_3CN, 25°C) δ (ppm): 177.4, 157.1 (CH), 151.4, 144.3,

130.1, 130.0, 127.7 (CH), 126.1, 116.3, 66.5 (OCH_2), 49.8 (NCH_2); HRMS (ESI^+) *m/z*: $[M + H]^+$ calcd for $C_{13}H_{11}N_6O_6S^+$: 379.0455; found: 379.0466.

5,7-Dinitro-4-(2-(piperidin-1-yl)thiazol-5-yl)benzo[c][1,2,5] oxadiazole (**59b**).

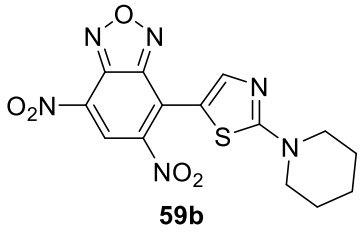

59b

Green-blue solid, 0.006 g, 22% yield. ^{1}H-NMR (300 MHz, CD_3CN, 25°C) δ, ppm: 8.90 (s, 1H), 8.79 (s, 1H), 3.83–3.73 (m, 4H), 1.80–1.70 (m, 6H); ^{1}H-NMR (600 MHz, $CDCl_3$, 25°C) δ, ppm: 9.06 (s, 1H), 8.79 (s, 1H), 3.79 (br. s, 4H), 1.79 (br. s, 6H); ^{13}C-NMR: (150 MHz, $CDCl_3$, 25 C) δ, ppm: 176.1, 159.3 (CH), 149.9, 142.9, 136.7, 129.1 (CH), 128.3, 125.4, 116.3, 50.7 (br. s. NCH_2), 25.5 (NCH_2CH_2), 23.8 ($NCH_2CH_2CH_2$); HRMS (ESI^+) *m/z*: $[M + H]^+$ calcd for $C_{14}H_{13}N_6O_5S^+$: 377.0663; found: 377.0680.

5,7-Dinitro-4-(2-(pyrrolidin-1-yl)thiazol-5-yl)benzo[c][1,2,5] oxadiazole (**59c**).

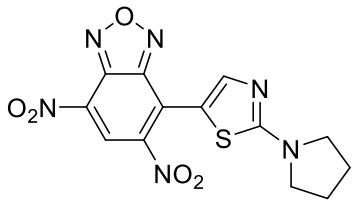

59c

Dark blue solid, 0.004 g, 15% yield. ^{1}H-NMR: (600 MHz, CD_3CN, 25°C) δ (ppm): 8.94 (s, 1H), 8.80 (s, 1H), 4.00–3.33 (br. m, 4H), 2.15–2.10 (br. m, 4H); ^{13}C-NMR: (150 MHz, CD_3CN, 25°C) δ (ppm): 174.0, 159.4 (CH), 151.4, 144.4, 138.1, 130.5 (CH), 129.4, 126.4, 116.8, 51.8 (br. s. NCH_2), 26.1 (br. s, NCH_2CH_2); HRMS (ESI^+) *m/z*: $[M + H]^+$ calcd for $C_{13}H_{11}N_6O_5S^+$: 363.0506; found: 363.0513.

General procedure for the synthesis of benzofuroxan derivatives 50 and 62a-f

A solution of aminothiazole derivative **49** or **61a-f** (2 eq) in 5 mL of $CHCl_3$ was added to a solution of 7-chloro-4,6-dinitrobenzofuroxan **48** (1 eq) in 5 mL of $CHCl_3$. The reaction was carried out at room temperature and the conversion was monitored through TLC analysis (eluent: 2/1 toluene/ethyl acetate). The crude mixture was precipitated in *n*-hexane (10 mL) and the obtained solid was filtered off, washed with cold water (100 mL) and dried under vacuum (0.06 mm Hg) at 40°C to constant weight. The crude products were purified by FC or crystallization to give the target compounds.

Synthesis of 4,6-dinitro-7-(thiazol-2-ylamino)benzo[c][1,2,5]oxadiazole 1-oxide (**50**)

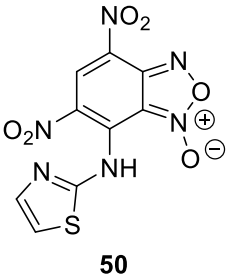

50

General procedure was used employing **48** (208 mg, 0.8 mmol) and aminothiazole **49** (160 mg, 1.6 mmol). ^{1}H-NMR (500 MHz, Acetone-d_6, 25 °C), δ (ppm): 9.08 (s, 1H, H5), 7.65 (d, *J*=4.4 Hz, 1H, H75), 7.30 (d, *J*= 4.4 Hz, 1H, H74); ^{13}C-NMR (125 MHz, Acetone-d_6, 25 °C), δ, ppm = 170.1 (C72), 147.2 (C3a), 143.7 (C6), 133.2 (C5), 128.8 (C75), 127.1 (C7), 124.1 (C4), 112.2 (C74), 109.2 (C7a). ^{15}N-NMR (51 MHz, Acetone-d_6) δ = N6, (N4), (N71), (N76) no observed cross-peaks in spectra.

Synthesis of 7-((5-methylthiazol-2-yl)amino)-4,6-dinitrobenzo[c][1,2,5]oxadiazole 1-oxide (**62a**)

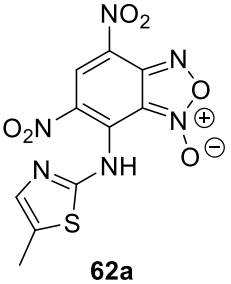

62a

General procedure was used employing **48** (208 mg, 0.8 mmol) and aminothiazole **61a** (182 mg, 1.6 mmol). FC (eluent: ethyl acetate pure) provided pure compound **62a** as wine-colored powder (167 mg, 0.49 mmol, 62% yield). m.p.: 210-212 °C; ^{1}H-NMR (500 MHz, Acetone-d_6, 25 °C), δ (ppm): 9.04 (s, 1H, H5), 7.33 (q, *J* = 1.2 Hz, 1H, H75), 2,44 (d, *J* = 1.2 Hz, 3H, CH3); ^{13}C-NMR (125 MHz, Acetone-d_6, 25 °C), δ, ppm = 171.1 (C72), 148.5 (C3a), 144.4 (C6), 134.5 (C5), 127.7 (C7), 127.3 (C75), 127.3 (C74), 123.4 (C4), 113.9 (C7a), 13.3 (CH_3); ^{15}N-NMR (51 MHz, Acetone-d_6) δ = 366.0 (N6), 362,2 (N4), 189.5 (N71), n/o/ (N76); IR (*v*, cm^{-1}): 1376 (NO_2 symm), 1548 (NO_2 asymm), 1620 (furoxan ring); Anal. calcd (%) for $C_{10}H_6N_6O_6S$: C 35.51; H 1.79; N 24.85; S 9.48. Found: C 35.59; H 1.82; N 24.79; S 9.42.

Synthesis of 7-((4-(ethoxycarbonyl)thiazol-2-yl)amino)-4,6-dinitrobenzo[c][1,2,5]oxadiazole 1-oxide (**62b**)

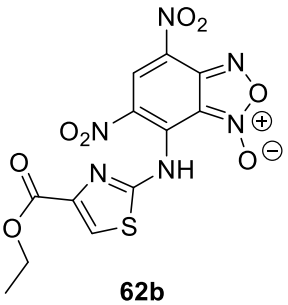

62b

General procedure was used employing **48** (208 mg, 0.8 mmol) and aminothiazole **61b** (275 mg, 1.6 mmol). Crystallization from a mixture of $CHCl_3$/n-hexane (3:1) provided pure compound **62b** as purple powder (294 mg, 0.74 mmol, 93% yield). m.p.: 188-189°C; ^{1}H-NMR (500 MHz, Acetone-d_6, 25 °C), δ (ppm): 9.09 (s, 1H, H5), 8.10 (s, 1H, H75), 4.38 (q, *J* = 7.1 Hz, 2H, H79), 1.38 (t, *J* = 7.1 Hz, 3H, CH3); ^{13}C-NMR (125 MHz, Acetone-d_6, 25 °C), δ, ppm = 165.1 (C72), 160.3 (C77), 148.0 (C3a), 140.0 (C6), 139.0 (C74), 133.0 (C5), 129.9 (C7), 127.5 (C4),

123.9 (C75), 114.0 (C7a), 63.0(C79), 15.1 (C80); ^{15}N-NMR (51 MHz, Acetone-d_6) δ = 365.2 (N6), 361,2 (N4), 223.2 (N71), n/o/(N76); IR (*v*, cm^{-1}): 1339 (NO_2 symm), 1551 (NO_2 asymm), 1624 (furoxan ring), 1691 (CO), 1712 (C=O), 3101 (C5H); Anal. calcd (%) for $C_{12}H_8N_6O_8S$: C 36.37; H 2.03; N 21.21; S 8.09. Found: C 36.36; H 2.05; N 21.21; S 8.13.

Synthesis of 4,6-dinitro-7-(phenyl(thiazol-2-yl)amino)benzo[c][1,2,5]oxadiazole 1-oxide (**62c**)

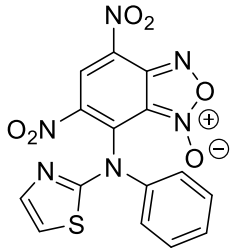

62c

General procedure was used employing **48** (208 mg, 0.8 mmol) and aminothiazole **61c** (281 mg, 1.6 mmol). FC (eluent: $CHCl_3$ pure) provided pure compound **62c** as violet powder (182 mg, 0.45 mmol, 57% yield). m.p.: 112-113 °C; ^{1}H-NMR (500 MHz, Acetone-d_6, 25 °C), δ (ppm): 8.96 (s, 1H, H5), 7.63 (d, *J* = 7.6 Hz, 2H, H78), 7.54 (t, *J* = 7.6 Hz, 2H, H79), 7.49 (d, *J* = 7.6 Hz, 1H, H80), 7.41 (d, *J* = 3.6 Hz, 1H, H75), 7.35 (d, *J* = 3.6 Hz, 1H, H74); ^{13}C-NMR (125 MHz, Acetone-d_6, 25 °C), δ, ppm = 168.1 (C72), 147.8 (C3a), 143.6 (C77), 141.5 (C75), 140.2 (C6), 135.4 (C7), 134.5 (C4), 131.7 (C5), 131.7 (C79), 130.3 (C80), 126.9 (C78), 117.1 (C74), 115.7 (C7a); ^{15}N-NMR (51 MHz, Acetone-d_6) δ = 363.8 (N6), 357.5 (N4), 285.1 (N71), 107.3 (N76); IR (*v*, cm^{-1}): 1336 (NO_2 symm), 1556 (NO_2 asymm), 1621 (furoxan ring); Anal. calcd (%) for $C_{15}H_8N_6O_6S$: C 45.00; H 2.01; N 20.99; S 8.01. Found: C 45.05; H 1.98; N 20.95; S 8.06.

Synthesis of 7-((5-methylthiazol-2-yl)(phenyl)amino)-4,6-dinitrobenzo[c][1,2,5]oxadiazole 1-oxide (**62d**)

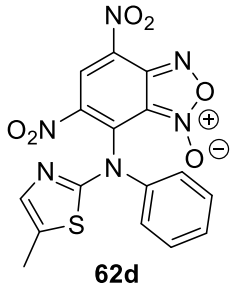

62d

General procedure was used employing **48** (208 mg, 0.8 mmol) and aminothiazole **61d** (304 mg, 1.6 mmol). FC (eluent: $CHCl_3$ pure) provided pure compound **62d** as blue powder (255 mg, 0.61 mmol, 77% yield). m.p.: 169-170 °C; ^{1}H-NMR (500 MHz, Acetone-d_6, 25 °C), δ (ppm): 8.94 (s, 1H, H5), 7.59 (d, *J* = 8.2 Hz, 2H, H78), 7.52 (t, *J* = 8.2 Hz, 2H, H79), 7.46 (t, *J* = 8.2 Hz, 1H, H80), 7.08 (q, *J* = 1.3 Hz, 1H, H75), 2.46 (d, *J* = 1.3 Hz, 3H, CH3); ^{13}C-NMR (125 MHz, Acetone-d_6, 25 °C), δ, ppm = 164.8 (C72), 146.8 (C3a), 142.5 (C77), 138.8 (C6), 137.8 (C75), 134.3 (C7), 133.0 (C4), 130.9 (C74), 130.6 (C5), 130.4 (C79), 129.1 (C80), 125.7 (C78), 114.7 (C7a), 11.6 (CH3); ^{15}N-NMR (51 MHz, Acetone-d_6) δ = 373.3 (N3), 366.1 (N6), 357.1 (N4), 287.0

(N71), 108.5 (N76); IR (*v*, cm^{-1}): 1380 (NO_2 symm), 1557 (NO_2 asymm), 1621 (furoxan ring); Anal. calcd (%) for $C_{16}H_{10}N_6O_6S$: C 46.38; H 2.43; N 20.28; S 7.74. Found: C 46.31; H 2.49; N 20.33; S 7.68.

Synthesis of 7-((4-methoxyphenyl)(thiazol-2-yl)amino)-4,6-dinitrobenzo[c][1,2,5]oxadiazole 1-oxide (**62e**)

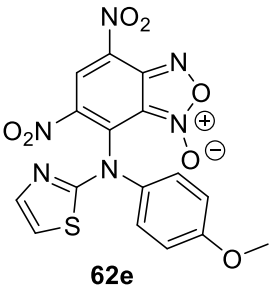

62e

General procedure was used employing **48** (208 mg, 0.8 mmol) and aminothiazole **61e** (329 mg, 1.6 mmol). FC (eluent: $CHCl_3$ pure) provided pure compound **62e** as blue powder (175 mg, 0.41 mmol, 51% yield). m.p.: 176-178 °C; ^{1}H-NMR (500 MHz, Acetone-d_6, 25 °C), δ (ppm): 8.94 (s, 1H, H5), 7.56 (d, *J* = 9.0 Hz, 1H, H78), 7.39 (d, *J* = 3.5 Hz, 1H, H75), 7.32 (d, *J* = 3.5 Hz, 1H, H74), 7.07 (d, *J* = 9.0 Hz, 2H, H79), 3.90 (s, 3H, CH3); ^{13}C-NMR (125 MHz, Acetone-d_6, 25 °C), δ, ppm = 168.8 (C72), 161.6 (C80), 147.8 (C3a), 141.6 (C75), 139.6 (C6), 136.1 (C77), 135.3 (C7), 133.9 (C4), 131.6 (C5), 129.1 (C79), 117.0 (C74), 116.7 (C79), 115.7 (C7a), 56.7 (CH3); ^{15}N-NMR (51 MHz, Acetone-d_6) δ = 364.2 (N6), 358.6 (N4), 281.2 (N71), 106.4 (N76); IR (*v*, cm^{-1}): 1378 (NO_2 symm), 1558 (NO_2 asymm), 1621 (furoxan ring), 3101 (C5H); Anal. calcd (%) for $C_{16}H_{10}N_6O_7S$: C 44.65; H 2.34; N 19.53; S 7.45. Found: C 44.62; H 2.37; N 19.49; S 7.49.

Synthesis of 7-((3-chlorophenyl)(thiazol-2-yl)amino)-4,6-dinitrobenzo[c][1,2,5]oxadiazole 1-oxide (**62f**)

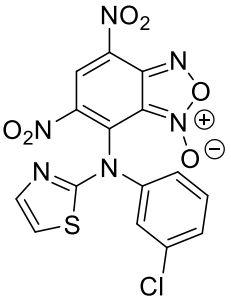

62f

General procedure was used employing **48** (208 mg, 0.8 mmol) and aminothiazole **61f** (336 mg, 1.6 mmol). FC (eluent: $CHCl_3$ pure) provided pure compound **62f** as wine-colored powder (218 mg, 0.50 mmol, 63% yield). m.p.: 74-75 °C; ^{1}H-NMR (500 MHz, Acetone-d_6, 25 °C), δ (ppm): 8.96 (s, 1H, H5), 7.62 (d, *J* = 7.6 Hz, 1H, H78), 7.53 (t, *J* = 7.6 Hz, 2H, H79), 7.48 (d, *J* = 7.6 Hz, 1H, H80), 7.41 (d, *J* = 3.6 Hz, 1H, H75), 7.35 (d, *J* = 3.6 Hz, 1H, H74); ^{13}C-NMR (125 MHz, Acetone-d_6, 25 °C), δ, ppm = 167.4 (C72), 147.7 (C3a), 144.6 (C79), 141.5 (C75), 140.1 (C6), 136.4 (C77), 134.9 (C7), 134.9 (C4), 132.8 (C81), 131.3 (C5), 130.0 (C80), 126.3 (C78), 125.3 (C82), 117.4 (C74), 115.7 (C7a); ^{15}N-NMR (51 MHz, Acetone-d_6) δ = 373.6 (N3), 363.6 (N6), 357.5 (N4), 285.4 (N71), 104.7 (N76); IR (*v*, cm^{-1}): 1360 (NO_2 symm),

1556 (NO_2 asymm), 1621 (furoxan ring); Anal. calcd (%) for $C_{15}H_7ClN_6O_6S$: C 41.44; H 1.62; Cl 8.15; N 19.33; S 7.38. Found: C 41.52; H 1.55; Cl 8.23; N 19.37; S 7.44.

Cytotoxicity Assay

Cytotoxic effects of the test compounds on human cancer and normal cells were estimated by means of the multifunctional Cytell Cell Imaging system (GE Health Care Life Science, Danderyd, Sweden) using the Cell Viability Bio App which precisely counts the number of cells and their viability evaluated from fluorescence intensity data. DAPI and propidium iodide were purchased from Sigma. Two fluorescent dyes that selectively penetrate the cell membranes and fluoresce at different wavelengths were used in the experiments. The M-HeLa clone 11 human, epithelioid cervical carcinoma, the strain of HeLa, a clone of M-HeLa; PANC-1 is a human pancreatic cancer cell line; human duodenal cancer cell line (HuTu 80) from the Type Culture Collection of the Institute of Cytology (Russian Academy of Sciences, S-Petersburg, Russia) and Chang liver cell line (human liver cells) from N. F. Gamaleya Research Center of Epidemiology and Microbiology (Moscow, Russia) were used in the experiments. The cells were cultured in a standard Eagle's nutrient medium manufactured at the Chumakov Institute of Poliomyelitis and Virus Encephalitis (PanEco company, Moscow, Russia) and supplemented with 10% fetal calf serum and 1% nonessential amino acids. The cells were plated into a 96-well plate (Nunc) at a concentration of 1 x 10^5 cells/mL, 150 µL of medium per well, and cultured in a CO_2 incubator at 37 °C. Twenty-four hours after seeding the cells into wells, the compound under study was added at a preset dilution, 150 µL to each well. The dilutions of the compounds were prepared immediately in nutrient media; 5% DMSO that does not induce the inhibition of cells at this concentration was added for better solubility. The experiments were repeated three times. Intact cells cultured in parallel with experimental cells were used as a control.

Flow Cytometry Assay

Cell Culture. M-HeLa cells at 1 x 10^6 cells/well in a final volume of 2 mL were seeded into 6-well plates. After 24 h of incubation, various concentrations of Compounds **61f** and **62f** were added to wells.

Cell Apoptosis Analysis. The cells were harvested at 2000 rpm for 5 min and, then, washed twice with ice-cold PBS, followed by resuspension in binding buffer. Next, the samples

were incubated with 5 µL of annexin V-FITC and 5 µL of propidium iodide for 15 min at room temperature in the dark. Finally, the cells were analyzed by flow cytometry (Guava easy Cyte, MERCK, Kenilworth Union County, NJ, USA). The experiments were repeated three times.

Mitochondrial Membrane Potential

The cells were harvested at 2000 rpm for 5 min and, then, washed twice with ice-cold PBS, followed by resuspension in JC-10 (10 µg/mL) and incubation at 37°C for 10 min. After the cells were rinsed three times and suspended in PBS, the JC-10 fluorescence was observed by flow cytometry.

References

[174] Micheletti, G.; Iannuzzo, L.; Calvaresi, M.; Bordoni, S.; Telese, D.; Chugunova, E.; Boga, C. *RSC Advances*, **2020**, *10(57)*, 34670-34680.
[175] Chugunova, E.; Micheletti, G.; Telese, D.; Boga, C.; Islamov, D.; Usachev, K.; Burilov, A.; Tulesinova, A.; Voloshina, A.; Lyubina, A.; Amerhanova, S; Gerasimova, T.; Gilfanova, A.; Syakaev, V. *Int. J. Mol. Sci.*, **2021**, *22*, 7497.
[176] Boulton, A. J.; Ghosh, P. B. *Advances in Heterocyclic Chemistry*, Vol. 10; Katritzky, A. R., Boulton, A. J., Eds.; Academic Press: New York, **1969**; pp. 1-41.
[177] Gasco, A., Boulton, A.J. *Furoxans and Benzofuroxans in Advances in Heterocyclic Chemistry* Vol. 29; A.R. Katritzky, A.J. Boulton Ed.s, Academic Press: New York, **1981**, pp.251-340.
[178] Fronabarger, J.W.; Williams, M.D.; Sanborn, W.B.; Parrish, D.A.; Bichay, M. *Propellants Explos. Pyrotech.*, **2011**, *36*, 459-470.
[179] Šarlauskas, J.; Anusevičius, Ž.; Misiūnas, A. *Central Eur. J. Energetic Mat.*, **2012**, *9*, 365-386.
[180] Noelting, E.; Kohn, O. *Chemische Apparatur*, **1894**, *18*, 1095.
[181] Drost P. *Justus Liebigs Ann. Chem.*, **1899**, *307*, 49-69.
[182] Drost P.; Zincke, T. *Justus Liebigs Ann. Chem.*, **1900**, *313*, 309-325.
[183] Green, A.G., Rowe F.M. *J. Chem. Soc.*, **1912**, *101*, 2452-2459.
[184] Harris, R.K.; Katritzky, A.R.; Oksne, S.; Bailey, A.S.; Pateson, W.G. *J. Chem. Soc.*, **1963**, 197-203.
[185] Guntram, R.; Jarzecki, A.A.; Pulay, P. *J. Comput. Chem.*, **1997**, *18*, 489-500.
[186] Mallory, F. B.; Manatt, S. L.; Wood, C. S. *J. Am. Chem. Soc.*, **1965**, *87*, 5433-5438.
[187] Mallory, F. B.; Cammarata, A. *J. Am. Chem. Soc.*, **1966**, *88*, 61-64.
[188] Friedrichsen, W. *J. Phys. Chem.*, **1994**, *98*, 12933-12937.
[189] Stevens, J.; Schweizer, M. Rauhut, G. *J. Am. Chem. Soc.*, **2001**, *123*, 7326-7333.
[190] Dunkin, I. R.; Lynch, M. A.; Boulton, A. J.; Henderson, N. *Chem. Commun.*, **1991**, 1178-1179.
[191] Abushanab, E.; Alteri, N. D. *J. Org. Chem.*, **1975**, *40*, 157-160.
[192] Bulacinski, A.B.; Scriven, E.F.V.; Suschitzky, H. *Tetrahedron Lett.*, **1975**, *41*, 3577-3578.
[193] (a). Buncel, E.; Terrier, F. *Org. Biomol. Chem.*, **2010**, *8*, 2285–2308 and ref therein. (b). Jovené, C.; Sebban, M.; Marrot, J.; Régis Goumont, R. *The Diels-alder reactivity of the furoxan ring of substituted benzofuroxans. Synthesis of substituted imines and evidence of the intermediacy of ortho-dinitrosoarenes in the 1-oxide/3-oxide interconversion* In Targets in Heterocyclic Systems Chemistry and Properties Vol. 16, Orazio A. Attanasi and Domenico Spinelli Ed.s, Società Chimica Italiana: Roma 2012, pp. 90-112.
[194] Chan, S.-C.; England, J.; Wieghardt, K.; Wong, C.Y. *Chem. Sci.*, **2014**, *5*, 3883-3887.
[195] Boulton, A. J.; Katritsky, A. R.; Hamid, A. M. *J. Chem. Soc. C*, **1967**, 2005–2007.
[196] Alan R. Katritzky, Christopher A. Ramsden, John A. Joule, Viktor V. Zhdankin, *Handbook of Heterocyclic Chemistry* 3rd Ed., Chap. 2.4 Elsevier: Amsterdam **2010**, pp 139-209.
[197] Rauhut, G.; Eckert, F. *Quantum Chemical Studies on Heterocyclic Rearrangements in Benzofuroxans: Reaction Paths, Vibnrational Spectra, and Rate Constants* in High Performance Computing in Science and Engineering '99 E. Krause, W. Jäger, Eds. Springer-Verlag: Heidelber **2000** pp. 183-211.
[198] Rauhut, G. *Recent Advances in Computing Heteroatom-Rich Five- and Six-Membered Ring Systems* in Advances in Heterocyclic Chemistry, Volume 81, Alan R. Katritzky Ed.; Academic Press London **2001**, p. 37.
[199] Terrier, F.; Lakhdar, S.; Boubaker, T.; Goumont, R. J. Org. Chem., **2005**, 70, 6242-6253.
[200] Lakhdar, S.; Goumont, R.; Terrier, F.; Boubaker, T.; Dust, J. M.; Buncel, E. *Org. Biomol. Chem.*, **2007**, *5*, 1744-1751.
[201] Boga C.; Forlani, L. *J. Chem. Soc., Perkin Trans. 2*, **2001**, 1408-1413.
[202] Micheletti, G.; Boga, C.; Cino, S.; Bordoni, S.; Chugunova, E. *RSC Adv.*, **2018**, *8*, 41663-41674.
[203] Boga, C.; Del Vecchio, E.; Forlani, L.; Mazzanti, A.; Todesco, P. E. *Angew. Chem.*, Int. Ed., **2005**, *44*, 3285-3289.
[204] Boga, C.; Del Vecchio, E.; Forlani, L.; Goumont, R.; F. Terrier, F.; Tozzi, S. *Chem. Eur. J.*, **2007**, *13*, 9600-9607.
[205] Forlani, L.; Boga, C.; Mazzanti, A.; N. Zanna, N. Eur. *J. Org. Chem.*, **2012**, *6*, 1123-1129.
[206] Boga, C.; Cino, S.; Micheletti, G.; Padovan, D.; Prati, L.; Mazzanti, A.; Zanna, N. *Org. Biomol. Chem.*, **2016**, *14*, 7061-7068.
[207] Cerecetto, H., González, M. *Heterocycl. Chem.*, **2007**, *10*, 265–308.
[208] Chugunova, E. A.; Burilov, A. R. *Curr. Top. Med. Chem.*, **2017**, *17*, 986-1005.
[209] Singh, K.; Singh, S.; Taylor, J.A. *Dye. Pigment.*, **2002**, *54*, 189–200.
[210] Trivette, C.D., Jr.; Morita, E.; Young, E.J. *Chem. Technol.*, **1962**, *35*, 1360–1429.

[211] Khan, E.; Khan, A.; Gul, Z.; Ullah, F.; Tahir, M.N.; Khalid, M.; Asif, H.M.; Asim, S.; Braga, A.A.C. *J. Mol. Struct.*, **2020**, *1200*, 127126.
[212] Venkatachalam, T.K.; Mao, C.; Uckun, F. *Bioorg. Med. Chem.*, **2004**, *12*, 4275–4284.
[213] Chugunova, E.; Boga, C.; Sazykin, I.; Cino, S.; Micheletti, G.; Mazzanti, A.; Sazykina, M.; Burilov, A.; Khmelevtsova, L.; Kostina, N. Eur. *J. Med. Chem.*, **2015**, *93*, 349–359.
[214] Mjambili, F.; Njoroge, M.; Naran, K.; De Kock, C.; Smith, P.J.; Mizrahi, V.; Warner, D.; Chibale, K. *Bioorg. Med. Chem. Lett.*, **2014**, *24*, 560–564.
[215] Wan, Y.; Long, J.; Gao, H.; Tang, Z. *Eur. J. Med. Chem.*, **2021**, *210*, 112953.
[216] Hussein, A.H.M.; Khames, A.A.; El-Adasy, A.-B.A.; Atalla, A.A.; Abdel-Rady, M.; Hassan, M.I.A.; Nemr, M.T.M.; Elshaier, Y.A.A.M. *RSC Adv.*, **2020**, *10*, 29723–29736.
[217] Mayr, H.; Patz, M. *Angew. Chem.*, Int. Ed. Engl. **1994**, *33*, 938–957.
[218] Mayr, H.; Kempf, B.; Ofial, A. R. *Acc. Chem. Res.*, **2003**, *36*, 66–77.
[219] Mayr, H.; Bug, T.; Gotta, M. F.; Hering, N.; Irrgang, B.; Janker, B.; Kempf, B.; Loos, R.; Ofial, A. R.; Remmenikov, G.; Schimmel, N. *J. Am. Chem. Soc.*, **2001**, *123*, 9500–9512.
[220] Tanja Kanzian, Tobias A. Nigst, Andreas Maier, Stefan Pichl, Herbert Mayr. *Eur. J. Org. Chem.*, **2009**, 6379–6385.
[221] Reichardt, C. *Solvents and Solvent Effects in Organic Chemistry*, Wiley-VCH Publishers, 3rd edn, **2003**.
[222] Micheletti, G.; Bordoni, S.; Chugunova, E.; Boga, C. *Molecules*, **2017**, *22*, 684.
[223] R. W. Read and W. P. Norris, *Aust. J. Chem.*, **1985**, *38*, 435–445.
[224] Micheletti, G.; Telese, D.; Boga, C. *Molbank*, **2020**, *2020*, M1165.
[225] (a) Verma, S. K.; Acharya, B. N. M.; Kaushik, P. *Org. Biomol. Chem.*, **2011**, *95*, 1324–1327; (b) Dutta, P. K.; Sen, S.; Saha D.; Dhar, B. *Eur. J. Org. Chem.*, **2018**, 657–665.
[226] (a) D. Keil and H. Hartmann, *Liebigs Ann.*, **1995**, *6*, 979–984; (b) Fei-Dong, H.; Chang, X.; Dong-Dong, L.; Dong-Sheng, S.; Tian, L.; Feng-Shou, L. *J. Org. Chem.*, **2018**, *83*, 9144–9155.
[227] Terrier, F.; Chatrousse, A. P.; Soudais, Y.; Hlaibi, M. *J. Org. Chem.*, **1984**, *49*, 4176–4181.

Chapter V: Synthesis and characterization of highly conjugated carbocycles with Fluorene core

5.1. Introduction

Optoelectronics deals with the study and application of electronic instruments that can convert electricity into light and *viceversa*.[228] The instruments used can work with γ-rays, X-rays, ultraviolet, infrared or visible light. There is an extremely large number of devices that are designed based on the possibility of emitting light or detecting it. Instruments designed to emit light use electric current to produce electromagnetic radiation. Instruments constructed with the objective of detecting light, on the contrary, must convert the electromagnetic radiation they receive into electric current.

The phenomenon that is observed when charged particles or electromagnetic radiation pass through matter and dissipate their energy, exciting the molecules of the material they pass through, is the principle on which all instruments used to detect and measure these particles or radiation are based.

In particular scintillators have the ability to convert high-energy photons, from X-rays or gamma rays, to lower-energy photons. The latter are emitted by the scintillator after interaction with the incident radiation and can be detected by another instrument, such as a photomultiplier, which converts them into an electrical signal (**Figure 51**). From the electric signal thus produced, it is possible to trace the light emitted from the scintillator. This feature makes the scintillators particularly suitable for detecting charged particles or electromagnetic radiations with high energy. In fact, scintillators and photomultipliers are coupled directly or through a light guide and the set of the two instruments allows us to detect the incident radiation and measure its parameters.

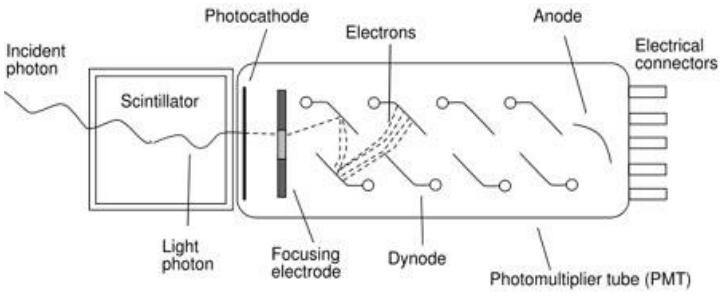

Figure 51. Outline diagram of a scintillator detector. (https://web.stanford.edu/group/scintillators/scintillators.html).

The phenomenon occurring in a scintillator is called scintillation, a property of luminescence, and can be observed in organic and inorganic crystals, as well as in fluids, gases, and polymeric materials. Three main types of luminescence can occur in these kinds of materials: fluorescence, if the emission occurs immediately after absorption (between 10^{-8} and 10^{-9} seconds later); phosphorescence, when the emission occurs at a wavelength greater than the fluorescence and with times of 10^{-4} seconds or more; delayed fluorescence, if the emission is of the same wavelength as the fluorescence but with longer times. In general, almost all scintillators have two re-emission components, one fast and one slow but for measurements, the fast component (fluorescence) is taken as the reference.

These materials have received extensive attention in recent years, as they can be used as radiation detectors for radiation exposure monitoring, security inspection, space exploration, and medical imaging.[228,229,230,231]

In the latter field, positron emission tomography (PET), single photon emission computed tomography (SPECT), X-ray computed tomography (TAC) or dosimetric probes are just some examples of techniques that use scintillator materials as detectors. In radiodiagnostics or nuclear medicine, the detection of the radiation and the subsequent processing of the signal allow to obtain multiple information, such as: a) biotopological, for the study of tumor processes, b) functional of the various organs analyzed, c) morphological, d) physicist. In addition, the measurements of the radiation flow carried out using dosimeters based on scintillator detectors allow the monitoring of the contamination of subjects and environment.

In general, there are some requirements for a material in order to be used as scintillator:

- Efficient conversion of kinetic energy into light;
- Conversion of kinetic energy into linear light;
- Transparency of the medium to the wavelength of the light emitted;
- Decay time sufficiently short to generate fast pulses;
- Good mechanical properties of the material;
- Refractive index of the material close to that of the glass (n=1.5).

Since no material allows to respect all the characteristics, the choice is to find a right compromise among these properties. Therefore, searching for low-cost, high-performance scintillation materials is still of great scientific and practical interest.

Another important aspect, to consider for the application of any material as a scintillator, is the scintillation efficiency, defined as the fraction of incident particles actually

transformed into light. We try to exploit materials in which this parameter is as wide as possible, but not always the phenomena associated with the return to the ground state of excited molecules of material translate into light emission. The set of effects that do not allow the emission of light are generically identified with the term *quenching*.

The scintillators are divided into two main groups: organic and inorganic. Inorganic scintillators are used as crystals, while organic can be liquid, plastic or crystalline. This differentiation is based on the fact that the phenomenon of luminescence has a different origin in these two categories. In fact, in organic materials, luminescence is an intrinsic molecular property, while for inorganics it is a crystal's property; for this reason they are not used in other phases. The different mechanism of luminescence defines an important difference in application terms: inorganics have slower emission rates but higher light yield, while organics produce minor light yield but have higher emission rates.

Below I will focus only on organic scintillators, because they are one of the themes of this doctoral project.

The first organic scintillators, polycyclic aromatic hydrocarbons such as anthracene and naphthalene,[232] used as single crystals, suffer from fragility and scalability. Moreover, they are characterized both by crystal growth limitations and high costs.

Liquid scintillators, where an organic scintillator is dissolved in a suitable solvent, based on alkyl benzenes were developed to overcome the scalability and cost issues and incorporate the excellent response speed of organic scintillators; but drawbacks such as encapsulation, toxicity and flammability have prevented wide scale adoption for larger productions.

Plastic scintillators contain at least one fluorophore, as fluorescent organic dye with optical absorption in UV or near-UV, dissolved in a polymeric matrix. The matrix material must possess high affinity to the guest molecules and high optical transparency in the visible range of light. Among polymer matrices known the ones containing aromatic moieties have higher performance due to possible energy transfer mechanism in them.[233] They are low cost, scalable, highly durable and have low flammability risks: they combine many of the advantages of liquid and crystalline organic scintillators without the corresponding drawbacks. For these characteristics they are particularly convenient and of great interest.

In all these configurations, the phenomenon of luminescence is attributed to the delocalized electron π-system of aromatic compounds. These electrons require less energy to be excited than those involved in the σ bond. Precisely the excited state of these electrons, which

consists in switching to higher energy singlet states, is responsible for the emission of light. The energy levels of an organic molecule for π electrons includes a series of singlet states (S_0, S_1, S_2, ...) with increasing energy, as shown in the Jablonsky energy diagram of **Figure 52**. Between each state, it is possible to associate various vibrational sub-levels, with an energy distance much lower than that which separates each state of singlet, which are denoted with a second suffix (*e.g.* S_{00}, S_{01}, S_{02}, ..., for the state S_0). In addition to singlet states, there are also triplet states (defined by the letter T and represented in the same way) that have lower energy than the respective singlet states. The passage from singlet to triplet states is prohibited. However, there is a possibility that the triplet states are occupied by σ electrons.

Overall, the phenomenon of luminescence is caused by the passage of electrons π from the ground state of singlet (S_{00}) to higher energy singlet states (S_{10}, S_{11}, S_{12}, ...) and the subsequent return to the ground state. A fluorescence emission is observed when electrons decay from the singlet excited state, while phosphorescence is observed when electrons decay from the triplet excited state. Instead, the decay of molecules between states of singlet at higher energy than the ground state does not produce light emission.

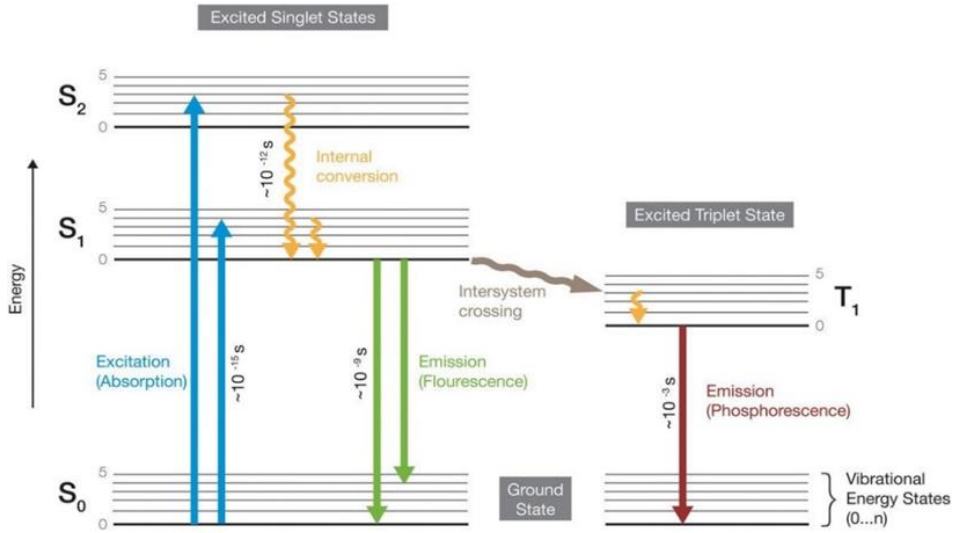

Figure 52. Jablonsky energy diagram with electronic states and transitions of an organic fluorophore in excited singlet or triplet states. (https://www.genetics.org/content/211/1/15.figures-only).

In the last few years, the fluorene moiety showed to be a promising building block for the design of emitting materials. The use of small organic molecules, including fluorene derivatives, ensures greater purity, better solubility and reproducibility. Fluorene

derivatives functionalized at 2,7- and/or 9- position are suitable candidates for extending π-conjugation and to obtain new materials with high luminescence quantum efficiency. For example, Pei & al. synthesized and characterized the fluorene trimer shown in **Figure 53**,[234] where the central fluorene core is functionalized in 2- and 7- position by other two fluorene moieties, while the 9- position contains two styrenyl groups.

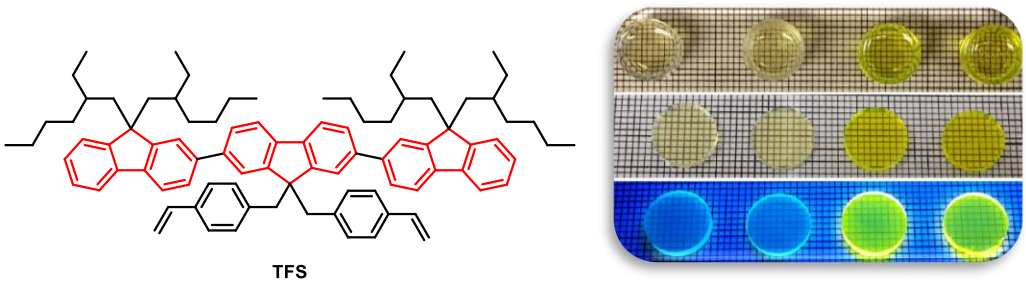

Figure 53. Fluorene derivative with properties as scintillator.

This compound, dubbed TFS, was employed as material in plastic scintillators to achieve an increase in light yield versus a commercial blue scintillator. The mixture TFS with vinyl toluene was undergone to bulk polymerization to produce cylindrical polymer monoliths (**Figure 53**) and coupled to either a photomultiplier tube to measure the scintillation light under exposure to Cs-137 gamma rays.

The design of highly π-extended fused conjugated fluorene-based systems is one effective approach to increasing charge transport for high mobility of electrons;[235,236] however some molecules show very weak fluorescence in solid state due to the quenching of excited states induced by condensed molecular packing.[237] Reducing the π-conjugation and then the intermolecular interactions enough may enhance the fluorescence efficiency.[238] Hu & al. designed and synthesized an organic semiconductor 2,7-diphenyl-9H-fluorene (**63**), conjugated in 2- and 7- position with two phenyl rings (**Figure 54**).[239] This material showed deep-blue lasing characteristics with high photoluminescence quantum yield; it is a promising building block for designing blue emitting materials and can behave potentially as organic scintillator.

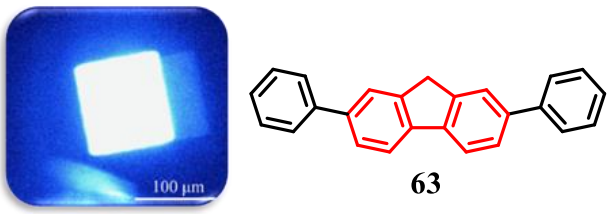

Figure 54. 2,7-Diphenyl-9H-fluorene, a potential organic scintillator.

However, different studies clearly demonstrate that fluorene-based substrates suffer from thermal and photochemical degradation over time, depending on the group introduced at 9-position of fluorene ring.[240,241] The fluorene-based structures, characterized by aryl moieties in 9-position, such as the spiro-bifluorene **A** (**Figure 55**) and diphenyl fluorene **B** (**Figure 55**), showed as aromatic substituents give rise to the most robust derivatives both from the thermal and photochemical point of view.[242,243] In fact replacing the aryl by alkyl substituents lead to loss of inertness.

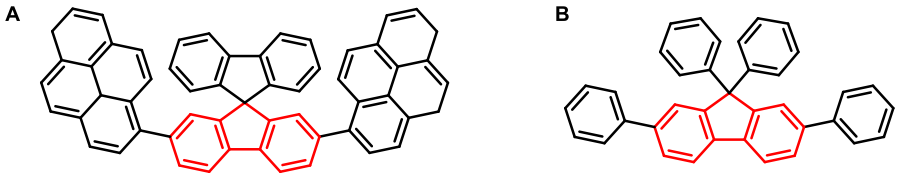

Figure 55. Fluorene-based structures functionalized in 9-position. A) spiro-fluorene derivative. B) diphenyl fluorene derivative.

In this context, with the aim to find novel π-extended aromatic materials with potential scintillatory properties of possible use in medical field (*e.g.* suitable for X-ray Imaging and Dosimetry), we designed to synthesize several fluorene derivatives functionalized at 2,7- and 9- position.

5.2. Results and discussion

The first approach was to functionalize fluorene in position 9 through Wittig reaction (**Scheme 36**). The phosphorane of fluorene **65**, in turn prepared from 9-bromofluorene (**64**) and triphenylphosphine in basic medium, was reacted with aldehydes **66a-q** (**Scheme 36**). Depending on the steric hindrance of the aldehyde used, two different reaction conditions have been adopted: under MW irradiations (300 W) or neat in oil bath at 225°C.

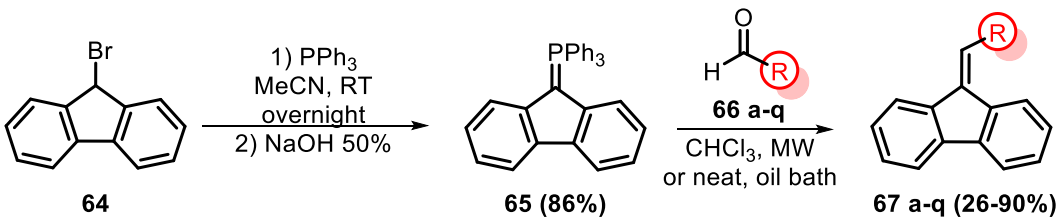

Scheme 36. Synthetic pathway to obtain 9-fluorene derivatives **67a-q**.

The fluorene derivatives functionalized in 9-position synthesized with related yields obtained after purification are listed in **Figure 55**.

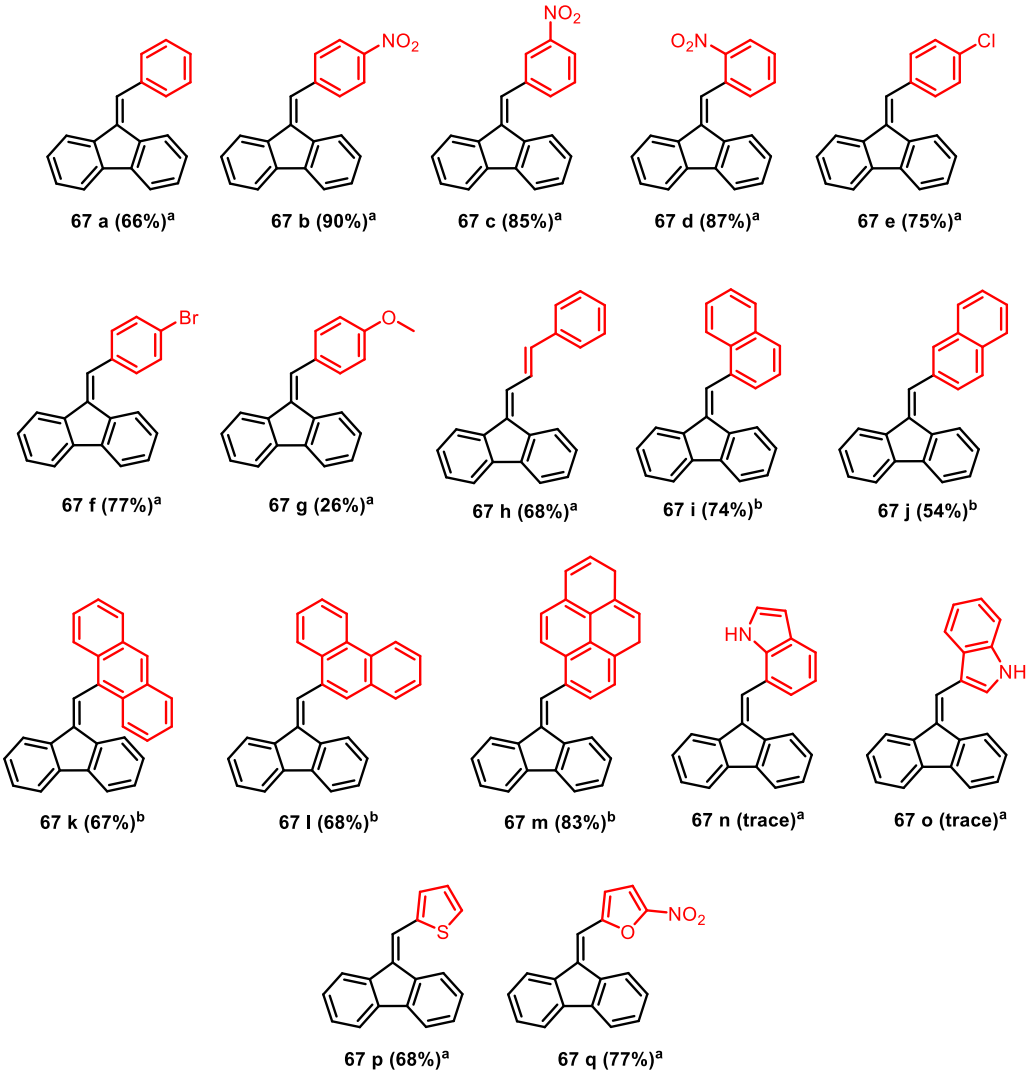

Figure 55. Fluorene derivatives **67a-q** obtained. [a] Product obtained under MW irradiation in $CHCl_3$. [b] Product obtained neat at 225°C.

An alternative route involving the Knoevenagel reaction was used to functionalize the 9-position of fluorene. With this procedure, the reaction between fluorene (**68a**) or 2,7-dibromofluorene (**68b**) and terephtaldehyde (**69**), carried out in the presence of potassium *tert*-butoxide in *tert*-butanol gave the desired products **70a** and **70b** in 64% and 53% of yield, respectively, after their precipitation from the reaction mixture (**Scheme 37**).

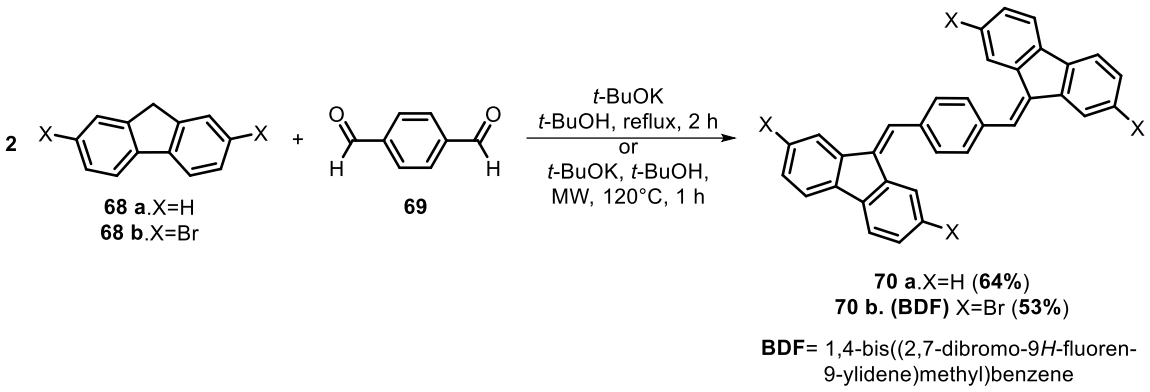

Scheme 37. Knoevenagel reaction to obtain the fluorene derivatives **70a,b**.

The presence of four bromine substituents in product **70b** (hereafter indicated as **BDF**) makes it an useful synthon for further functionalizations to obtain more highly-conjugated systems through C-C cross coupling reactions. Thus, we planned to increase the π-conjugation through Suzuki-Miyaura reaction on **BDF**.

At first the optimal reaction conditions were investigated using the cross-coupling reaction between 2,7-dibromofluorene (**68b**) and phenyl boronic acid (**71**) as a model reaction (**Table 13**).

Table 13. Investigation on optimal conditions of Suzuki-Miyaura reaction on **68b**.

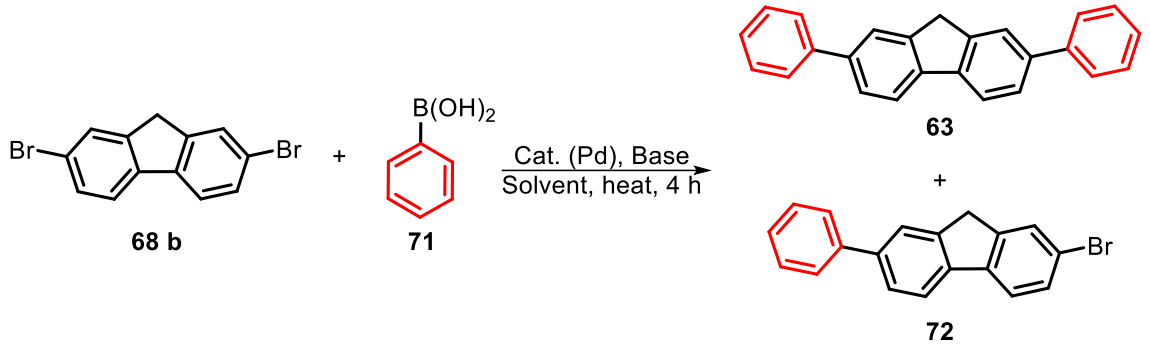

Entry	Cat. (0.1 mol%)	Base (1M)	Solvent	T (°C)	Ratio[a] (63/72)	Yield (63)[b]
1	$Pd(Ph_3)_4$	Cs_2CO_3	EtOH:H_2O (3:1)	Reflux	5:1	30%
2	$Pd(Ph_3)_4$	Cs_2CO_3	THF:H_2O (9:1)	Reflux	1:3	10%
3	$Pd(dppf)Cl_2$*CH_2Cl_2	Cs_2CO_3	THF:H_2O (9:1)	Reflux	7:1	70%

[a] Data calculated through ^{1}H-NMR analysis of the crude reaction mixture; [b] data referred to **63** after purification of the product.

From data of entries 1 and 2 of **Table 13** it is possible to underline that the solvent affects not only the ratio between **63** and **72**, but also the conversion. Despite the THF:H_2O solvent mixture (entry 2, **Table 13**) increases the solubility of the starting materials, the yield of product **63**, under the same experimental conditions, was lower (10%) than in EtOH:H_2O (30%). The change of the catalyst increased (in THF:H_2O 9:1) the yield to 70% (entry 3, **Table 13**).

Once optimized the reaction conditions, the Suzuki cross-coupling between **BDF** and phenyl boronic acid (**71**) was carried out for 24 hours (**Scheme 38**) but compound **73** was obtained in only 10% yield. This result requires further deepening of this reaction to find a more selective catalyst and to optimize the other reaction conditions.

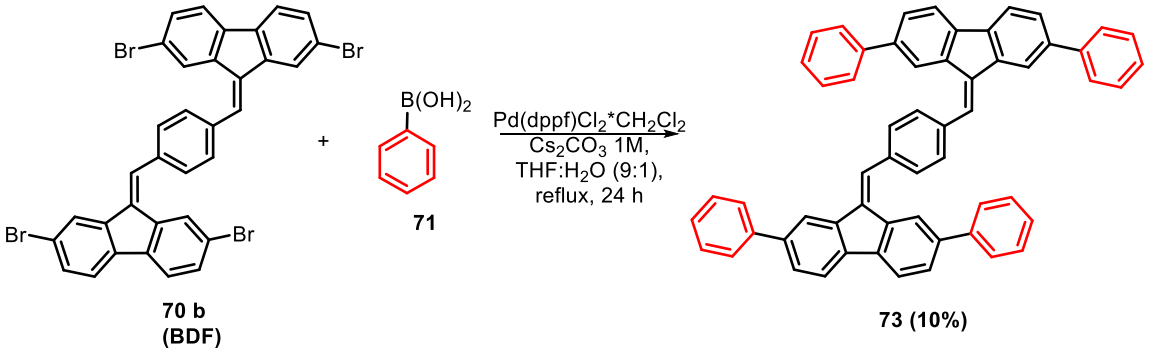

Scheme 38. C-C cross coupling reaction to obtain the highly conjugated fluorene-based system **73**.

Photophysical analyses

In order to gain information on photophysical properties of compounds obtained, UV/Vis spectrophotometric analyses were performed. The fluorene-based derivatives **63**, **67b-m**, **67p-q** and **70a,b** were dissolved in DCM, recording the spectrum in the 260-650 nm wavelength range. The molar extinction coefficient ε was calculated measuring the absorbance at λ_{max} at three different concentrations (10^{-6}, 10^{-5}, 10^{-4} M) for each compound. The data obtained are resumed in **Table 14**.

Table 14. UV/Vis absorbtion λ_{max} values of fluorene derivatives dissolved in DCM at 25 °C.

Entry	Compound	λ_{max} (nm)	ε (M^{-1} cm^{-1})	R^2
1[a]	**68a**	265	19700	-
2	**63**	324	26970	0.991
3[a]	**67a**	327	13000	-
4	**67b**	357	66356	0.981
5	**67c**	322	121812	0.985
6	**67d**	314	16637	0.993
7	**67e**	330	14857	0.999
8	**67f**	331	14371	0.996
9	**67g**	346	16410	0.995
10	**67h**	375	17608	0.998
11	**67i**	340	10568	0.990
12	**67j**	343	17176	0.989
13	**67k**	390	10521	0.997
14	**67l**	346	13557	0.999
15	**67m**	379	19916	0.998
16	**67p**	359	15402	0.997
17	**67q**	423	18114	0.999
18	**70a**	366	17133	0.994
19	**70b**	303	19122	0.998

[a]Data reported from literature[244]

From data above reported, it is possible to underline how an increase of the π-conjugation in fluorene-based structures leads to a bathochromic effect (*Red shift*) for each compound with respect to fluorene (**68a**, entry 1, **Table 14**). Different effects can be evidenced depending on the substituent bound to phenyl ring of 9-benzylidenyl scaffold. In nitrofluorene derivatives **67b-d** the electronic delocalization of the system decreases depending on the position of the nitro group causing a hypsochromic effect (*Blue shift*) of maximum absorption: 357 nm for **67b** (*p*-NO_2), 322 nm for **67c** (*m*-NO_2) and 314 nm for **67d** (*o*-NO_2) (entries 4-6, **Table 14**).[245,246] Instead the presence of a halogen group causes an auxochrome effect (entries 7-8, **Table 14**). The presence of electron donor groups with +M effect, such as OMe (entry 9, **Table 14**) or electron-rich five-membered heteroaromatic substituents (entries 16-17, **Table 14**) contributes to π-system extension, with consequent increase of wavelenght and ε for iperchromic effect.

In order to evaluate the photoluminescence properties, emission spectra of some of compounds synthesized were performed in solid state recording the spectrum in the 250-

800 nm wavelength range using a spectrofluorometer equipped with a Xenon lamp (**Figure 56**).

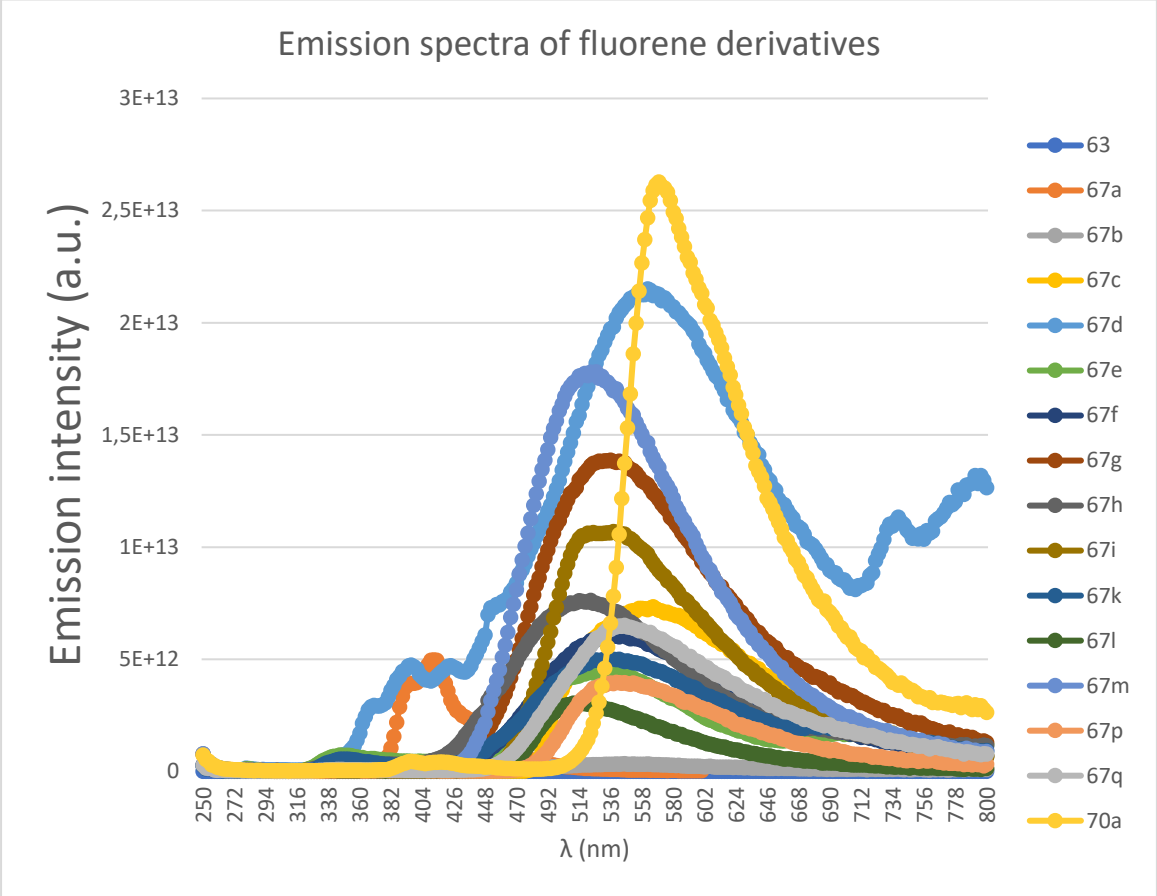

Figure 56. Emission spectra of some fluorenylidene derivatives in solid state with λ_{exc}= 280 nm.

A well-defined peak is visible with a maximum at 574 nm for the compound **70a** (yellow line, **Figure 56**). The compounds **67d**, **67m** and **67g** (light blue, blue and brown line, respectively, **Figure 56**) are characterized by a more large peaks with maxima ranging from 502-556 nm. These samples show also the higher relative intensity. Moreover, the emission peaks are in the blue-yellow visible spectrum, thus can be good candidates for scintillators in the range of the X-rays as they have a relative high photoluminescence in the visible range. The other samples have a lower intensity and therefore are hypothetically less interesting as potential scintillators.

5.3. Conclusions

A series of 9-fluorenylidene derivatives, of interest in medical and optoelectronic field as organic scintillators, was synthesized through Wittig or Knoevenagel reaction. Among them, the tetrabromoderivative **BDF** can be a useful synthon for further functionalizations via C-C coupling reactions to obtain more highly conjugated systems. It has been used to synthesize more π-conjugated systems through Suzuki cross-coupling.

All the compounds have been fully characterized. In particular, the photophysical analyses evidenced as compound **70a**, with absorption λ_{max} at 366 nm and emission λ_{max} at 574 nm, could be a suitable candidate as organic scintillator in the X-rays field.

Selected fluorenylidene derivatives among those synthesized will be analyzed by Prof. Daniele Rinaldi's research group at Università Politecnica delle Marche (AN, Italy) to test their potential scintillatory properties.

5.4. Experimental section

The reagents used, unless stated otherwise, were purchased from Sigma-Aldrich (Milan, Italy). Chromatographic purifications (FC) were carried out on glass columns packed with silica gel Geduran Si 60, 0.063–0.200 mm, (Sigma-Aldrich, Milan, Italy). Thin-layer chromatography (TLC) was performed on silica gel 60 F254-coated aluminum foils (Fluka, Buchs, Switzerland). The nuclear magnetic resonance spectra were recorded at 25°C on Varian spectrometers Mercury 400 or Inova 600 (Varian, Palo Alto, CA, USA) operating at 400 or 600 MHz (for ^{1}H-NMR) and 100.56 or 150.80 MHz (for ^{13}C-NMR), respectively. Frequencies are reported in Hz and the chemical shifts were referenced to the solvent ($CDCl_3$, δ =7.27 and 77.0 ppm for ^{1}H and ^{13}C-NMR, respectively). Signal multiplicities were established by DEPT-135 experiments. Characterization data of known compounds agree with those reported in literature, thus only selected data are reported below for them. ^{13}C NMR data for compounds **70b** and **73** are not reported because of they very poor solubility. ESI-MS spectra have been recorded using a Waters 2Q 4000 instrument (Waters Corporation, Milford, MA, USA). Melting points were measured on a Büchi apparatus (Stone, Staffs, UK) and are not corrected. Reactions under microwave irradiation were carried out using a Milestone Start Synth (Milestone Inc, Shelton, CT, USA) apparatus at 300W. The UV/Vis analyses were recorded at room temperature using a Perkin Elmer Lambda 12 spectrophotometer UV/Vis using quartzite cuvettes with 1 cm of lenght path. Uncorrected steady-state emission spectra were recorded on an Edinburgh FLSP920 spectrometer equipped with a 450 W xenon arc lamp, double excitation and single emission monochromators, and a Peltier-cooled Hamamatsu R928P photomultiplier tube (185–850 nm). Emission spectra were acquired with a cut-off filter (295 nm) and corrected for source intensity (lamp and grating) and emission spectral response (detector and grating) by a calibration curve supplied with the instrument. The wavelengths for the emission spectra were determined using the absorption maxima of the MLCT transition bands (emission spectra) and at the maxima of the emission bands (excitation spectra).

Synthesis of (9*H*-fluoren-9-ylidene)triphenyl-λ^5-phosphane (**65**) AD_7

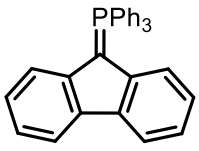

65

In a round bottom flask, equipped with a magnetic bar, PPh_3 (516 mg, 1.97 mmol) was added to a solution of 9-bromo-9H-fluorene **64** (500 mg, 2.04 mmol) in CH_3CN (10 mL). The mixture was stirred overnight at room temperature. The white solid precipitated was filtered on a Büchner

funnel and washed with Et_2O (3 x 15 mL). The solid collected was transferred on a separating funnel using Et_2O (10 mL) where it was added an acqueous solution of NaOH 50% (10 mL, 0.1 M). Once separated, the organic phase was dried over anhydrous $MgSO_4$, filtered and concentrated under reduced pressure. Compound **65** was obtained as yellow solid (745 mg, 1.75 mmol, 86% yield). m.p.: 247-250 °C; ^{1}H-NMR (400 MHz, $CDCl_3$, 25 °C), δ (ppm): 8.20 (d, *J*=7.8 Hz, 2H), 7.86-7.75 (m, 6H), 7.67 (dt, J_1=7.5 Hz, J_2=1.1 Hz, 3H), 7.54 (dt, J_1=8.1 Hz, J_2=3.0 Hz, 6H), 7.02 (t, *J*=7.4 Hz, 2H), 6.92 (t, *J*=7.2 Hz, 2H), 6.37 (d, *J*=7.9 Hz, 2H). ^{13}C-NMR (100 MHz, DMSO-d6, 25 °C), δ, ppm = 141.7 (d, J_{P-C}=14.85), 134.3 (d, J_{P-C}=10.3), 132.7 (d, J_{P-C}=2.87), 131.9, 130.9 (d, J_{P-C}=14.3), 129.2 (d, J_{P-C}=12.4), 125.8 (d, J_{P-C}=88.5), 122.9, 119.4, 116.2 (d, J_{P-C}=49.3), 53.1 (d, J_{P-C}=129.6).

General procedure for the synthesis of fluorene derivatives (**A**)

A solution of phosphane of fluorene **65** (1 eq) in $CHCl_3$ (0.03 M) was introduced in a vessel for MW experiments equipped with a magnetic bar under nitrogen atmosphere to avoid the oxidation to fluorenone. The corresponding aldehyde (1 eq) was added to the solution and the mixture was heated at 85 or 100°C for 30 minutes, or 3-5 hours under MW irradiation (300 W) then allowed to stand at room temperature. After removal of the solvent, the crude was purified through crystallization or FC on silica gel.

General procedure for the synthesis of fluorene derivatives (**B**)

In a three necked bottom flask, previously dried with heat gun under nitrogen atmosphere, partially immersed in an oil bath and equipped with a reflux condenser and a magnetic bar, phosphane of fluorene **65** (1 eq) and the corresponding aldehyde (1.56 eq) are added. The reaction mixture was heated neat at 160 or 225 °C for 1 hour then allowed to stand at room temperature. The crude was purified through crystallization or FC on silica gel.

Synthesis of 9-benzylidene-9*H*-fluorene (**67a**)

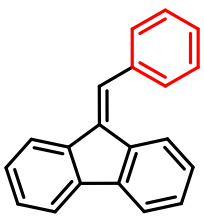

67 a

General procedure **A** was used employing **65** (213 mg, 0.5 mmol) and aldehyde **66a** (53 mg, 0.5 mmol) in $CHCl_3$ (15 mL). The reaction was heated at 85°C for 3 hours. Crystallization in MeOH/EtOH (1/1) provided pure compound **67a** as yellow solid (87 mg, 0.33 mmol, 66% yield). m.p.: 71-73 °C; ^{1}H-NMR (400 MHz, $CDCl_3$, 25 °C), δ (ppm): 7.83 (d, *J*=7.2 Hz, 1H), 7.79-7.75 (m, 2H), 7.74 (s, 1H) 7.67-7.61 (m, 3H), 7.54-7.48 (m,

2H), 7.47-7.41 (m, 2H), 7.37 (dq, J_1= 7.5 Hz, J_2= 1.2 Hz, 2H), 7.12 (dt, J_1=7.5 Hz, J_2=1.2 Hz, 1H); ^{13}C-NMR (100 MHz, $CDCl_3$, 25 °C), δ, ppm =141.2, 139.4, 139.1, 136.8, 136.5, 136.4, 129.2, 128.49, 128.47, 128.2, 127.9, 127.2, 126.9, 126.6, 124.3, 120.2, 119.7, 119.5.

Synthesis of 9-(4-nitrobenzylidene)-9*H*-fluorene (67b)

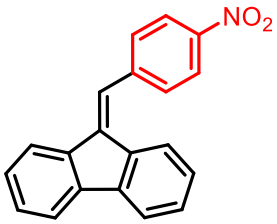

67 b

General procedure **A** was used employing **65** (213 mg, 0.5 mmol) and aldehyde **66b** (75 mg, 0.5 mmol) in $CHCl_3$ (15 mL). The reaction was heated at 85°C for 30 minutes. Crystallization in MeOH provided pure compound **67b** as yellow solid (135 mg, 0.45 mmol, 90% yield). m.p.: 169-171 °C; ^{1}H-NMR (400 MHz, $CDCl_3$, 25 °C), δ (ppm): 8.27 (d, *J*=9.0 Hz, 2H), 7.75 (d, *J*=7.9 Hz, 1H), 7.70 (d, *J*=7.8 Hz, 4H, 2 segnali sovrapposti), 7.54 (s, 1H), 7.41 (t, *J*=6.9 Hz, 2H), 7.35 (dt, J_1=7.5 Hz, J_2=1.1 Hz, 2H), 7.07 (dt, J_1=7.6 Hz, J_2=1.1 Hz, 1H); ^{13}C-NMR (100 MHz, $CDCl_3$, 25 °C), δ, ppm = 147.1, 143.8, 141.7, 139.4, 138.78, 138.76, 135.7, 130.1, 129.4, 129.0, 127.2, 126.9, 124.2, 123.8, 123.7, 120.5, 120.0, 119.7.

Synthesis of 9-(3-nitrobenzylidene)-9*H*-fluorene (67c)

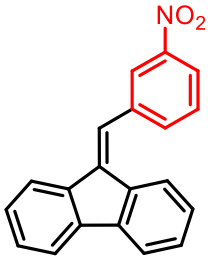

67 c

General procedure **A** was used employing **65** (213 mg, 0.5 mmol) and aldehyde **66c** (75 mg, 0.5 mmol) in $CHCl_3$ (15 mL). The reaction was heated at 85°C for 3 hours. FC (eluent: 2/8 *n*-hexane/DCM) provided pure compound **67c** as yellow solid (127 mg, 0.42 mmol, 85% yield). m.p.: 112-114 °C; ^{1}H-NMR (400 MHz, $CDCl_3$, 25 °C), δ (ppm): 8.4 (s, 1H), 8.25- 8.21 (m, 1H), 7.89-7.85 (m, 1H), 7.74 (d, *J*=7.8 Hz, 1H), 7.70 (d, *J*=7.2 Hz, 2H), 7.58 (t, *J*=8.9 Hz, 1H), 7.53 (s, 1H), 7.41 (dt, J_1=7.5 Hz, J_2=1.2 Hz, 1H), 7.39-7.31 (m, 3H), 7.07 (dt, J_1=7.64 Hz, J_2=1.23 Hz, 1H); ^{13}C-NMR (100 MHz, $CDCl_3$, 25 °C), δ, ppm = 148.2, 141.5, 139.3, 138.8, 138.5, 138.4, 135.7, 135.3, 129.4, 129.2, 128.8, 127.2, 126.8, 124.0, 123.9, 123.5, 122.6, 120.4, 119.9, 119.6.

Synthesis of 9-(2-nitrobenzylidene)-9*H*-fluorene (67d)

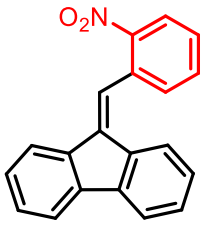

67 d

General procedure **A** was used employing **65** (213 mg, 0.5 mmol) and aldehyde **66d** (75 mg, 0.5 mmol) in $CHCl_3$ (15 mL). The reaction was heated at 85°C for 3 hours. Crystallization in MeOH provided pure compound **67d** as yellow solid (129 mg, 0.43 mmol, 87% yield). m.p.: 123-124.5 °C; ^{1}H-NMR (400 MHz, $CDCl_3$, 25 °C), δ (ppm): 8.26 (dd, J_1=8.2 Hz, J_2=1.2 Hz, 1H), 7.87 (s,1H), 7.84 (d, J=7.3 Hz, 1H), 7.76-7.68 (m, 3H), 7.66 (dt, J_1=7.6 Hz, J_2=1.1 Hz, 1H), 7.58 (dt, J_1=7.8 Hz, J_2=1.3 Hz, 1H), 7.42 (dt, J_1=7.7 Hz, J_2=1.2 Hz, 1H), 7.37 (dt, J_1=7.5 Hz, J_2=1.4 Hz, 1H), 7.31 (dt, J_1=7.3 Hz, J_2=1.3 Hz, 1H), 7.04-6.93 (m, 2H); ^{13}C-NMR (100 MHz, $CDCl_3$, 25 °C), δ, ppm = 147.5, 141.5, 139.2, 138.8, 136.9, 136.0, 133.4, 132.8, 132.6, 129.1, 128.8, 128.7, 127.2, 126.6, 125.0, 124.1, 122.8, 120.7, 119.9, 119.6.

Synthesis of 9-(4-chlorobenzylidene)-9*H*-fluorene (67e)

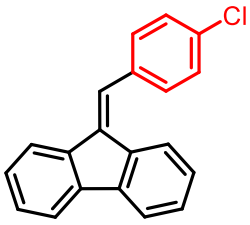

67 e

General procedure **A** was used employing **65** (213 mg, 0.5 mmol) and aldehyde **66e** (70 mg, 0.5 mmol) in $CHCl_3$ (15 mL). The reaction was heated at 85°C for 3 hours. Crystallization in MeOH provided pure compound **67e** as yellow solid (107 mg, 0.37 mmol, 75% yield). m.p.: 148-149 °C; ^{1}H-NMR (400 MHz, $CDCl_3$, 25 °C), δ (ppm): 7.78 (d, J=9.1 Hz, 1H), 7.73 (d, J=8.5 Hz, 2H), 7.61-7.49 (m, 4H), 7.48-7.39 (m, 3H), 7.35 (t, J=7.3 Hz, 2H), 7.11 (t, J=7.6 Hz, 1H); ^{13}C-NMR (100 MHz, $CDCl_3$, 25 °C), δ, ppm = 141.3, 139.2, 139.1, 136.9, 136.2, 135.2, 133.8, 130.6, 128.72, 128.69, 128.4, 127.0, 126.7, 125.6, 124.2, 120.2, 119.8, 119.6.

Synthesis of 9-(4-bromobenzylidene)-9*H*-fluorene (67f)

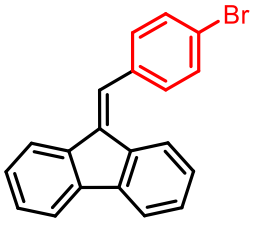

67 f

General procedure **A** was used employing **65** (213 mg, 0.5 mmol) and aldehyde **66f** (70 mg, 0.5 mmol) in $CHCl_3$ (15 mL). The reaction was heated at 85°C for 3 hours. Crystallization in MeOH provided pure compound **67f** as yellow solid (128 mg, 0.38 mmol, 77% yield). m.p.: 142-143 °C; ^{1}H-NMR (400 MHz, $CDCl_3$, 25 °C), δ (ppm): 7.77 (d, J=7.4 Hz, 1H), 7.73 (d, J=7.8 Hz, 2H), 7.62-7.54 (m, 4H), 7.46 (d, J=8.2 Hz, 2H), 7.41 (dt, J_1=7.6 Hz, J_2=1.2 Hz, 1H), 7.35 (dt, J_1=7.5 Hz, J_2= 1.2 Hz, 2H), 7.11 (dt, J_1=7.6 Hz, J_2=1.1 Hz, 1H); ^{13}C-NMR (100 MHz, $CDCl_3$, 25 °C), δ, ppm

=141.3, 139.2, 139.1, 136.9, 136.2, 135.7, 131.6, 130.8, 128.7, 128.4, 127.0, 126.7, 125.6, 124.2, 122.0, 120.2, 119.8, 119.6.

Synthesis of 9-(4-methoxybenzylidene)-9*H*-fluorene (67g)

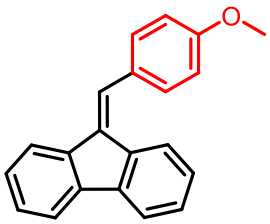

67 g

General procedure **A** was used employing **65** (213 mg, 0.5 mmol) and aldehyde **66g** (68 mg, 0.5 mmol) in $CHCl_3$ (15 mL). The reaction was heated at 85°C for 3 hours. FC (eluent: 1/1 *n*-hexane/DCM) provided pure compound **67g** as yellow solid (37 mg, 0.13 mmol, 26% yield). m.p.: 130-132 °C; ^{1}H-NMR (400 MHz, $CDCl_3$, 25 °C), δ (ppm): 7.79 (d, *J*=7.6 Hz, 1H), 7.77-7.71 (m, 3H), 7.67 (s, 1H), 7.57 (d, *J*=8.6 Hz, 2H), 7.42-7.30 (m, 3H), 7.11 (dt, J_1=7.7 Hz, J_2=1.2 Hz, 1H), 7.01 (d, *J*=8.7 Hz, 2H, 2 signals overlapped), 3.90 (s, 3H); ^{13}C-NMR (100 MHz, $CDCl_3$, 25 °C), δ, ppm = 159.5, 141.1, 139.6, 138.9, 136.6, 135.4, 130.8, 129.0, 128.3, 127.8, 127.3, 126.9, 126.6, 124.1, 120.0, 119.7, 119.5, 113.9, 55.3.

Synthesis of (*E*)-9-(3-phenylallylidene)-9*H*-fluorene (67h)

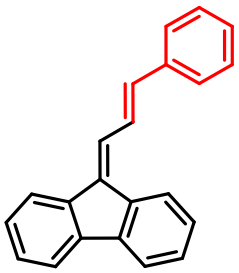

67 h

General procedure **A** was used employing **65** (213 mg, 0.5 mmol) and aldehyde **66h** (60 mg, 0.5 mmol) in $CHCl_3$ (15 mL). The reaction was heated at 85°C for 3 hours. FC (eluent: 1/1 *n*-hexane/DCM) provided pure compound **67h** as yellow solid (96 mg, 0.34 mmol, 68% yield). m.p.: 155-156 °C; ^{1}H-NMR (400 MHz, $CDCl_3$, 25 °C), δ (ppm): 8.1-8.0 (m, 1H), 8.02-7.95 (m, 1H), 7.81-7.71 (m, 3H), 7.61 (d, *J*=7.6 Hz, 2H), 7.44 (t, *J*=7.8 Hz, 2H), 7.42-7.32 (m, 6H), 7.00 (d, *J*=15.2 Hz, 1H); ^{13}C-NMR (100 MHz, $CDCl_3$, 25 °C), δ, ppm = 140.8, 139.5, 138.9, 138.6, 137.2, 136.9, 135.0, 128.8, 128.5, 127.8, 127.7, 127.1, 127.0, 126.9, 126.8, 125.0, 124.7, 120.0, 119.9, 119.6.

Synthesis of 9-(naphthalen-1-ylmethylene)-9*H*-fluorene (67i)

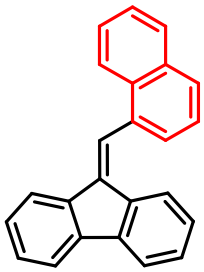

67 i

General procedure **B** was used employing **65** (213 mg, 0.5 mmol) and aldehyde **66i** (122 mg, 106 µL, 0.78 mmol). The reaction was heated at 160°C for 1 hour. FC (eluent: 7/3 *n*-hexane/DCM) provided pure compound **67i** as yellow solid (113 mg, 0.37 mmol, 74% yield). m.p.: 120-124°C;

^{1}H-NMR (400 MHz, $CDCl_3$, 25 °C), δ (ppm): 8.10-8.05 (m, 2H), 7.98-7.91 (m, 3H), 7.79-7.70 (m, 3H), 7.60-7.53 (m, 2H), 7.52-7.48 (m, 1H), 7.45-7.39 (m, 2H), 7.27 (dt, J_1= 7.4 Hz, J_2= 1.0 Hz, 1H), 7.09 (d, J= 7.8 Hz, 1H), 6.91 (dt, J_1= 7.6 Hz, J_2= 1.1 Hz, 1H); ^{13}C-NMR (100 MHz, $CDCl_3$, 25 °C), δ, ppm = 141.2, 139.4, 139.1, 137.9, 136.7, 134.3, 133.6, 131.7, 128.6, 128.5, 128.4, 128.3, 127.1, 127.0, 126.7, 126.4, 126.2, 125.4, 125.3, 125.1, 124.7, 120.4, 119.7, 119.6.

Synthesis of 9-(naphthalen-2-ylmethylene)-9*H*-fluorene (67j)[247]

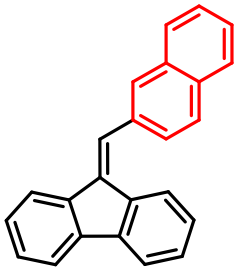

67 j

General procedure **B** was used employing **65** (213 mg, 0.5 mmol) and aldehyde **66j** (122 mg, 0.78 mmol). The reaction was heated at 225°C for 1 hour. Crystallization in MeOH provided pure compound **67j** as yellow solid (82 mg, 0.27 mmol, 54% yield). m.p.: 98-100°C; ^{1}H-NMR (400 MHz, $CDCl_3$, 25 °C), δ (ppm): 8.10 (s, 1H), 7.98-7.81 (m, 5H), 7.79-7.69 (m, 3H), 7.62 (d, J= 7.9 Hz, 1H), 7.59-7.51 (m, 2H), 7.45-7.29 (m, 3H), 7.03 (dt, J_1= 7.7 Hz, J_2=1.1 Hz, 1H).

Synthesis of 9-((9*H*-fluoren-9-ylidene)methyl)anthracene (67k)[248]

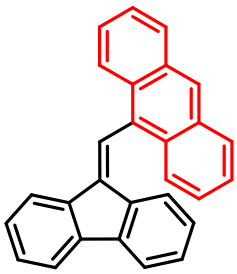

67 k

General procedure **B** was used employing **65** (213 mg, 0.5 mmol) and aldehyde **66k** (160 mg, 0.78 mmol). The reaction was heated at 225°C for 1 hour. Crystallization in MeOH provided pure compound **67k** as yellow solid (125 mg, 0.35 mmol, 67% yield). m.p.: 238-240°C; ^{1}H-NMR (400 MHz, $CDCl_3$, 25 °C), δ (ppm): 8.56 (s, 1H), 8.23 (s, 1H), 8.18 (dd, J_1= 8.7 Hz, J_2= 0.7 Hz, 2H), 8.13-8.04 (m, 3H), 7.83-7.76 (m, 1H), 7.68 (d, J= 7.7 Hz, 1H), 7.54-7.44 (m, 4H), 7.43-7.34 (m, 2H), 7.16 (dt, J_1= 7.6 Hz, J_2= 0.9 Hz, 1H), 6.63 (dt, J_1= 7.7 Hz, J_2= 1.0 Hz, 1H), 6.12 (d, J= 7.9, 1H).

Synthesis of 9-((9*H*-fluoren-9-ylidene)methyl)phenanthrene (67l)[245]

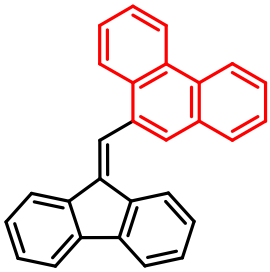

67 l

General procedure **B** was used employing **65** (213 mg, 0.5 mmol) and aldehyde **66l** (160 mg, 0.78 mmol). The reaction was heated at 225°C for 1 hour. FC (eluent: 3/7 *n*-hexane/DCM) provided pure compound **67l** as yellow solid (121 mg, 0.34 mmol, 68% yield). m.p.: 183-186°C; ^{1}H-NMR (400 MHz, $CDCl_3$, 25 °C), δ (ppm): 8.86-8.75 (m, 2H), 8.17 (dd, J_1= 8.2 Hz, J_2= 1.1 Hz, 1H), 8.08 (d, J= 1.4 Hz,1H), 8.02 (s, 1H), 7.98-7.95 (m, 1H), 7.89 (dd, J_1= 7.9 Hz, J_2= 1.4 Hz, 1H), 7.81-7.78 (m, 1H), 7.77-7.71 (m, 3H), 7.69-7.65 (m, 1H), 7.64-7.59 (m, 1H), 7.49-7.40 (m, 2H), 7.32-7.25 (m, 2H), 6.89 (dt, J_1= 7.6 Hz, J_2= 1.1 Hz, 1H).

Synthesis of 6-((9*H*-fluoren-9-ylidene)methyl)-1,5a^{1}-dihydropyrene (67m)

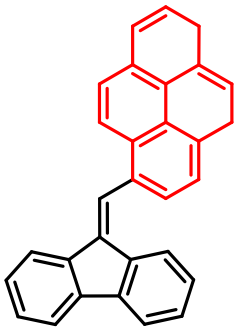

67 m

General procedure **B** was used employing **65** (213 mg, 0.5 mmol) and aldehyde **66m** (179 mg, 0.78 mmol). The reaction was heated at 225°C for 1 hour. FC (eluent: 1/1 *n*-hexane/DCM) provided pure compound **67m** as yellow solid (158 mg, 0.42 mmol, 83% yield). m.p.: 207-210°C; ^{1}H-NMR (600 MHz, $CDCl_3$, 25 °C), δ (ppm): 8.35-8.09 (m, 8H), 8.08-7.95 (m, 3H), 7.80-7.67 (m, 2H), 7.48- 7.37 (m, 2H), 7.27-7.19 (m, 1H), 6.97-6.74 (m, 2H); ^{13}C-NMR (150 MHz, $CDCl_3$, 25 °C), δ, ppm = 141.2, 139.4, 139.3, 138.2, 136.7, 131.6, 131.3, 131.2, 131.1, 129.1, 128.5, 128.4, 127.9, 127.8, 127.5, 127.4, 127.1, 126.7, 126.1, 125.5, 125.44, 125.43, 124.9, 124.8, 124.7, 124.68, 124.59, 120.5, 119.7, 119.6; ESI-MS^{+} (*m/z*): 381 $[M+H]^{+}$, 403 $[M+Na]^{+}$.

Synthesis of 7-((9*H*-fluoren-9-ylidene)methyl)-1*H*-indole (67n)

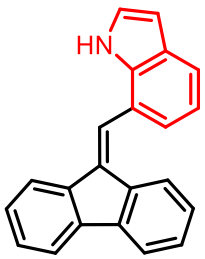

67 n

General procedure **A** was used employing **65** (213 mg, 0.5 mmol) and aldehyde **66n** (72 mg, 0.5 mmol) in $CHCl_3$ (15 mL). The reaction was heated at 100°C for 5 hours. FC (eluent: 9/1 *n*-hexane/EtOAc) provided pure compound **67n** as yellow solid (10 mg, 0.03 mmol, 7% yield). m.p.: 137-139°C; ^{1}H-NMR (600 MHz, $CDCl_3$, 25 °C), δ (ppm): 8.27 (s, 1H), 8.01 (s, 1H), 7.91 (d, J=7.6 Hz, 1H), 7.77 (d, J=7.5 Hz, 1H), 7.73 (d, J=7.5 Hz, 1H), 7.46 (t, J=7.2 Hz, 3H), 7.41 (dt, J_1=7.6 Hz, J_2=1.2 Hz, 1H), 7.38 (td, J_1=7.3 Hz, J_2=1.2 Hz, 1H), 7.31-7.28 (m, 2H), 7.24 (t, J=2.7 Hz, 1H), 7.00 (dt, J_1=7.6 Hz, J_2= 1.1

Hz, 1H), 6.56-6.55 (m, 1H); ^{13}C-NMR (150 MHz, $CDCl_3$, 25 °C), δ, ppm = 141.0, 139.7, 139.2, 136.8, 136.4, 135.9, 129.0, 128.2, 128, 127.0, 126.9, 126.6, 125.7, 125.0, 124.6, 121.9, 120.9, 120.3, 119.5, 119.4, 111.1, 102.5; ESI-MS$^-$ (*m/z*): 292 [M-H]$^-$; ESI-MS$^+$ (m/z): 294 [M+H]$^+$, 316 [M+Na]$^+$, 332 [M+K]$^+$.

Synthesis of 3-((9*H*-fluoren-9-ylidene)methyl)-1*H*-indole (67o)

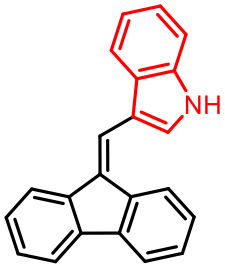

67 o

General procedure **A** was used employing **65** (213 mg, 0.5 mmol) and aldehyde **66o** (72 mg, 0.5 mmol) in $CHCl_3$ (15 mL). The reaction was heated at 100°C for 5 hours. FC (eluent: 8/2 *n*-hexane/EtOAc) provided pure compound **67o** as yellow solid (7 mg, 0.02 mmol, 5% yield). m.p.: 142-143 °C; ^{1}H-NMR (600 MHz, $CDCl_3$, 25 °C), δ (ppm): 8.41 (s, 1H), 7.94 (d, *J*=7.8 Hz, 1H), 7.88 (d, *J*=7.5 Hz, 1H), 7.85 (s, 1H), 7.77 (d, *J*=8.0 Hz, 2H), 7.70-7.65 (m, 2H), 7.48 (d, *J*=8.1 Hz, 1H), 7.37 (qt, *J*=6.7 Hz, 2H), 7.31 (q, *J*=7.5 Hz, 2H), 7.21 (t, *J*=7.5 Hz, 1H), 7.11 (t, *J*=7.7 Hz, 1H); ^{13}C-NMR (150 MHz, $CDCl_3$, 25 °C), δ, ppm = 140.7, 140.0, 138.5 137.1, 136.0, 134.5 127.8, 127.4, 127.1, 126.8, 126.5, 125.3, 124.1, 122.9, 120.6, 120.2, 120.0, 119.6, 119.5, 119.1, 113.3, 111.4; ESI-MS$^-$ (*m/z*): 292 [M-H]$^-$; ESI-MS$^+$ (m/z): 316 [M+Na]$^+$, 332 [M+K]$^+$.

Synthesis of 2-((9*H*-fluoren-9-ylidene)methyl)thiophene (67p)[245]

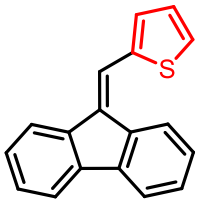

67 p

General procedure **A** was used employing **65** (176 mg, 0.4 mmol) and aldehyde **66p** (45 mg, 37 µL, 0.4 mmol) in $CHCl_3$ (15 mL). The reaction was heated at 85°C for 3 hours. FC (eluent: 6/4 *n*-hexane/DCM) provided pure compound **67p** as yellow solid (71 mg, 0.27 mmol, 68% yield). m.p.: 69-71°C; ^{1}H-NMR (400 MHz, $CDCl_3$, 25 °C), δ (ppm): 8.16-8.13 (m, 1H), 7.79-7.70 (m, 3H), 7.64 (d, *J*= 1.0 Hz, 1H), 7.50-7.44 (m, 2H), 7.42-7.30 (m, 3H), 7.24-7.15 (m, 2H).

Synthesis of 2-((9*H*-fluoren-9-ylidene)methyl)-5-nitrofuran (67q)

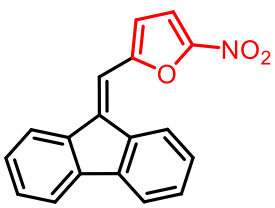

67 q

General procedure **A** was used employing **65** (213 mg, 0.5 mmol) and aldehyde **66q** (70 mg, 52 µL, 0.5 mmol) in $CHCl_3$ (15 mL). The reaction was heated at 85°C for 3 hours. FC (eluent: 3/7 *n*-hexane/DCM) provided pure compound **67q** as orange solid (111 mg, 0.38 mmol, 77% yield). m.p.: 196-197 °C; ^{1}H-NMR (600

MHz, $CDCl_3$, 25 °C), δ (ppm): 8.83 (d, *J*=7.7 Hz, 1H), 7.71-7.65 (m, 3H), 7.45-7.40 (m, 3H), 7.37 (t, *J*=7.2 Hz, 1H), 7.29 (d, *J*=7.5 Hz, 1H), 7.09 (s, 1H), 6.80 (d, *J*=3.6 Hz, 1H); ^{13}C-NMR (150 MHz, $CDCl_3$, 25 °C), δ, ppm = 154.1, 151.9, 141.9, 139.9, 139.8, 139.3, 135.0, 130.3, 129.6, 128.1, 127.3, 126.6, 120.5, 119.8 (two signals overlapped), 116.0, 113.7, 109.2; ESI-MS$^+$ (*m/z*): 312 $[M+Na]^+$, 328 $[M+K]^+$.

Synthesis of 1,4-bis((9*H*-fluoren-9-ylidene)methyl)benzene (70a)[245]

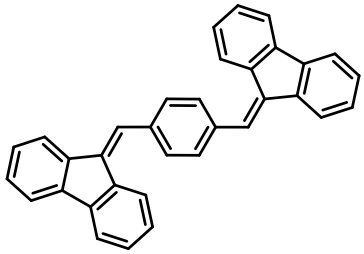

70 a

In a dried three necked bottom flask, partially immersed in an oil bath and equipped with a reflux condenser and a magnetic bar, a solution of fluorene **68a** (182 mg, 1.1 mmol) in *t*-BuOH (15 mL) was heated under reflux conditions under nitrogen atmosphere. Once dissolved, *t*-BuOK (369 mg, 3.3 mmol) was added in small portions, then terephthaldehyde **69** (67 mg, 0.5 mmol) was added and the reaction carried out for 2 hours under reflux conditions. The solid precipitated was filtered on a Büchner funnel and washed with MeOH (3 x 10 mL), affording the desired product **70a** as yellow solid (137 mg, 0.32 mmol, 64% yield). m.p.: 216-219°C; ^{1}H-NMR (300 MHz, $CDCl_3$, 25 °C), δ (ppm): 7.83 (d, *J*= 7.3 Hz, 2H), 7.78-7.68 (m, 12H), 7.44-7.30 (m, 6H), 7.12 (t, *J*= 7.3 Hz, 2H).

Synthesis of 1,4-bis((2,7-dibromo-9*H*-fluoren-9-ylidene)methyl)benzene (70b)

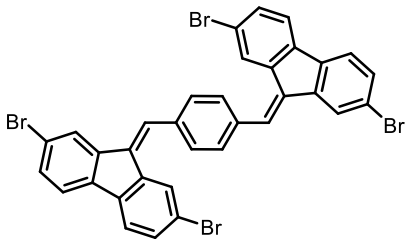

70 b

A solution of fluorene derivative **68b** (356 mg, 1.1 mmol), *t*-BuOK (369 mg, 3.3 mmol) and terephthalaldehyde **69** (67 mg, 0.5 mmol) in *t*-BuOH (20 mL) was introduced in a vessel for MW experiments equipped with a magnetic bar under nitrogen atmosphere to avoid the oxidation to fluorenone. The mixture was heated at 120 °C for 1 hour under MW irradiation (300 W) then allowed to stand at room temperature. The solid precipitated was filtered on a Büchner funnel and washed with MeOH (3 x 10 mL), affording the desired product **70b** as yellow solid (198 mg, 0.26 mmol, 53% yield). m.p.: >303°C; ^{1}H-NMR (400 MHz, $CDCl_3$, 25 °C), δ (ppm): 7.93 (s, 2H), 7.84 (s, 2H), 7.77-7.67 (m, 6H), 7.60-7.43 (m, 8H).

Synthesis of 2,7-diphenyl-9*H*-fluorene (63)[239]

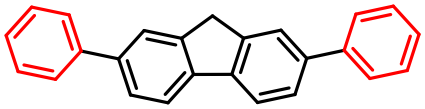

63

In a dried three necked bottom flask, partially immersed in an oil bath and equipped with a reflux condenser and a magnetic bar, fluorene derivative **68b** (162 mg, 0.5 mmol) and boronic acid **71** (134 mg, 1.1 mmol) were dissolved in THF (10 mL). An aqueous solution of Cs_2CO_3 (1 M, 1 mL), previously degassed with nitrogen flow in an ultrasound bath for 1 hour, and $Pd(dppf)Cl_2*CH_2Cl_2$ (8.17 mg, 0.01 mmol) were added to the solution and heated under reflux in nitrogen atmosphere for 4 hours. The crude mixture was filtered on a plug of Celite, washed with DCM (4 x 30 mL) and extracted in continuous with DCM. The organic phase was dried over $MgSO_4$, filtered and concentrated under reduced pressure. FC on silica gel (eluent: 9/1 *n*-hexane/DCM) and a crystallization from MeOH/EtOH 1/1 provided the compound **63** as white solid (110 mg, 0.34 mmol, 70% yield). m.p.: 284-286°C; ^{1}H-NMR (400 MHz, $CDCl_3$, 25 °C), δ (ppm): 8.05-7.14 (m, 16H), 4.02 (s, 2H).

Synthesis of 1,4-bis((2,7-diphenyl-9*H*-fluoren-9-ylidene)methyl)benzene (73)

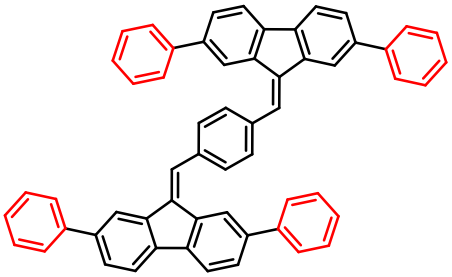

73

In a dried three necked bottom flask, partially immersed in an oil bath and equipped with a reflux condenser and a magnetic bar, fluorene derivative **70b** (430 mg, 0.576 mmol) and boronic acid **71** (309 mg, 2.536 mmol) were dissolved in THF (120 mL). An aqueous solution of Cs_2CO_3 (1 M, 10 mL), previously degassed with nitrogen flow in an ultrasound bath for 1 hour, and $Pd(dppf)Cl_2*CH_2Cl_2$ (18 mg, 0.02 mmol) were added to the solution and heated under reflux in nitrogen atmosphere overnight. The crude mixture was diluted with water (20 mL) and extracted with $CHCl_3$ (100 mL) at 50°C for 18 hours. The organic phase was dried over $MgSO_4$, filtered and concentrated under reduced pressure. FC on silica gel (eluent: 8/2 *n*-hexane/DCM) provided the desired product **73** as yellow solid (40 mg, 0.05 mmol, 10% yield). m.p.: >303 °C; ^{1}H-NMR (600 MHz, $CDCl_3$, 25 °C), δ (ppm): 8.07 (s, 2H), 7.98 (s, 2H), 7.87 (s, 2H), 7.85-7.78 (m, 6H), 7.74 (d, J= 7.7 Hz, 4H), 7.66 (dd, J_1= 7.8 Hz, J_2= 1.4 Hz, 2H), 7.59 (dt, J_1= 7.7 Hz, J_2= 1.4 Hz, 2H), 7.51 (t, J= 7.7 Hz, 4H), 7.45-7.33 (m, 6H), 7.23 (t, J= 7.5 Hz, 6H), 7.19-7.13 (m, 2H); ESI-MS$^+$ (*m/z*): 735 $[M+H]^+$, 757 $[M+Na]^+$, 773 $[M+K]^+$.

References

[228] Zhuravleva, M., Friedrich, S. & Melcher, C. L. *Appl. Phys. Lett.*, **2012**, *101*, 101902.
[229] Weber, M. J. J. *Lumin.*, **2002**, *100*, 35–45.
[230] Lecoq, P. *Nucl. Instrum. Meth. A*, **2016**, *809*, 130–139.
[231] Kramer, K. W., Dorenbos, P., Gudel, H. U. & van Eijk, C. W. E. *J. Mater. Chem.*, **2006**, *16*, 2773–2780.
[232] Niese, S. *J. Radioanal, Nucl. Chem.*, **1999**, *241*, 499-501.
[233] Birks, J.B. Ed. *Organic Molecular Photophysics*; John Wiley & Sons: London; **1973**; Vol. 1.
[234] Kishpaugh, D.; Hajagos, T.; Liu, C.; Chen, Q.; Pei, Q. *Nucl. Instrum. Methods Phys. Res. A*, **2017**, *868*, 59-65.
[235] Samuel, I. D. W.; Turnbull, G. A. *Chem. Rev.*, **2007**, *107*, 1272−1295.
[236] Zhang, X.; Dong, H.; Hu, W. *Adv. Mater.*, **2018**, *30*, 1801048.
[237] Zimmerman, P. M.; Bell, F.; Casanova, D.; Head-Gordon, M. *J. Am. Chem. Soc.*, **2011**, *133*, 19944−19952.
[238] Grimsdale, A. C.; Chan, K. L.; Martin, R. E.; Jokisz, P. G.; Holmes, A. B. *Chem. Rev.*, **2009**, *109*, 897−1091.
[239] Liu, D.; De, J.; Gao, H.; Ma, S.; Ou, Q.; Li, S.; Qin, Z.; Dong, H.; Liao, Q.; Xu, B.; Peng, Q.; Shuai, Z.; Tian, W.; Fu, H.; Zhang, X.; Zhen, Y.; Hu, W. *J. Am. Chem. Soc.*, **2020**, *142*, 6332-6339.
[240] Yu, W.-L.; Pei, J.; Huang, W.; Heeger, A. *J. Adv. Mater.*, **2000**, *12*, 828−831.
[241] Wu, Y.; Li, J.; Fu, Y.; Bo, Z. *Org. Lett.*, **2004**, *6*, 3485−3487.
[242] Kobin, B.; Behren, S.; Braun-Cula, B.; Hecht, S. *J. Phys. Chem.*, **2016**, *120*, 5474-5480.
[243] Tao, S.; Peng, Z.; Zhang, X.; Wang, P.; Lee, C.; Lee, S. *Adv. Funct. Mater.*, **2005**, *15*, 1716-1721.
[244] Eakins, L.; Cooper, W.; Gerasimchuk, N.; Phillips, J.; Breyfogle, E.; Stearman, J. *Can. J. Chem.*, **2013**, *91(11)*, 1059 – 1071.
[245] Brown, W.; Reagan, H. *J. Am. Chem. Soc.*, **1947**, *69(5)*, 1032-1033.
[246] Meng-Chi Chen, Deng-Gao Chen, Prof. Pi-Tai Chou *ChemplusChem*, **2021**, *86*, 11-27
[247] Ma, Y.; Luo, J.; Zhang, S.; Lu, S.; Du, G.; He, Lin *Org. Biomol. Chem.*, **2021**, *19*, 3717-3721.
[248] Becker, H.; Andersson, K. *J. Org. Chem.*, **1983**, *48(24)*, 4542-4549.

CHAPTER VI: Meanwhile in Denmark: Synthesis of Bicyclic Phenol Derivatives by a Base-Promoted One-Pot Cascade Reaction

6.1. Introduction

During the third year of doctorate, I spent 6 months at the Department of Drug Design and Pharmacology, University of Copenaghen (DK), under supervision of prof. Lennart Bunch. In this period I focused my efforts in the investigation of different reaction conditions about anion-accelerated electrocyclic ring-opening in 2-π electrocyclic systems with potential interest in medicinal chemistry. In particular I focused on the '*in situ*' generation of benzyne as reactive intermediate for cycloaddition reactions with several arynophiles at low temperature for the synthesis of phenol derivatives.

Phenols are ubiquitous building blocks in medicinal chemistry and found in many drugs in their free form or incorporated. Nedless to say, a good number of substituted phenols are commercially available and many more are readily synthesized by employing well-described methodologies such electrophilic aromatic substitution reactions, functional group transformations and/or transition metal catalysis. As an alternative strategy, a late stage aromatization strategy has been pursued. This strategy allows for access to phenols with substitution patterns and/or multiple substituents, which are difficult to access by means of the before mentioned well-known methodologies.

In regard to late stage aromatization strategies, the Bunch's group has recently disclosed the one-step synthesis of *meta*-bromo phenols **76** from cyclopentenones **74** by a base-promoted 2π-electrocyclic ring-opening of the key intermediate 6,6-dihalobicyclo[3.1.0]hexan-2-ones **75** (**Figure 57A**).[249] The methodology gives access to multi-functionalized phenols, which are otherwise difficult to synthesize, including fused bicyclic heterocyclic systems exemplified by the synthesis of the natural product *caramboxin*.[245] From that point, the work continued and the methodology was expanded to the recently reported synthesis of *meta*-bromo anilins **78** (**Figure 57B**) and *meta*-triflouromethyl anilins **80** (**Figure 57C**), from their corresponding cyclopentanones **77** and **79**, respectively.[250]

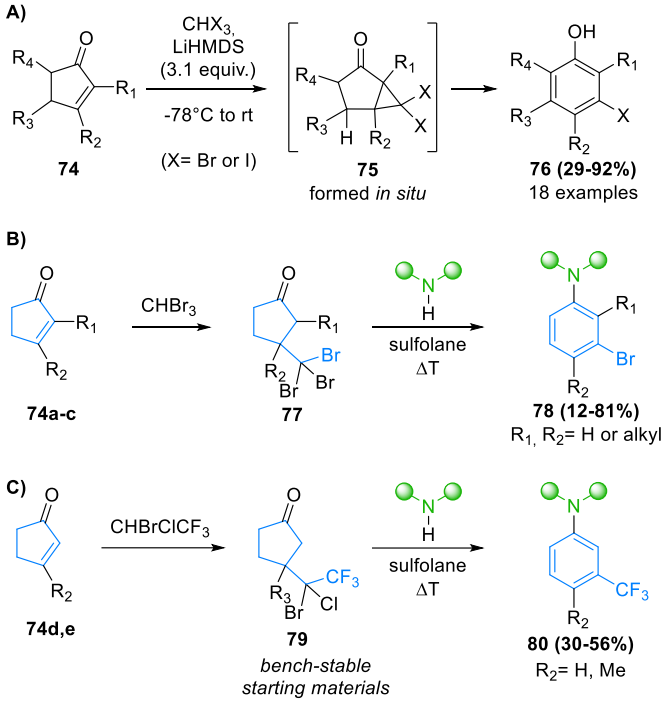

Figure 57. A) Reported one-step synthesis of *meta*-bromo phenols **76** from cyclopentenones **74** via a base-promoted 2π-electrocyclic ring-opening of the key intermediate 6,6-dihalobicyclo[3.1.0]hexan-2-ones (**75**). **B**) Synthesis of *meta*-bromo anilins **78** from bench-stable 3-substituted cyclopentanones **77**. **C**) Synthesis of *meta*-trifluoromethyl anilins **80** from bench-stable 3-substituted cyclopentanones **79**.

In the Brook rearrangement, first described by Brook et al., an α-silylcarbinol isomerizes to its corresponding *O*-silyl ether.[251,252] Recently, Kim and co-workers reported the *in situ* formation of benzyne from a Brook-like rearrangement of 2-methylsilyl-3-triflate-phenol with base (**Figure 58**). The highly reactive aryne was captured with a range of different arynophiles to give their corresponding ring-fused phenols.[253]

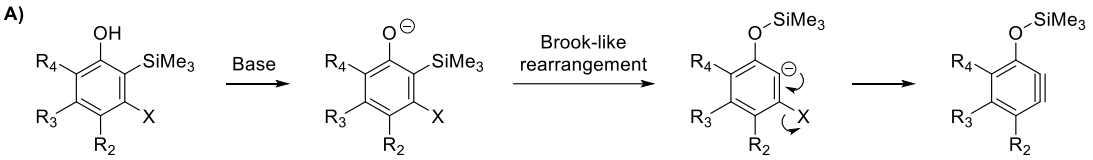

Figure 58. Treatment of 2-methylsilyl-3-triflate-phenol with base leads to *in situ* formation of the corresponding benzyne by a Brook-like rearrangement.[236]

The combination of the work of Kim et al. with the recently reported base-mediated one-step reaction seemed to be an interesting opportunity for the synthesis of phenols from cyclopentenones.[232] Taking notice of the recent report on the synthesis of substituted 2-trimethylsilylcyclopentenones by Morandi and coworkers,[254] the analog 2-trimethylsilyl-3-

methyl-5-phenyl-cyclopentenone **81** (**Scheme 39**) seemed attractive as starting material for the synthesis of phenols due to its physicochemical (non-volatile) and spectroscopic (easily identified by ^{1}H-NMR) properties.

6.2. Results and discussion

At first an intermolecular palladium-catalyzed reaction under microwaves irradiation (300W) allowed to obtain the starting material **81** for the next synthetic step. By reacting an alkyne **81b**, an α,β-unsaturated acid chloride **81a**, which serves as both the alkene and carbon monoxide source, and a hydrosilane **81c** it was possible to create three new C−C bonds (**Scheme 39**).

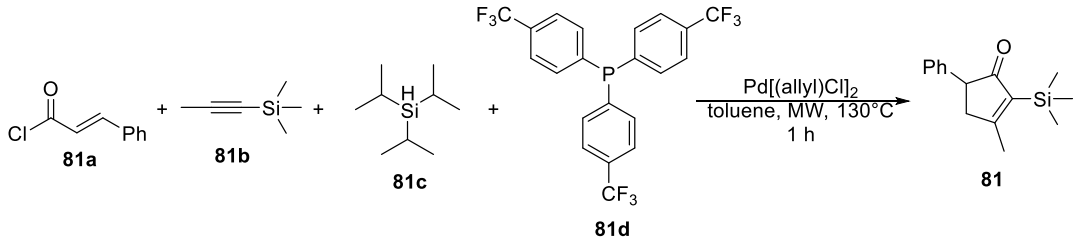

Scheme 39. Synthesis of cyclopentenone **81** as starting material for the next step.

We envisaged the putative cascade reaction (**Scheme 40**) to commence with base-mediated conjugate addition of a haloform to cyclopentenone **81**, to give enolate **82**, which upon cyclization gives dihalo-cyclopropane analogue **83**. Subsequent base induced 2π-electrocyclic ring-opening of **83** at low temperature provides phenoxide **84**, which undergoes Brook-like rearrangement followed by elimination to reactive aryne **85**. Upon the reaction of **85** – in situ -with a suitable arynophile, adduct **86** is obtained.

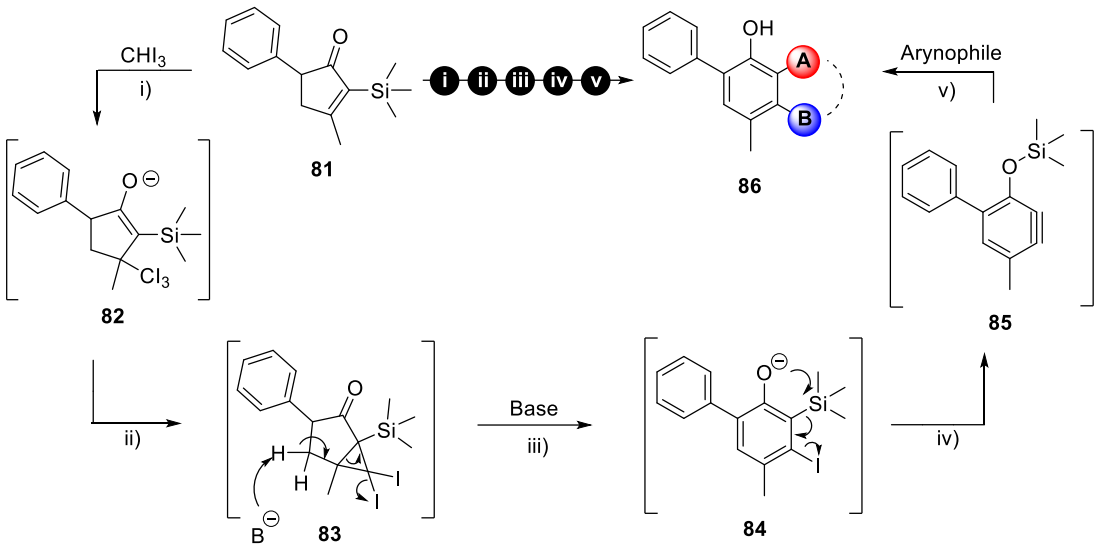

Scheme 40. One-pot synthesis of substituted phenols. i) 1,4-Addition reaction; ii) cyclopropane formation; iii) Anion-accelerated 2π-disrotatory electrocyclic ring-opening reaction; iv) Brook-like rearrangement, aryne formation; v) *in situ* cycloaddition or nucleophilic addition reaction.

First the nature of the halide leaving group for this putative cascade reaction was investigated. As the standard arynophile for this study, furan was chosen. Upon addition of 1 equiv of bromoform at -78 ºC in THF and allowing the reaction mixture to warm to room temperature over one hour, no desired furan adduct **88** was observed (**Table 15**, entry 1). On the other hand, when adding 1 equiv of iodoform, and retaining the general reaction conditions, the furan adduct **88** was isolated in 20% yield (**Table 15**, entry 2). The fact that product is only obtained with iodide as the leaving group, is in line with general observations that bromine is only rarely reported as a suitable leaving group in these transformations.[255] Deprotection of the TMS ether took place during work-up to give phenol **88**, exclusively. Extending the reaction time by slowly warming the reaction mixture to room temperature over night (**Table 15**, entry 3) led to reduced yield of **88** (8%). As an alternative it was decided to increase the equivalents of arynophile to 10, and under these conditions, the furan adduct **88** was isolated in 40% yield.

Table 15. Optimization of [4+2] cycloaddition reaction with furan.

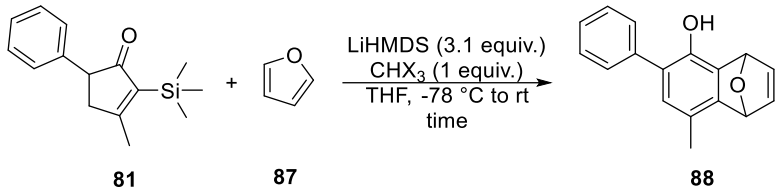

81 87 88

Entry	CHX_3	Furan Equiv. (87)	Time [h]	Yield[a] [%]
1	$CHBr_3$	2	1	0
2	CHI_3	2	1	20
3	CHI_3	2	18	8
4	CHI_3	10	2	40

[a] Isolated yields.

Next, solvent effects were investigated (**Table 16**) with point in the optimized reaction conditions just described (**Table 15**, entry 3). When the reaction was carried out in the slightly less polar solvent Me-THF, adduct **88** was isolated in significantly lower yield (22%) (**Table 16**, entry 2). Switching to the acyclic solvent cyclopentylmethylether (CPME) led to a complete loss of the desired product (**Table 16**, entry 3). The use of dimethyl ether (DME) prompted us to initiate the reaction at -40°C, being the melting point of DME = -58°C. However, the reaction furnished **88** in only 15% yield (**Table 16**, entry 4) suggesting that not only the solvent polarity negatively influences the reaction outcome, but perhaps also the initial temperature.

Table 16. Investigation of solvent effect on the reaction outcome.

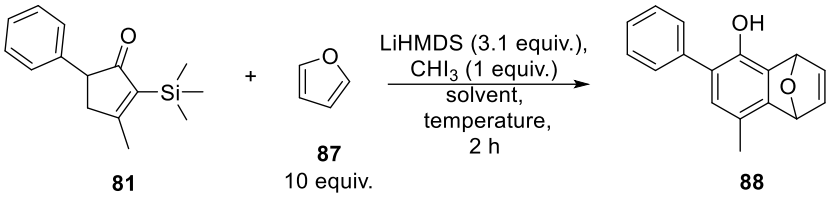

81 87 10 equiv. 88

Entry	Solvent	Temperature	Yield[a] [%]
1	THF	-78°C to rt	40
2	Me-THF	-78°C to rt	22
3	CPME	-78°C to rt	n.d.[b]
4	DME	-40°C to rt	15

[a] Isolated yields. [b] n.d.=not detected.

We now turned to investigate the scope of this cascade transformation on a variety of arynophiles representing [4+2], [3+2], and [2+2] cycloaddition reactions as well as nucleophilic addition reactions (**Table 17**). For the [4+2] cycloaddition reactions, it was

surprising to learn that 2,5-dimethylfuran **89a** did not allow for detection of the desired product (**Table 17**, entry 2). The same was true for *N*-methyl pyrrole (**89b**), cyclohexadiene (**89c**), Danishefsky's diene (**89d**), and anthracene (**89e**) (**Table 17**, entries 3-6). In fact, a side-product was isolated in various yields and its structure idenfied by ^{1}H- and ^{13}C-NMR to be 3-iodo,5-phenylphenol (**91**). We propose that the formation of **91** originates from competition reaction between the arynophile and the iodide anion, at the *in situ* generated benzyne **85**, or as a result of *in situ* protonation of the arylic anion. The proton source could be the aryne.

For the class of intermolecular [3+2] cycloaddition reactions, the desired product was not detected when azides **89f** and **89g** were employed (**Table 17**, entry 7-8). However, the [2+2] cycloaddition reaction with 2-methoxypropene (**89h**) did proceed to give **90h** in 4% together with iodophenol (**91**) in 8% yield (**Table 17**, entry 9). In accordance with charge-, aryne distortion- and steric model,[256] regioisomers **90d**, **90g** and **90h** are expected as favored products. In fact considering the benzyne **85**, where the OTMS group has an inductively electron-withdrawing effect, the arynophile attacks the aryne terminus that is more positively charged, more distorted towards linearity and less sterically hindered. Finally, the electrophilic nature of benzyne **85** was probed by applying morpholine **89i** as a nucleophile. For this class, the expected phenol derivative **90i** was isolated in 18% yield after warming the reaction at room temperature over 3 hours, and using only 3 equivalents of **89i** (**Table 17**, entry 10). Interestingly, phenol **91** was not obtained in this reaction.

Table 17. Investigation of reactivity of several arynophiles towards the benzyne precursor **81**.

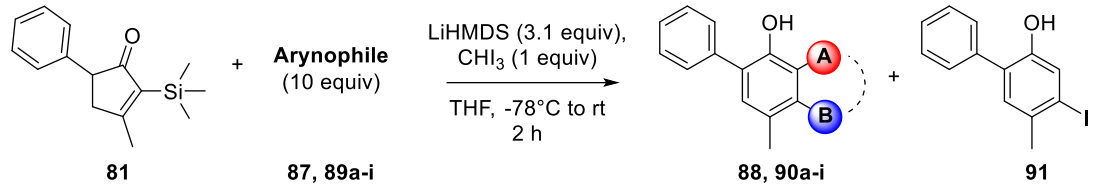

Arynophiles used:

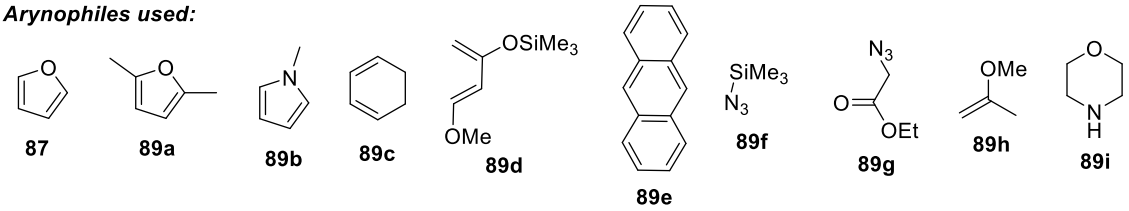

Entry	Arynophile	Reaction class	Product	Yield (88+90) [%][a]	Yield (91) [%][a]
1	**87**	[4+2]	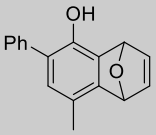 **88**	40	8
2	**89a**	[4+2]	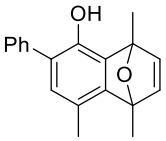 **90a**	n.d.[b]	16
3	**89b**	[4+2]	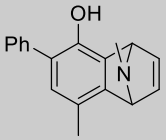 **90b**	n.d.[b]	8
4	**89c**	[4+2]	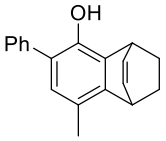 **90c**	n.d.[b]	13
5	**89d**	[4+2]	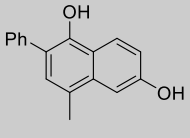 **90d**	n.d.[b]	10

6[d]	**89e**	[4+2]	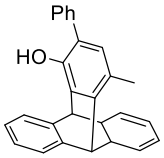 **90e**	n.d.[b]	5
7[d]	**89f**	[3+2]	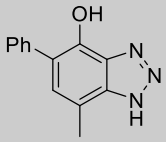 **90f**	n.d.[b]	/[c]
8	**89g**	[3+2]	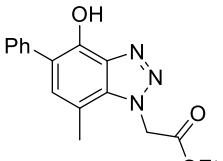 **90g**	n.d.[b]	/[c]
9	**89h**	[2+2]	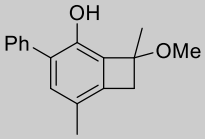 **90h**	4	8
10[e]	**89i**[f]	Nu	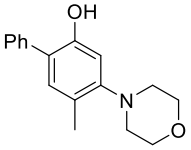 **90i**	18	n.d.[b]

[a] Isolated yields. [b] n.d.=not detected. [c] Crude product not purified.

Variation from standard conditions 2h, 10 equiv: [d] 18 h; [e] 3 h; [f] 3 equiv. of morpholine used.

6.3. Conclusions

In conclusion we have investigated the principles for a cascade reaction of a 2-trimethylsilylcyclopentenone **81**, iodoform and an arynophile to give the corresponding substituted phenol. The influence of temperature, time and solvent effects were addressed and it was shown that the increase of the equivalents of arynophile led to higher yields. Not all [4+2] arynophiles were successful, and also the [3+2] reactions were non-productive. However, the investigated [2+2] arynophile gave the product in low yield, whereas the amine nucleophile morpholine was quite efficient in providing the corresponding phenol in 18% yield. The prime example was with furan as arynophile which gave the desired phenol **88** in 40% isolated yield. While this yield may seem only moderate, when taken into consideration that this cascade transformation holds five individual synthetic steps, the average conversion for each step is an impressive 83%.

6.4. Experimental section

All reactions requiring inert conditions were performed under argon atmosphere in flame dried glassware. Commercially available chemicals were used without further purification. THF was dried using a SG WATER solvent purification system from Pure Process Technology. Remaining anhydrous solvents were prepared by storing them over molecular sieves for at least 48 h. R_F values and reaction controls were performed on F254 silica gel 60 thin-layer chromatography alumina sheets from Merck. Chromatographic purification was performed using either flash chromatography on silica gel 60A (40-63 μm). NMR-spectra were acquired using a 400 MHz Bruker Avance II equipped with a 5 mm broad band probe. Samples were dissolved in deuterated solvent and analysed at 300 K. Proton spectra, at 400.09 MHz, were acquired using 30°-pulses, a spectral width of 8 kHz, collecting 16 scans with a length of 65536 data points with a relaxation delay of 1.0 sec. FID's were zero-filled to twice the size and exponentially multiplied with a line broadening factor of 0.3 Hz before Fourier transform. Carbon spectra were acquired at 100.60 MHz with 30°-pulses, a spectral width of 24 kHz, collecting 256 scans with a length of 65536 data points and with a relaxation delay of 2.0 sec. The ^{13}C nuclei were ^{1}H-decoupled using the Waltz-16 composite pulse decoupling scheme. FID's were exponentially multiplied with a line broadening factor of 1.0 Hz before Fourier transform. NMR-spectra were acquired using a 600 MHz Bruker Avance III HD equipped with a cryogenically cooled 5 mm dual probe optimized for ^{13}C and ^{1}H. Samples were dissolved in deuterated solvent and analysed at 300 K. Proton spectra, at 600.03 MHz, were acquired using 30°-pulses, a spectral width of 12 kHz, collecting 16 scans with a length of 65536 data points with a relaxation delay of 1.0 sec. FID's were zero-filled to twice the size and exponentially multiplied with a line broadening factor of 0.3 Hz before Fourier transform. Carbon spectra were acquired at 150.88 MHz with 30°-pulses, a spectral width of 36 kHz, collecting 256 scans with a length of 65536 data points and with a relaxation delay of 2.0 sec. The ^{13}C nuclei were 1H-decoupled using the Waltz-16 composite pulse decoupling scheme. FID's were exponentially multiplied with a line broadening factor of 1.0 Hz before Fourier transform. LC-MS spectra were recorded using a Waters Acquity UPLC-MS with dual wavelength detection with electrospray ionization. Gradients of 5% aqueous MeCN + 0.1% HCO_2H (solvent A), and 95% aqueous MeCN + 0.05% HCO_2H (solvent B) were employed. LC-MS analysis is in agreement with the structure of all compounds obtained.

Synthesis of 3-methyl-5-phenyl-2-(trimethylsilyl)cyclopent-2-en-1-one (**81**).

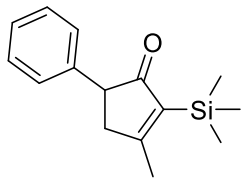

81

In a flame-dried vessel for MW experiments equipped with a magnetic stirrer, phosphine **81d** (36 mg, 78 µmol, 1 mol%) and $Pd[(allyl)Cl]_2$ (14 mg, 39 µmol, 0.5 mol%) are dissolved in anhydrous toluene (15 mL) at r.t. for 15 minutes. Then, acyl chloride **81a** (1.950 g, 11.8 mmol), **81b** (1.15 mL, 7.8 mmol), **81c** (2.4 mL, 11.8 mmol) were added in sequence and the resulting orange solution was heated under MW irradiation at 130°C for 1 hour. After cooling, the green solution was filtered on Celite and washed with DCM (3 x 10 mL). After removal of the solvent on rotovap, the crude product was purified by flash chromatography (heptane : DCM : Et_2O 8:1:1) to give compound **81** (520 mg, 2.13 mmol, 27%) as a yellow oil. R_F= 0.38 (heptane/DCM/Et_2O 8:1:1); ^{1}H-NMR (400 MHz, $CDCl_3$, 25°C): δ= 7.33-7.27 (m, 2H; Ar-H), 7.24-7.19 (m, 1H; Ar-H), 7.14-7.09 (m, 2H; Ar-H), 3.54 (dd, J_1=7.6 Hz, J_2=3.2 Hz, 1H), 3.11 (dd, J_1=18.8 Hz, J_2=0.6 Hz, 1H), 2.71 (m, 1H), 2.25 (s, 3H; CH_3), 0.25 ppm (s, 9H; $Si(CH_3)_3$); ^{13}C-NMR (150 MHz, $CDCl_3$, 25°C): δ= 212.15, 184.2, 140.3, 138.7, 128.64, 128.63, 127.5, 126.6, 52.8, 45.1, 20.2, 17.7, -0.58 ppm; IR: *v*= 3710, 2982, 2904, 2365, 2352, 2348, 1614, 1405, 1229, 1073, 1065, 1057 cm^{-1}; LC-MS^+ (*m/z*): 245 $[M+H]^+$.

General procedure for preparation of substituted phenols

In a flame-dried round-bottom flask, equipped with a magnetic stirrer and under argon atmosphere, cyclopentenone **81** (1 eq) and CHI_3 (1 eq) were dissolved in THF (0.1 M) at room temperature. After cooling to -78°C in an acetone dry ice bath for 10 minutes, arynophile (3 or 10 equiv.) and LiHMDS (1 M in THF, 3.1 eq) were added dropwise. After removal of the cooling bath, the reaction mixture was allowed to warm to r.t. After 2 (or 3) hours, the reaction was quenched with saturated aqueous NH_4Cl (40 mL/mmol), extracted with DCM (120 mL/mmol) and the combined organic layers were dried over $MgSO_4$. After removal of the solvent under reduced pressure, the crude product was purified by flash column chromatography.

Synthesis of 8-methyl-6-phenyl-1,4-dihydro-1,4-epoxynaphthalen-5-ol (**88**).

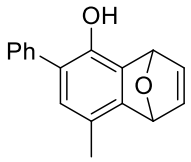

88

General procedure was used employing cyclopentenone **81** (50 mg, 0.20 mmol), furan **87** (145 µL, 2 mmol), CHI_3 (80 mg, 0.20 mmol) and LiHMDS (1 M in THF, 0.63 mL, 0.63 mmol). The reaction time was 2 hours. Flash column chromatography on silica gel using heptane:EtOAc (8:2) provided compound **88** (20 mg, 0.08 mmol, 40%) as a colorless oil. R_F= 0.20 (heptane/EtOAc 8:2); ^{1}H-NMR (400 MHz, $CDCl_3$, 25°C): δ= 7.50-7.43 (m, 2H), 7.42-7.35 (m, 3H), 7.12 (dd, J_1= 1.82 Hz, J_2= 5.57 Hz, 1H), 7.07 (dd, J_1= 1.82 Hz, J_2= 5.52 Hz, 1H), 6.68 (s, 1H), 5.98 (s, 1H), 5.80 (s, 1H), 5.05 (bs, 1H), 2.28 ppm (s, 3H). ^{13}C-NMR (100 MHz, $CDCl_3$, 25°C): δ= 149.2, 144.1, 143.0, 142.3, 136.8, 133.1, 129.3, 129.1, 128.9, 127.8, 127.5, 122.8, 81.2, 80.2, 17.6 ppm. IR: *v*= 2982, 2904, 2361, 2345, 1407, 1393, 1379, 1247, 1229, 1077, 1065, 1055 cm^{-1}; LC-MS^+ (*m/z*): 251 $[M+H]^+$.

Synthesis of 8-methoxy-5,8-dimethyl-3-phenylbicyclo[4.2.0]octa-1,3,5-trien-2-ol (**90h**).

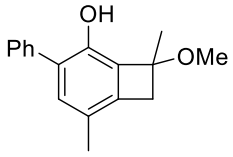

90h

General procedure was used employing the cyclopentenone **81** (50 mg, 0.20 mmol), 2-methoxypropene **89h** (191 µL, 2 mmol), CHI_3 (80 mg, 0.20 mmol) and LiHMDS (1 M in THF, 0.63 mL, 0.63 mmol). The reaction time was 2 hours. Flash column chromatography on silica gel using heptane:EtOAc (8:2) provided compound **90h** (2 mg, 0.008 mmol, 4%) as a yellow oil. R_F= 0.16 (heptane/EtOAc 8:2); ^{1}H-NMR (400 MHz, $CDCl_3$, 25°C): δ= 7.50-7.40 (m, 4H), 7.39-7.34 (m, 1H), 6.98 (s, 1H), 5.20 (bs, 1H), 3.43 (s, 3H), 3.29 (d, *J*=3.1 Hz, 1H), 2.99 (d, *J*=2.8 Hz, 1H), 2.17 (s, 3H), 1.72 ppm (s, 3H); LC-MS^+ (*m/z*): 255 $[M+H]^+$.

Synthesis of 5-methyl-4-morpholino-[1,1'-biphenyl]-2-ol (**90i**).

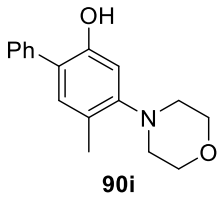

90i

General procedure was used employing the cyclopentenone **81** (50 mg, 0.20 mmol), morpholine **89i** (54 µL, 0.60 mmol), CHI_3 (80 mg, 0.20 mmol) and LiHMDS (1 M in THF, 0.63 mL, 0.63 mmol). The reaction time was 3 hours. Flash column chromatography on silica gel using heptane:EtOAc (8:2) provided compound **90i** (10 mg, 0.037 mmol, 18%) as a yellow oil. R_F= 0.28 (heptane/EtOAc 8:2); ^{1}H-NMR (400 MHz, $CDCl_3$, 25°C): δ= 7.51-7.42 (m, 4H), 7.40-7.33 (m, 1H), 7.07 (s, 1H), 6.69 (s, 1H), 5.14 (s, 1H), 3.87 (t, *J*=4.4 Hz, 4H), 2.96 (t, *J*=4.4 Hz, 4H), 2.28 ppm (s, 3H); ^{13}C-NMR (150 MHz, $CDCl_3$, 25°C): δ= 151.5 (bs), 151.1,

137.0, 132.6, 129.2, 128.9, 127.5, 124.3, 123.2 (bs), 106.8, 67.1, 52.2, 17.2 ppm; IR: *v*= 3237, 2961, 2850, 2161, 1730, 1612, 1487, 1449, 1400, 1298, 1262, 1194, 1143, 1110, 1025, 1106, 910, 889, 768 cm^{-1}; LC-MS^+ (*m/z*): 270 $[M+H]^+$.

4-iodo-5-methyl-[1,1'-biphenyl]-2-ol (**91**).

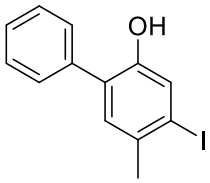

91

Yellow oil; R_F= 0.28 (heptane/EtOAc 8:2); ^{1}H-NMR (400 MHz, $CDCl_3$, 25°C): δ= 7.52-7.46 (m, 3H), 7.45-7.38 (m, 3H), 7.09 (s, 1H), 5.06 (bs, 1H), 2.39 (s, 3H); ^{13}C-NMR (150 MHz, $CDCl_3$, 25°C): δ= 150.6, 136.3, 133.5, 130.4, 129.3, 128.8, 128.2, 128.1, 125.9, 99.8, 26.8.

References

[249] Staudt, M.; Sølling, T.; Bunch, L. *Chem. - A Eur. J.*, **2021**, *27*, 10941–10947.
[250] Staudt, M.; Cétin, A.; Bunch, L. Transition Metal-Free Synthesis of Meta-Bromo- and Meta-Trifluoromethylanilines from Cyclopentanones by a Cascade Reaction. *Chem. - A Eur. J.*, **2021**, in press.
[251] Brook, A. G.; Warner, C. M.; McGriskin, M. E. *J. Am. Chem. Soc.*, **1959**, *81*, 981–983.
[252] Brook, A. G. *J. Am. Chem. Soc.*, **1958**, *80*, 1886–1889.
[253] Kwon, Y. J.; Jeon, Y. K.; Sim, H. Bin; Oh, I. Y.; Shin, I.; Kim, W. S. *Org. Lett.*, **2017**, *19*, 6224–6227.
[254] Lee, Y. H.; Denton, E. H.; Morandi, B. *J. Am. Chem. Soc.*, **2020**, *142*, 20948–20955.
[255] Kitamura, T.; Yamane, M.; Inoue, K.; Todaka, M.; Fukatsu, N.; Meng, Z.; Fujiwara, Y. A *J. Am. Chem. Soc.*, **1999**, *121(50)*, 11674–11679.
[256] Medina, J. M.; Mackey, J. L.; Garg, N. K.; Houk, K. N. *J. Am. Chem. Soc.*, **2014**, *136(44)*, 15798–15805.

Abstract

This PhD project has been mainly focused on the synthesis of novel organic compounds containing heterocyclic and/or carbocyclic scaffold and on the study of stearic acid derivatives and their applications in biological field. Particular attention has been devoted at the synthesis of compounds whose anticancer activity was investigated owing the collaboration with biochemists.

The synthesis of novel derivatives of 9-hydroxystearic acid (9-HSA) evidenced how the presence of substituents on C9, able to make hydrogen bonds is of crucial importance for the biological activity. Moreover, the *R* or *S* configuration of the C-9 influences the antiproliferative activity. Also the position of the hydroxy group along the chain of hydroxystearic acids was investigated: regioisomers with the hydroxy group bound to odd carbons resulted more active than those bearing the hydroxy group on even carbons. Further, the insertion of (*R*)-9-HSA in magnetic nanoparticles gave a novel material which characterization remarked its suitability for drug delivery because of the magnetic monodomain structure, the dimension inside the range 10 nm < d < 100 nm and the high magnetization saturation.

Structural hybrids between amino aza-heterocycles and azelaic acid have been synthesized and some of them showed a selective activity towards osteosarcoma cell line U2OS.

Several Apcin analogues bearing indole, benzothiazole, benzofurazan moieties connected to tryptaminyl-, amino pyridinyl-, pyrimidinyl- and pyrazinyl ring through a 1,1,1-trichloroethyl group were synthesized. Biological tests showed the importance of both the tryptaminyl and the pyrimidinyl moieties, confirming the effectiveness against acute leukemia models. Benzothiazole and benzofurazan derivatives were active at nanomolar concentration, against cervical, colon, breast and bone cancer cell lines.

The S_NAr between 2-aminothiazole derivatives and 7-chlorodinitrobenzofuroxan revealed different behaviour depending from amino substituent of the thiazole. The reaction with 2-*N*-piperidinyl-, 2-*N*-morpholinyl-, or 2-*N*-pyrrolidinyl thiazole gave two isomeric species derived from the attack on C-5 of thiazole ring; the reaction mechanism was investigated mainly via NMR experiments. Thiazoles substituted with primary- or not-cyclic secondary amines reacted with the exocyclic amino nitrogen atom giving a series of compounds whose biological activity have highlighted as they might be promising candidates for further development of antitumor agents.

A series of 9-fluorenylidene derivatives, of interest in medical and optoelectronic field as organic scintillators, was synthesized through Wittig or Suzuky reaction and will be analyzed to test their potential scintillatory properties.

Finally, base-promoted cascade reaction allowed me to access phenol derivatives from the corresponding cyclopentenones under mild conditions. The reaction will be improved and tested on other several arynophiles to confirm the strength of the methodology.